UNIVERSITY OF CALIFORNIA,
IRVINE

Comprehensive Cardiac Computed Tomography: Translating Medical Physics Into Medical Practice

DISSERTATION

submitted in partial satisfaction of the requirements
for the degree of

DOCTOR OF PHILOSOPHY

in Biomedical Engineering

by

Logan Charles Hubbard

Dissertation Committee:
Professor Sabee Molloi, Chair
Professor Bruce Tromberg
Associate Professor Shaista Malik

2018

DEDICATION

To

the people I love

without whom none of my success would be possible

TABLE OF CONTENTS

	PAGE
LIST OF FIGURES	**iv**
LIST OF TABLES	**viii**
ACKNOWLEDGMENTS	**x**
CURRICULUM VITAE	**xi**
ABSTRACT OF THE DISSERTATION	**xv**
CHAPTER 1: Coronary Artery Disease and The Current State of Cardiac Computed Tomography Cardiac Computed Tomography	**1**
CHAPTER 2: Accuracy of Absolute Perfusion Measurement as Compared to Ultrasonic Perfusion Measurement in a Cardiac Phantom	**8**
CHAPTER 3: Accuracy of Coronary Perfusion Territory Assignment as Compared to Myocardial Blush in Swine	**38**
CHAPTER 4: Accuracy of Relative Perfusion Measurement as Compared to Invasive Fractional Flow Reserve Measurement in Swine	**66**
CHAPTER 5: Accuracy of Absolute Perfusion Measurement as Compared to Quantitative Microsphere Perfusion Measurement in Swine	**92**
CHAPTER 6: Low-Dose Prospective Global Stress Perfusion Measurement as Compared to Retrospective Perfusion Measurement in Swine	**117**
CHAPTER 7: Low-Dose Prospective Vessel-Specific Rest Perfusion, Stress Perfusion, Coronary Flow Reserve, and Angiography as Compared to Retrospective Perfusion Measurement in Swine	**143**
CHAPTER 8: Prospective Acquisition Timing Using a Diluted Test Bolus as Compared to a Pure Bolus in Swine	**171**
CHAPTER 9: Prospective Acquisition Timing Using an Optimal Bolus Timing Theory as Compared to a Pure Bolus in Swine	**195**
CHAPTER 10: Clinical Translation and Future Directions of Low-Dose Comprehensive Cardiac Computed Tomography in Human Subjects	**222**
REFERENCES	**239**

LIST OF FIGURES

PAGE

Figure 1.1. Graphical display of coronary arterial architecture **7**

Figure 2.1: Single compartment model used in the first-pass analysis technique. **29**

Figure 2.2: Photograph and schematic diagram of the cardiac perfusion phantom. **30**

Figure 2.3: Myocardial compartment around the contrast filled left ventricle. **31**

Figure 2.4: Pulsatile flow profile in the cardiac perfusion phantom. **32**

Figure 2.5: Arterial input function and myocardial tissue time attenuation curve with five-volume FPA sampling protocol. **33**

Figure 2.6: FPA perfusion and MSM perfusion regression and Bland-Altman analysis. **34**

Figure 2.7: Arterial input function and myocardial tissue time attenuation curve with two-volume FPA sampling protocol. **35**

Figure 2.8: Temporal optimization of volume scan selection for the FPA technique. **36**

Figure 2.9: FPA perfusion measurement with the new two-volume sampling scheme as compared to reference standard ultrasonic-flow-probe perfusion measurement. **37**

Figure 3.1: Minimum-Cost Path (MCP) assignment method summary. **61**

Figure 3.2: MCP Image Processing Methods. **62**

Figure 3.3: Linear regression and Bland-Altman analysis of mass correspondence of M_{MCP} and M_{RS} for LCA and RCA territories. **63**

Figure 3.4: Mass correspondence of MCP and reference standard myocardial perfusion territories from a single animal. **64**

Figure 3.5: Evaluation of myocardium at-risk distal of a stenosis in the LAD using MCP. **65**

Figure 4.1: Coronary perfusion compartment model used for FPA perfusion measurement. **85**

Figure 4.2: Arterial input function and myocardial tissue time attenuation curve used for FPA perfusion measurement. **86**

Figure 4.3: CT projection and angiographic images of the interventional setup. **87**

Figure 4.4: Image processing scheme for the FPA technique. **88**

Figure 4.5: Regression and Bland-Altman analysis comparing the result of relative FPA perfusion measurement to reference standard FFR measurement. **89**

Figure 4.6: Regression and Bland-Altman analysis comparing the result of relative MSM perfusion measurement to reference standard FFR measurement. **90**

Figure 4.7: Diagnostic performance of relative FPA and relative MSM perfusion measurement as compared to reference standard FFR measurement. **91**

Figure 5.1: Myocardial perfusion compartment model used for quantitative first-pass analysis (FPA) perfusion measurement. **110**

Figure 5.2: Arterial input function and myocardial tissue time attenuation curve used for FPA perfusion measurement. **111**

Figure 5.3: Contrast-enhanced CT projection and angiographic images of the interventional setup in the swine model. **112**

Figure 5.4: Image processing scheme for FPA perfusion measurement. **113**

Figure 5.5: Combined angiography and perfusion maps generated by the FPA technique. **114**

Figure 5.6: Regression of FPA perfusion measurement in all three coronary arteries combined as compared to reference standard microsphere perfusion measurement. **115**

Figure 5.7: FPA- and MSM based detection of physiologically significant stenoses in the LAD at maximal hyperemia. **116**

Figure 6.1: Figure 6.1: First-pass analysis theory and implementation. **138**

Figure 6.2: Reduced tube current rest perfusion measurement analysis. **139**

Figure 6.3: Low-dose prospective stress perfusion measurement analysis. **140**

Figure 6.4: Low-dose stress perfusion measurement distribution in the presence of a physiologically significant left anterior descending coronary artery stenosis. **141**

Figure 6.5: Effective dose of the low-dose prospective FPA technique using automatic exposure control. **142**

Figure 7.1: Low-dose comprehensive cardiac CT theory and implementation. **166**

Figure 7.2: Low-dose comprehensive cardiac CT image processing scheme. **167**

Figure 7.3: Low-dose vessel-specific perfusion measurement analysis with the comprehensive cardiac CT technique. **168**

Figure 7.4: Low-dose vessel-specific coronary flow reserve versus stress perfusion in the absence and presence of increasing severity LAD stenosis in a single swine. **169**

Figure 7.5: Application of the of the low-dose comprehensive cardiac CT technique. **170**

Figure 8.1: Standard, diluted, and reference CT angiography bolus injection protocol comparison. **188**

Figure 8.2: Image processing scheme. **189**

Figure 8.3: Standard, combined, and reference CT angiography acquisition protocol comparison. **190**

Figure 8.4: Test bolus and reference CT angiography bolus time-to-peak enhancement comparison. **191**

Figure 8.5: Standard, combined, and reference CT angiography peak enhancement and CNR comparison.. **192**

Figure 8.6: Standard, combined, and reference CT angiography peak enhancement regression analysis.. **193**

Figure 8.7: Standard, combined, and reference CT angiography CNR regression analysis. **194**

Figure 9.1: Contrast bolus injection protocol and bolus dispersion theory. **214**

Figure 9.2: Automatic gamma variate fitting of the aortic enhancement in two swine. **215**

Figure 9.3: Prospective Acquisition Protocol Simulation **216**

Figure 9.4: Gamma fit time-to-peak data as compared to 0.5* injection time data. **217**

Figure 9.5: Pair-wise gamma fit comparison under rest and stress conditions. **218**

Figure 9.6: Prospective V1 enhancement as a function of left atrial trigger threshold. **219**

Figure 9.7: Prospective simulation V2 peak acquisition using an optimal delay time as compared to the ideal peak. **220**

Figure 9.8: FPA perfusion data using the simulated prospective acquisition protocol as compared to the previously validated reference standard retrospective FPA perfusion data. **221**

Figure 10.1: Preemptive diluted test bolus and low-dose comprehensive cardiac CT technique protocol. **235**

Figure 10.2: Low-dose comprehensive cardiac CT technique protocol that employs an optimal injection-time-based acquisition. **236**

Figure 10.3: Co-registered stress perfusion and CT angiography with the low-dose comprehensive cardiac CT technique in a 100 kg patient with coronary artery disease. **237**

Figure 10.4: Vessel-specific CFR versus stress perfusion measurement with the low-dose comprehensive cardiac CT technique in a 100 kg patient with coronary artery disease. **238**

LIST OF TABLES

PAGE

Table 2.1: Summary of the linear regression analysis between different CT perfusion methods and known perfusion measurements. **28**

Table 3.1: Per-animal results for LCA and RCA territories in the left ventricle, right ventricle, and whole heart myocardium. **56**

Table 3.2: Mass correspondence of MCP and reference standard coronary perfusion territories in the left ventricle, right ventricle, and whole heart myocardium. **57**

Table 3.3: Linear regression analysis of MCP and reference standard perfusion territories in the left ventricle, right ventricle, and whole heart myocardium. **58**

Table 3.4: Spatial correspondence of MCP and reference standard coronary territories in the left ventricle, right ventricle, and whole heart myocardium. **59**

Table 3.5: Absolute and relative coronary perfusion distributions for LAD_{MCP}, LCx_{MCP} and RCA_{MCP} in the left ventricle myocardium. **60**

Table 4.1: Animal parameters. **83**

Table 4.2: Comparison of dynamic CT perfusion to quantiative [^{15}O] H_2O PET. **84**

Table 5.1: FPA and MSM perfusion compared to reference standard microsphere perfusion. **107**

Table 5.2: FPA- and MSM-based detection of physiologically significant LAD stenosis. **108**

Table 5.3: FPA, MSM, and microsphere perfusion in the LAD compared to dynamic PET. **109**

Table 6.1: Rest perfusion measurement at reduced tube current and reference standard rest perfusion measurement mean comparison with corresponding dose metrics. **134**

Table 6.2: Low-dose prospective stress perfusion measurement and reference standard retrospective stress perfusion measurement mean comparison with corresponding low-dose prospective stress perfusion dose metrics. **135**

Table 6.3: Low-dose prospective stress perfusion measurement and reference standard retrospective stress perfusion measurement accuracy and precision analysis. **136**

Table 6.4: Low-dose prospective stress perfusion distribution in the left ventricle of a single animal in the absence and presence of physiologically significant LAD stenosis. **137**

Table 7.1: Low-dose perfusion and CFR measurement and reference standard perfusion and CFR measurement mean comparison. **163**

Table 7.2: Low-dose comprehensive cardiac CT dose metrics. **164**

Table 7.3: Low-dose perfusion measurement and reference standard perfusion measurement accuracy and precision analysis. **165**

Table 8.1: Standard, combined, and reference retrospective CT angiogram peak enhancement and CNR mean comparison. **186**

Table 8.2: Standard, combined, and reference CT angiogram peak enhancement and CNR regression analysis. **187**

Table 9.1: Rest and stress comparison. **212**

Table 9.2: Prospective peak acquisition simulation as compared to ideal peak acquisition. **213**

Table 10.1: Low-dose comprehensive cardiac CT stress perfusion distribution in the left ventricle of a 100 kg patient. **233**

Table 10.2: Low-dose comprehensive cardiac CT CFR distribution in the left ventricle of a 100 kg patient. **234**

ACKNOWLEDGMENTS

To my Mentor, Dr. Sabee Molloi. Thank you for making me into the scientist that I am today. With your guidance and support, you have pushed me to achieve more than I ever thought possible, and for that I truly grateful.

To my Committee Members, Dr. Bruce Tromberg and Dr. Shaista Malik. Thank you for your constant commitment to my training.

To the Medical Scientist Training Program. Thank you for providing me with such an incredible opportunity to become a physician-scientist.

To the support of the AHA (Award Number: 17CPRE33650059), the CARE Program (NIH NHLBI Award Number: T32-HL116270), and the MSTP (NIH Award Number: T32-GM008620). Thank you for making my training and my research possible.

To Shant. Thank you for being an amazing colleague, teammate, and friend. This project would not have been possible without you.

To my Family. Thank you for your unwavering love, support, encouragement, and belief in me. Thank you for never allowing me to say that I "can't" do something, for never letting me quit on myself or my goals, and for teaching me to be accountable and responsible for my own actions. Thank you for always supporting my creativity and my passions, and for fostering in me a constant desire to learn and to grow. I truly could not have done any of this without you.

To my Friends. Thank you for never giving up on me. I am so appreciative and so grateful to have all of you in my life.

Finally, to Lauren. Thank you for supporting me, for believing in me, and for loving me. I would not have made it through this without you. I truly cannot wait to begin our next chapter together, and I am so excited for what our future holds. I love you to the moon.

CURRICULUM VITAE

Logan Charles Hubbard
Medical Scientist Training Program
Department of Biomedical Engineering
University of California, Irvine

Education

University of California, Irvine
Ph.D. – Biomedical Engineering; Emphasis of Medical Physics (09/2018)
M.D. – School of Medicine (06/2020)
Case Western Reserve University
B.S. – Biomedical Engineering; Emphasis on Biomedical Imaging (05/2012)

Fellowships

AHA Award Number: 17CPRE33650059
AWRP Winter 2017 Clinical Health Profession Student Training Program
Title of Project: Anatomical and Functional Assessment of Coronary Artery Disease Using Whole-Heart Computed Tomography
Start Date: 07/01/2017, End Date: 06/30/2019
CARE Award Number: T32-HL116270
Edwards Lifesciences Center for Advanced Cardiovascular Technology T32 Grant
Start Date: 06/01/2015, End Date: 05/30/2017
Ruth L. Kirschstein National Research Service Award Number: T32-GM008620
Medical Scientist Training Program, University of California - Irvine
Start Date: 07/01/2012, End Date: 06/30/2020

Honors & Awards

2018 Medical Arts Exhibit Award Winner
2017 1 of 2 Featured in AHA's Western States Affiliate Research Insights Newsletter
2013 Letter of Commendation, Medical Immunology, UCI School of Medicine
2013 Letter of Commendation, Human Histology, UCI School of Medicine
2012 Gheorge and Claudia Mateescu Research in Imaging Award Winner
2012 CWRU Magna cum laude, CWRU

Other Experience and Professional Memberships

2017 UC Irvine Medical Scientist Training Program Admission Committee Member
2016 American Heart Association Member

Positions and Employment:

2012 MD/PhD Student, Medical Scientist Training Program, UCI, CA
2010 - 2012 Research Assistant, Biomedical Imaging, CWRU, OH
2011 - 2012 Biomedical Design Director, Biomedical Engineering, CWRU, OH
2010 - 2012 Research Assistant, Pathology, CWRU, OH
2009 - 2011 Biomedical Design Engineer, Biomedical Engineering, CWRU, OH
2008 - 2010 Research Assistant, Nuclear Medicine, CWRU, OH

Manuscripts in Preparation

- **Hubbard L,** Malkasian S, Zhao Y, Abbona P, Molloi S. A simple solution to patient-specific computed tomography angiography optimization: preliminary investigation in a swine animal model. ***In Preparation. 2018***
- **Hubbard L,** Malkasian S, Zhao Y, Abbona P, Molloi S. Comprehensive cardiac CT: preliminary investigation in a swine animal model. ***In Preparation. 2018***
- **Hubbard L**, Malkasian S, Zhao Y, Abbona P, Molloi S. Submillisievert stress myocardial perfusion measurement using first-pass analysis dynamic computed tomography: preliminary investigation in a swine animal model. ***In Preparation. 2018***

Publications

- **Hubbard L,** Malkasian S, Zhao Y, Abbona P, Molloi S. Contrast-to-noise ratio optimization in coronary computed tomography angiography: validation in a swine model. ***In Review***. **2018**
- Zhao Y, **Hubbard L**, Malkasian S, Abbona P, Molloi S. Volumetric Dynamic CT Perfusion of the Lung: Validation in a Swine Model. ***In Review. 2018***
- Malkasian S**, Hubbard L**, Dertli B, Kwon J, Molloi S. Quantification of vessel-specific coronary perfusion territories using minimum-cost path assignment and computed tomography angiography: validation in a swine model. ***In Review.*****2018**
- Molloi S, Johnson T, Lipinski J, Ding H, **Hubbard L**. Accurate quantification of arterial cross-sectional area using coronary CT angiography: A phantom study. ***In Review.*** **2018**
- **Hubbard L**, Lipinski J, Ziemer B, Malkasian S, Sahdegi B, Javan H, Dertli B, Groves EM, Molloi S. Comprehensive assessment of coronary artery disease using first-pass analysis dynamic computed tomography perfusion. *Radiology*. 2017; 286(1)
- **Hubbard L**, Ziemer B, Lipinski J, Sahdegi B, Javan H, Groves EM, Malkasian S, Molloi S. Functional assessment of coronary artery disease using whole-heart dynamic computed tomography perfusion. *Circ Cardiovasc Imaging.* 2016; 9(12).
- Ziemer B, **Hubbard L**, Lipinski J, Molloi S. Dynamic CT perfusion measurement in a cardiac perfusion phantom. *Int. J. Cardiovasc Imaging*. 2015; 31(7).

- Lee K*, **Hubbard L***, Hern S, Yildiz I, Gratzl M, Steinmetz N. Shape matters: The diffusion rates of TMV rods and CPMV icosohedrons in a spheroid tumor model of extracellular matrix are distinct. *Biomaterials Science.* 2013; 1(6): 581-588.

Abstracts & Presentations

- **Hubbard L**, et al. Comprehensive cardiac CT: Providing angiography and perfusion with a single exam. Oral presentation. *Radiology Grand Rounds.* March 20, 2018, University of California – San Diego
- **Hubbard L**, et al. Comprehensive assessment of coronary artery disease using first-pass analysis dynamic computed tomography angiography and perfusion. Oral presentation. *Medical Scientist Training Program Symposium.* January 19, 2018, University of California – Irvine.
- **Hubbard L,** et al. Comprehensive assessment of coronary artery disease using first-pass analysis dynamic computed tomography angiography and perfusion. Oral presentation. *Biomedical Engineering Seminar Series*. November 11, 2017; University of California – Irvine.
- **Hubbard L**, Malkasian S, Dertli B, Kwon J, Abbona P, Molloi S. A low-dose prospective first-pass analysis dynamic CT perfusion technique for accurate myocardial perfusion measurement. Oral presentation. *Med Phys*. July 2017; 44(6):3021
- **Hubbard L**, Malkasian S, Dertli B, Kwon J, Abbona P, Molloi S. The effect of dose reduction on the accuracy of first-pass analysis dynamic CT myocardial perfusion measurement. Oral presentation. *Med Phys*. July 2017; 44(6):3021
- Malkasian S, ***Hubbard L**, Dertli B, Kwon J, Abbona P, Molloi S. TH-CD-601-2: Determining patient-specific myocardial perfusion territories using computed tomography coronary angiography. Oral presentation. *Med Phys.* July 2017 ***Presentation given by Hubbard L**
- Zhao Y, ***Hubbard L**, Malkasian S, Abbona P, Molloi S. Pulmonary blood flow measurement using low-dose computed tomography. Oral presentation. *Med Phys*. July 2017; 44(6):3300 ***Presentation given by Hubbard L**
- Molloi S, **Hubbard L**, Malkasian S, Abbona P. Quantification of myocardial blood flow using low-dose computed tomography. Oral presentation. *Journal of Cardiovascular Computed Tomography*. June 2017 11(4):S31.
- Molloi S, Malkasian S, **Hubbard L**, Abbona P. Quantification of regional myocardial mass at risk using computed tomography angiography. Poster presentation. *Journal of Cardiovascular Computed Tomography*. June 2017 11(4):S14.
- **Hubbard L,** et al. Comprehensive assessment of coronary artery disease using first-pass analysis dynamic computed tomography. Oral presentation. *Cardiovascular Applied Research and Entrepreneurship Retreat.* November 8, 2016; University of California – Irvine.
- **Hubbard L,** et al. Comprehensive assessment of coronary artery disease using whole-heart computed tomography. Oral presentation. *UC Irvine Medical Scientist Training Program Research Retreat*; October 29, 2016; Lake Arrowhead, CA.

- **Hubbard L**, Ziemer B, Lipinski J, Malkasian S, Sahdegi B, Javan H, Dertli B, Groves EM, Molloi S. Abstract TH-AB-207A-11: Anatomical and functional assessment of coronary artery disease using low-dose whole-organ dynamic computed tomography. Oral presentation. *Med Phys.* July 2016; 43(6): 3862.
- **Hubbard L**, Ziemer B, Malkasian S, Lipinski J, Sahdegi B, Javan H, Dertli B, Groves EM, Molloi S. Abstract TH-CD-206-07: Determination of patient-specific myocardial mass at risk using computed tomography angiography. Oral presentation. *Med Phys.* July 2016; 43(6): 3884.
- **Hubbard L**, et. Noninvasive assessment of cardiovascular disease with first-pass analysis dynamic computed tomography perfusion measurement. Oral presentation. *Edwards Lifesciences Center for Advanced Cardiovascular Technology Seminar Series*; March 8, 2016; University of California – Irvine.
- **Hubbard L**, Ziemer B, Lipinski J, Sahdegi B, Javan H, Groves EM, Molloi S. Abstract 19530: Functional assessment of coronary artery disease using low-dose dynamic computed tomography perfusion. Poster presentation. *Circulation.* November 2015; 132:A19530
- **Hubbard L,** et al. Functional assessment of coronary artery disease using low-dose dynamic computed tomography perfusion. Oral presentation. *UC Irvine Medical Scientist Training Program Research Retreat*; November 1, 2015; Lake Arrowhead, CA.
- **Hubbard L**, Ziemer B, Sahdegi B, Javan H, Lipinski J, Groves E, Molloi S. TU-G-204-03: Dynamic CT myocardial perfusion measurement using first pass analysis and maximum slope models. Oral presentation. *Med Phys.* July 2015; 42(6): 3633.
- Ziemer B, **Hubbard L**, Groves EM, Sadeghi B, Javan H, Lipinski J, Molloi S. TU-G-204-01: BEST IN PHYSICS (IMAGING): Dynamic CT myocardial Perfusion measurement and its comparison to fractional flow reserve. Oral presentation. *Med Phys*. July 2015; 42(6):3633 DOI 10.1118/1.4925765.
- Molloi S, Ziemer B, **Hubbard L**, Lipinski J, Sadeghi B, Javan H, Groves EM. SP171.4 - Myocardial perfusion imaging by low-dose CT. Oral presentation. IUPESM 2015 World Congress on Medical Physics and Biomedical Engineering. June 2015. Toronto, Canada
- **Hubbard L,** et al. CT myocardial perfusion. Oral presentation. *Edwards Lifesciences Center for Advanced Cardiovascular Technology Seminar Series*; December 9, 2014; University of California – Irvine.
- Ziemer B, **Hubbard L**, Lipinski J, Molloi S. TU-A-12A-09: Absolute blood flow measurement in a cardiac phantom using low dose CT. Oral presentation. *Med Phys.* July 2014; 41(6): 451-452. DOI 10.1118/1.4889255.
- **Hubbard L,** et al. Wide-volume contrast enhanced CT of a dynamic cardiovascular imaging phantom to measure volumetric flow. Poster presentation. *UC Irvine Medical Scientist Training Program Research Retreat*; October 5, 2013; Lake Arrowhead, CA.
- **Hubbard L,** et al. The diffusion rates of TMV rods and CPMV icosohedrons in a spheroid tumor model of extracellular matrix are distinct. Poster presentation. *UC Irvine Medical Scientist Training Program Research Retreat*; October 6, 2012; Lake Arrowhead, CA.

ABSTRACT OF THE DISSERTATION

Comprehensive Cardiac Computed Tomography:

Translating Medical Physics Into Medical Practice

By

Logan Charles Hubbard

Doctor of Philosophy in Biomedical Engineering

University of California, Irvine, 2018

Professor Sabee Molloi, Chair

Coronary artery disease (CAD) is the leading cause of morbidity and mortality worldwide. As a risk factor, CAD and its resultant ischemic cardiomyopathy are strongly predicative of future cardiac events. While coronary computed tomography (CT) angiography is a powerful tool for assessing CAD risk, it is fundamentally limited in that it can only assess the morphological severity of segmental CAD, but cannot define the physiological severity of concurrent mutli-vessel, diffuse, and microvascular disease. Hence, guidelines recommend additional physiological assessment of CAD, in conjunction with CT angiography, for more objective indication of patient risk. The primary modalities used for physiological assessment are single-photon emission computed tomography (SPECT), stress echocardiography, cardiac magnetic resonance (CMR), static positron emission tomography (PET), and static CT. However, such modalities only provide metrics of relative perfusion; hence, they still cannot appreciate

the true physiological severity of multiform CAD. Fortunately, absolute perfusion measurement with dynamic CT can overcome these limitations, where the spatial distribution of absolute rest and stress perfusion in mL/min/g combined with physiological cutoff thresholds can be used to reliably stratify patient risk and properly guide intervention. Nevertheless, current dynamic CT perfusion techniques are known to be quantitatively inaccurate and deliver unacceptably high effective radiation doses per imaging exam, precluding their widespread clinical use. As such, there is a major unmet clinical need for an accurate, low-dose CT technique for combined morphological and physiological assessment of multiform CAD.

This dissertation research addresses that unmet clinical need through the development, validation, and preliminary clinical translation of an accurate, low-dose, comprehensive cardiac CT technique based on first-pass analysis (FPA). The comprehensive technique can accurately assess vessel-specific stress and rest perfusion, while simultaneously providing cardiac functional analysis (CFA), CT angiography, and coronary flow reserve (CFR), respectively. Thus, morphological and physiological assessment of CAD is feasible using a single low-dose exam, making comprehensive CT-based assessment of multiform CAD more accurate, accessible, and impactful to patients in need.

CHAPTER 1: CORONARY ARTERY DISEASE AND THE CURRENT STATE OF CARDIAC COMPUTED TOMOGRAPHY

Coronary Artery Disease (CAD)

Coronary artery disease (CAD) is the leading cause of morbidity and mortality worldwide, with the extent of CAD and its resultant ischemic cardiomyopathy strongly predictive of future cardiac events. There are three main coronary arteries that are most commonly affected - the left anterior descending (LAD), the left circumflex (LCx), and the right coronary artery (RCA) - with each supplying their own unique distribution of myocardial tissue. Moreover, there are three main types of coronary artery disease that affect the aforementioned arteries and their downstream architectures - segmental disease, diffuse disease, and microvascular disease - where segmental disease affects the conducting epicardial vessels, diffuse disease affects the resistive arterioles, and microvascular disease affects the microcirculation, as shown in **Figure 1.1**. Interestingly, these CAD etiologies can exist in isolation or in any combination; hence, a spectrum of disease presentations are possible. As such, accurate resolution of each CAD etiology is absolutely necessary to reliably stratify patient risk and properly guide downstream medical or surgical intervention[1].

Morphological Assessment of CAD

Noninvasive coronary computed tomography (CT) angiography is a powerful diagnostic tool for assessing CAD severity[2-4]. However, CT angiography alone can only assess the morphological severity of segmental stenosis, i.e., it cannot resolve the physiological

severity of concurrent mutli-vessel, diffuse, and microvascular disease. As a result, there is often poor correlation between lesion severity and downstream myocardial ischemia and cardiomyopathy, and percutaneous coronary intervention (PCI) and optimal medical therapy outcomes are often the same[5]. Furthermore, as CT angiographic severity is based solely on CT angiographic morphology, vessel collateralization, coronary calcification, and imaging artifacts also confound diagnostic results[3, 4]. Moreover, in instances where CAD is detected, subjective visual grading of lesions has also been shown to result in high intra- and inter-observer variability[6, 7], especially for intermediate severity stenoses (approximately 30-70% luminal narrowing)[8-10]. Hence, guidelines[11-14] recommend additional physiological assessment of CAD, in conjunction with CT angiography, to more reliably stratify patient risk and more properly guide downstream intervention[4, 9].

Physiological Assessment of CAD

In general, physiological assessment of CAD is performed with fractional flow reserve (FFR), stress echocardiography, cardiac magnetic resonance (CMR), single-photon emission computed tomography (SPECT), static positron emission tomography (PET), or static CT [15] [16] [17] [15, 16, 18-21] and have been shown to improve PCI outcomes when used in conjunction with CT angiography[23]. Nevertheless, up to a 40% discordance exists between FFR and perfusion[22], while stress echocardiography, CMR, SPECT, static PET, and static CT only provide metrics of relative perfusion[15, 16, 18-21]. Hence, they still cannot accurately resolve the physiological severity of multi-vessel, diffuse, and microvascular disease[20, 21]. Fortunately, absolute stress perfusion measurement in

mL/min/g or coronary flow reserve (CFR) measurement, i.e., the ratio of absolute stress perfusion and absolute rest perfusion, can overcome these limitations, where the spatial distribution of stress perfusion or CFR measurement combined with physiologic cutoff thresholds[23, 24] may be used to more reliably stratify patient risk and more properly guide downstream intervention.

Absolute stress perfusion and CFR are most commonly measured with dynamic PET[14, 25, 26]. However, limited radiotracer access and high cost preclude the routine clinical use of dynamic PET[27]. Fortunately, the latest research suggests that absolute stress perfusion and CFR measurement are also feasible with dynamic CT[13, 28-32], which is much more clinically convenient and cost-effective[33], and can be used in conjunction with CT angiography for improved comprehensive work-up of multiform CAD[28, 34].

Dynamic CT

Many dynamic CT techniques have been developed[29, 31, 32, 35, 36], with recent reports confirming the value of dynamic CT perfusion and CFR in physiological assessment of CAD[31, 32, 35]. In general, these techniques monitor myocardial uptake of contrast material, i.e., changes in myocardial enhancement, over time to derive absolute perfusion data. Unfortunately, despite positive correlation with single-photon emission computed tomography (SPECT)[32], invasive coronary fractional flow reserve (FFR)[37], and quantitative microsphere perfusion measurements[31], dynamic CT techniques, such as the maximum slope model (MSM), are quantitatively inaccurate and systematically underestimate myocardial perfusion17-19[38]. Specifically, such techniques operate under

the mathematical assumption that contrast material does not leave the myocardial tissue volume-of-interest (VOI) over the measurement time. However, given the limited cranio-caudal coverage of most CT scanners, such techniques rely on small tissue volumes-of-interest (VOI) to derive perfusion. Thus, when considering the rapid transit time of contrast material throughout the myocardium[39], contrast material loss from those VOIs over the measurement duration is unavoidable, resulting in underestimation of perfusion(17-19). Furthermore, small VOI's measurements also suffer from poor signal-to-noise ratio (SNR); hence, dynamic CT techniques acquire data over many cardiac cycles to improve measurement reliability, leading to estimated effective radiation doses of up to 10 mSv per exam[37, 40-42]. While some radiation dose reduction is possible through tube voltage (kVp) and tube current (mA or mAs) optimization, as well as through iterative reconstruction techniques[43, 44], the fundamental limitations of measurement inaccuracy and large radiation dose have hampered the widespread clinical utility and overall impact of dynamic CT[18, 37, 42]. It is also important to note that dynamic CT techniques cannot simultaneously acquire CT angiographic data; thus, additional contrast dose and radiation dose are necessary for separate acquisition of a CT angiogram. Hence, there is an absolute need for an accurate, low-dose CT technique for combined morphological and physiological assessment of CAD, i.e., there is an absolute need for comprehensive cardiac CT.

Comprehensive Cardiac CT

Specifically, whole-heart 320-slice CT scanner technology with 16 centimeters of cranio-caudal coverage and a 350 ms gantry rotation time allows the entire heart to be imaged

within a single cardiac cycle[44]. Such increases in coverage and rotation speed enable simultaneous first-pass acquisition of dynamic CT perfusion data and CT angiography data using only two whole-heart volume scans and a single contrast injection, i.e., the radiation and contrast dose associated with dynamic CT perfusion and CT angiography acquisition can be dramatically reduced. Moreover, the accuracy of absolute perfusion measurement can be significantly improved[45]. As with the aforementioned dynamic CT techniques, the comprehensive cardiac CT technique still assumes that contrast material does not leave the myocardial tissue VOI over the measurement time. However, by dramatically increasing the size of the tissue VOI to encompass that of the entire myocardium, while simultaneously making measurements faster than the myocardial transit time, the comprehensive cardiac CT technique improves dynamic CT perfusion measurement accuracy by eliminating the problem of contrast material loss from the measurement volume over the measurement time. Furthermore, given the simultaneous addition of coregistered CT angiography data, automatic algorithmic delineation of vessel-specific perfusion territories[46, 47] enables further dynamic CT perfusion measurement in the LAD, LCx, and RCA. Thus, the comprehensive cardiac CT technique is fundamentally different from current dynamic CT perfusion and CT angiography techniques in its approach to CAD risk stratification. By integrating dynamic CT perfusion and CT angiography into a single low-dose exam, comprehensive morphological and physiological assessment of multi-form CAD can be used to more reliably stratify patient risk and more properly guide downstream intervention[4, 9].

The research outlined in this dissertation details the development and validation of the new comprehensive cardiac CT technique. More specifically, chapters 2 – 5 retrospectively validate perfusion measurement accuracy, while chapters 6 and 7 retrospectively validate effective dose reduction. Chapters 8 and 9 go on to validate prospective acquisition timing, and chapter 10 concludes with preliminary implementation of the comprehensive cardiac CT technique in one human subject, as well as future directions. In combination, the body of this work improves upon the field of cardiac CT and has the potential to make CT-based assessment of multiform CAD more accessible and impactful to patients in need.

Figures

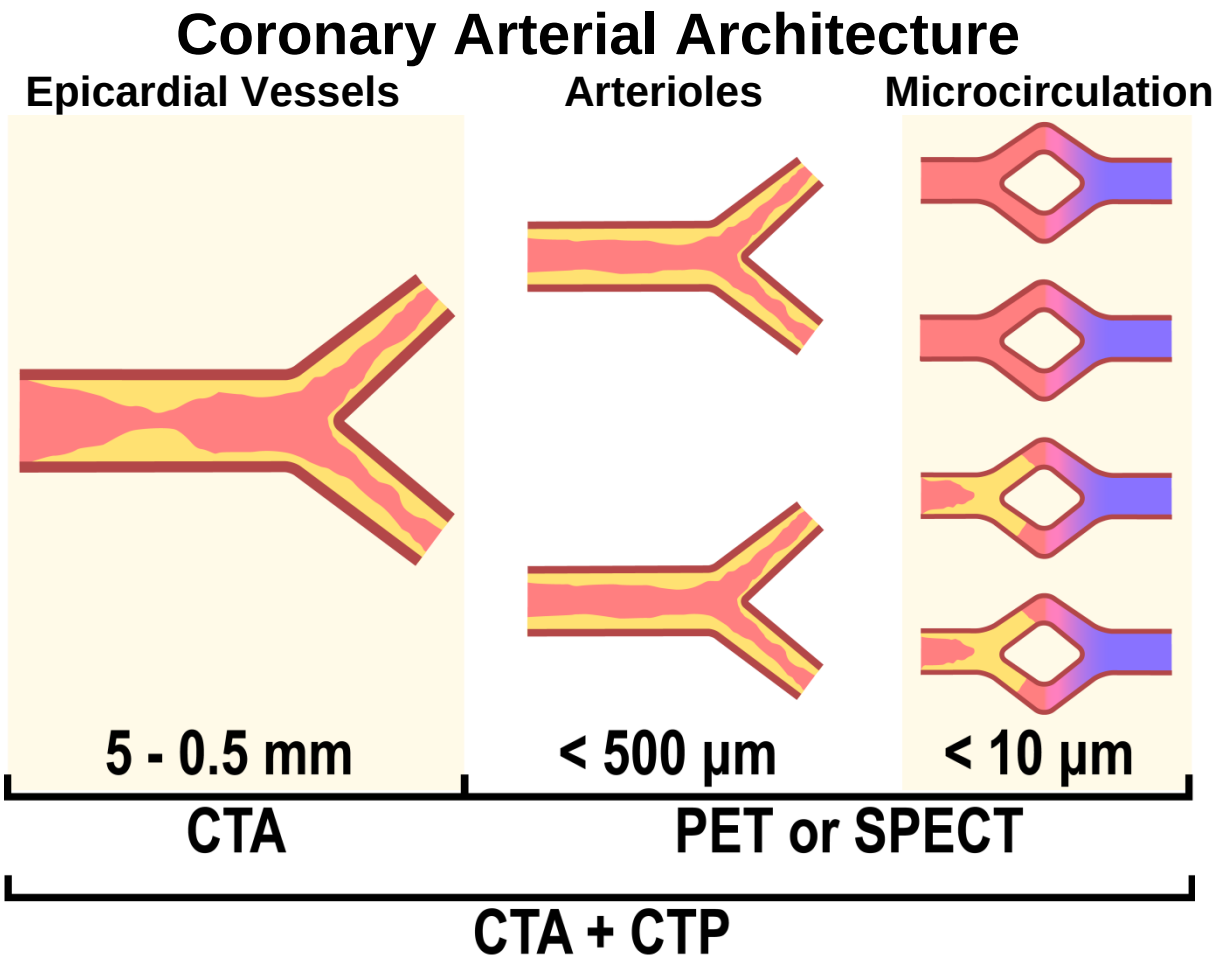

Figure 1.1. Graphical display of coronary arterial architecture, showing three different types of coronary artery disease. More specifically, segmental disease affects the conducting epicardial vessels, diffuse disease affects the resistive arterioles, while microvascular disease affects the microcirculation. CT angiography can resolve segmental disease, while SPECT and PET can resolve diffuse and microvascular disease, but no single modality can resolve all three disease etiologies. Hence, combining CT angiography and dynamic CT perfusion into a single exam enables simultaneous resolution of segmental, diffuse, and microvascular coronary artery disease at a low contrast and radiation dose.

CHAPTER 2: ACCURACY OF ABSOLUTE PERFUSION MEASUREMENT AS COMPARED TO ULTRASONIC PERFUSION MEASUREMENT IN A CARDIAC PHANTOM

Abstract

Widespread clinical implementation of dynamic CT myocardial perfusion has been hampered by its limited accuracy and high radiation dose. The purpose of this study was to evaluate the accuracy and radiation dose reduction of a dynamic CT myocardial perfusion technique based on first pass analysis (FPA). To test the FPA technique, a pulsatile pump was used to generate known perfusion rates in a range of 0.96-2.49 mL/min/g. All the known perfusion rates were determined using an ultrasonic flow probe and the known mass of the perfusion volume. FPA and maximum slope model (MSM) perfusion rates were measured using volume scans acquired from a 320-slice CT scanner, and then compared to the known perfusion rates. The measured perfusion using FPA (P_{FPA}), with two volume scans, and the maximum slope model (P_{MSM}) were related to known perfusion (P_K) by $P_{FPA} = 0.91P_K + 0.06$ ($r = 0.98$) and $P_{MSM} = 0.25P_K - 0.02$ ($r = 0.96$), respectively. The standard error of estimate (SEE) for the FPA technique, using two volume scans, and the MSM was 0.14 mL/min/g and 0.30 mL/min/g, respectively. The estimated radiation dose required for the FPA technique with two volume scans and the MSM was, 2.6 mSv and 11.7-17.5 mSv, respectively. Therefore, the FPA technique can yield accurate perfusion measurements using as few as two volume scans, corresponding to approximately a factor of 4 reduction in radiation dose as compared with the currently available MSM. In conclusion, the results of the

study indicate that the FPA technique can make accurate dynamic CT perfusion measurements over a range of clinically relevant perfusion rates, while substantially reducing radiation dose, as compared to currently available dynamic CT perfusion techniques.

Introduction

Computed tomography (CT) angiography is a well-established, noninvasive method used to detect coronary artery stenoses. However, CT angiography is limited in its ability to determine whether an intermediate lesion (35-75% diameter stenoses) is the cause of ischemia[9, 48]. Although multimodal techniques such as PET/CT and SPECT/CT can provide functional information, these techniques are limited by the cost and availability of radiotracers, preventing their widespread clinical implementation. Therefore, it would be clinically useful to combine the anatomic information of CT angiography with the physiologic information of CT myocardial perfusion into a single, low-dose procedure to better stratify a patient's risk.

Several different techniques of dynamic CT perfusion have been reported[35, 36, 49-51], most of which are based on some variation of the Mullani-Gould method[52]. These techniques, such as the maximum slope model, monitor the mean enhancement of a small volume of myocardium over time. The resulting contrast pass curve is then used to measure myocardial perfusion using fitting parameters from different models. While such techniques have shown positive correlation with coronary fractional flow reserve[51] and microsphere measurements[29], overall they tend to underestimate perfusion[38]. This

problem of underestimation stems fundamentally from the rapid transit time of contrast through the myocardium. Specifically, these techniques operate under the assumption that no contrast leaves the myocardial tissue volume of interest over the time of measurement. However, these techniques generally make measurements using small volumes of interest (VOI), over many cardiac cycles; therefore, they are inherently subject to contrast loss from those VOIs, especially at hyperemia. In addition, such techniques require multiple volume scans over many cardiac cycles to generate perfusion measurements, leading to cumulative radiation doses of up to 30 mSv for combined rest and stress scans[37]. Therefore, the issues of measurement accuracy and radiation dose need to be addressed before dynamic CT perfusion can be implemented as a clinical standard.

To resolve such limitations, much larger VOIs, defined as an entire perfusion bed of an artery or major arterial branch, distal to a stenosis [47, 53], could be used to make vessel-specific perfusion measurements. Further, measurement in large VOIs would improve the signal-to-noise-ratio (SNR). Unfortunately, CT technology has been limited by the total myocardial volume coverage per cardiac cycle. Hence, dynamic CT perfusion techniques have been limited in the accurate quantification of myocardial perfusion[54, 55]. However, with recent advances in CT technology, the coverage has been extended, allowing the entire heart to be imaged within a fraction of a second. Such advances have enabled implementation of the first pass analysis (FPA) technique for dynamic CT myocardial perfusion measurement. By increasing the VOI size, SNR is improved, and the problem of contrast loss from VOIs over the time of measurement is eliminated.

Hence, the FPA technique is able to measure the total volume of contrast material that has entered a given perfusion bed between two volume scans. As a result, the complicated problems of myocardial contrast dynamics and blood flow quantification can be distilled down into the much simpler concept of conservation of mass.

In this study, the ability of the FPA technique to accurately measure myocardial perfusion over a range of known, clinically relevant perfusion rates were evaluated in a cardiac phantom using a 320-slice CT scanner. The possibility of radiation dose reduction was also investigated by assessing the accuracy of FPA perfusion measurements using a limited number of volume scans.

Materials and Methods

Perfusion Theory

The proposed FPA perfusion measurement technique is based on a first pass distribution model[56-59] and the principle of conservation of mass. Specifically, any myocardial perfusion volume supplied by a coronary artery may be modeled as a compartment with a unique entrance and exit vessel, as seen in **Figure 2.1**. Given this model, no assumptions about the compartment shape, internal structure, vascular permeability, or nature of the exit conduits need to be made. In order to measure flow (Q) through the compartment, it is necessary to determine the volume (ΔV) of blood entering the compartment within a certain time interval (Δt), as well as the input blood iodine concentration (C_{in}) using (see **Appendix 2.1 and Appendix 2.2**):

$$\boldsymbol{Q = \frac{\Delta V}{(\Delta t)(C_{in})}} \qquad \textbf{(1)}$$

It is possible to calculate $\frac{\Delta V}{\Delta t}$ by determining the change in the integrated Hounsfield units (HU) of all voxels within the compartment per unit time. Additionally, C_{in} may be estimated from the integrated HU per unit volume (HU/cm^3) of a calibration VOI close to the compartment entrance. Thus, using the proposed FPA technique, the flow through any large myocardial tissue compartment, or perfusion volume of interest, can be calculated as the average slope of the integrated HU in the VOI per unit time, divided by the average input concentration from the calibration volume, assuming no contrast agent has exited the myocardial VOI before measurements are completed. Further, because the mass of the myocardial VOI is known, the perfusion rate can be derived directly from the calculated flow rate. As a result, many intra-compartment parameters, such as capillary permeability and extraction, do not need to be considered when determining perfusion. Thus, such a technique eliminates the need to acquire multiple volume scans over many cardiac cycles and has the potential to substantially reduce the radiation dose of dynamic CT perfusion.

Cardiac Perfusion Phantom

The cardiac perfusion phantom was designed to model the pulsatile mixing dynamics of the heart with a femoral contrast injection site[60]. A photograph and a schematic of the cardiac perfusion phantom are shown in **Figure 2.2**. Proximally, the components of the phantom served to generate a realistic stroke volume and cardiac output and ensured sufficient mixing prior to the myocardial compartment. Distally, a myocardial compartment with a coronary vessel input was constructed from a 10 cm diameter polymethyl methacrylate (PMMA) tube filled with small diameter plastic beads of

different sizes. The beads simulated myocardial tissue packing and reduced the interstitial fluid distribution volume within the myocardial compartment, such that the measured density of the simulated myocardial tissue was 0.97 g/mL. Another PMMA chamber was also placed in the center of the myocardial compartment and was filled with contrast media with an iodine concentration of 20 mg/mL to simulate a contrast-filled ventricle. Further, the total volume of the simulated myocardial tissue was designed to approximate the total tissue volume of the myocardium. Lastly, the entire myocardial compartment was imaged inside an average adult-sized anthropomorphic thorax to generate realistic radiation dose, x-ray attenuation, and image noise properties (Cardio; QRM, Mohrendorf, Germany) [61]. Overall, the design of the myocardial compartment simulates a first pass distribution model. An axial cross section of the myocardial compartment before and after contrast injection is shown in **Figure 2.3**.

Water was circulated through the phantom using a pulsatile pump (Harvard Apparatus, Holliston Mass). The stroke volume and cardiac output were held constant at 100 mL per stroke and 5 L/min total through the system. Separate input and output reservoirs were used to eliminate recirculation of contrast material. An ultrasonic flow probe (Transonic Systems Inc., Ithaca NY) was used to determine instantaneous flow through the myocardial compartment, and all known flow rates were continuously recorded (MP150, Biopac Systems Inc., Goleta CA). The known flow rates were converted to perfusion using the known mass of the perfusion volume. The known perfusion was used as the reference standard for comparison to the measured CT perfusion. An example of the pulsatile flow profile through the phantom can be found in **Figure 2.4** and is characteristic of *in vivo* systolic and diastolic flow properties. In order to modulate

the perfusion rate through the myocardial compartment, variable resistance was applied downstream of the perfusion compartment and at the termination of the distal aorta (see **Figure 2.2**). A range of known perfusion rates between 0.96-2.49 mL/min/g were evaluated. The minimum and maximum perfusion rates are approximately representative of perfusion in resting and stress conditions and correspond to a coronary flow reserve (CFR) of 2.6. The range of perfusion rates evaluated is also approximately representative of perfusion deficits caused by stenoses of increasing severity in stress conditions.

CT Imaging Protocol

CT imaging was performed using a 320-slice Aquilion One CT scanner (Toshiba America Medical Systems, Tustin CA). An ECG emulator was used to generate a heart rate that matched the frequency of the pulsatile pump, allowing the cardiac phantom to be imaged using a prospective, ECG-gated cardiac perfusion protocol. The CT imaging parameters were: 320 x 0.5 mm detector collimation, 100 kVp tube voltage, 200 mA tube current, and 0.35 s rotation time. For each perfusion measurement approximately 20 volume scans were acquired following a 15 mL bolus injection of contrast material (Isovue 370, Bracco Diagnostics, Princeton, NJ) and a 15 mL bolus injection of saline. All injections were made using a power injector (Empower CTA, Acist Medical Systems, Eden Prairie MN) at a rate of 5 mL/s. While transient increases in flow, on the order of 5-10%, were measured immediately after contrast injection, all flow rates equilibrated well before CT perfusion measurements were made. Hence, any effects of the contrast injection on measured perfusion rates were negligible. CT images were reconstructed

from full projection data sets with a slice thickness of 0.5 mm using a medium-smooth FC03 kernel with beam hardening corrections. The voxel size was 0.43 x 0.43 x 0.5 mm^3 and images were reconstructed at 75% of the ECG cycle, as is customary in diastolic imaging.

Perfusion Measurement Using the FPA Technique

All FPA perfusion measurements were made using a VOI with an outer diameter of 9 cm, an inner diameter of 5.7 cm, and a slab thickness of 1.5 cm, defined inside the myocardial compartment. The contrast filled ventricle was excluded from the VOI. Given these dimensions and the packing fraction of the beads, the total volume inside the VOI was 57 mL, corresponding to approximately 55 grams of simulated myocardial tissue. Example images of the phantom before and after contrast infusion are shown in **Figure 2.3**. For each perfusion measurement, the integrated HU (sum of all voxel HU) within the myocardial VOI was used to generate the tissue time attenuation curve (TAC). To obtain the input concentration C_{in} in equation 1, a calibration VOI with a cross-sectional area of approximately 2 cm^2 and a thickness of 0.3 cm was defined directly upstream from the myocardial compartment. The integrated HU within this calibration VOI was determined and divided by the known VOI volume to yield the arterial input function (AIF). Perfusion was calculated by measuring the change in iodinated blood volume within the known time interval and dividing by the myocardial mass.

Perfusion Measurement Using the Maximum Slope Model

For comparison purposes, perfusions rates were also measured using the maximum slope model. In this case, several small VOIs, measuring approximately 0.3 cm^3, were defined inside the myocardial compartment. The VOI size was chosen based on previously reported maximum slope model implementations[29, 62]. The average HU in the small VOIs, instead of the integrated HU, was determined and plotted as a function of time. Curve fitting was performed, and maximum slope model perfusion was calculated using the following equation[38].

$$\boldsymbol{Q = \frac{\max\left(\frac{d}{dt}V\right)}{\max\left(C_{in}\right)}} \qquad \textbf{(2)}$$

Radiation Dose Reduction

The radiation dose reduction capacity of the FPA technique was evaluated by successively reducing the number of volume scans per perfusion measurement from the original 20 volume scans, in order to determine the minimum number of volume scans necessary for accurate perfusion measurement. A small VOI inside the aorta is normally monitored to determine the start of image acquisition using a preset HU. In order to simulate a clinical protocol, a threshold of 180 HU was set for the AIF. After a threshold of 180 HU was reached in the AIF, five volume scans over five consecutive cardiac cycles (V1-V5) were used for perfusion measurements. The first-pass analysis perfusion calculations were performed based on two (V1 and V5), three (V1, V3 and V5), and five (V1-V5) volume scans (see **Figure 2.5**). The initial volume scan (V1) used was one cardiac cycle after a triggering threshold of 180 HU in the AIF. The input

concentration C_{in} used for FPA perfusion measurement was always acquired from the final volume scan (V5) and approximates the maximum of the arterial input function. The total dose-length-product (DLP) was determined for each measurement, and converted to an effective dose (ED) in mSv using an ED/DLP conversion factor (k = 0.014)[63]. The reduced radiation dose was calculated using the radiation dose per volume scan multiplied by the number of volume scans used for perfusion measurement.

Results

Perfusion Measurements

FPA and maximum slope model measurements were made for known flow rates between 60-140 mL/min corresponding to known perfusion rates between 0.96-2.49 mL/min/g. An example arterial input function for the 2.49 mL/min/g perfusion measurement is shown in **Figure 2.5**. The corresponding FPA tissue time attenuation curve (TAC) is also shown in **Figure 2.5**, where the upslope of the TAC between V1 and V5 is proportional to the average perfusion rate. For both the arterial input function and tissue time attenuation curve, clinically realistic enhancement was achieved. FPA and maximum slope model perfusion measurements versus known perfusion are shown in **Table 2.1** and **Figure 2.6**. The results show an excellent correlation between the known and measured perfusion using 2, 3, and 5 volume scans with no significant difference between the results from 2 and 5 volume scans. On the other hand, the maximum slope model showed a significant, systematic underestimation of the known perfusion.

Radiation Dose Reduction

FPA perfusion measurements were calculated using two, three, and five volume scans. The average difference between FPA perfusion measurements made using two volume scans versus five volume scans was 0.00±0.02 mL/min/g, suggesting the FPA technique can yield accurate perfusion measurements using as few as two volume scans. The radiation dose incurred per volume scan was 1.32 mSv, resulting in a total radiation dose of 2.64, 3.96, and 6.6 mSv for two, three, and five volume scans, respectively. Furthermore, depending on the perfusion rate, the radiation dose for the maximum slope model was in the range of 11.69 – 17.51 mSv. Based on the radiation dose of a two volume scan FPA acquisition compared to the radiation dose of the maximum slope model, the FPA technique offers more than a 4-fold reduction in radiation dose and is more accurate in perfusion quantification.

Discussion

Existing CT Perfusion Techniques

Existing dynamic CT perfusion techniques, such as the maximum slope model, use a relative index of myocardial blood flow to measure perfusion. Previous reports have indicated that CT perfusion is positively correlated with coronary fractional flow reserve (FFR) and microsphere measurements[29, 51]. However, in these reports perfusion was always underestimated, as illustrated by a less-than-unity slope and non-zero offset, when compared to reference standard microsphere measurements[29]. Such perfusion underestimation is due to the use of small VOIs (~1 mL) to generate myocardial tissue time attenuation curves. Smaller VOIs are subject to shorter transit times of contrast,

and as a result are highly susceptible to contrast loss and perfusion underestimation, especially at hyperemia[37]. Such problems of underestimation were also described in a recent simulation study[38] and are in agreement with the maximum slope model perfusion results from this study (see **Figure 2.6**).

The FPA technique differs from previously reported dynamic CT perfusion techniques in that it does not suffer from perfusion underestimation and can determine perfusion with near unity slope and minimal offset when compared to reference standard microsphere perfusion measurements. Specifically, it takes advantage of whole organ CT scanners to prospectively image the entire heart within a fraction of a second. The extended coverage allows perfusion measurement of the entire perfusion bed of an arterial tree or a major branch, eliminating the problem of contrast loss by increasing the transit time window; a requirement that is not satisfied by most dynamic CT perfusion techniques. Additionally, measurements in large perfusion beds are much less sensitive to image noise, making it easier to extract accurate perfusion information from fewer volume scans.

In the current study, a single, large VOI, which encompassed the entire myocardial tissue volume, was used for perfusion measurements. However, clinical implementation of this technique will require vessel-specific VOIs determined from CT angiographic images[47, 53]. Such VOIs will be defined as the entire perfusion bed of an artery or major arterial branch, distal to a stenosis, and will allow for vessel-specific perfusion measurements to be made.

Perfusion Measurement Using the FPA Technique

The results of the study indicate that the proposed FPA technique accurately measures perfusion using CT image data over a range of clinically relevant perfusion rates. FPA derived perfusion measurements had a standard deviation of 0.08 mL/min/g with an average RMS error of 0.083 mL/min/g. Maximum slope model derived perfusion measurements had a standard deviation of 0.03 mL/min/g and an average RMS error of 1.30 mL/min/g. The results indicate that the FPA technique is both accurate and reproducible (see **Table 2.1**). The results also indicate that the maximum slope model greatly underestimates perfusion (see **Figure 2.6**), which is in agreement with previous reports[38]. Overall, the accuracy and reproducibility of the perfusion results validate the FPA technique and its underlying assumptions. Additionally, the FPA technique has previously been validated for flow measurement using invasive 2D coronary angiographic images[56-59], further supporting its potential as a CT perfusion technique.

Dose Reduction

A major limitation of existing dynamic CT perfusion techniques is the high radiation dose required. Previous reports indicate that the average radiation dose delivered during a single dynamic CT perfusion stress scan is approximately 9-12 mSv[29, 32, 35, 40-42, 50, 51, 62, 64-67]. In the cases where both rest and stress perfusion scans are acquired, the total radiation dose is further increased and can be as high as 30 mSv[29, 35, 42, 50, 51, 64, 66]. Therefore, there is a specific need for dose reduction before dynamic CT perfusion techniques can be implemented as a routine clinical standard.

The results from this study indicate that the proposed FPA technique has the potential to substantially reduce radiation dose in addition to improving the accuracy of perfusion measurements. The reduction in radiation dose is accomplished by minimizing the number of volume scans necessary for accurate perfusion measurement. Compared to current dynamic CT perfusion techniques, which require approximately 15 volume scans for perfusion measurement [37], the FPA technique requires as few as two volume scans for perfusion measurement, resulting in more than a 4-fold reduction in radiation dose, as well as more accurate perfusion quantification.

The FPA technique also acquires both CT angiography and dynamic CT perfusion data during the same low-dose protocol, which further reduces the total radiation dose and contrast loading to the patient. Furthermore, the FPA technique can be used in conjunction with standard dose reduction methods such as tube voltage optimization, tube current modulation, and iterative reconstruction techniques[43, 66] to further reduce the radiation dose.

Clinical Application and Study Limitations

While the FPA technique was validated in a static cardiac phantom, there are a few limitations for *in vivo* application of this technique. The first limitation is the effect of potential motion artifacts on perfusion measurement. To address such motion artifacts, prospective ECG-gating can be used to minimize cardiac motion during data acquisition. Additionally, image processing techniques, such as deformable image registration based on mutual information, can be used to further reduce motion artifacts.

Another potential limitation is beam hardening due to large volumes of contrast pooling inside the ventricles. The phantom was designed to simulate such hardening artifacts. However, the associated artifacts can be minimized by applying beam-hardening corrections available with CT scanners, as well as additional corrections that take into account the dynamic nature of contrast in the heart [68, 69]. A single VOI, which encompassed the entire myocardial tissue compartment, was also used in the phantom study. Since the setup was used to develop and validate the FPA technique, less emphasis was placed on dividing the myocardial tissue compartment into multiple VOIs of complex shape. However, the accuracy of the FPA technique does not depend on the shape of a compartment. Hence, in the current phantom study, the shape of the compartment was chosen to be cylindrical for convenience. That being said, myocardial segmentation and multiple VOIs need to be used *in vivo* for relevant perfusion measurement. CT angiography data can be used to automatically generate vessel-specific VOIs[47, 53], allowing the perfusion in each coronary artery perfusion bed or major coronary branch to be determined. Another potential limitation of the study is the time-to-peak of each arterial input function and the corresponding tissue time attenuation curve. *In vivo,* the time-to-peak of these functions is relatively short due to the hyperemic transit time of blood from coronary artery to coronary sinus[39, 70]. Fortunately, since the FPA technique only requires a minimum of two volume scans, as long as those volume scans are acquired during the upslope of the myocardial tissue time attenuation curve *in vivo*, and include the peak of the arterial input function, absolute myocardial perfusion can be measured independent of the time-to-peak. The actual timing and total number of volume scans will require more investigation and will be

determined in future *in vivo* studies. Lastly, full projection data reconstruction was used in the study, resulting in reduced temporal resolution as compared with partial scan reconstructions. This was done to avoid the previously reported partial scan artifacts[35] that limit the quantitative nature of CT perfusion.

Conclusions

The results of the phantom study indicate the FPA technique can be used to make accurate dynamic CT perfusion measurements over a range of clinically relevant perfusion rates using a minimum of two volume scans. This technique has the potential to substantially reduce the radiation dose as compared with existing dynamic CT perfusion techniques by reducing the total number of volume scans necessary for accurate perfusion measurement.

Appendix 2.1: Original First-Pass Analysis (FPA) Derivation

To measure perfusion through a compartment, it is necessary to determine the volume ($V(t)$) of contrast material entering the compartment within a certain time interval, and this volume can be described as:

$$\boldsymbol{V(t) = \int_0^t Q_i(t)C_i(t)dt - \int_{t_{min}}^t Q_o(t)C_o(t)dt} \qquad \textbf{(1)}$$

where $Q_i(t)$ and $Q_o(t)$ are the incoming and outgoing flow rates, and $C_i(t)$ and $C_o(t)$ are the incoming and outgoing concentrations of contrast agent, respectively. Equation 1 represents the fluid dynamic form of mass conservation indicating that the total amount of contrast material in the compartment equals the amount that has entered minus the amount that has exited. The term t_{min} denotes the minimum transit time of contrast material through the compartment, from entrance to exit. Hence, if $V(t)$ is calculated before any contrast material has exited the vascular compartment, at $t < t_{min}$, the outgoing contrast concentration is zero (i.e. $C_o(t) = 0$) and the latter integral can be ignored.

$$\boldsymbol{V(t) = \int_0^{t<t_{min}} Q(t)C_{in}(t)\,dt} \qquad \textbf{(2)}$$

The derivative of both sides of equation 2, divided by the input iodine concentration, $C_{in}(t)$, yields:

$$\boldsymbol{Q(t < t_{min}) = C_{in}^{-1}(t < t_{min})\frac{d}{dt}V(t < t_{min})}\ \textbf{(3)}$$

Integrating from t to $t + \Delta t$ and dividing by Δt to give the time-averaged value of equation 3 over the sampling period, the final form of flow derived via the proposed first-pass analysis (FPA) technique is:

$$\boldsymbol{Q_{ave} = (C_{in}^{-1}\frac{d}{dt}V)_{ave}} \qquad \textbf{(4)}$$

Where $Q_{ave}$is the calculated flow, $\frac{\mathrm{d}}{\mathrm{dt}}\mathrm{V}$ is the rate of change of contrast volume in the vascular compartment per unit time, and C_{ave} is the average input concentration of incoming contrast material at the time of measurement. The measured flow can be further simplified as:

$$\boldsymbol{Q = \frac{\Delta V}{(\Delta t)(C_{ave})}} \qquad \textbf{(5)}$$

Appendix 2.2 Modified First-Pass Analysis Derivation

As previously described in **Appendix 2.1**, the first-pass flow (Q_{ave}) of iodine volume (V) into organ compartment of interest is defined as:

$$\boldsymbol{Q_{ave} = (C_{in}^{-1}\frac{d}{dt}V)_{ave}} \qquad \textbf{(4)}$$

or more simply as:

$$\boldsymbol{Q = \frac{\Delta V}{(\Delta t)(C_{ave})}} \qquad \textbf{(5)}$$

Where $\boldsymbol{\Delta V/\Delta t}$ corresponds to the integrated change in iodine volume or mass over the measurement time, while $\boldsymbol{C_{ave}}$ corresponds to the average incoming concentration of iodine over the measurement time, respectively. As such, if the tissue mass within the compartment, M_T, is also known, the compartmental perfusion is further defined as:

$$\boldsymbol{P = \frac{\Delta V}{(\Delta t)(C_{ave})(M_T)}} \qquad \textbf{(6)}$$

Given the results of the phantom study, only two volume scans were found to be necessary for absolute perfusion measurement. However, the impact of the timing of those volume scans on the accuracy of the FPA technique was not fully assessed. Hence, additional analysis was performed later on to determine the optimal first-pass

timing of the volume scans (now denoted as **V1** and **V2** in **Figure 2.8**), such that the accuracy of the FPA technique was maximized. Specifically, different trigger thresholds were used to specify the temporal location of **V1**, while the cardiac cycle delay of **V2** was incrementally increased (one cardiac cycle at a time) up to a maximum of five cardiac cycles after the peak. The mean ± standard deviation of the percent error for all FPA perfusion measurements as compared to reference standard ultrasonic perfusion measurement was then computed for each **V1** and **V2** combination, with the results displayed in **Figure 2.9**. Overall, the results indicate that in order to maximize the accuracy of FPA perfusion measurement, **V2** must be retrospectively selected or prospectively acquired at or near the peak enhancement of the arterial input function (AIF). Moreover, the **V1** trigger threshold does not dramatically impact the accuracy of the technique. Thus, the new, two-volume FPA sampling protocol was assessed using the phantom data, where the first volume scan after triggering at 180 HU was specified as **V1** (180HU was used to prevent false triggering), while the volume scan at or after the peak enhancement of the AIF was specified as **V2**. The results of the new, two-volume FPA sampling protocol are shown in **Figure 2.10.** Using the new protocol, FPA perfusion measurements were in better agreement with reference standard ultrasonic-flow-probe measurements (P_{FPA} = 0.99 P_{ULTRA} + 0.06, R^2 = 0.99) than previously reported. The RMSE was 0.07 mL/min/g while the RMSD was 0.05 mL/min/g, also indicating improved accuracy and precision. The concordance correlation coefficient (CCC)[33] was computed and found to be ρ = 0.99, indicating excellent agreement with the reference standard. **Given these results, the updated two-volume FPA protocol was used for the remainder of all validation studies.**

Tables

Table 2.1 Summary of the linear regression analysis between different CT perfusion methods and known perfusion measurements. The associated radiation dose is also included.

Method	Slope	Intercept	Pearson's r	SEE (mL/min/g)	Dose (mSv)
2 Scans	0.91	0.06	0.98	0.14	2.64
3 Scans	0.91	0.06	0.98	0.14	3.96
5 Scans	0.92	0.05	0.98	0.13	6.60
MSM	0.25	- 0.02	0.97	0.30	11.69-17.51

Figures

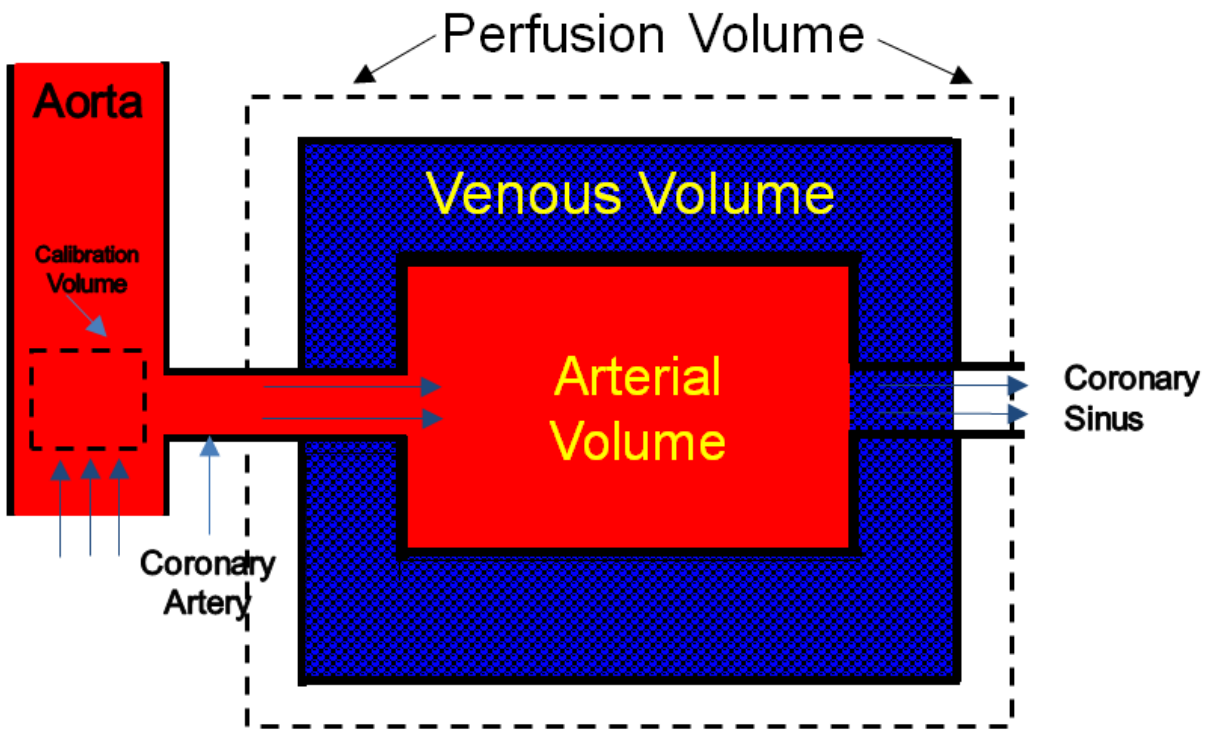

Figure 2.1: Single compartment model used in the first-pass analysis technique showing calibration and perfusion volumes.

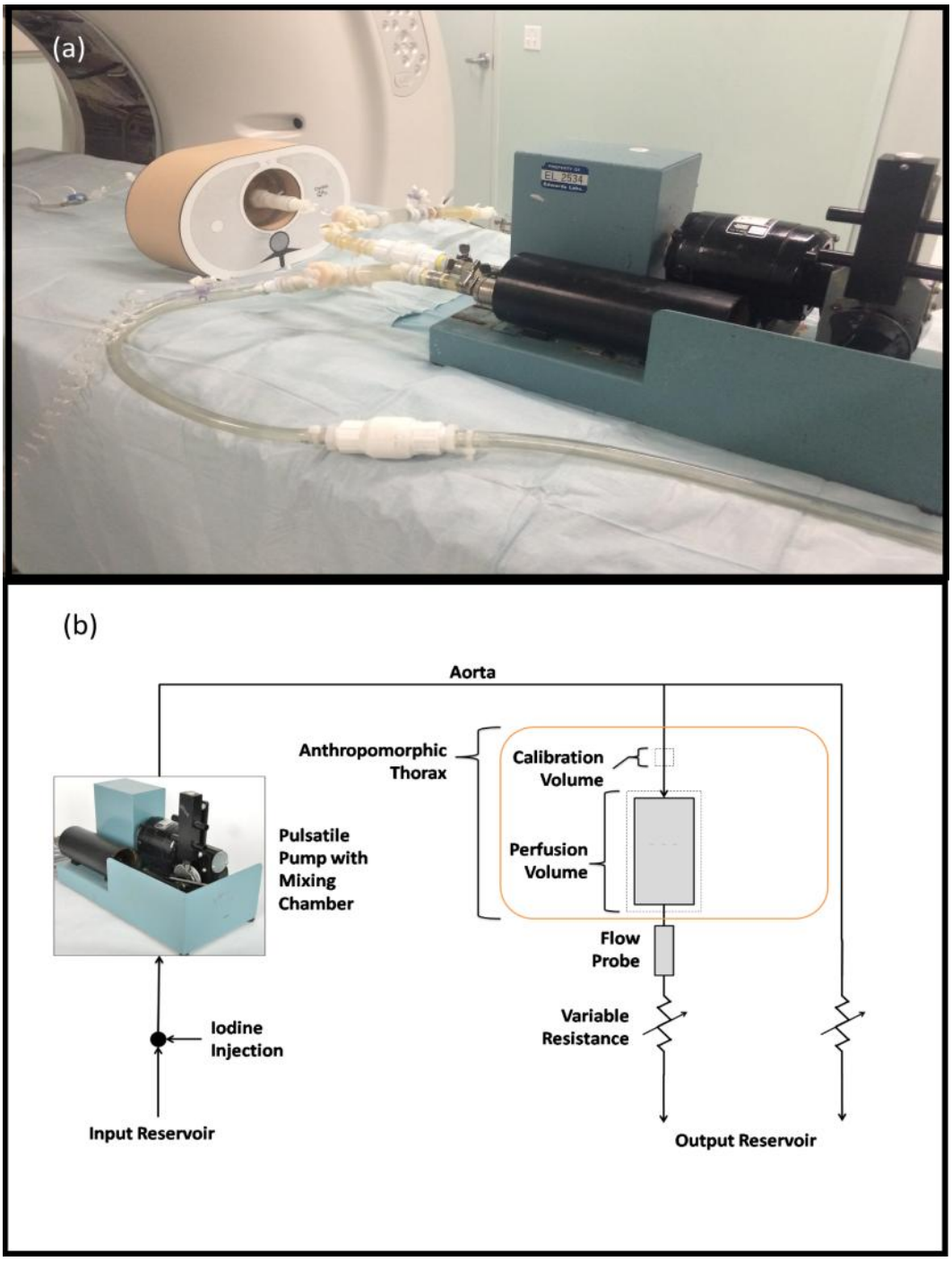

Figure 2.2: (a) A photograph of the cardiac perfusion phantom inside the anthropomorphic thorax along with the pulsatile pump, (b) a schematic diagram of the cardiac perfusion phantom.

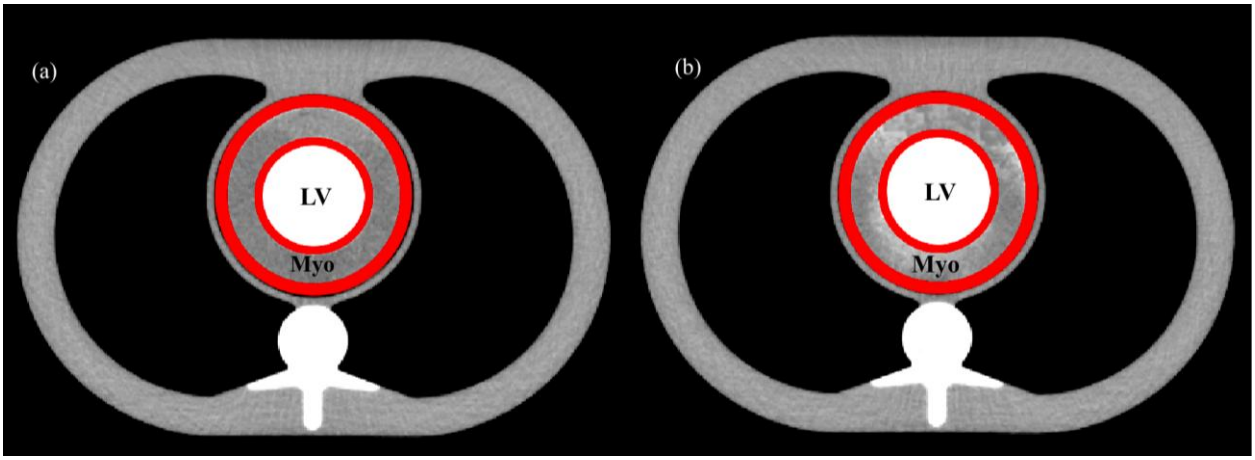

Figure 2.3: Myocardial compartment (Myo) around the contrast filled left ventricle (LV). The VOI (denoted in red) is overlaid before (a) and after (b) contrast infusion.

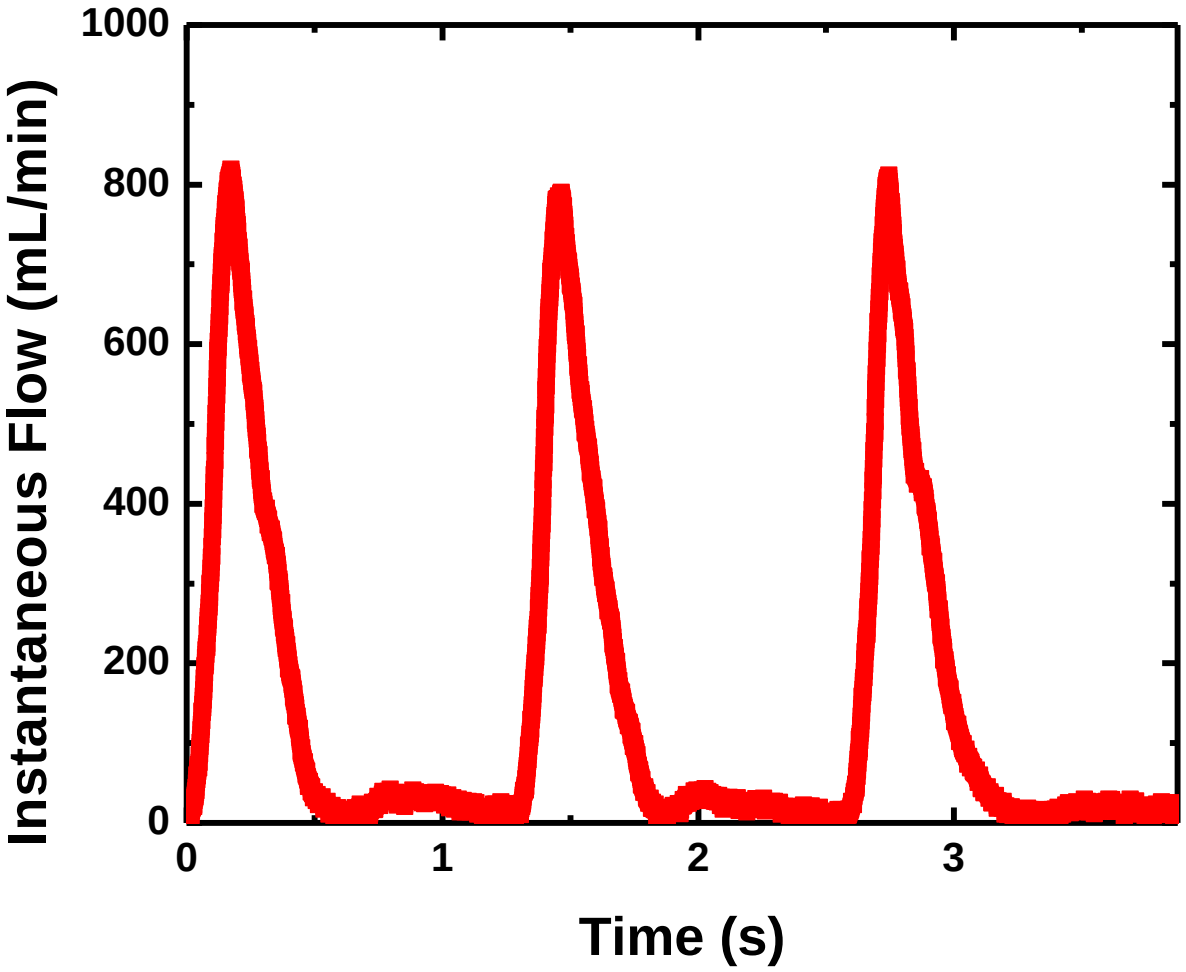

Figure 2.4: Pulsatile flow profile corresponding to an average perfusion rate of 2.49 mL/min/g.

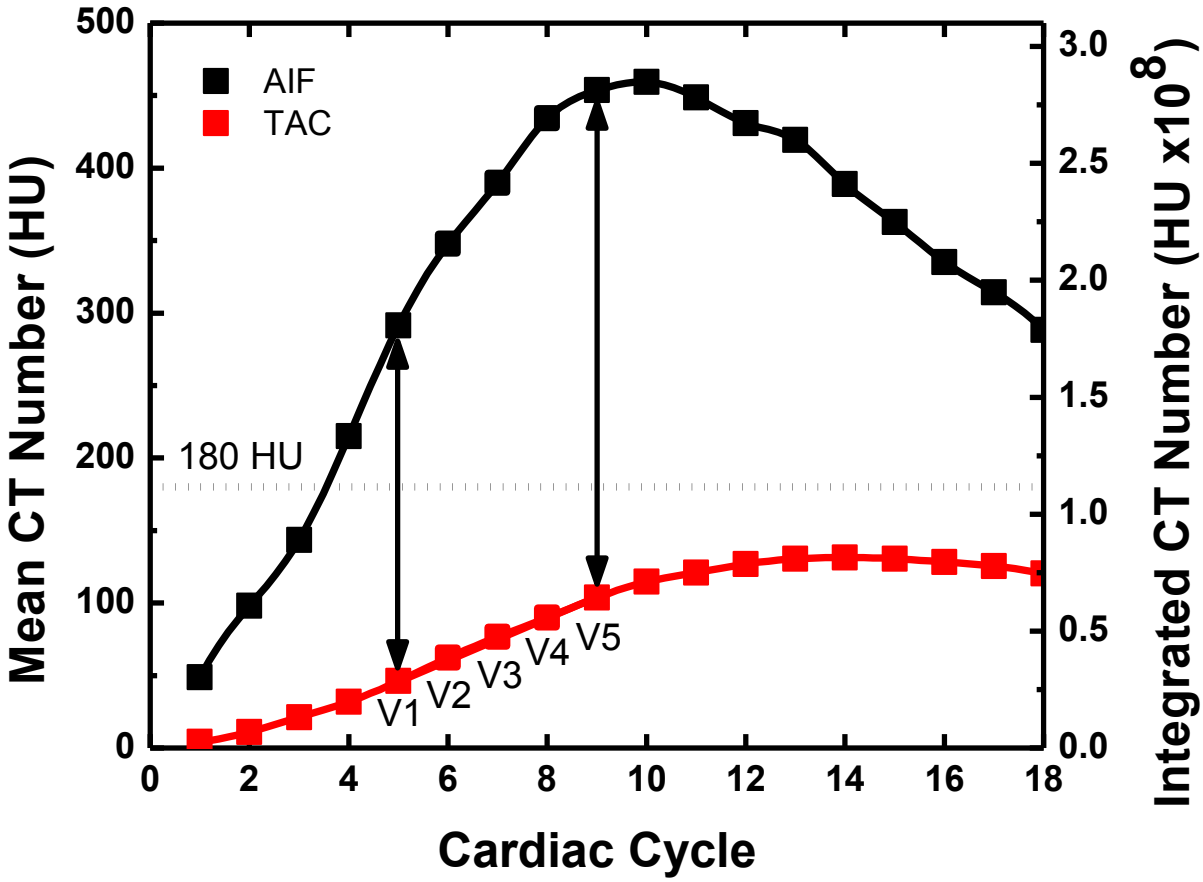

Figure 2.5: ***Example arterial input function (AIF) and the corresponding myocardial tissue time attenuation curve (TAC) showing the five volume scans (V_1-V_5) used for FPA perfusion calculations.***

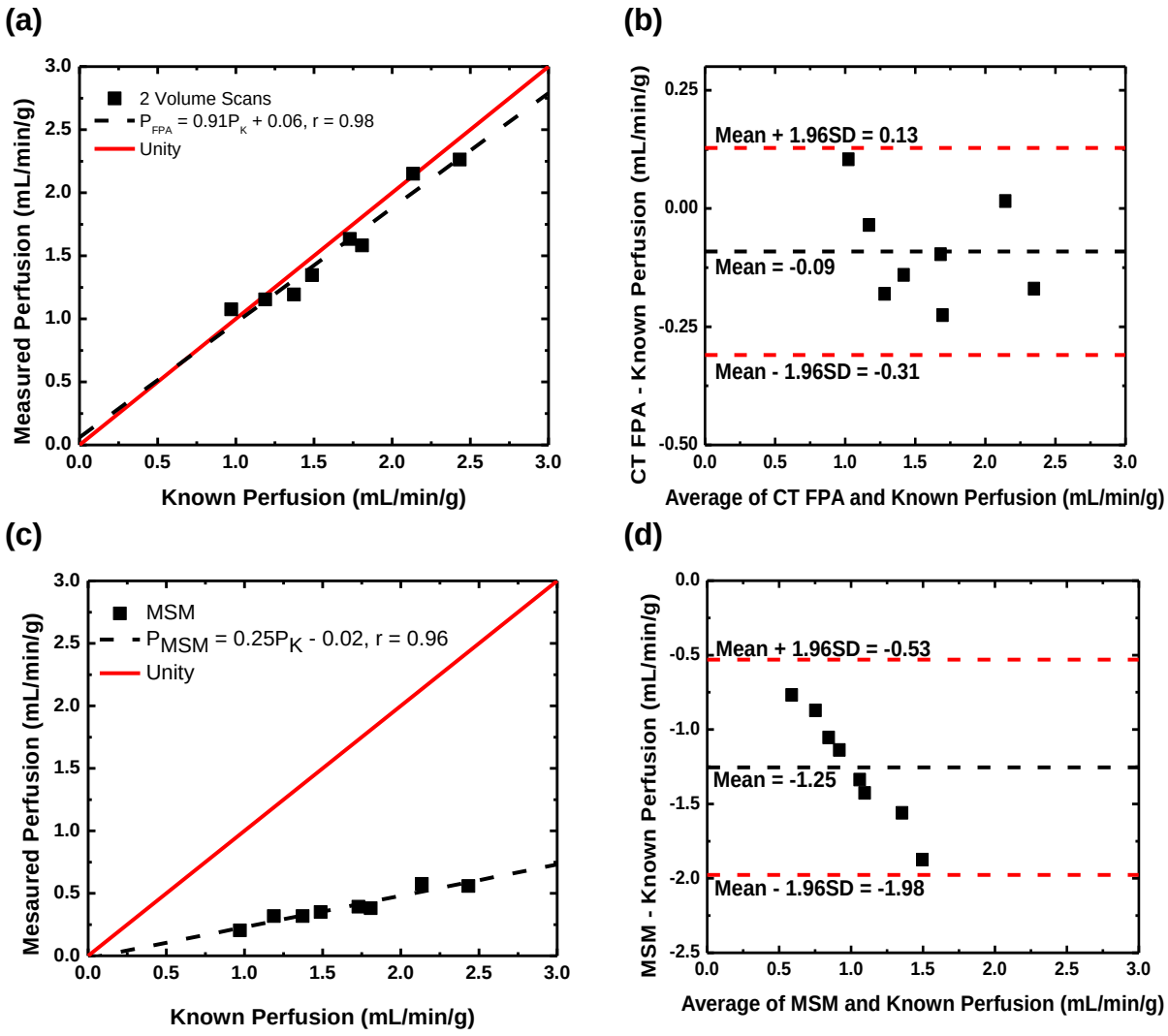

Figure 2.6: Two-volume scan FPA perfusion (a) and maximum slope model (MSM) perfusion (c) versus known perfusion with respective Bland-Altman plots (b, d).

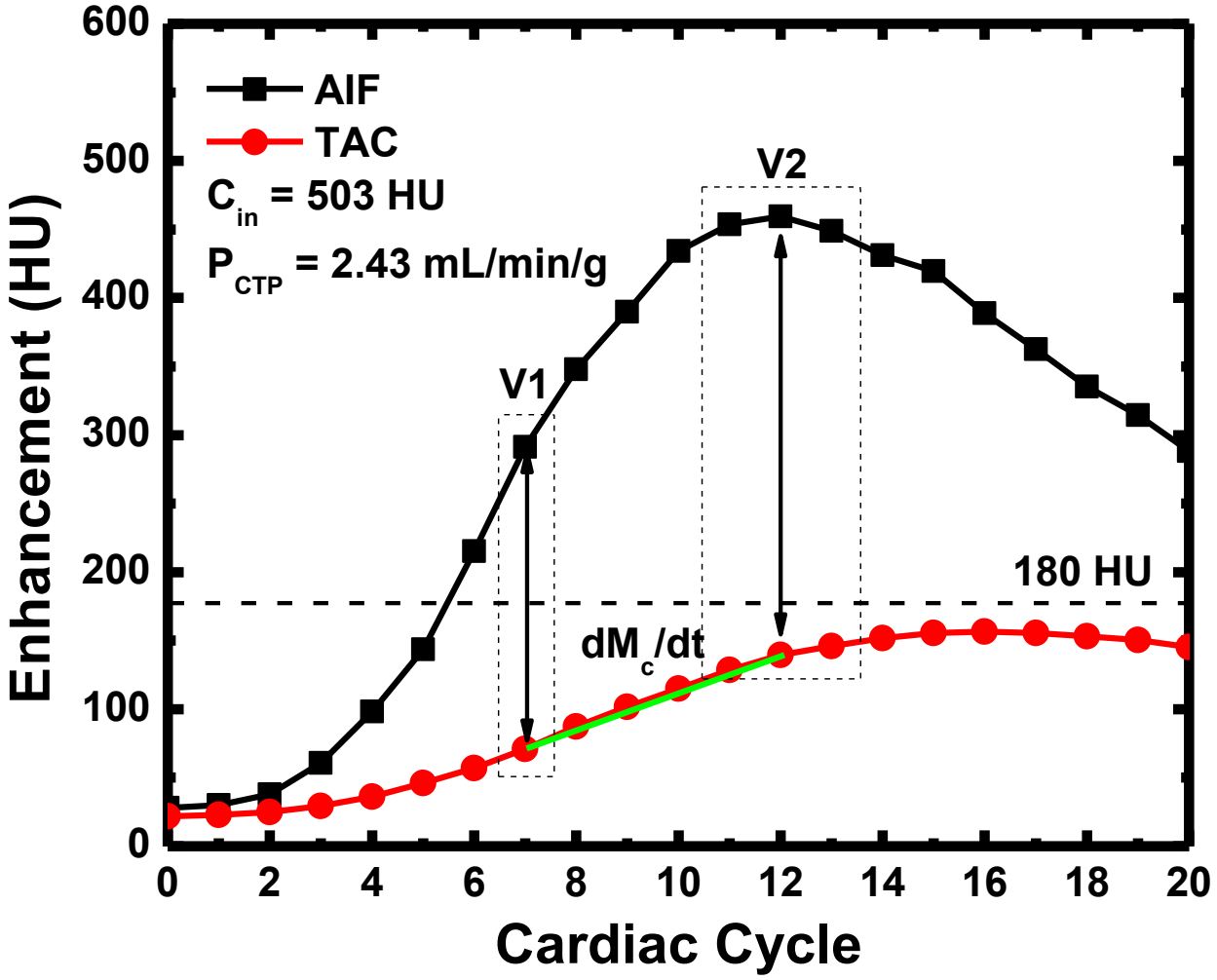

Figure 2.7: Example arterial input function (AIF) curve from the aorta and corresponding myocardial tissue enhancement curve (TAC) from the model, with a 180 HU "trigger" threshold and the new FPA V1 and V2 volume scan selection protocol displayed.

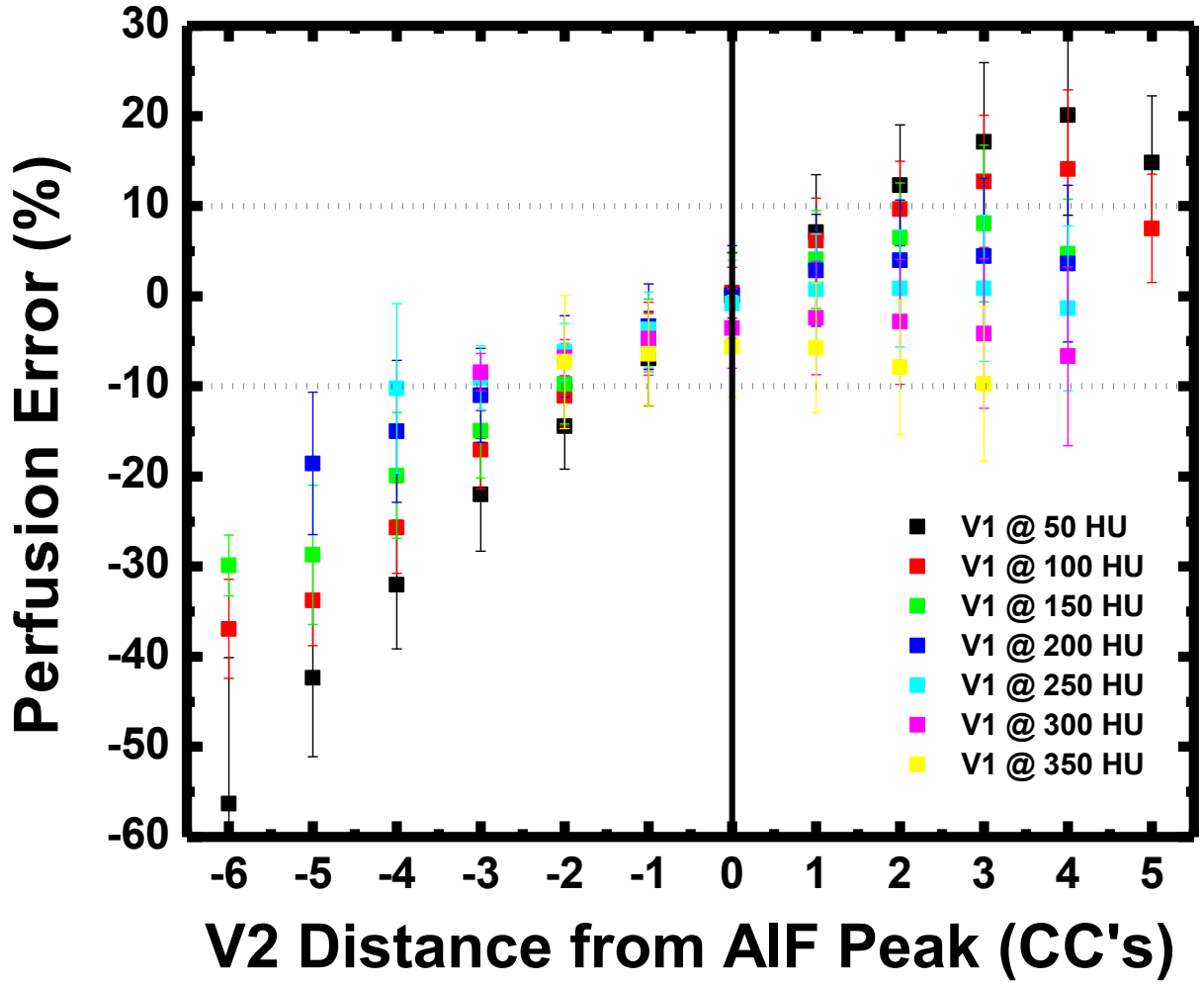

Figure 2.8: Temporal optimization of volume scan selection for the FPA technique. Different trigger thresholds were used to specify the temporal location of V1, while the cardiac cycle delay of V2 was incrementally increased (one cardiac cycle at a time) up to a maximum of five cardiac cycles after the peak. The mean ± standard deviation of the percent error for all FPA perfusion measurements as compared to reference standard ultrasonic perfusion measurement was then compared for each V1 trigger and V2 temporal combination. V1 and V2 indicate the first and second volume scans necessary for accurate FPA perfusion measurement. CC's indicates cardiac cycles, where FPA perfusion error is displayed as a function of the cardiac cycle distance of V2 away from the peak enhancement of the arterial input function (AIF).

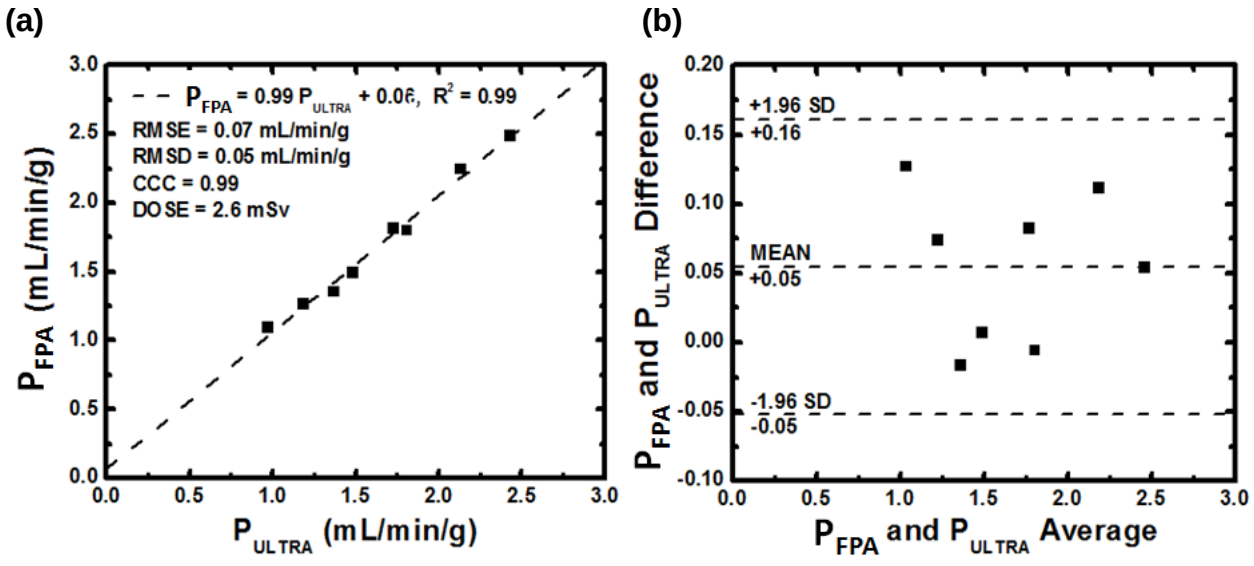

Figure 2.9: FPA perfusion measurement with the new two-volume sampling scheme as compared to reference standard ultrasonic-flow-probe perfusion measurement. (a) Regression analysis was performed with the coefficient of determination (R^2), accuracy (RMSE), precision (RMSD), concordance correlation (CCC), and "simulated" effective radiation dose also determined. (b) Bland-Altman analysis was also performed, with the limits of agreement displayed (bottom right).

CHAPTER 3: ACCURACY OF CORONARY PERFUSION TERRITORY ASSIGNMENT AS COMPARED TO MYOCARDIAL BLUSH IN SWINE

Abstract

As combined morphological and physiological assessment of coronary artery disease (CAD) is necessary to reliably resolve CAD severity, the objective of this study was to validate an automated minimum-cost path assignment (MCP) technique which enables accurate, vessel-specific assignment of the left (LCA) and right (RCA) coronary perfusion territories using computed tomography (CT) angiography data for both left and right ventricles. Six swine were used to validate the MCP technique. In each swine, a dynamic acquisition comprised of twenty consecutive volume scans was acquired with a 320-slice CT scanner following peripheral injection of contrast material. From this acquisition the MCP technique was used to automatically assign LCA and RCA perfusion territories for the left and right ventricles, independently. Each animal underwent another dynamic CT acquisition following direct injection of contrast material into the LCA or RCA. Using this acquisition, reference standard LCA and RCA perfusion territories were isolated from the myocardial blush. The accuracy of the MCP technique was evaluated by quantitatively comparing the MCP-derived LCA and RCA perfusion territories to these reference standard territories. All MCP perfusion territory masses ($Mass_{MCP}$) and all reference standard perfusion territory masses ($Mass_{RS}$) in the left ventricle were related by $Mass_{MCP}=0.99Mass_{RS}+0.35g$ ($r=1.00$). $Mass_{MCP}$ and $Mass_{RS}$ in the right ventricle were related by $Mass_{MCP}=0.94Mass_{RS}+0.39g$ ($r=0.96$). The MCP technique was validated in a swine animal model and has the potential to be used for

accurate, vessel-specific assignment of LCA and RCA perfusion territories in both the left and right ventricular myocardium using CT angiography data.

Introduction

Coronary artery disease (CAD) and its resultant ventricular dysfunction are strongly predictive of future cardiac events. However, when CAD risk is appropriately stratified and managed, long term outcomes are significantly improved[1, 71]. Appropriate stratification of CAD requires both morphological and physiological data to reliably assess the true severity of disease[2, 72-75]. Such stratification is often accomplished noninvasively with single-photon emission computed tomography (SPECT), cardiac magnetic resonance (CMR), positron-emission tomography (PET), or dynamic computed tomography (CT) perfusion; modalities that provide relevant perfusion data.

To incorporate corresponding morphological information with this perfusion data, the American Heart Association's (AHA) 17-segment model[76] of the heart is commonly used in the absence of angiographic data. In the 17-segment model, the left ventricle is segmented into seventeen virtual perfusion territories that are assigned to the left anterior descending (LAD), left circumflex (LCx), or right coronary artery (RCA), respectively. Nevertheless, despite the 17-segment model's clinical merit, it is unable to account for coronary morphological variation; thus, coronary perfusion territories are commonly miss-assigned by the model, leading to misinterpretation of perfusion defects[77-81]. Additionally, the 17-segment model does not provide any assessment of the right ventricular myocardium, yet CAD in the RCA is highly prevalent[82]. Given these

limitations, there exists a clinical need for improved vessel-specific morphological and physiological assessment of CAD in both ventricles[79].

With the advent of CT and MR angiography, in addition to hybrid PET/CT and SPECT/CT imaging methods, morphological data is becoming increasingly accessible. Several studies have even gone on to illustrate that such morphological data can be used to algorithmically assign vessel-specific perfusion territories[47, 83-87]. Nonetheless, most of these reports lack robust quantitative validation of their myocardial assignment algorithm's accuracy versus a true reference standard. Additionally, many of these studies have only validated coronary perfusion territory assignment on the epicardial surface of the left ventricle.

Hence, the purpose of this study was to thoroughly validate a minimum-cost path assignment (MCP) technique that enables accurate, vessel-specific assignment of the left and right coronary arterial perfusion territories throughout the full thickness of the left and right ventricular myocardium using computed tomography (CT) angiography data.

Materials and Methods

General Methods

The study was approved by the Animal Care Committee and Institutional Review Board for the Care of Animal Subjects and was performed in agreement with the "Position of the American Heart Association on Research Animal Use." All data was prospectively acquired between 12/2014 and 07/2016. Specifically, the MCP technique was validated

in six male Yorkshire swine (42 ± 9 kg). All swine underwent dynamic CT imaging, once following peripheral intravenous contrast injection and at least once following intracoronary contrast injection in the left or right main coronary arteries (LCA and RCA). A total of six peripheral intravenous contrast injection acquisitions were acquired, while a total of fifteen reference standard intracoronary injection datasets were acquired. The peripheral contrast injection acquisitions were used for MCP perfusion territory quantification, while the intracoronary injection data was used for extraction of "blushed" and "non-blushed" reference standard perfusion territories. The LCA and RCA perfusion territories obtained with the MCP technique (LCA_{MCP} and RCA_{MCP}) were quantitatively compared to the "blushed" and "non-blushed" reference standard LCA and RCA perfusion territories (LCA_{RS} and RCA_{RS}) obtained from intracoronary LCA and RCA contrast injections through mass and spatial correspondence analysis. Overall, MCP territories were independently derived and validated for the left and ventricular right ventricular myocardium. Additionally, MCP territories were independently derived and validated for the whole heart myocardium, which, in turn, included both the left and right ventricular myocardium.

Animal Protocol

Anesthesia was induced via intramuscular injection of Telazol (4.4 mg/kg), Ketamine (2.2 mg/kg), and Xylazine (2.2 mg/kg), and was maintained after intubation (Covedien, Mansfield, MA) through ventilation (Highland Medical Equipment, Temecula, CA) with an oxygen-air-mixture containing 1.5 -2.5% Isoflurane (Baxter, Deerfield, IL). Electrocardiogram, O_2 saturation, temperature, blood pressure, and end-tidal CO_2 were

monitored and a warming blanket (HTP-1500, Adroit Medical Systems, Loudon, TN) was used to prevent hypothermia.

Using the modified Seldinger technique under ultrasound guidance (Vivid E9, GE Healthcare, IL), catheter sheaths (AVANTI®, Cordis Corporation, Miami Lakes, FL) were placed in both femoral veins and in the right carotid artery. The right femoral vein was used for drug and fluid administration. The left femoral vein was used for peripheral contrast injection. The carotid sheath was used for invasive blood pressure monitoring as well as coronary catheter introduction. Specifically, under fluoroscopic guidance, a Judkins right guide catheter (Cordis Corporation, Miami Lakes, FL) was used to engage the left and right coronary ostia. The guide catheter was then used for intracoronary injection of contrast into the LCA or RCA during dynamic CT imaging, resulting in myocardial "blush" in each perfusion territory, respectively.

Computed Tomography (CT) Imaging Protocol

To derive MCP perfusion territories (LCA_{MCP} and RCA_{MCP}), dynamic CT data was acquired following peripheral contrast (Isovue 370 mg/mL, 1 mL/kg, 5 mL/s) and saline (0.5 mL/kg, 5 mL/s) injection via the femoral vein. For the determination of reference standard perfusion territories (LCA_{RS} and RCA_{RS}), dynamic CT data was acquired following intracoronary contrast (Isovue 50 mg/mL, 15 mL, 2 mL/s) injection via the guide catheter into the LCA or RCA. For both injection schemes, twenty consecutive volume scans were prospectively acquired with a multi-detector CT scanner (Aquilion One, Toshiba American Medical Systems, Tustin, CA) at 100 kVp and 200 mA using

320 x 0.5 mm detector collimation. Full projection data was used to avoid partial scan artifacts and all volume scans were reconstructed at 75% of the R-R interval using standard beam hardening corrections. Image datasets from the same animal were reconstructed with the same voxel size. Depending on the field-of-view, the reconstruction voxel size ranged from 0.43 x 0.43 x 0.50 mm to 0.79 x 0.79 x 0.50 mm. To allow for adequate renal clearance of contrast, each intracoronary contrast injection acquisition was performed at least 10 minutes after each peripheral intravenous contrast injection acquisition. Subsequent intracoronary contrast injection acquisitions were also acquired at least 10 minutes apart.

Minimum-Cost Path (MCP) Image Processing

Based on previous post-mortem swine analysis, it is known that myocardial tissue is perfused by its nearest coronary artery[46, 47]. Hence, the MCP technique was designed to model these prior findings, by determining the minimum distance, bounded within the heart, between each voxel of myocardium and each coronary artery. To validate the MCP technique, the peripheral intravenous contrast injection scans and intracoronary injection volume scans from the same animal were first registered[88] to a single maximally enhanced intravenous injection volume. The registered intravenous injection volume scans were then combined into a single maximum intensity projection (MIP) volume, from which the left ventricle, right ventricle and whole heart (both left and right ventricle) myocardium were semi-automatically segmented using a Vitrea workstation (Vitrea fX version 6.0, Vital Images, Inc., Minnetonka, MN). Semi-automatic extraction of

the LAD, LCx and RCA centerlines was also performed using the same Vitrea workstation.

Using a myocardial mask and centerlines of the LAD, LCx, and RCA, MCP was then performed separately on the left ventricle, right ventricle and whole heart, using the Insight Segmentation and Registration Toolkit[89]. Specifically, the vessel centerlines were used as seed points to create three separate distance maps through the myocardium using a Fast-Marching algorithm[90]. Using these distance maps, the minimum–cost path from each voxel of myocardium to each coronary centerline was used to assign each voxel to its closest supplying artery. This resulted in a vessel-specific perfusion territory for each coronary artery (LAD_{MCP}, LCx_{MCP} and RCA_{MCP}). This same process was performed three separate times, using the left ventricle, right ventricle, and whole heart masks, independently. This yielded coronary-specific assignment of the LAD_{MCP}, LCx_{MCP} and RCA_{MCP}, for each segmentation. The MCP technique, performed using the whole heart segmentation, is detailed in **Figure 3.1**.

Reference Standard (RS) Image Processing

The registered reference standard intracoronary injection volume scans were also combined into separate LCA injection and RCA injection MIP volumes, from which the "blushed" and "non-blushed" LCA and RCA perfusion territories were automatically segmented. As no ventricular blood pool opacification was present in intracoronary contrast injection acquisition MIPs, the whole heart myocardial mask from the former semi-automatic segmentation was first used to segment the entire myocardium from

these MIPs. A median filter was applied to each MIP, followed by automated region growing segmentation to extract the "blushed" and "non-blushed" LCA and RCA perfusion territories. For each region growing segmentation, the ostium of the coronary artery which was cannulated and directly injected with contrast was chosen as a seed point, and was iteratively grown into the whole heart myocardium, with the median Hounsfield Unit (HU) between "blushed" and "non-blushed" myocardium used as the cutoff. As such, each intracoronary injection acquisition resulted in two separate reference standard perfusion territories, one from the "blushed" myocardium and one from the "non-blushed" myocardium. A summary of these image processing steps is illustrated in **Figure 3.2.**

After MCP perfusion territories (LAD_{MCP}, LCx_{MCP} and RCA_{MCP}) were determined, and reference standard perfusion territory (LCA_{RS} and RCA_{RS}) extraction was complete, LAD_{MCP} and LCx_{MCP} were combined into a single left coronary artery MCP perfusion territory (LCA_{MCP}). All "blushed" and "nonblushed" reference standard perfusion territories of the same vessel were pooled together. The LCA_{MCP} and RCA_{MCP} perfusion territories were then quantitatively compared to LCA_{RS} and RCA_{RS} perfusion territories. LCA_{RS} and RCA_{RS} were first determined for the whole heart myocardium, after which they were segmented for only the left and right ventricle using the previously described left and right ventricular masks. These whole heart and ventricle-specific segmentations allowed direct and independent comparison of MCP to the corresponding reference standard whole heart, left ventricle, and right ventricle perfusion territories.

Bull's Eye Plot Visualization

Two-dimensional bull's eye plots were also provided for the right and left ventricles to further detail the coronary perfusion territories. This was achieved using a previously reported method[91]. Both the left and right ventricles were sampled into 100 slabs, perpendicular to the long axis of the heart through averaging. Within each slab, 360 equidistant samples were then taken radially from the center of the left ventricle. This was done for both the left and right ventricles, as well as for the rastered coronary centerlines, to yield bull's eye plots for the entire myocardium.

Myocardium At-Risk Simulation

Myocardium at-risk distal to a stenosis in a single animal was also assessed through simulation. Specifically, after determining LAD_{MCP}, LCx_{MCP} and RCA_{MCP} in the left ventricle, the position of a hypothetical stenosis was designated along the LAD centerline. MCP assignment was then performed in the LAD_{MCP} territory alone using the LAD vessel centerlines proximal and distal to the simulated stenosis, resulting in further delineation of the LAD_{MCP} territory into proximal and distal components. In total, three different LAD stenosis locations were evaluated for myocardium at-risk comparison.

Statistical Approach

In order to rigorously evaluate the accuracy of the MCP technique, MCP and reference standard perfusion territories for the same coronary artery were directly compared, using both mass and spatial correspondence. To evaluate mass correspondence, the myocardial mass of the MCP territories were compared to the myocardial mass of

reference standard territories via linear regression, root-mean-square error (RMSE), adjusted R^2 (Adj. R^2) concordance correlation coefficient (CCC) [92], Pearson's r (r), and Bland-Altman analysis. 95% Confidence intervals for RMSE, Adj. R^2, CCC and r provided, as [CI_{lower}, CI_{upper}]. Myocardial mass was estimated by multiplying the volume of each MCP or RS territory by the average density of myocardium tissue (1.035 g/mL). To further detail mass correspondence between MCP and reference standard perfusion territories, mass correspondence was performed on each axial slice of one animal. Additionally, the mass and mass-percent of LAD_{MCP}, LCx_{MCP} and RCA_{MCP}, in the left ventricle only, was measured and compared to a previously reported study[85]. To evaluate spatial correspondence between MCP and reference standard coronary perfusion territories, Dice's similarity coefficient and mean minimum Euclidean distance were computed. Dice's similarity coefficient is an established method used to quantitatively compare the overlap between separate volume segmentations[93, 94]. Mean minimum Euclidean distance was used to compute the mean minimum Euclidean distance between the boundaries of separate volume segmentations. For the calculation of mean minimum Euclidean distance, only non-overlapping boundary points were used, to remove possible bias caused by utilizing the same myocardial segmentation for both MCP and reference standard perfusion datasets. With the exception of Bland-Altman analysis, reference standard territories of the same coronary artery and acquired from the same animal were averaged together, yielding a total of 12 measurements for each assessment metric (6 LCA_{RS} and 6 RCA_{RS}). Mass and spatial correspondence between MCP and reference standard perfusion territories was

performed on the left ventricle, right ventricle and whole heart myocardium, independently.

Results

Animal Model

A total of six swine (42.0 ± 9.0 kg) were imaged. The average heart rate and mean arterial pressure during imaging were 84±10 beats per minute and 77±9 mmHg, respectively. The average mass of the whole heart for all six animals was 81.44±13.91 g. The average masses of the left and right ventricles were 68.42±11.60 g and 13.02±2.58 g, respectively. Seven LCA and eight RCA intracoronary injections were made, yielding a total of fifteen reference standard perfusion territory pairs (15 LCA_{RS} and 15 RCA_{RS}). Mass and percent mass correspondence from every intracoronary contrast injection acquisition are detailed in **Table 3.1**.

Mass Correspondence of Left and Right Ventricle MCP Perfusion Territories

In the left ventricular myocardium, the average mass of LCA_{MCP} was 55.90±9.98 g and the average mass of LCA_{RS} was 56.00±10.15 g, while the average mass of RCA_{MCP} was 12.52±2.60 g and the average mass of RCA_{RS} was 12.42±3.66 g. Left ventricle MCP mass correspondence is further detailed in **Table 3.2a**. For the right ventricular myocardium, the average mass of LCA_{MCP} and LCA_{RS} was 5.11±1.64 g and 5.39±2.03 g, respectively, while the average mass of RCA_{MCP} and RCA_{RS} was 7.90±2.20 g and 7.63±2.35 g, respectively. Right ventricle myocardial mass correspondence is detailed in **Table 3.2b**. From linear regression analysis, the left ventricular mass of LCA_{MCP} and

LCA_{RS} were related by $Mass_{MCP} = 0.97\ Mass_{RS} + 1.48$ g, while the RCA_{MCP} and RCA_{RS} were related by $Mass_{MCP} = 0.66\ Mass_{RS} + 4.29$ g. Combined, the left ventricular mass of all MCP territories, i.e. both LCA_{MCP} and $RCA_{MCP,}$ were related to the mass of all reference standard territories by $Mass_{MCP} = 0.99\ Mass_{RS} + 0.35$ g. Comprehensive linear regression analysis is provided in **Table 3.3a** and **Figure 3.3a**. Similar analysis for right ventricle myocardial perfusion territories are described in **Table 3.3b** and **Figure 3.3b**.

Mass Correspondence of Whole Heart MCP Perfusion Territories

Additionally, mass correspondence analysis was performed on MCP territories derived for the whole heart by combining both the left and right ventricular masks. For the whole heart myocardium, the average masses of LCA_{MCP} and LCA_{RS} were 61.02±10.21 g and 61.02±10.21 g, respectively, while the average masses of RCA_{MCP} and RCA_{RS} were 20.60±4.42 g and 20.18±5.69 g, respectively. Mass correspondence in the whole heart myocardium is further detailed in **Table 3.2c**. For the whole heart myocardium, the mass of all MCP territories were related to all reference standard territories by $Mass_{MCP} = 0.97\ Mass_{RS} + 1.19$ g. Linear regression analysis for the whole heart myocardium is shown in **Table 3.3c** and **Figure 3.3c**. Whole heart mass correspondence in one animal was also assessed on a per-axial slice basis, as detailed in **Figure 3.4**.

Spatial Correspondence of Left and Right Ventricle MCP Perfusion Territories

The mean minimum Euclidean distance between the left ventricle myocardium LCA_{MCP} and LCA_{RS} was 2.56±0.30 mm, while the mean minimum Euclidean distance between

the left ventricle myocardium RCA_{MCP} and RCA_{RS} was 3.60±1.08 mm. Overlap of left ventricle myocardium LCA_{MCP} with LCA_{RS} yielded a mean Dice's similarity coefficient of 0.97±0.01. Overlap of left ventricle myocardium RCA_{MCP} with RCA_{RS} yielded a mean Dice's similarity coefficient of 0.86±0.06. Spatial correspondence of the left ventricle myocardial perfusion territories is further described in **Table 3.4a**. The mean minimum Euclidean distance between right ventricle myocardium LCA_{MCP} and LCA_{RS} was 9.01±2.78 mm, while the mean minimum Euclidean distance between the right ventricle myocardium RCA_{MCP} and RCA_{RS} was 7.05±3.02 mm. Overlap of right ventricle myocardium LCA_{MCP} with LCA_{RS} yielded a mean Dice's similarity coefficient of 0.86±0.04. Overlap of right ventricle myocardium RCA_{MCP} with RCA_{RS} yielded a mean Dice's similarity coefficient of 0.87±0.05. Spatial correspondence of the right ventricle myocardial perfusion territories is further described in **Table 3.4b**.

Spatial Correspondence of Whole Heart MCP Perfusion Territories

Spatial correspondence of MCP to reference standard perfusion territories was performed on MCP territories derived for the whole heart by combining both left and right ventricular masks. The mean minimum Euclidean distance between the whole heart myocardium LCA_{MCP} and LCA_{RS} was 4.10±0.86 mm, while the mean minimum Euclidean distance between the whole heart myocardium RCA_{MCP} and RCA_{RS} was 4.65±1.67 mm. Overlap of LCA_{MCP} with LCA_{RS} yielded a mean Dice's similarity coefficient of 0.96±0.01 in the whole heart myocardium. Overlap of RCA_{MCP} with RCA_{RS} yielded a mean Dice's similarity coefficient of 0.87±0.05 in the whole heart myocardium. Whole heart MCP perfusion territory spatial correspondence is detailed in **Figure 3.3c**.

LAD_{MCP}, LCx_{MCP}, and Myocardium At-Risk

Beyond validation of LCA_{MCP}, preliminary analysis of LAD_{MCP} and LCx_{MCP} was also performed, and compared with previously reported LAD and LCx left ventricle mass distributions[85]. Myocardial mass and mass-percent distributions of LAD_{MCP}, LCx_{MCP} and RCA_{MCP} are provided in **Table 3.5**. Furthermore, MCP was also used to simulate assessment of myocardium at-risk, distal to a simulated stenosis in one animal, as described in **Figure 3.5**. The figure shows that it is possible to determine myocardial mass at risk distal to a stenosis.

Discussion

General Discussion

Le et al.[47] initially validated a method to quantify coronary perfusion territories. The MCP technique improves Le et al.'s method by constraining distance calculations between myocardial voxels and coronary arteries within the myocardial tissue volume, rather than through unbound space. In the current study, both LCA_{MCP} and RCA_{MCP} showed excellent correspondence to LCA_{RS} and RCA_{RS}, respectively, throughout the whole heart, including the right ventricle. However, as the swine in this study all had an average heart rate of 80 beats per minute, motion artifacts were common, causing incomplete segmentation of the right ventricle and RCA, especially with respect to the septal branch of the posterior descending coronary artery. Hence, higher discordance was seen between RCA_{MCP} and $RCA_{RS,}$ likely due to suboptimal assignment of the posterior septum. Additionally, the mean minimum Euclidean distance between right ventricle MCP and reference standard perfusion territories was much higher than that of

the left ventricle, due to suboptimal right ventricle reference standard territory segmentation. Overall, however, MCP showed excellent agreement with reference standard perfusion territories.

Comparison to Previously Reported Methods

Previous studies have proposed several techniques to improve the assessment of coronary perfusion territories[47, 83-87]. Currently, the AHA 17-segment model[76] is widely used, but several reports demonstrate its limitations[77-81]. An improved model-based approach to determining coronary perfusion territories has been proposed[86], but is still limited by a predefined model.

Other methods to determine vessel-specific coronary perfusion territories[84, 85, 87], based on Seiler et al.[46], have also been proposed, where each voxel of the left ventricular myocardium is assumed to be perfused by its nearest coronary artery. Faber et al.[87] applied Seiler's method using CT angiography and SPECT for validation ($Mass_{Faber}$ = $0.92Mass_{SPECT}$ + 10.32 g, R^2 = 0.59). Kurata et al.[84] conducted a study to assess the accuracy of CTA-derived myocardium at-risk using the Voronoi algorithm and SPECT for validation (r = 0.81 [0.74, 0.87] and mass error = 10%). Ide et al.[85] also conducted a histological validation of CTA-derived perfusion territories for the LAD, LCx and RCA using the Voronoi algorithm and *ex vivo* porcine hearts (r = 0.92 for LAD; r = 0.96 for LCx; r = 0.96 for RCA). Additionally, methods to determine coronary perfusion territories using coronary magnetic resonance have also been proposed[83], but require invasive cannulation of each coronary artery. However, in nearly all previously reported

methods, quantification of coronary perfusion territories was only performed on the left ventricle and only mass correspondence analysis was provided.

In comparison to these prior studies, the MCP technique performs equivalently with respect to mass correspondence analysis. Furthermore, the MCP technique was also assessed for spatial correspondence. These spatial correspondence metrics, such as Dice's similarity coefficient and mean minimum Euclidean distance, show that the MCP technique can accurately determine the spatial distribution of the LCA and RCA perfusion territories in the left ventricle, as well as in the right ventricle and whole heart. Additionally, while direct validation of LAD_{MCP} and LCx_{MCP} was not evaluated in this study, comparisons to mass distributions of LAD, LCx and RCA perfusion territories in the left ventricle, as previously reported by Ide et al.[85], show that MCP has the potential to provide accurate assessment of the LAD and LCx perfusion territories. Finally, preliminary evaluation of myocardium at-risk distal to a stenosis using MCP illustrates that a clinically significant myocardial defect could be discerned.

Study Limitations

There were limitations associated with this study. First, this study utilized a swine model with high heart rates and significant motion artifact in some cases. The thin right ventricle wall is especially susceptible to motion artifact, causing difficulties in blush segmentation and underestimation of right ventricle mass. To amend this, a dedicated study to further validate the MCP technique in the right ventricle could be implemented, with systolic phase reconstructions used instead. By reconstructing systolic phase

datasets, the right ventricular myocardium would be thicker, allowing for more consistent segmentation of right ventricle myocardial blush. This study also was performed on a small sample size; further assessment of the MCP technique on a larger population is still necessary. Additionally, this study utilized healthy swine without CAD. Further investigation is necessary to fully understand how significant CAD will affect the performance of the MCP technique. For example, in the case of a complete coronary occlusion where digital extraction of the coronary artery distal to the occlusion is not possible, the MCP technique may be limited. Yet, given recent work illustrating reliable coronary centerline extraction in patients with coronary calcification and stents[95], it is anticipated that the MCP technique will be able to accurately determine vessel-specific perfusion territories, even in the presence of moderate focal or diffuse CAD. Beyond CAD, the MCP technique will be limited in assessing collateralization, as they may be too small to visualize.

It is also important to note that in this study, the left ventricle, right ventricle and whole heart MCP perfusion territories were derived using a dynamic CT acquisition, rather than a standard CTA acquisition. However, such an acquisition scheme was used solely to validate MCP in the right ventricle and whole heart, but is not necessary for MCP in the left ventricle. Specifically, MCP in the left ventricle can be derived using only a standard CTA dataset to yield left ventricle, coronary-specific perfusion territories. Hence, the MCP technique could be integrated with current clinical CTA methods to provide assessment of coronary perfusion territories in the left ventricle. Nevertheless, whole heart and right ventricle assessment using the MCP technique require

simultaneous coronary and biventricular opacification. Fortunately, low-dose clinical CTA examinations that acquire biventricular and coronary opacification have already been proposed and implemented using a 64-slice CT system[96]. Additionally, CT perfusion conveniently acquires biventricular and coronary opacification, as well as myocardial perfusion, in a single low dose examination[97-99]. While CT was used exclusively in this study, the MCP technique has the potential to be applied to any imaging modality that provides an image of the myocardium and coronary arteries.

Conclusions

The MCP technique may provide a means to objectively delimit vessel-specific perfusion territories in the heart. Using mass correspondence, as well as spatial correspondence, such as mean minimum Euclidean distance and Dice's similarity coefficient, the MCP technique has been robustly validated in the left and right ventricular myocardium, as well as in the whole heart. Furthermore, it is anticipated that the MCP technique may have the potential to accurately assign the coronary perfusion territories of the LAD and LCx, as well as quantify the myocardial mass at-risk distal to a stenosis, although further validation is necessary. Thus, given the results, the MCP technique has the potential to improve CAD assessment through accurate and automatic delineation of vessel-specific myocardial perfusion territories using CT angiography data.

Tables:

Table 3.1: Per-animal results for LCA and RCA territories, in the (a) left ventricle, (b) right ventricle, and (c) whole heart myocardium.

(a) Left Ventricle		**LCA**		**RCA**	
	Injection Site	M_{MCP}(g)	M_{RS}(g)	M_{MCP}(g)	M_{RS}(g)
Animal 1	LCA	54.27[79.53%]	53.60[78.56%]	13.96[20.47%]	14.63[21.44%]
	RCA		50.47[74.56%]		17.22[25.44%]
Animal 2	LCA	62.14[82.72%]	61.30[81.59%]	12.98[17.28%]	13.83[18.41%]
	RCA		63.75[84.86%]		11.38[15.14%]
Animal 3*	LCA	52.70[83.73%]	55.46[88.13%]	10.24[16.27%]	7.47[11.87%]
Animal 4	LCA	40.60[76.88%]	40.75[77.17%]	12.21[23.12%]	12.06[22.83%]
	LCA		39.69[75.16%]		13.12[24.84%]
	RCA		39.95[75.65%]		12.86[24.35%]
	RCA		39.67[75.13%]		13.14[24.87%]
Animal 5	LCA	70.42[81.04%]	71.25[82.01%]	16.47[18.96%]	15.63[17.99%]
	LCA		68.90[79.30%]		17.99[20.70%]
	RCA		70.15[80.74%]		16.73[19.26%]
	RCA		70.36[80.98%]		16.53[19.02%]
Animal 6	LCA	55.57[85.72%]	57.42[88.58%]	9.26[14.28%]	7.40[11.42%]
	RCA		54.23[83.65%]		10.60[16.35%]
(b) Right Ventricle		**LCA**		**RCA**	
	Injection Site	M_{MCP}(g)	M_{RS}(g)	M_{MCP}(g)	M_{RS}(g)
Animal 1	LCA	3.86[31.26%]	3.59[29.04%]	8.49[68.74%]	8.77[70.96%]
	RCA		3.64[29.44%]		8.71[70.56%]
Animal 2	LCA	7.20[43.47%]	8.89[53.72%]	9.36[56.53%]	7.66[46.28%]
	RCA		6.77[40.92%]		9.78[59.08%]
Animal 3*	LCA	5.49[47.43%]	6.92[59.79%]	6.09[52.57%]	4.66[40.21%]
Animal 4	LCA	6.08[57.34%]	7.40[69.79%]	4.52[42.66%]	3.20[30.21%]
	LCA		5.87[55.36%]		4.73[44.64%]
	RCA		5.35[50.39%]		5.26[49.61%]
	RCA		4.86[45.80%]		5.75[54.20%]
Animal 5	LCA	5.45[34.18%]	7.87[49.38%]	10.50[65.82%]	8.07[50.62%]
	LCA		5.82[36.52%]		10.12[63.48%]
	RCA		4.43[27.80%]		11.51[72.20%]
	RCA		4.51[28.29%]		11.43[71.71%]
Animal 6	LCA	2.61[23.54%]	2.27[20.48%]	8.46[76.46%]	8.80[79.52%]
	RCA		2.59[23.37%]		8.48[76.63%]
(c) Whole Heart		**LCA**		**RCA**	
	Injection Site	M_{MCP}(g)	M_{RS}(g)	M_{MCP}(g)	M_{RS}(g)
Animal 1	LCA	58.13[72.13%]	57.19[70.97%]	22.46[27.87%]	23.40[29.03%]
	RCA		54.10[67.60%]		25.93[32.40%]
Animal 2	LCA	69.34[75.64%]	70.19[76.56%]	22.34[24.36%]	21.49[23.44%]
	RCA		70.52[76.92%]		21.16[23.08%]
Animal 3*	LCA	58.19[78.09%]	62.39[83.72%]	16.33[21.91%]	12.13[16.28%]
Animal 4	LCA	46.68[73.61%]	48.15[75.93%]	16.73[26.39%]	15.26[24.07%]
	LCA		45.56[71.85%]		17.85[28.15%]
	RCA		45.30[71.42%]		18.12[28.58%]
	RCA		44.53[70.22%]		18.89[29.78%]
Animal 5	LCA	75.87[73.77%]	79.13[76.95%]	26.97[26.23%]	23.71[23.05%]
	LCA		74.72[72.66%]		28.11[27.34%]
	RCA		74.59[72.53%]		28.25[27.47%]
	RCA		74.87[72.81%]		27.96[27.19%]
Animal 6	LCA	58.18[76.65%]	59.69[78.65%]	17.72[23.35%]	16.21[21.35%]
	RCA		56.81[74.85%]		19.09[25.15%]

*Animal 3 expired after the first LCA intracoronary contrast injection acquisition.
Data expressed as mass [percent mass].(LCA = left coronary artery, M_{MCP} = mass of minimum-cost path coronary territory, M_{RS} = mass of reference standard coronary territory, RCA = right coronary artery)

Table 3.2. Mass correspondence of MCP and reference standard coronary perfusion territories in the (a) left ventricle, (b) right ventricle and (c) whole heart myocardium.

(a) Left Ventricle

	LCA		**RCA**	
	$Mass_{MCP}$ (g)	$Mass_{RS}$ (g)	$Mass_{MCP}$ (g)	$Mass_{RS}$ (g)
Animal 1	54.00	52.04±2.22	13.96	15.92±1.83
Animal 2	62.14	62.52±1.73	12.98	12.6±1.73
Animal 3*	52.70	55.46	10.24	7.47
Animal 4	40.60	40.02±0.51	12.21	12.79±0.51
Animal 5	70.42	70.17±0.97	16.47	16.72±0.97
Animal 6	55.57	55.82±2.26	9.26	9.00±2.26
MEAN±STD	55.90±9.98	56.00±10.15	12.52±2.60	12.42±3.66

(b) Right Ventricle

	LCA		**RCA**	
	$Mass_{MCP}$ (g)	$Mass_{RS}$ (g)	$Mass_{MCP}$ (g)	$Mass_{RS}$ (g)
Animal 1	3.86	3.61±0.03	8.49	8.74±0.04
Animal 2	7.20	7.83±1.50	9.36	8.72±1.50
Animal 3*	5.49	6.92	6.09	4.66
Animal 4	6.08	5.87±1.10	4.52	4.74±1.10
Animal 5	5.45	5.66±1.61	10.50	10.29±1.61
Animal 6	2.61	2.43±0.23	8.46	8.64±0.23
MEAN±STD	5.11±1.64	5.39±2.03	7.90±2.20	7.63±2.35

(c) Whole Heart

	LCA		**RCA**	
	$Mass_{MCP}$ (g)	$Mass_{RS}$ (g)	$Mass_{MCP}$ (g)	$Mass_{RS}$ (g)
Animal 1	57.86	55.65±2.18	22.46	24.67±1.80
Animal 2	69.34	70.35±0.23	22.34	21.32±0.23
Animal 3*	58.19	62.39	16.33	12.13
Animal 4	46.68	45.89±1.57	16.73	17.53±1.58
Animal 5	75.87	75.83±2.20	26.97	27.01±2.20
Animal 6	58.18	58.25±2.03	17.72	17.65±2.04
MEAN±STD	61.02±10.21	61.39±10.70	20.60±4.42	20.18±5.69

****Animal 3 expired after only one intracoronary contrast injection acquisition***

Data expressed as mass, or mean mass ± standard deviation.

(LCA = left coronary artery, $Mass_{MCP}$ = mass of minimum-cost path coronary territory, $Mass_{RS}$ = mass of reference standard coronary territory, RCA = right coronary artery)

Table 3.3: Linear regression analysis of MCP and reference standard perfusion territories in the (a) left ventricle, (b) right ventricle and (c) whole heart myocardium.

(a) Left Ventricle

	Linear Regression	RMSE (g)	Adj. R^2	CCC	r
LCA	$Mass_{MCP} = 0.97Mass_{RS} + 1.48$ g	1.71	0.97 [0.75, 1.00]	0.99 [0.89, 1.00]	0.99 [0.89, 1.00]
RCA	$Mass_{MCP} = 0.66Mass_{RS} + 4.29$ g	1.05	0.84 [0.08, 0.98]	0.88 [0.24, 0.99]	0.93 [0.50, 0.99]
LCA+RCA	**$Mass_{MCP} = 0.99Mass_{RS} + 0.35$ g**	**1.54**	**0.99 [0.98, 1.00]**	**1.00 [0.99, 1.00]**	**1.00 [0.99, 1.00]**

(b) Right Ventricle

	Linear Regression	RMSE (g)	Adj. R^2	CCC	r
LCA	$Mass_{MCP} = 0.77Mass_{RS} + 0.95$ g	0.53	0.90 [0.30, 0.99]	0.93 [0.46, 0.99]	0.96 [0.65, 1.00]
RCA	$Mass_{MCP} = 0.90Mass_{RS} + 1.06$ g	0.69	0.90 [0.34, 0.99]	0.95 [0.61, 0.99]	0.96 [0.67, 1.00]
LCA+RCA	**$Mass_{MCP} = 0.94Mass_{RS} + 0.39$ g**	**0.71**	**0.91 [0.70, 0.97]**	**0.96 [0.85, 0.99]**	**0.96 [0.85, 0.99]**

(c) Whole Heart

	Linear Regression	RMSE (g)	Adj. R^2	CCC	r
LCA	$Mass_{MCP} = 0.93Mass_{RS} + 3.65$ g	2.28	0.95 [0.60, 0.99]	0.98 [0.79, 1.00]	0.98 [0.82, 1.00]
RCA	$Mass_{MCP} = 0.72Mass_{RS} + 5.94$ g	1.74	0.83 [0.05, 0.98]	0.90 [0.32, 0.99]	0.93 [0.48, 0.99]
LCA+RCA	**$Mass_{MCP} = 0.97Mass_{RS} + 1.19$ g**	**2.08**	**0.99 [0.97, 1.00]**	**1.00 [0.98, 1.00]**	**1.00 [0.99, 1.00]**

Bolded row is plotted in Figure 3.3.

For Adj. R^2, CCC and r, 95% confidence intervals (CI) are expressed as [CI_{Lower}, CI_{Upper}].

(Adj. R^2 = Adjusted R^2; CCC = concordance correlation coefficient, LCA = left coronary artery, $Mass_{MCP}$ = mass of minimum-cost path coronary territory, $Mass_{RS}$ = mass of reference standard coronary territory, RCA = right coronary artery, RMSE = root-mean-square error)

Table 3.4: Spatial correspondence of MCP and reference standard coronary territories in the (a) left ventricle, (b) right ventricle, and (c) whole heart myocardium.

(a) Left Ventricle

	LCA		**RCA**	
	MMD (mm)	DSC	MMD (mm)	DSC
Animal 1	2.37±0.01	0.97±0.01	2.56±0.16	0.90±0.01
Animal 2	2.38±0.04	0.96±0.01	5.65±3.69	0.82±0.03
Animal 3*	3.03	0.97	3.78	0.79
Animal 4	2.43±0.23	0.97±0.00	3.10±1.05	0.91±0.01
Animal 5	2.28±0.25	0.98±0.00	3.45±1.82	0.91±0.02
Animal 6	2.84±0.33	0.97±0.01	3.06±0.23	0.81±0.06
MEAN±STD	2.56±0.30	0.97±0.01	3.60±1.08	0.86±0.06

(b) Right Ventricle

	LCA		**RCA**	
	MMD (mm)	DSC	MMD (mm)	DSC
Animal 1	4.44±0.36	0.92±0.01	4.23±1.24	0.96±0.00
Animal 2	12.23±0.90	0.86±0.07	5.62±1.82	0.88±0.08
Animal 3*	8.30	0.82	10.08	0.80
Animal 4	11.42±2.72	0.87±0.01	11.42±1.79	0.83±0.05
Animal 5	9.54±2.01	0.87±0.06	4.38±0.91	0.92±0.05
Animal 6	8.14±4.85	0.81±0.11	6.55±3.63	0.94±0.03
MEAN±STD	9.01±2.78	0.86±0.04	7.05±3.02	0.89±0.07

(c) Whole Heart

	LCA		**RCA**	
	MMD (mm)	DSC	MMD (mm)	DSC
Animal 1	2.54±0.25	0.97±0.01	3.04±0.32	0.92±0.01
Animal 2	4.98±2.38	0.95±0.02	5.90±3.69	0.85±0.05
Animal 3*	4.33	0.95	5.36	0.79
Animal 4	4.37±0.50	0.96±0.00	5.92±0.61	0.89±0.02
Animal 5	4.62±1.93	0.97±0.01	3.78±0.78	0.92±0.03
Animal 6	3.75±0.83	0.96±0.01	4.53±1.85	0.88±0.04
MEAN±STD	4.10±0.86	0.96±0.01	4.65±1.67	0.87±0.05

****Animal 3 expired after only one intracoronary contrast injection acquisition***

Data expressed as mean ± standard deviation.

(DSC = Dice's similarity coefficient, LCA = left coronary artery, MMD = mean minimum Euclidean distance, myocardium, RCA = right coronary artery)

Table 3.5: Absolute and relative coronary perfusion distributions for LAD_{MCP}, LCx_{MCP} and RCA_{MCP} in the left ventricle myocardium.

	LAD $Mass_{MCP}(g)$	**LCx** $Mass_{MCP}(g)$	**RCA** $Mass_{MCP}(g)$
Animal 1	36.46[53.65%]	17.54[25.81%]	13.96[20.54%]
Animal 2	38.35[51.05%]	23.79[31.67%]	12.98[17.28%]
Animal 3	31.91[50.71%]	20.78[33.03%]	10.24[16.27%]
Animal 4	28.79[54.52%]	11.81[22.36%]	12.21[23.12%]
Animal 5	43.94[50.57%]	26.48[30.47%]	16.47[18.96%]
Animal 6	32.03[49.40%]	23.54[36.32%]	9.26[14.28%]
MEAN±STD	35.25±5.47[51.65±1.99%]	20.66±5.29[29.94±5.06%]	12.52±2.60[18.41±3.16%]
Ide et al.[85]	49.8%	32.2%	25.9%

Data expressed as mass [percent mass], or mass ± standard deviation [percent mass ± standard deviation].

(LAD = left anterior descending coronary artery, LCx = left circumflex coronary artery, M_{MCP} = mass of Minimum-Cost Path-derived coronary territory, RCA = right coronary artery)

Figures:

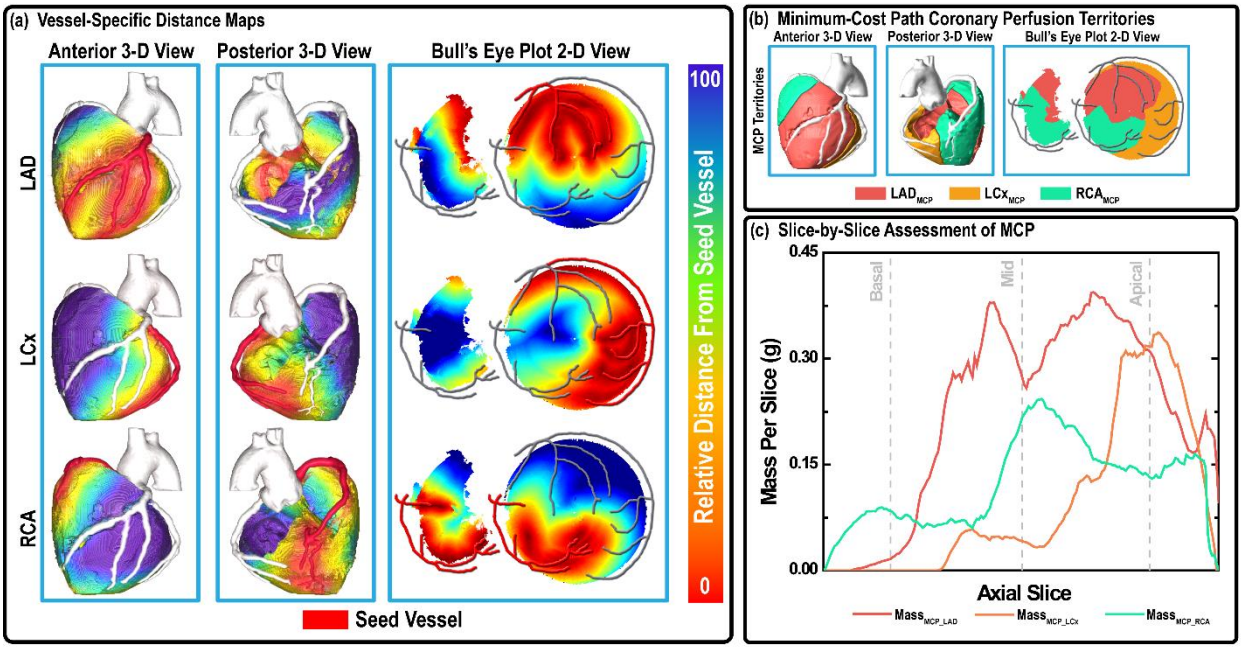

Figure 3.1: Minimum-Cost Path assignment method summary. (a) Distance maps through a whole heart myocardial mask were generated for the LAD, LCx and RCA, using the Fast-Marching algorithm and respective vessel centerline as seed points (red). (b) These distance maps were used to determine the minimum-cost path of each myocardial voxel to each coronary artery, yielding three discrete vessel perfusion territories for each coronary artery in the whole heart. (c) Assessment of mass distribution of LAD_{MCP}, LCx_{MCP} and RCA_{MCP} is also provided, on a per-axial slice basis in the whole heart. This method was applied using only the left ventricle and right ventricle masks, independently, in the same manner, to yield left ventricle and right ventricle MCP territories.

(2-D = Two Dimensional, 3-D = Three-Dimensional, LAD = left anterior descending coronary artery, LAD_{MCP} = Minimum-Cost Path assigned LAD myocardial perfusion territory, LCx = left circumflex coronary artery, LCx_{MCP} = Minimum-Cost Path assigned LCx myocardial perfusion territory, RCA = right coronary artery, RCA_{MCP} = Minimum-Cost Path assigned RCA myocardial perfusion territory)

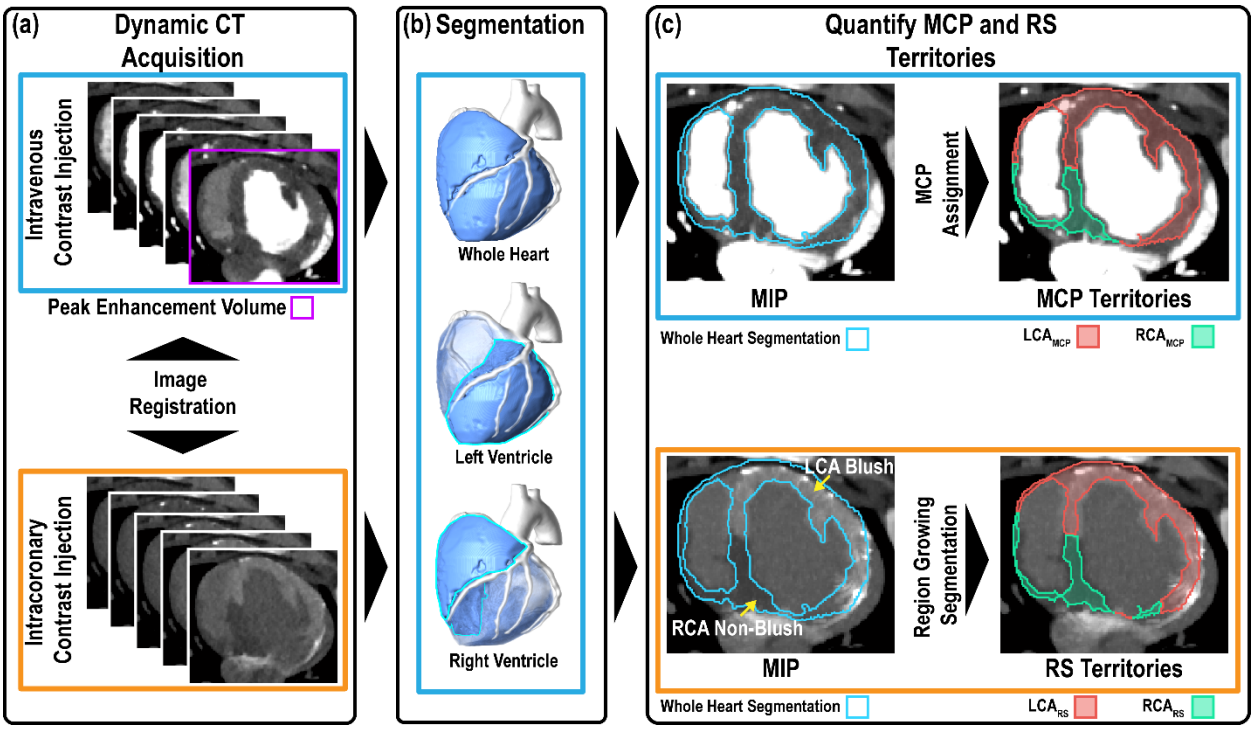

***Figure 3.2:** Image Processing Methods. (a) First, an intracoronary contrast injection CT acquisition was registered to the peak enhancement volume from the intravenous contrast injection CT acquisition from the same animal. (b) MCP assignment was then performed on the segmented whole heart to yield LCA_{MCP} and RCA_{MCP}, while automated region growing segmentation was performed on the intracoronary contrast injection MIP, using the same whole heart segmentation. Panels outlined in blue depict steps performed on intravenous contrast injection data, while panels outlined in orange depict steps performed on intracoronary contrast injection data. The images shown were acquired from the same animal. While processing in the whole heart is depicted, the same steps were followed, using left and right ventricle masks to derive MCP perfusion territories.*

(LCA = left coronary artery, LCA_{MCP} = minimum-cost path assigned LCA myocardial perfusion territory, LCA_{RS} = reference standard LCA myocardial perfusion territory, MCP = minimum-cost path assignment, MIP = maximum intensity projection image, RCA = right coronary artery, RCA_{MCP} =minimum-cost path assigned RCA myocardial perfusion territory, RCA_{RS} = reference standard RCA myocardial perfusion territory)

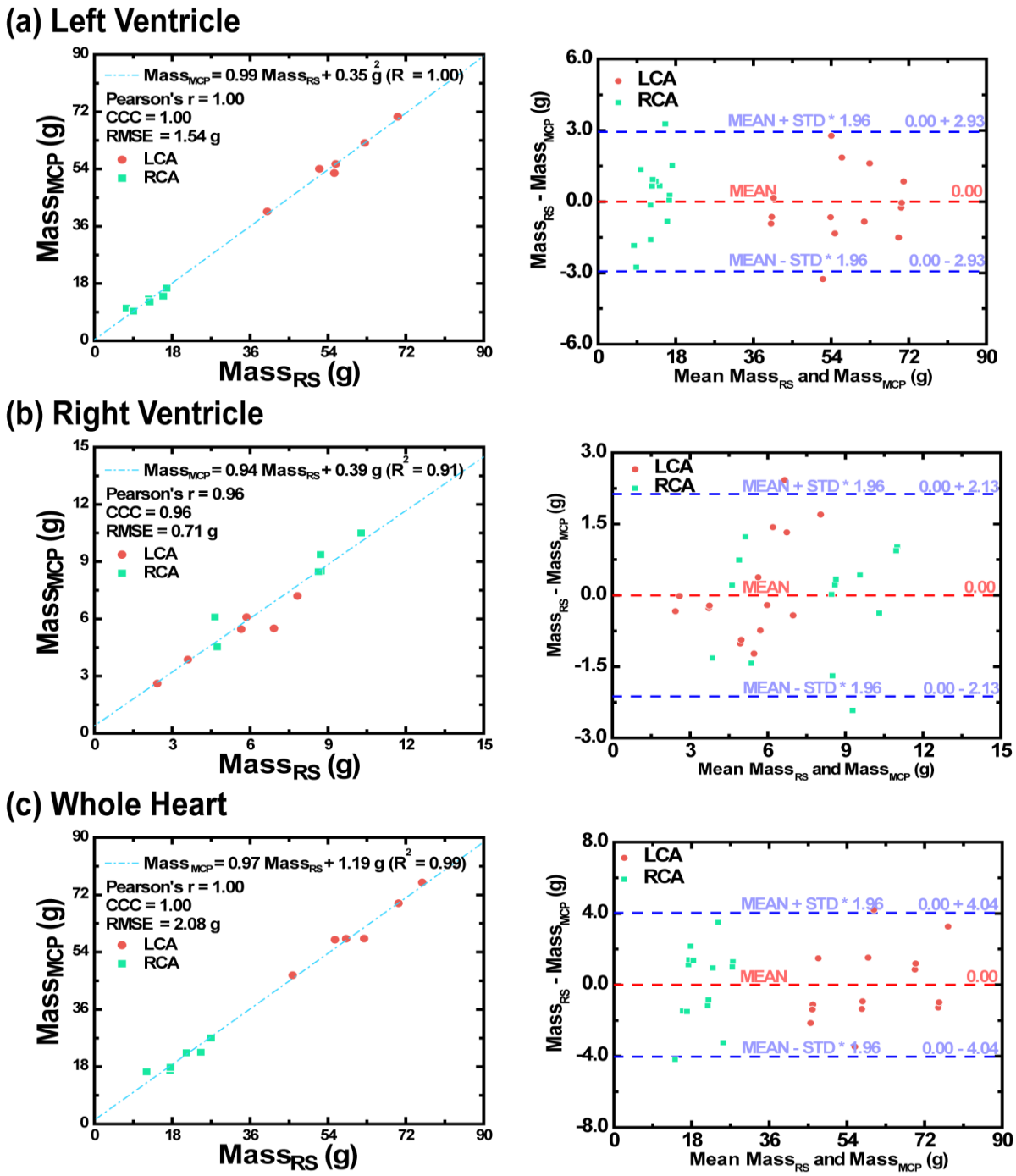

Figure 3.3: *Linear regression and Bland-Altman analysis of mass correspondence of M_{MCP} and M_{RS} for LCA and RCA territories, in the (a) left ventricle, (b) right ventricle, and (c) whole heart myocardium. Linear regression analysis displayed above was computed using both LCA and RCA correspondence together.*
(CCC = concordance correlation coefficient; LCA = left coronary artery; $Mass_{MCP}$ = mass of minimum-cost path-derived coronary territory; $Mass_{RS}$ = mass of reference standard coronary territory; RCA = right coronary artery; RMSE = root-mean-square error)

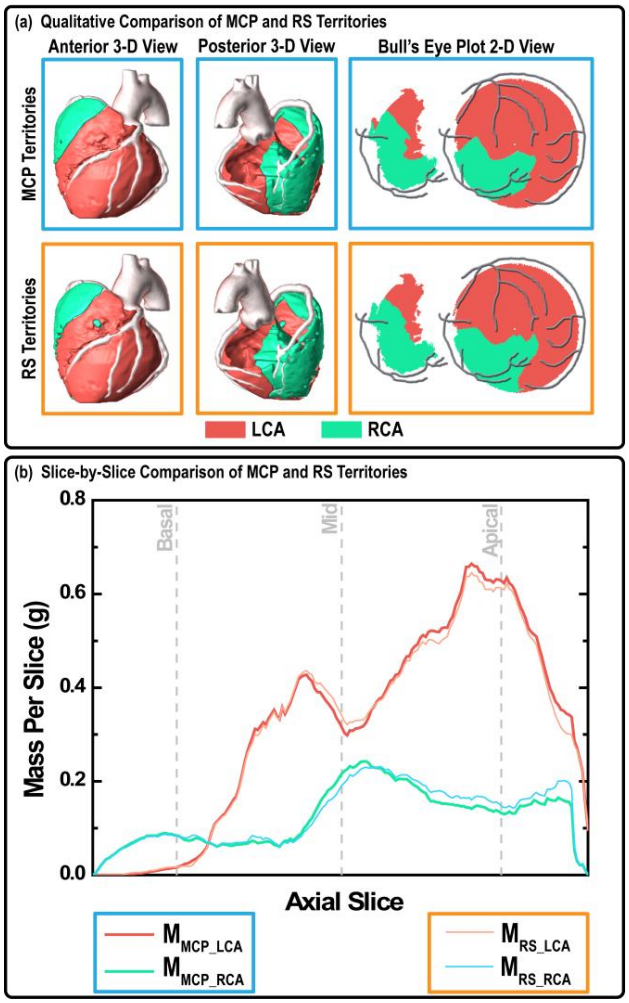

Figure 3.4: Whole heart slice-by-slice analysis of mass correspondence of MCP and reference standard myocardial perfusion territories from a single animal. Slice-by-slice comparison was performed using the Animal 1 dataset. (a) LCA_{MCP} and RCA_{MCP} (blue panels), and LCA_{RS} and RCA_{RS} (orange panels) volumes are shown. Anterior and posterior 3-D volumetric views of MCP and reference standard territories are shown. Right and left ventricle 2-D bull's eye plot projections of MCP and reference standard territories are also shown. The right ventricle 2-D bull's eye plot projection is shown superimposed with the RCA vessel centerline. The left ventricle 2-D bull's eye plot projection is shown superimposed with the LAD, LCx and RCA vessel centerlines. Quantitative, slice-by-slice analysis is performed by comparing the $Mass_{MCP\_LCA}$ and $Mass_{RS\_LCA}$, as well as $Mass_{MCP\_RCA}$ and $Mass_{RS\_RCA}$.

(2-D = Two Dimensional, 3-D = Three Dimensional, MCP = minimum-cost path assignment, LCA = left coronary artery, $Mass_{MCP\_LCA}$ = minimum-cost path assigned LCA myocardial perfusion territory, $Mass_{RS\_LCA}$ = reference standard LCA myocardial perfusion territory, RCA = right coronary artery, $Mass_{MCP\_RCA}$ = minimum-cost path assigned RCA myocardial perfusion territory, $Mass_{RS\_RCA}$ = reference standard RCA myocardial perfusion territory, RS = reference standard)

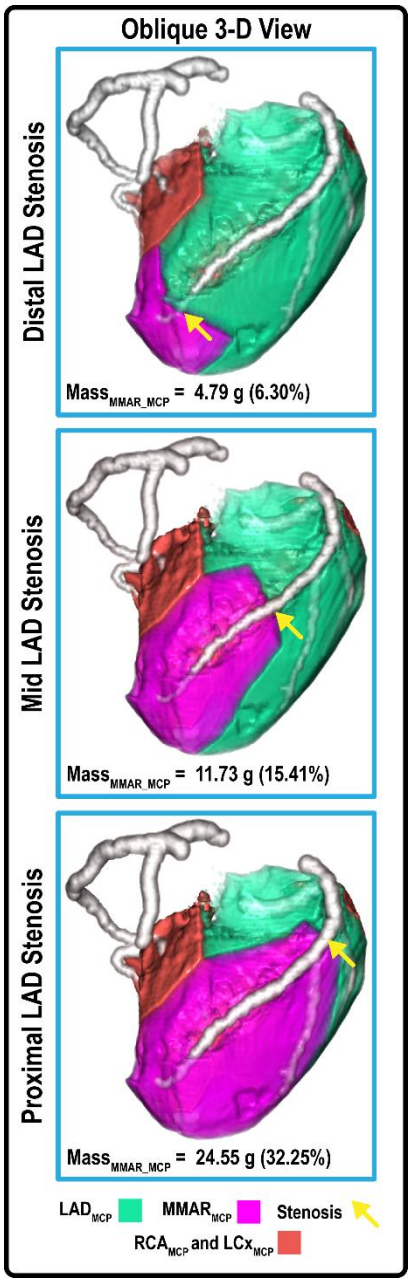

Figure 3.5: Evaluation of myocardium at-risk distal of a stenosis in the LAD, using MCP. An increasingly proximal stenosis was simulated in the LAD. MCP was then used to determine the myocardial mass at-risk distal of the stenosis, in each case. Mass of myocardium at-risk distal of each stenosis is reported as MASS (MASS PERCENT OF TOTAL LEFT VENTRICULAR MYOCARDIUM).

(3-D = Three-Dimensional, LAD = left anterior descending coronary artery, LAD_{MCP} = minimum-cost path assigned LAD myocardial perfusion territory, LCx = left circumflex coronary artery, LCx_{MCP} = minimum-cost path assigned LCx myocardial perfusion territory, $MMAR_{MCP}$ = minimum-cost path assigned myocardial mass at-risk; RCA = right coronary artery, RCA_{MCP} = minimum-cost Path assigned RCA myocardial perfusion territory)

CHAPTER 4: ACCURACY OF RELATIVE PERFUSION MEASUREMENT AS COMPARED TO INVASIVE FRACTIONAL FLOW RESERVE MEASURMENT IN SWINE

Abstract

Computed tomography (CT) angiography is an important tool for evaluation of coronary artery disease (CAD), but often correlates poorly with myocardial ischemia. Current dynamic CT perfusion techniques can assess ischemia but have limited accuracy and deliver high radiation dose. Therefore, an accurate, low-dose, dynamic CT perfusion technique is needed**.** A total of 20 contrast enhanced CT volume scans were acquired in 5 swine (40 ± 10 kg) to generate CT angiography and perfusion images. Varying degrees of stenosis were induced using a balloon catheter in the proximal left anterior descending (LAD) coronary artery and a pressure wire was used for reference fractional flow reserve (FFR) measurement. Perfusion measurements were made with only two volume scans using a new first-pass analysis (FPA) technique and with 20 volume scans using an existing maximum slope model (MSM) technique. Perfusion (P) and FFR measurements were related by P_{FPA} = 1.01 FFR - 0.03 (R^2 = 0.85) and P_{MSM} = 1.03 FFR - 0.03 (R^2 = 0.80) for FPA and MSM techniques, respectively. Additionally, the effective radiation doses were calculated to be 2.64 and 26.4 mSv for FPA and MSM techniques, respectively. A new FPA-based dynamic CT perfusion technique was validated in a swine animal model. The results indicate that the FPA technique can potentially be used for improved anatomical and functional assessment of CAD at a relatively low radiation dose.

Introduction

Coronary artery disease (CAD) is the leading cause of morbidity and mortality worldwide, with extensive CAD and its resultant ventricular dysfunction strongly predictive of future cardiac events. Fortunately, morbidity and mortality are significantly reduced when patients are risk stratified using computed tomography (CT) angiography[3, 4] and treated appropriately with medical therapy or revascularization[1, 71]. However, CT angiography is fundamentally limited in that lesion severity is based solely on lesion morphology; hence, vessel collateralization, coronary calcification, and image artifacts confound diagnostic results[3, 4, 10]. Furthermore, subjective visual grading of lesions results in high intra- and interobserver variability[6, 7, 100], with poor correlation between lesion severity and myocardial ischemia, especially for intermediate stenoses (30-70% luminal narrowing)[2, 9, 10]. Hence, CT angiography alone cannot fully characterize coronary lesions[2, 101], and functional assessment techniques, in concert with CT angiography, are needed for more objective indication of coronary lesion significance[6, 7, 100, 102-104]. As an initial solution, many dynamic CT perfusion techniques, such as the maximum slope model (MSM), have been developed and implemented using 64-slice CT technology, with recent reports confirming the value of dynamic CT perfusion in the functional assessment of CAD[31, 32, 35]. In general, these techniques monitor myocardial uptake of contrast material, i.e., changes in myocardial enhancement, within a tissue slab of interest over time to derive relevant perfusion data. Unfortunately, despite positive correlation with single-photon emission computed tomography (SPECT)[32] and invasive fractional flow reserve (FFR)[31, 105], such techniques are inaccurate and underestimate absolute perfusion[38]. Specifically, most

dynamic CT perfusion techniques operate under the assumption that contrast material does not exit the myocardial tissue volume-of-interest (VOI) over the measurement time. However, due to the limited cranio-caudal coverage of 64-slice CT technology, such techniques utilize small tissue VOIs to derive perfusion. Thus, when considering the myocardial transit time of 3-5 seconds from coronary artery to coronary sinus at maximal hyperemia[39], significant contrast material loss from those small VOIs is unavoidable, resulting in underestimation of perfusion. Furthermore, due to the poor signal-to-noise ratio (SNR) associated with small volume measurement, such techniques require image acquisition over many cardiac cycles to generate reliable perfusion metrics, leading to cumulative radiation doses of up to 10-15 mSv per exam[37, 40, 42]. While some radiation dose reduction is possible through tube voltage (kVp) and photon fluency (mAs) optimization, as well as through iterative reconstruction[43, 66], the fundamental limitations of measurement inaccuracy and large radiation dose have hampered dynamic CT perfusion's widespread clinical utility.

To overcome such obstacles, this study validated a new CT-based approach to anatomical and functional assessment of CAD. Specifically, simultaneous acquisition of CT angiography and dynamic CT perfusion data with a whole-heart CT scanner, combined with a novel first-pass analysis (FPA) technique, enables reliable assessment of CAD, with invasive fractional flow reserve (FFR) as the reference standard. Further, by using a two volume scan acquisition protocol, both the radiation and contrast dose per exam can be reduced, making comprehensive CT-based evaluation of CAD more accessible and impactful to patients in need.

Materials and Methods

First-Pass Analysis Model

Our low-dose dynamic CT perfusion technique is based on a first-pass analysis (FPA) model and conservation of contrast material mass[56, 59]. Specifically, any coronary perfusion territory distal to a stenosis may be modeled as a single compartment with a unique entrance and exit vessel, as described in **Figure 4.1**. By definition, the compartmental perfusion (P_{FPA}) is proportional to the mass of contrast material that accumulates in the compartment per unit time (dM_C/dt), divided by the incoming contrast concentration (C_{in}) and compartment tissue mass (M_T), prior to significant contrast exit. Using cardiac CT data, dM_C/dt may be derived from the change in integrated Hounsfield Units (HU) within the compartment, while C_{in} may be estimated from the arterial input function (AIF)[45].

$$\boldsymbol{P_{FPA} = \left(M_T^{-1} C_{in}^{-1} \frac{dM_c}{dt}\right)_{ave}} \qquad \textbf{(1)}$$

As previously reported[45], only two volume scans, denoted as V1 and V2 in **Figure 4.2**, are necessary for perfusion measurement with our FPA technique. V1 is used for dynamic CT perfusion measurement and is the first volume scan after the AIF exceeds 180 HU, while V2 is used for both dynamic CT perfusion measurement and CT angiography and is the first volume scan after the AIF reaches its peak. In general, such volume scans always occur less than five seconds apart and ensure that the maximum rate of contrast material mass accumulation (dM_C/dt) in any perfusion compartment of interest is always captured for dynamic CT perfusion measurement prior to significant

contrast exit, while maximal coronary opacification is always achieved for CT angiography.

Maximum Slope Model

The maximum slope model (MSM) is a dynamic CT perfusion technique that defines perfusion (P_{MSM}) as the maximum upslope of the tissue time attenuation curve (TAC), divided by the maximum of the AIF and tissue density (ρ). In general, the MSM generates tissue TACs using small volumes-of-interest (VOI), on the order of 1.5 cm^2 x 0.5 cm each, that are placed in a coronary perfusion territory of interest distal to a stenosis and assumes no contrast exit from those VOIs over the measurement time. Unfortunately, given the low SNR of the resulting tissue TACs, the maximum upslope is difficult to determine, therefore, the average upslope is more often used[37, 38], as seen in ***Equation 2.***

$$\boldsymbol{P_{MSM}} = \frac{ave\left(\frac{d}{dt}(\boldsymbol{TAC})\right)}{max(\boldsymbol{AIF})} \cdot \frac{\mathbf{1}}{\boldsymbol{\rho}} \qquad \textbf{(2)}$$

Animal Preparation

The study was approved by the animal care committee and institutional review board for the care of animal subjects and was performed in agreement with the position of the American Heart Association on research animal use. Specifically, an animal model was created that allowed several levels of single vessel disease to be induced in the proximal left anterior descending (LAD) coronary artery. Sex-based differences in disease were not present; hence, five male Yorkshire swine (weight: 40 ± 10 kg) were

sufficient for validation of the FPA technique. Anesthesia was induced with Telazol (4.4mg/kg), Ketamine (2.2 mg/kg), and Xylazine (2.2 mg/kg). After induction, each animal was intubated (Covedien, Mansfield, MA) and ventilated (Highland Medical Equipment, Temecula, CA) with an oxygen-air-mixture containing 1.5 -2.5% Isoflurane anesthetic (Baxter, Deerfield, IL). ECG, O_2 saturation, temperature, and end-tidal CO_2 were monitored and a warming blanket (HTP-1500, Adroit Medical Systems, Loudon, TN) was used to prevent hypothermia.

The right carotid artery, right femoral artery, and both femoral veins were cannulated under ultrasonic guidance (Vivid E9, GE Healthcare). 6 and 7F sheaths (Terumo Interventional Systems, Somerset, NJ) were placed in the arteries and veins respectively. Blood pressure was monitored from the carotid sheath, the left femoral vein was used for contrast injection, and the right femoral vein was used for drug and fluid administration. Prior to cardiac catheterization, heparin was administered (10,000 unit bolus followed by 1,000 units/hour). A 6F Judkins right guiding catheter (Cordis Corporation, Miami, FL) was used to engage the left main coronary artery and a 0.014" intracoronary pressure wire (PrimeWire PRESTIGE® Pressure Guide Wire, Volcano Corp, Rancho Cordova, CA) was placed into the distal LAD. A balance middleweight (BMW) 0.014" coronary guide wire (Abbott Vascular, Abbott Park, IL) was also placed in the distal LAD and a balloon catheter was passed over the BMW wire into the proximal LAD.

Prior to stenosis induction, intracoronary adenosine was infused at a rate of 240 μg/min (Harvard Apparatus, Model 55-2222) to produce maximal hyperemia in the LAD. Intracoronary adenosine was used rather than intravenous adenosine to prevent reflex-tachycardia-dependent motion artifact, as swine under anesthesia experience profound hypotension from intravenous adenosine. Once hyperemia was achieved in the LAD, the balloon was inflated to induce several different levels of stenosis. Stenosis severity was assessed via fractional flow reserve (FFR) measurement (ComboMap, Volcano Corp., Rancho Cordova, CA). Specifically, FFR is defined as the ratio of pressure distal to a stenosis (P_d) to the pressure proximal to a stenosis (P_a) at maximal hyperemia and has a normal value of 1.0. FFR is particularly useful in characterizing the functional significance of intermediate severity stenoses[106, 107]; hence, it was used as the reference standard for validation of the FPA technique. The entire interventional setup is illustrated in **Figure 4.3**. Finally, after all equipment was in place, each animal was positioned in the CT gantry and imaged. At each stenosis level, reference standard FFR was recorded continuously (MP150, Biopac Systems, Inc., Goleta, CA). Overall, FFRs from 0.4 to 1.0 were evaluated.

CT Imaging Protocol

At each stenosis level, contrast-enhanced (Isovue 370, Bracco Diagnostics, Princeton, NJ) whole-heart imaging was performed with a 320-slice CT scanner (Aquilion One, Toshiba American Medical Systems, Tustin, CA) using 320 x 0.5 mm collimation at 100 kVp and 200 mA. All contrast injections (Empower CTA, Acist Medical Systems, Eden Prairie, MN) were made peripherally (50 mL at 5 mL/s) and were followed by a saline

chaser (25 mL at 5 mL/s). Twenty consecutive volume scans were acquired for MSM implementation. However, only two volume scans less than five seconds apart, denoted as V1 and V2 in **Figure 4.2**, were used for FPA perfusion measurement. For all acquisitions, diastolic-phase images were reconstructed at 75% of the R-R interval using an FC03 kernel with standard beam hardening corrections and a voxel size of 0.43 x 0.43 x 0.5 mm. Full projection data was used to avoid partial scan artifacts, but limited temporal resolution to 0.35 seconds[70]. The dose-length product was also recorded and was converted into effective radiation dose using an adult chest conversion factor of 0.015. However, given that the kV, mA, and volume scan number were all fixed, the effective radiation dose per volume scan was the same for all acquisitions across all animals, independent of animal size.

Image Processing

FPA perfusion was derived in the distal LAD using a novel image processing scheme, as summarized in **Figure 4.4**. First, the volume scans of interest were registered[88] and combined into a single maximum intensity projection (MIP) volume. Semi-automatic segmentation of the MIP was performed, yielding a binary myocardial mask. The coronary vessel centerlines of the LAD, left circumflex coronary artery (LCx), and right coronary artery (RCA) were then extracted with a Vitrea workstation (Vitrea fX ver6.0, Minnetonka, MN, USA). From the myocardial mask and coronary centerlines, vessel-specific myocardial assignment was performed using a minimum-cost-path approach[47, 53], yielding three separate perfusion territories, one for each major coronary vessel, with the LAD territory further partitioned to isolate the diseased distal tissue compartment.

Using the compartment mass, the average of the AIF, and the integrated change in myocardial HU between V1 and V2, FPA perfusion was derived for each acquisition. Finally, MSM perfusion was derived in the distal LAD using a single VOI, measuring 1.5 cm^2 x 0.5 cm, placed within the anterior wall of the left ventricle distal to the stenosis. Given the average rate of dynamic enhancement within that VOI, the maximum of the AIF, and the myocardial density, MSM perfusion was derived for each acquisition.

Relative Perfusion

The FPA technique can accurately measure absolute perfusion[45]. However, for the purposes of this study, absolute perfusion measurement could not be validated against FFR as FFR is a relative metric. Thus, respective absolute perfusion measurements (P_{FPA} and P_{MSM}) were normalized into relative perfusion measurements, where relative perfusion was defined as the ratio of perfusion in the presence of a stenosis to perfusion in the absence of a stenosis, at maximal hyperemia. Such a ratio corrected for the semi-quantitative nature of the MSM technique, enabling one-to-one comparison between FPA and MSM perfusion measurements. Additionally, the ratio enabled validation of two-volume FPA perfusion measurement against reference standard FFR measurement.

Statistical Approach

As a wide range of stenotic disease was evaluated in each animal, with no repeat measurements made per stenosis level, all measurements were assumed to be independent. Relative FPA and MSM perfusion measurements were compared to

reference standard FFR measurements using linear regression and Bland-Altman analysis. The coefficient of determination (R^2), root-mean-square error (RMSE), root-mean-square deviation (RMSD), and concordance correlation coefficient (CCC)[92] were also computed. Based on a recent study, a correlation of at least r = 0.76 was expected between relative perfusion and reference standard FFR measurement[105]. However, as indicated by our previous work[45], the FPA technique improves perfusion measurement correlation. Therefore, given a significance level of 0.05 and a power of 0.80, a sample size of 15 independent measurements was projected to adequately power the study. Finally, the area under the curve (AUC) of the receiver operator characteristic (ROC) was computed, with reference standard FFR measurement less than or equal to 0.8 classified as functionally significant, in order to determine the diagnostic sensitivity and specificity of relative FPA and MSM perfusion measurement in detection of functionally significant stenoses.

Results

The average heart rate and mean arterial pressure (MAP) during imaging were 84 beats per minute and 77 mmHg, respectively, as shown in **Table 4.1.** The average radiation dose of FPA perfusion measurement was 2.64 mSv; much lower than the 26.4 mSv dose of MSM perfusion measurement. Additionally, as indicated by **Table 4.2**, the result of absolute FPA perfusion measurement at baseline and maximal hyperemia agreed well with corresponding quantitative [^{15}O] H_2O PET perfusion measurement reported by the literature[108], while MSM perfusion measurement systematically underestimated flow. As shown in **Figure 4.5**, the result of relative FPA perfusion measurement was in good

agreement with reference standard FFR measurement (P_{FPA} = 1.01 FFR – 0.03 (95% CI = [0.87 1.14]), R^2 = 0.85 (95% CI = [0.74 0.92]) , P < 0.001). The RMSE was 0.07, and Bland-Altman analysis demonstrated negligible systematic measurement bias. The RMSD was 0.07, and the majority of the data fell within the limits of agreement. Additionally, the CCC was found to be ρ = 0.91 (95% CI = [0.84 0.95]), indicating excellent agreement between relative FPA perfusion measurement and reference standard FFR measurement. As shown in **Figure 4.6,** the result of relative MSM perfusion measurement was in good agreement with reference standard FFR measurement (P_{MSM} = 1.03 FFR – 0.03 (95% CI = [0.87 1.18]), R^2 = 0.80 (95% CI = [0.67 0.89]), P < 0.001). The RMSE was 0.08, and Bland-Altman analysis demonstrated negligible systematic measurement bias. The RMSD was 0.08, and the majority of the data fell within the limits of agreement. Additionally, the CCC was found to be ρ = 0.89 (95% CI = [0.81 0.94]), indicating good agreement between relative MSM perfusion measurement and reference standard FFR measurement.

Detection of functionally significant stenoses, classified as having FFRs less than or equal to 0.80, was also evaluated. For relative FPA perfusion measurement, the diagnostic sensitivity, specificity, positive predictive value, and negative predictive value was 93% (95% CI = [78% - 99%]), 79% (95% CI = [49% - 95%]), 90% (95% CI = [74% - 98%]), and 85% (95% CI = [55% - 98%]), respectively, while the diagnostic accuracy was 94% (95% CI = [88% - 100%]), as indicated by the AUC of the ROC in **Figure 4.7a**. For relative MSM perfusion measurement, the diagnostic sensitivity, specificity, positive predictive value, and negative predictive value was 87% (95% CI = [69% - 96%]), 79%

(95% CI = [49% - 95%]), 90% (95% CI = [73% - 98%]), and 73% (95% CI = [45% - 92%]), respectively, while the diagnostic accuracy was 91% (95% CI = [82% - 99%]), as indicated by the AUC of the ROC in **Figure 4.7b**.

Discussion

We have developed a technique to improve anatomical and functional assessment of CAD using whole-heart CT scanner technology and a novel FPA approach. As previously described[45, 56, 59], our technique assumes that contrast material does not exit the myocardial tissue VOI over the measurement time. However, by dramatically increasing the size of that VOI to encompass the entire coronary perfusion territory distal to a stenosis, while also reducing the time necessary to measure perfusion, the problem of contrast material loss from the VOI over the measurement time is eliminated, i.e., the problem of perfusion underestimation[38] is solved. Isolation of entire coronary perfusion territories and reduced measurement time is made possible by whole-heart CT scanner technology[44] which allows the entire heart to be imaged in a single cardiac cycle. Furthermore, such technology enables simultaneous acquisition of CT angiography and dynamic CT perfusion data using a single contrast injection, ultimately reducing radiation and contrast dose to patients per CAD exam. Moreover, the improvements in measurement SNR afforded by whole-heart CT scanner technology and the FPA technique minimizes the number of volume scans necessary for perfusion measurement, reducing the radiation dose to 2.64 mSv; much lower than the 10-15 mSv dose of current dynamic CT perfusion techniques[37, 40-42]. Thus, the proposed FPA technique is novel in its approach to CAD diagnosis and evaluation. By isolating patient-

specific coronary anatomy from CT angiography, low-dose, vessel-specific dynamic CT perfusion measurement in the LAD, LCx and RCA perfusion territories is feasible.

Given the results of the study, the FPA technique performed as well as the MSM technique in characterization of functionally significant lesions, as indicated by the ROC curve analysis, with additional gains in sensitivity and negative predictive value. While both techniques agreed well with reference standard FFR measurement, the FPA technique demonstrated better concordance correlation and tighter limits of agreement, as compared to the MSM technique. Such findings suggest that large reductions in radiation dose are possible, without sacrificing measurement reliability, by using the FPA technique for noninvasive assessment of CAD.

Despite the apparent advantages of the FPA technique, limitations do exist. Specifically, for the purposes of this study, absolute perfusion measurements were normalized into relative perfusion measurements for one-to-one comparison to reference standard FFR, with relative perfusion defined as the ratio of perfusion in the presence of a stenosis to perfusion in the absence of a stenosis, at maximal hyperemia. However, since intracoronary adenosine was used, hyperemic perfusion measurements in the presence and absence of stenoses were derived solely from the distal LAD. This differs from clinical practice in that such a ratio is normally computed using perfusion measurements from diseased and healthy remote perfusion territories. In either case, relative perfusion is still a valuable metric for assessing the functional severity of single vessel disease. However, it cannot accurately assess multi-vessel or balanced three-vessel disease.

Only absolute perfusion (mL/min/g) measurement can overcome such deficiencies[20], enabling evaluation of single vessel, multi-vessel, balanced three-vessel, and even microvascular disease. Fortunately, the FPA technique can also measure absolute perfusion, as previously reported[45] and demonstrated by general comparison to quantitative [^{15}O] H_2O PET from the literature[108]. Specifically, absolute FPA perfusion measurement at baseline was found to be slightly higher than corresponding quantitative PET perfusion measurement. However, such increases in baseline flow are expected and can be attributed to contrast-induced vasodilation[109]. Absolute FPA perfusion measurement at maximal hyperemia was also found to be higher than corresponding quantitative PET perfusion measurement. Such increases in hyperemic flow are also expected, however, as the use of intracoronary adenosine enabled full coronary vasodilation while maintaining a high mean systemic driving pressure; a difficult condition to achieve when using intravenous stress agents due to peripheral vasodilation and systemic pressure drop.

Nevertheless, this study only validated FPA-based assessment of proximal vessel disease as compared to FFR and did not compute branch-specific measurements. While evaluation of such major arterial distributions was sufficient for comparison to FFR, in clinical practice, decision making relies on stress flow mapping of the entire heart. Fortunately, our minimum-cost-path myocardial assignment algorithm enables sub-segmental and branch-specific coronary territory assignment, possibly allowing for more focal FPA perfusion measurement, although further validation is necessary. Furthermore, simultaneous acquisition of whole-heart CT angiography and dynamic CT

perfusion data is not possible with 64-slice CT scanners due to limited cranio-caudal coverage that necessitates helical scanning or step-and-shoot acquisition modes for whole-heart imaging. Hence, widespread utilization of the FPA technique depends largely on the availability of whole-heart imaging systems. Fortunately, such systems are becoming more prevalent. Additionally, 128- and 256-slice CT scanners with eight centimeters of cranio-caudal coverage are also becoming more prevalent, with a recent report[110] indicating that it is possible to image the entire heart within eight centimeters of cranio-caudal coverage if systolic-phase data is acquired during an end-expiratory breath hold. Hence, the reach of our FPA technique may also be extended to clinical centers with 128- and 256-slice CT scanner technology, although further validation is necessary.

The diagnostic performance of the FPA technique is also directly impacted by several error contributors: physiology, physics, protocol, and processing. Regarding physiology, when imaging at heart rates above 65 beats per minute, blurring of coronary vasculature on CT angiography and spatial misalignment of myocardial voxels between temporally separate dynamic CT perfusion images is bound to occur. Fortunately, the FPA technique derives perfusion from the integrated change in HU within large tissue compartments of interest over the measurement time, thus the relative error contributed by motion artifact is small, as such artifacts generally only affect the voxels along a compartment's periphery. As a result, the FPA technique is much less affected by heart-rate-dependent motion artifact, as compared to current dynamic CT perfusion techniques, which rely on small volume imaging. Nevertheless, to minimize the effects

of high heart rate on FPA and MSM computation, intracoronary adenosine was used rather than intravenous adenosine, preventing hypotension and its associated reflex tachycardia, but was invasive and limited the study to the LAD alone. If intravenous adenosine were to be used instead, as is the clinical standard, concurrent beta blockade could help to reduce heart rate, while enabling functional evaluation of all three major coronary perfusion territories. Moreover, deformable image registration can be used for additional improvements in voxel alignment. Specifically, a 3D image-based motion correction algorithm[88] was already integrated into the FPA technique. Finally, with respect to physics, highly attenuating contrast material, as well as metal from the balloon catheter and pressure wire, can generate significant beam hardening artifacts. While manufacturer-specific beam hardening correction algorithms were already used, additional image-based correction algorithms[68] could be implemented.

Regarding the imaging protocol, 20 volume scans were used for MSM computation, at a total radiation dose of 26.4 mSv. However, only two volume scans less than five seconds apart were used for FPA computation, at a total radiation dose of 2.64 mSv, indicating the potential for substantial dose reduction in dynamic CT perfusion. That being said, validation of a true, prospective, two-volume FPA acquisition scheme is still necessary. Fortunately, such a scheme is realizable, with only minor increases in dose, through the use dynamic bolus tracking. Hence, a three- to four-fold reduction in radiation dose is achievable with the FPA technique, as compared to the 10-15 mSv dose of current dynamic CT perfusion techniques[37, 40-42], with additional reduction possible through mA optimization and iterative reconstruction[43, 66]. Finally, with respect

to image processing, vessel-specific FPA perfusion measurement depends on accurate minimum-cost-path myocardial assignment[47, 53]. While our assignment algorithm enables the perfusion compartment distal to any coronary stenosis to be isolated, regardless of stenosis location, the accuracy of assignment depends on the spatial resolution of the CT angiogram, i.e., the more extensive the angiogram, the better the result of assignment. While preliminary data suggest that our angiogram quality and assignment algorithm are sufficient, additional validation to determine the minimum vessel sparseness necessary for accurate assignment is still needed.

Conclusions

The results of this work indicate the potential for low-dose, vessel-specific, anatomical and functional assessment of CAD using the FPA technique, as compared to the MSM technique, with invasive FFR as the reference standard. By validating a combined approach to anatomical and functional assessment of CAD, the FPA technique could improve CAD diagnosis and treatment. Furthermore, by reducing the number of volume scans necessary for reliable perfusion measurement, the FPA technique could substantially reduce both radiation and contrast dose per CAD imaging exam, making CT-based assessment of CAD more accessible and impactful to patients in need.

Tables

Table 4.1: Animal parameters

Parameter	Mean ± SD
Weight (kg)	40 ± 10
HR (beats/min)	84 ± 10.4
MAP (mmHg)	77 ± 9.4

Table 4.2: Comparison of dynamic CT perfusion to quantiative [^{15}O] H_2O PET

Modality	Baseline Perfusion (mL/min/g)	Hyperemic Perfusion (mL/min/g)
PET	1.00 ± 0.25	3.26 ± 1.04
FPA	1.18 ± 0.58	5.44 ± 1.44
MSM	0.54 ± 0.12	1.82± 0.43

Figures

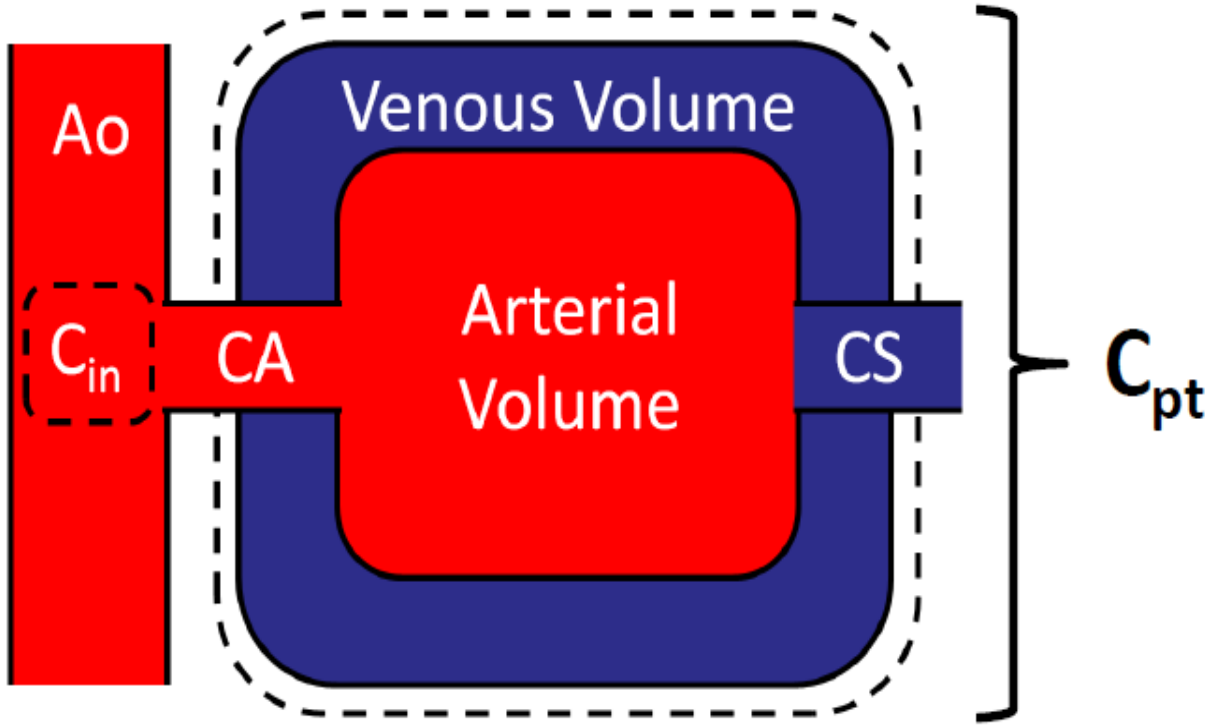

Figure 4.1: Coronary perfusion compartment model used for FPA perfusion measurement, indicating the aortic (Ao) input (Cin), coronary artery of interest (CA), distal perfusion territory of interest (Cpt), and coronary sinus (CS). The compartment tissue mass is defined as M_T in Equation 1.

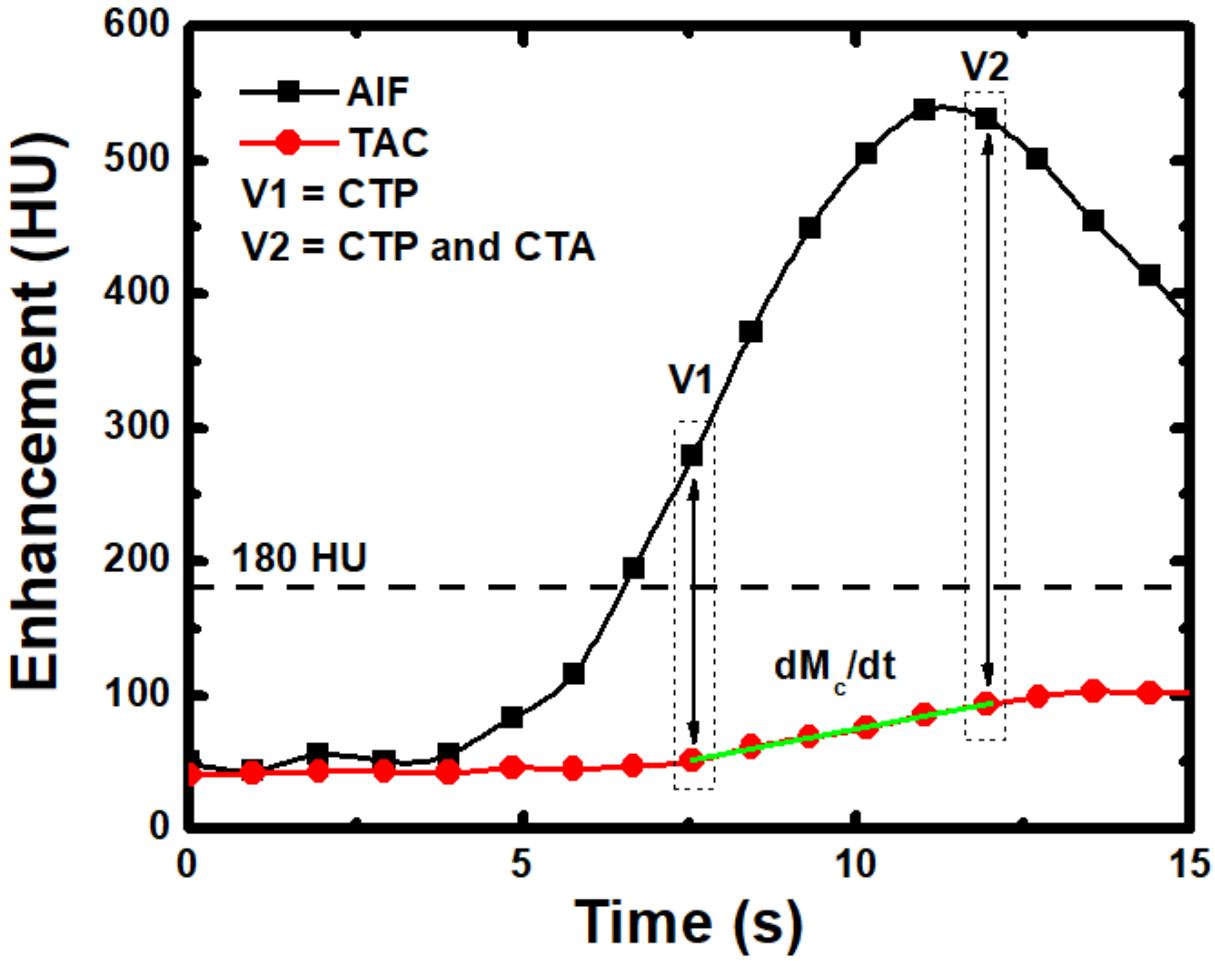

Figure 4.2: Two volume scans, denoted as V1 and V2, are used for FPA perfusion measurement. The integrated change in myocardial HU is derived from the tissue time attenuation curve (TAC), while the average input concentration is estimated from the arterial input function (AIF). The volume scan at maximal enhancement (V2) is also used for CT angiography.

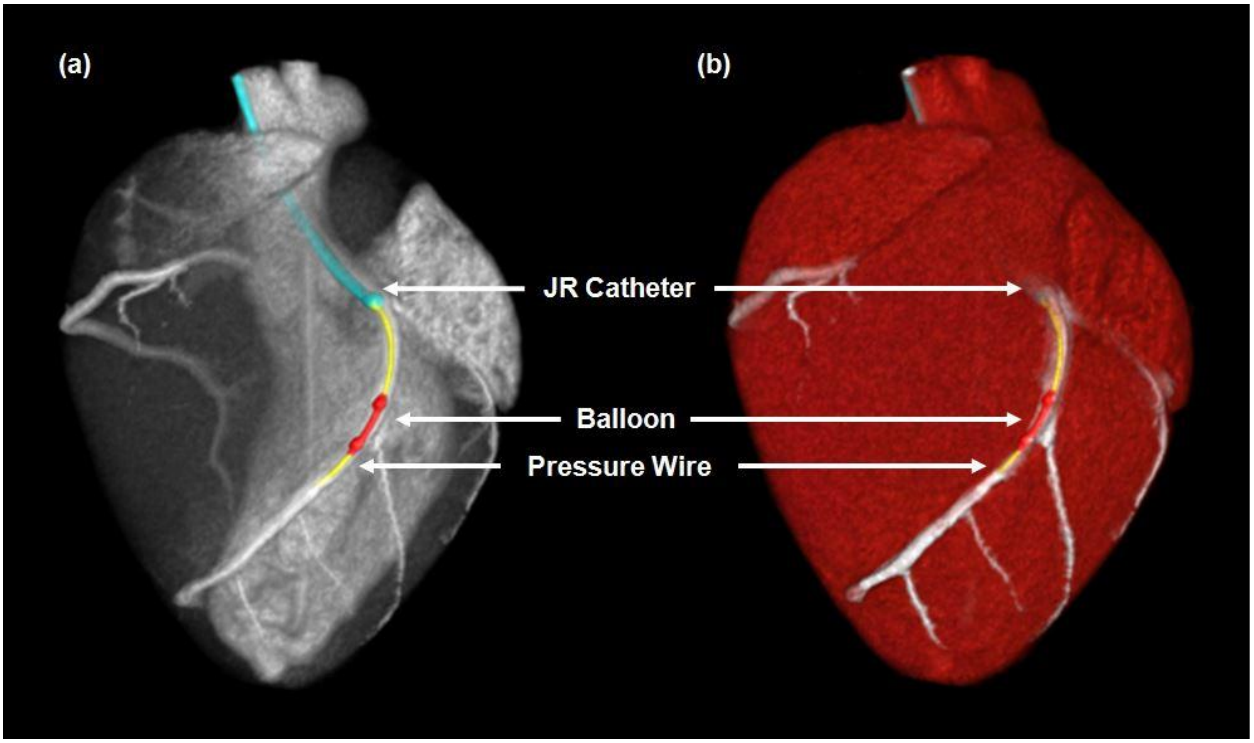

Figure 4.3: CT projection (a) and angiographic (b) images of the interventional setup, with the Judkins right (JR) catheter (blue), pressure wire (yellow), and balloon catheter (red) displayed.

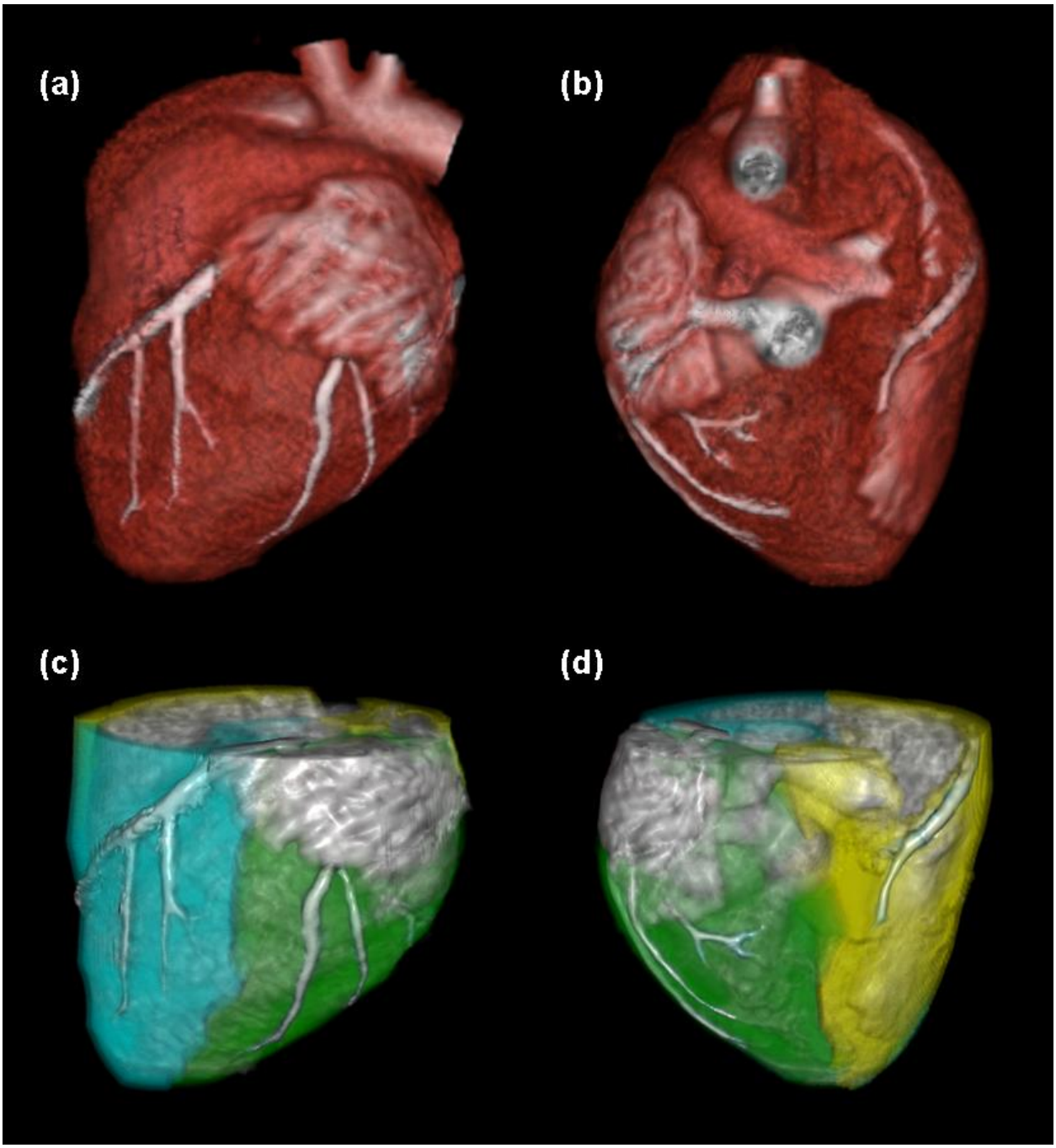

Figure 4.4: Image processing scheme for the FPA technique. The myocardium is segmented and coronary centerlines are extracted (a, b). Myocardial assignment is performed, with the LAD territory further partitioned to isolate the diseased distal tissue (c, d: cyan = total LAD territory, green = total LCX territory, yellow = total RCA territory).

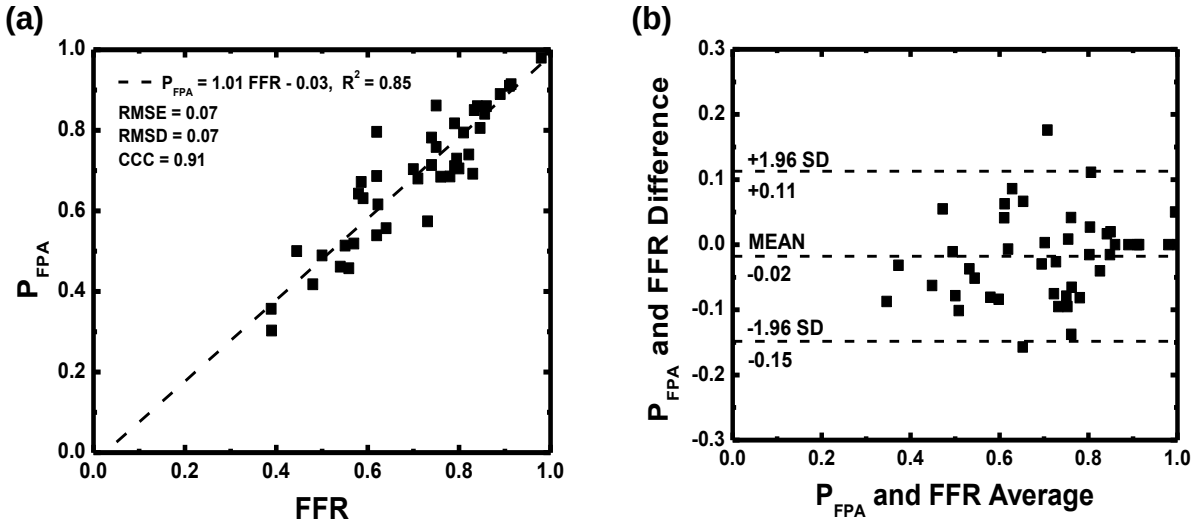

Figure 4.5: Regression analysis comparing the result of relative FPA perfusion measurement to reference standard FFR measurement (a). Bland-Altman analysis was also performed (b).

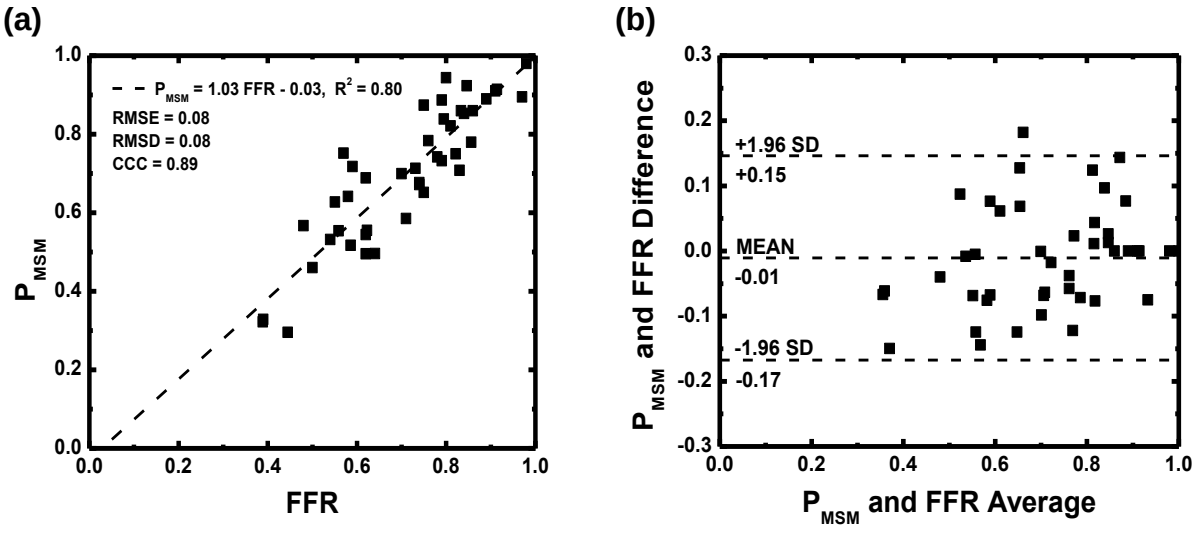

Figure 4.6: Regression analysis comparing the result of relative MSM perfusion measurement to reference standard FFR measurement (a). Bland-Altman analysis was also performed (b).

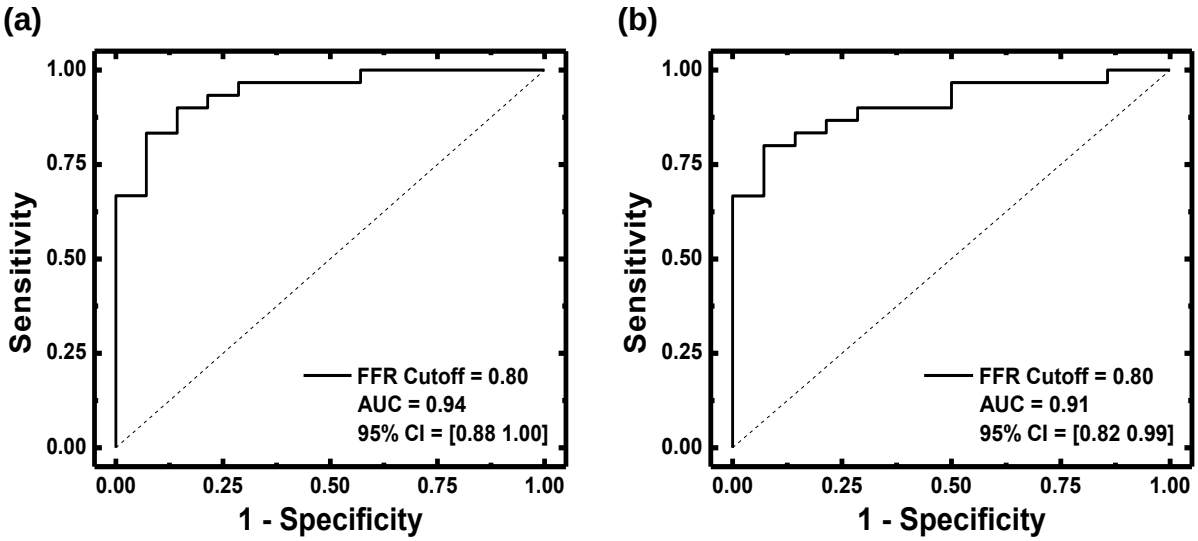

Figure 4.7: Diagnostic performance of relative FPA and relative MSM perfusion measurement as compared to reference standard FFR measurement (a, b). Functionally significant stenoses were classified as having FFRs less than or equal to 0.8.

CHAPTER 5: ACCURACY OF ABSOLUTE PERFUSION MEASUREMENT AS COMPARED TO QUANTITATIVE MICROSPHERE PERFUSION MEASUREMENT IN SWINE

Abstract

The purpose of this study was to retrospectively validate a first-pass analysis (FPA) technique that combines CT angiography and dynamic CT perfusion measurement for accurate, low-dose, vessel-specific morphological and physiological assessment of coronary artery disease (CAD). The study was approved by the Animal Care Committee. The FPA technique was retrospectively validated in six swine (37.3 ± 7.5 kg) between 04/2015 and 10/2016. Four to five intermediate severity stenoses were generated in the left anterior descending (LAD) coronary artery of each swine and twenty contrast-enhanced volume scans were prospectively acquired per stenosis. All volume scans were retrospectively reconstructed and used for maximum slope model (MSM) perfusion measurement, but only two first-pass volume scans were used for FPA perfusion measurement. FPA and MSM perfusion measurements in the LAD, left circumflex (LXc), right coronary artery (RCA), and in all three coronary arteries combined were compared to reference standard microsphere perfusion measurements using regression. The $\mathrm{CTDI}_{\mathrm{vol}}^{32}$ and size-specific dose estimate (SSDE) per two-volume FPA perfusion measurement were also determined. FPA and MSM perfusion measurements in all three coronary arteries combined were related to reference standard microsphere perfusion measurements by $P_{FPA\_COMBINED} = 1.02\ P_{MICRO\_COMBINED} + 0.11$ ($r = 0.96$) and $P_{MSM\_COMBINED} = 0.28\ P_{MICRO\_COMBINED} + 0.23$ ($r = 0.89$). The

$\mathrm{CTDI}_{\mathrm{vol}}^{32}$ and SSDE per two-volume FPA perfusion measurement were estimated to be 10.8 mGy and 17.8 mGy, respectively. The FPA technique was retrospectively validated in a swine model and has the potential to be used for accurate, low-dose, vessel-specific morphological and physiological assessment of CAD.

Introduction

Coronary artery disease (CAD) is a major global health concern. Fortunately, when CAD is accurately assessed with coronary angiography or CT angiography, long-term outcomes are improved[111]. Unfortunately, morphological assessment of CAD often correlates poorly with the physiological significance of intermediate severity disease (30-70% luminal narrowing)[112]. Hence, guidelines recommend further physiological assessment of CAD with fractional flow reserve (FFR)[17], cardiac magnetic resonance (CMR)[16], single-photon emission computed tomography (SPECT)[15], or static positron emission tomography (PET)[19]. Nevertheless, up to a 40% discordance exists between FFR and perfusion[22], while CMR, SPECT, and static PET only estimate relative perfusion, i.e., they cannot accurately assess multi-vessel, diffuse, and microvascular disease[20, 21]. Only quantitative perfusion measurement (mL/min/g) can overcome such deficiencies, where hyperemic perfusion less than 1.0 mL/min/g indicates significant disease[113].

Fortunately, quantitative perfusion measurement is possible with both dynamic PET[26] and dynamic CT[31, 32], with the latter being more clinically convenient and cost-effective[33]. Nevertheless, despite correlation with microsphere perfusion

measurement[29, 114], dynamic CT perfusion techniques, such as the maximum slope model (MSM), underestimate perfusion[38, 115, 116]. Specifically, given the limited cranio-caudal coverage of most CT scanners, such techniques rely on small tissue volumes-of-interest (VOI) to derive perfusion. Coupled with the rapid 3-5 second hyperemic transit of contrast material from coronary artery to coronary sinus[39], such small VOIs are subject to contrast material exit over the measurement duration, resulting in perfusion underestimation[38, 115, 116]. Small VOI measurements also suffer from poor signal-to-noise ratio (SNR); hence, dynamic CT perfusion techniques acquire data over many cardiac cycles to improve measurement reliability, leading to estimated effective radiation doses of up to 10 – 15 mSv[37, 42]. Furthermore, dynamic CT perfusion techniques cannot simultaneously acquire angiographic data; thus, additional contrast and radiation dose are necessary for separate CT angiography. Thus, the purpose of this study was to retrospectively validate a first-pass analysis (FPA) technique that combines CT angiography and dynamic CT perfusion measurement for accurate, low-dose, vessel-specific morphological and physiological assessment of CAD.

Materials and Methods

General Methods

The study was approved by the Animal Care Committee. The FPA technique was retrospectively validated in six male Yorkshire swine (37.3 ± 7.5 kg) using microsphere perfusion measurement as the reference standard[29, 114], with the MSM technique implemented for additional comparison. Data was prospectively acquired between 04/2015 and 06/2015 and was retrospectively analyzed between 06/2015 and 10/2016.

All authors conducted the data acquisition and had control of the data. Five authors (LH, JL, BZ, SM, BD) conducted the data analysis and generated the information for publication.

First-Pass Analysis Technique

First-pass analysis (FPA) and conservation of mass[117] state that the average perfusion (P_{AVE}) within a tissue compartment is proportional to the first-pass entry of contrast material mass into that compartment over time (dM_C/dt), normalized by the incoming contrast material concentration (C_{in}) and compartment tissue mass (M_T), assuming no contrast material exits over the measurement duration. Thus, the FPA technique models the entire myocardium as a single compartment, as described by **Figure 5.1**, and is computationally convenient as it lumps the vascular, interstitial, and cellular compartments together; hence, no assumptions about vascular permeability, interstitial drainage, or cellular composition are needed. From this compartment, dM_C/dt is derived from the integrated change in myocardial Hounsfield Units (HU) over time, while C_{in} is approximated from the aortic input function (AIF)[97, 98], as described by **Equation 1**.

$$\boldsymbol{P_{AVE} = \left(M_T^{-1} C_{in}^{-1} \frac{dM_c}{dt} \right)_{AVE}} \qquad \textbf{(1)}$$

Finally, as the average perfusion (P_{AVE}) is also proportional to the rate of contrast material concentration change in the compartment; i.e., the average change in myocardial Hounsfield Units (ΔHU_{AVE}), over time, the voxel-by-voxel concentration change (ΔHU) is used to derive voxel-by-voxel perfusion (P_{FPA}), as described by

Equation 2.

$$P_{FPA} = P_{AVE} \frac{\Delta HU}{\Delta HU_{AVE}} \qquad (2)$$

Such perfusion measurement is feasible using only two first-pass volume scans, labeled V1 and V2 in **Figure 5.2**, simulating a low-dose prospective acquisition protocol. V1 is the first volume scan after the AIF exceeds 180 HU, while V2 is the first volume scan after the AIF reaches its peak. V1 and V2 are used for perfusion measurement, while V2 is also used for CT angiography[97, 98].

Maximum Slope Model Technique

The MSM technique uses small tissue VOIs (~1.0 cm^3) to generate myocardial time attenuation curves (TACs), and assumes no contrast material exits those VOIs over the measurement duration. Perfusion (P_{MSM}) is defined as the maximum upslope of those TACs ($dTAC/dt_{MAX}$), divided by the maximum of the AIF (AIF_{MAX}) and tissue density (ρ_T). However, due to poor measurement SNR, the average upslope ($dTAC/dt_{AVE}$) is more commonly used [37, 38], as described by **Equation 3**.

$$P_{MSM} = \rho_T^{-1} AIF_{MAX}^{-1} \left(\frac{dTAC}{dt} \right)_{AVE}$$

Animal Model

Anesthesia was induced with Telazol (4.4 mg/kg), Ketamine (2.2 mg/kg), and Xylazine (2.2 mg/kg), and was maintained through ventilation (Highland Medical Equipment, Temecula, CA) with 1.5-2.5% Isoflurane (Baxter, Deerfield, IL). Catheter sheaths were placed (AVANTI®, Cordis Corporation, Miami Lakes, FL) in the femoral arteries and veins, the right jugular vein, and the right carotid artery. Using the femoral artery sheaths, a pigtail catheter was passed into the left ventricle for microsphere injection and a multipurpose catheter was passed into the aorta for blood sample withdrawal. The femoral vein sheaths were used for drug and fluid administration, while the jugular sheath was used for contrast material injection.

Using the carotid sheath, the left coronary ostium was engaged with a Judkins right catheter (Cordis Corporation, Miami Lakes, FL) and a pressure wire (PrimeWire PRESTIGE® Pressure Guide Wire, Volcano Corp, Rancho Cordova, CA) was advanced into the distal left anterior descending (LAD) coronary artery. A balloon was passed over the wire into the proximal LAD and was used to generate four to five different intermediate severity stenoses (30 – 70% luminal narrowing) during maximal intracoronary hyperemia (240 µg adenosine/min, Harvard Apparatus, Model 55-2222). Stenosis severity was monitored with fractional flow reserve (FFR) measurement (ComboMap, Volcano Corp., Rancho Cordova, CA). The interventional setup is shown in **Figure 5.3**.

CT Imaging Protocol

For each stenosis, contrast material (1 mL/kg, Isovue 370, Bracco Diagnostics, Princeton, NJ) and saline (0.5 mL/kg) were injected (7 mL/s, Empower CTA, Acist Medical Systems, Eden Prairie, MN) and twenty whole-heart volume scans were prospectively acquired (Aquilion One, Toshiba America Medical Systems, Tustin, CA) at 100 kVp and 200 mA with 320 x 0.5 mm collimation and 16 cm of cranio-caudal coverage. All twenty volume scans were retrospectively reconstructed from full projection data at 75% of the R-R interval and were used for MSM perfusion measurement, but only two first-pass volume scans were used for FPA perfusion measurement, simulating a low-dose prospective acquisition protocol. Additionally, the $\mathrm{CTDI}_{\mathrm{vol}}^{32}$ per two-volume FPA perfusion measurement was recorded, and a size-specific dose estimate (SSDE) was also computed to account for the small ~22 cm effective chest diameter of the swine[118].

Microsphere Perfusion Measurement

NuFlow Hydro-Coat™ fluorescent microspheres (15.5 μm diameter, IMT Laboratories, Irvine, CA) were used as the reference standard for perfusion measurement[29, 114]. For each stenosis, microspheres were injected into the left ventricle and blood samples were withdrawn from the aorta at 10 mL/min over two minutes (GenieTouch, Kent Scientific, Torrington, CT). Each animal was then euthanized, and tissue samples were excised from the distal LAD, left circumflex (LCx), and right coronary artery (RCA) perfusion territories. All tissue and blood samples were analyzed independently (IMT Laboratories, Irvine, CA).

FPA Image Processing

The two first-pass volume scans were registered, combined into a maximum intensity projection (MIP) volume, and segmented semi-automatically to produce a myocardial mask, i.e., a whole-heart perfusion compartment. Given the compartment mass, the average of the AIF, and the integrated and average change in myocardial HU between the two volume scans, voxel-by-voxel perfusion measurement was computed. The centerlines of the LAD, LCx, and RCA were then extracted from the MIP (Vitrea fX version 6.0, Vital Images, Inc., Minnetonka, MN) and were used, along with the mask, for minimum-cost-path (MCP) myocardial assignment [47], yielding three separate coronary perfusion territories, with the LAD territory further partitioned past the stenosis. Voxel-by-voxel perfusion measurements were then averaged within each territory and compared to the microsphere perfusion measurements. The FPA image processing scheme is summarized in **Figure 5.4.**

MSM Image Processing

VOIs measuring 1.0 cm^3 were placed in the anterior wall of the left ventricle, the lateral wall of the left ventricle, and the inferior septal wall between ventricles. Given the dynamic enhancement within each VOI, the maximum of the AIF, and the myocardial tissue density, vessel-specific perfusion measurements were derived and compared to microsphere perfusion measurements.

Statistical Approach

To appropriately demonstrate improved agreement of FPA over MSM perfusion measurement, as compared to microsphere perfusion measurement, power analysis was performed[119]. In a similar study[29], a slope of 0.25 and a correlation of 0.67 was found between MSM perfusion measurement and microsphere perfusion measurement, with a microsphere standard deviation of 1.25 mL/min/g. However, the FPA technique has been shown to improve the slope with comparable correlation as compared to the MSM technique[97, 98]. Hence, twenty independent microsphere perfusion measurements were deemed necessary to reject the null hypothesis of equal slopes, assuming a conservative FPA slope improvement of at least 0.25 over the MSM slope, a microsphere standard deviation of 1.25 mL/min/g, a type 1 error probability of 0.05, and a power of 0.80. The combined variance of microsphere perfusion measurements (LAD, LCx, and RCA for all stenoses) within each animal was also compared to the combined variance of microsphere perfusion measurements between each animal using intra-cluster correlation (ICC)[120]. The ICC was found to be $\rho = 0.12$, indicating negligible correlation between intra-animal measurements; hence, all measurements were assumed to be independent. For the primary outcome measure, the accuracy and precision of FPA and MSM perfusion measurement in the LAD, LCx, RCA, and in all three coronary arteries combined was assessed using regression, root-mean-square-error (RMSE), and root-mean-square deviation (RMSD). Lin's concordance correlation coefficient (CCC)[92] was also computed as a measure of true agreement with the reference standard. For the secondary outcome measure, the performance of FPA- and MSM-based detection of significant stenoses in the LAD was assessed. The sensitivity,

specificity, positive predictive value, negative predictive value, and area under the curve (AUC) of the receiver operator characteristic (ROC) were computed, with LAD microsphere perfusion measurements less than 1.0 mL/min/g at maximal hyperemia classified as physiologically significant[113]. Statistical software was used for all analysis (PS, Version 3.0, Vanderbilt University, Nashville, TN, and SPSS, Version 22, IBM Corporation, Armonk, NY).

Results

The average heart rate and mean arterial pressure were 78.6 ± 5.3 beats per minute and 73.4 ± 9.9 mmHg, respectively. The $\mathrm{CTDI}_{\mathrm{vol}}^{32}$ and SSDE per two-volume FPA perfusion measurement were 10.8 mGy and 17.8 mGy, respectively. Based on the result of MCP assignment, the LAD, LCx, and RCA perfused 43.0 ± 3.4%, 38.2 ± 2.2%, and 18.8 ± 5.3% of the left ventricular mass, respectively, and perfused 39.9 ± 8.8%, 0.1 ± 0.3%, and 60.0 ± 8.7% of the right ventricular mass, respectively. Additionally, combined angiography and perfusion maps were generated by the FPA technique for baseline, hyperemic, and stenotic perfusion conditions in the LAD and are shown in **Figure 5.5**.

FPA perfusion measurement in all three coronary arteries combined was related to microsphere perfusion measurement by $P_{FPA\_COMBINED} = 1.02\ P_{MICRO\_COMBINED} + 0.11$, with a Pearson's correlation of $r = 0.96$, a CCC of $\rho = 0.95$, a RMSE of 0.54 mL/min/g, and a RMSD of 0.52 mL/min/g, as shown in **Figure 5.6a**, with the individual LAD, LCx, and RCA perfusion measurements shown in **Table 5.1**. MSM perfusion measurement in

all three coronary arteries combined was related to microsphere perfusion measurement by $P_{MSM\_COMBINED} = 0.28\ P_{MICRO\_COMBINED} + 0.23$, with a Pearson's correlation of $r = 0.89$, a CCC of $\rho = 0.35$, a RMSE of 1.69 mL/min/g, and a RMSD of 0.24 mL/min/g, as shown in **Figure 5.6b**, with the individual LAD, LCx, and RCA measurements also shown in **Table 5.1**.

For FPA-based detection of significant stenoses, the area under the curve (AUC) of the receiver operator characteristic (ROC) was 0.96, as shown in **Table 5.2** and **Figure 5.7a**. For MSM-based detection of significant stenoses, the AUC of the ROC was 0.91, as shown in **Table 5.2** and **Figure 5.7b**. The diagnostic sensitivity, specificity, positive predictive value, and negative predictive value of both techniques is also shown in **Table 5.2**. A general comparison between FPA, MSM, microsphere, and dynamic PET perfusion measurement as previously reported[26] is shown in **Table 5.3**.

Discussion

The FPA technique performed better than the MSM technique in vessel-specific perfusion measurement, demonstrating higher slope of agreement and higher concordance correlation[92] as compared to microsphere perfusion measurement. The FPA technique also performed better than the MSM technique in detection of significant stenoses, with additional gains in accuracy, specificity, and positive predictive value, although the MSM technique demonstrated higher sensitivity and negative predictive value. However, such high sensitivity and negative predictive value can be attributed to

a high false positive rate, as indicated by the poor specificity, low positive predictive value, and underestimation of perfusion by the MSM technique[38, 115, 116].

Baseline and hyperemic perfusion measurement with the FPA technique also agreed with dynamic PET as previously reported[26], while the MSM technique underestimated perfusion. That being said, perfusion measured with the FPA technique was slightly higher than that of dynamic PET[26] due to contrast-induced vasodilation[109] and due to intracoronary adenosine use. Specifically, intracoronary adenosine reduced hypotension and reflex-tachycardia [121], but permitted full coronary vasodilation with high mean systemic pressure; a difficult condition to achieve under intravenous stress due to mean systemic pressure drop. Hence, if intravenous adenosine were used instead, hyperemic perfusion measured with the FPA technique would likely be more comparable to that of dynamic PET[26]. Regardless, the combined angiography and perfusion maps generated by the FPA technique agreed well with baseline, hyperemic, and stenotic perfusion conditions in the LAD.

Nevertheless, the clinical feasibility of the FPA technique depends on proper prospective volume scan acquisition. Specifically, only two first-pass volume scans were retrospectively selected for FPA perfusion measurement, simulating a low-dose prospective acquisition protocol, and corresponding to a $\mathrm{CTDI}_{\mathrm{vol}}^{32}$ and SSDE of 10.8 mGy and 17.8 mGy, respectively. While such a first-pass protocol ensured that bi-ventricular enhancement was present for myocardial segmentation, that the maximum rate of contrast material mass entry (dM_C/dt) was captured for dynamic CT perfusion

measurement, and that maximal coronary opacification was achieved for CT angiography, validation of a true prospective, two-volume FPA acquisition protocol is still necessary. Fortunately, such a protocol is realizable through the use of dynamic bolus tracking[122], where V1 can be triggered and acquired after the AIF exceeds 180 HU, while V2 can be acquired 4-5 seconds later following the AIF peak. Nevertheless, the accuracy of such a protocol depends on proper dynamic bolus tracking-based triggering; hence, inaccurate triggering may lead to inaccurate FPA perfusion measurement. That being said, such dependency can be circumvented by instead using a low-dose test contrast bolus acquisition to determine the timing of the V1 and V2 volume scans prior to low-dose prospective FPA perfusion measurement. Given that timing, the V1 and V2 volume scans can be acquired a fixed amount of time after contrast injection, eliminating the need for dynamic bolus tracking, while guaranteeing measurement accuracy with only minor increases in contrast and radiation dose. Hence, if using an adult chest conversion factor of k = 0.014, prospective clinical implementation of the FPA technique at 100 kVp and 200 – 500 mA may ultimately yield an estimated effective radiation dose of 2.4 – 6.0 mSv for combined CT angiography and dynamic CT perfusion measurement, which is comparable to that of current CT angiography techniques, but is much lower than that of current dynamic CT perfusion techniques (10 – 15 mSv)[37, 42]. Nevertheless, the clinical feasibility of the FPA technique also depends on the accessibility of 320-slice CT technology with 16 cm of cranio-caudal coverage[44], as simultaneous acquisition of whole-heart CT angiography and dynamic CT perfusion data is not possible with 64-slice CT scanners. Fortunately, such technology is becoming more prevalent. A recent report [110] also suggests that whole-

heart imaging is possible with 128- and 256-slice CT technology if systolic-phase data is acquired at end-expiration. Hence, the FPA technique could be implemented with 128- and 256-slice CT technology, but further validation is necessary.

Regarding the limitations of the study, only proximal vessel disease was assessed in the LAD, i.e., multivessel disease, distal or branch disease, diffuse disease, and microvascular disease were not considered. Fortunately, the FPA technique can spatially resolve perfusion on a voxel-by-voxel and vessel-specific basis; hence, detection of focal, gradient, and global perfusion deficits is still feasible. Nevertheless, the accuracy of voxel-by-voxel perfusion measurement depends on image noise. Fortunately, as a clinically relevant volume of ischemic myocardium is on the order of 1 cm^3, moderate binning of voxel-by-voxel perfusion measurements can be used to suppress image noise while maintaining adequate spatial perfusion resolution. Accurate vessel-specific perfusion measurement also depends on the accuracy of MCP assignment [47]. Fortunately, the preliminary results of this study indicate adequate assignment performance. However, the minimum vessel sparseness needed for accurate MCP assignment still requires validation.

Conclusions

The FPA technique enables CT angiography data and dynamic CT perfusion data to be acquired simultaneously using only two first-pass volume scans and a single contrast injection. Specifically, the FPA technique defines the entire myocardium as a single VOI while also making measurements prior to hyperemic transit; hence, contrast material

loss from the measurement VOI over the measurement time is circumvented and the problem of perfusion underestimation[38, 115, 116] is solved. Isolation of whole-heart VOIs in a single cardiac cycle and improved measurement SNR is enabled by whole-heart CT technology; thus, reducing the number of volume scans necessary for accurate perfusion measurement. Such a reduction in volume scan number also results in a lower radiation exposure. Hence, by using only two volume scans for combined CT angiography and dynamic CT perfusion measurement, prospective clinical implementation of the FPA technique has the potential to substantially reduce the radiation and contrast dose associated with noninvasive CAD workup, making comprehensive CT-based assessment of CAD more accessible and impactful to patients in need. In summary, the FPA technique was retrospectively validated in a swine model and has the potential to be used for accurate, low-dose, vessel-specific morphological and physiological assessment of CAD.

Tables

Table 5.1: FPA and MSM perfusion compared to reference standard microsphere perfusion

Technique	Slope	Intercept	Pearson's r	Lin's CCC	RMSE (mL/min/g)	RMSD (mL/min/g)
FPA (N)						
LAD (27)	1.01** [0.90, 1.13]	0.19 [-0.25, 0.62]	0.97 [0.93, 0.99]	0.96** [0.91, 0.98]	0.63	0.58
LCx (27)	0.99** [0.58, 1.4]	0.18 [-0.27, 0.63]	0.70 [0.44, 0.85]	0.63 [0.33, 0.81]	0.44	0.41
RCA (27)	0.87** [0.63, 1.10]	0.18 [-0.25, 0.60]	0.84 [0.68, 0.92]	0.84** [0.68, 0.92]	0.56	0.55
Combined (81)	**1.02** [0.94, 1.09]**	**0.11 [-0.07, 0.29]**	**0.96** [0.94, 0.97]**	**0.95** [0.92, 0.97]**	**0.54**	**0.52**
MSM (N)						
LAD (27)	0.27 [0.21, 0.33]	0.25 [0.02, 0.47]	0.89 [0.77, 0.95]	0.27 [-0.12, 0.59]	2.63	0.30
LCx (27)	0.34 [0.12, 0.56]	0.13 [-0.11, 0.37]	0.54 [0.20, 0.76]	0.21 [-0.18, 0.55]	0.65	0.21
RCA (27)	0.27 [0.19, 0.35]	0.28 [0.14, 0.42]	0.83 [0.66, 0.92]	0.31 [-0.08, 0.62]	1.11	0.18
Combined (81)	**0.28 [0.24, 0.31]**	**0.23 [0.14, 0.31]**	**0.89 [0.83, 0.93]**	**0.35 [0.14, 0.53]**	**1.69**	**0.24**

Brackets indicate 95% confidence intervals. FPA indicates first-pass analysis; MSM, maximum slope model perfusion; LAD, left anterior descending; LCx, left circumflex; RCA, right coronary artery; N, number of perfusion measurements; Lin's CCC, Lin's concordance correlation coefficient; RMSE, root-mean-square error; RMSD, root-mean-square deviation. **Indicates non-overlap of the 95% confidence intervals, i.e., significant differences between corresponding FPA and MSM parameters.

Table 5.2: FPA- and MSM-based detection of physiologically significant LAD stenosis

Technique	SN (%)	SP (%)	PPV (%)	NPV (%)	AUC of ROC
FPA	60 (3/5) [15, 95]	95 (21/22) [77,100]	75 (3/4) [19, 99]	91 (21/23) [72, 99]	0.96 [0.90, 1.00]
MSM	100 (5/5) [48,100]	64 (14/22) [41, 83]	38 (5/13) [14, 68]	100 (14/14) [77, 100]	0.91 [0.80, 1.00]

Parentheses indicate the fractional representation of measurements; Brackets indicate 95% confidence intervals; LAD indicates left anterior descending; SN, sensitivity; SP, specificity; PPV, positive predictive value; NPV, negative predictive value; AUC of ROC, area under the curve of the receiver operator characteristic.

Table 5.3: FPA, MSM, and microsphere perfusion in the LAD compared to dynamic PET [26]

Method	Baseline Perfusion (mL/min/g)	Hyperemic Perfusion (mL/min/g)
FPA	0.94 ± 0.55	5.22 ± 1.61**
MSM	0.41 ± 0.29	1.61 ± 0.47**
MICRO	0.81 ± 0.35	4.95 ± 1.49**
PET	0.85 ± 0.19	3.89 ± 1.01‡‡

Unless otherwise stated, all perfusion data are MEAN ± STD; FPA indicates first-pass analysis; MSM, maximum slope model; MICRO, reference standard microspheres; PET, dynamic positron emission tomography; LAD, left anterior descending; **Indicates hyperemia induced by an intracoronary stress agent; ‡‡Indicates hyperemia induced by an intravenous stress agent.

Figures

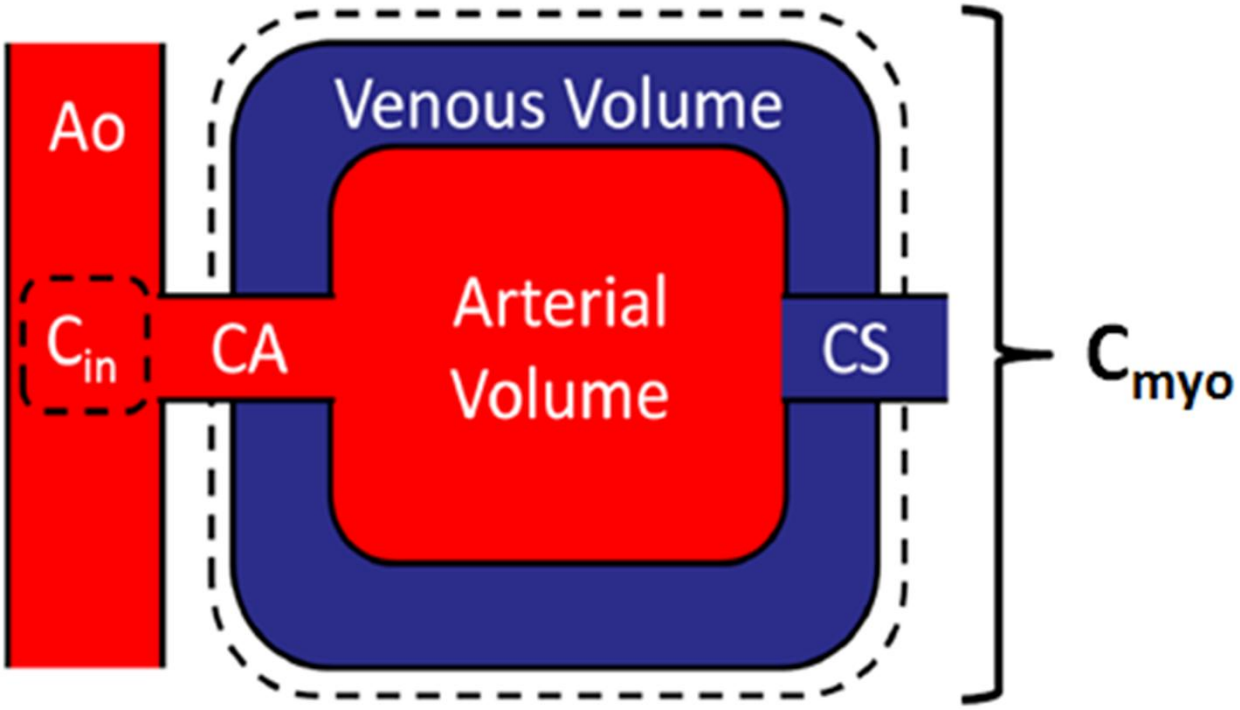

Figure 5.1: Myocardial perfusion compartment model used for quantitative first-pass analysis (FPA) perfusion measurement, indicating the aortic input (Ao) and input concentration (C_{in}), coronary arterial input (CA), whole-heart myocardial tissue compartment (C_{myo}), and coronary sinus (CS). The compartment tissue mass is defined as M_T in Equation 1.

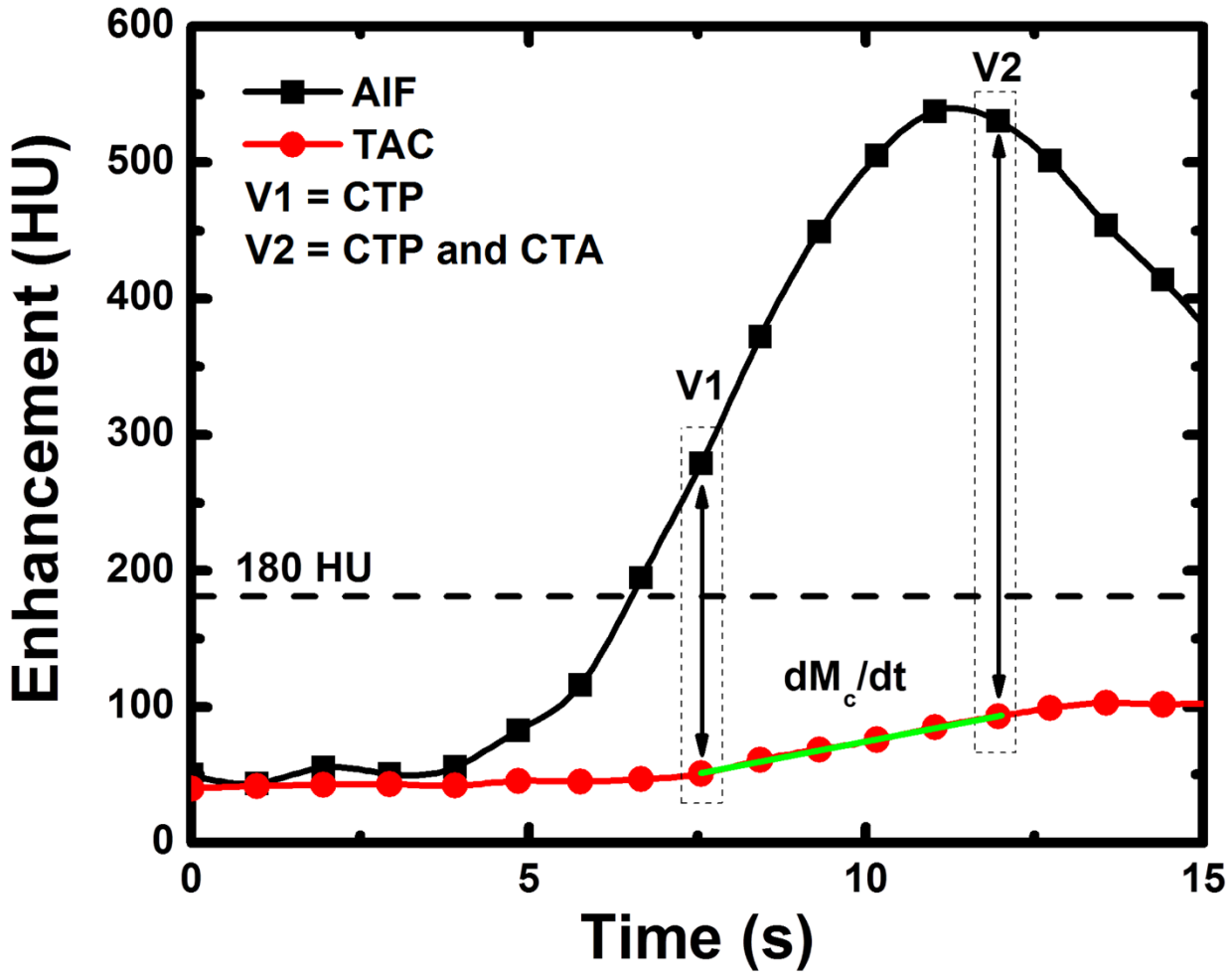

Figure 5.2: Two first-pass volume scans, denoted as V1 and V2, are used for FPA perfusion measurement, simulating a low-dose prospective acquisition protocol based on dynamic bolus tracking. The integrated change in myocardial Hounsfield units (dM_C/dt) is derived from the tissue time attenuation curve (TAC) and the average input concentration (C_{in}) is estimated from the aortic input function (AIF). Both first-pass volume scans (V1 and V2) are used for dynamic computed tomography perfusion (CTP) measurement, while the volume scan after maximal enhancement (V2) is also used for computed tomography angiography (CTA).

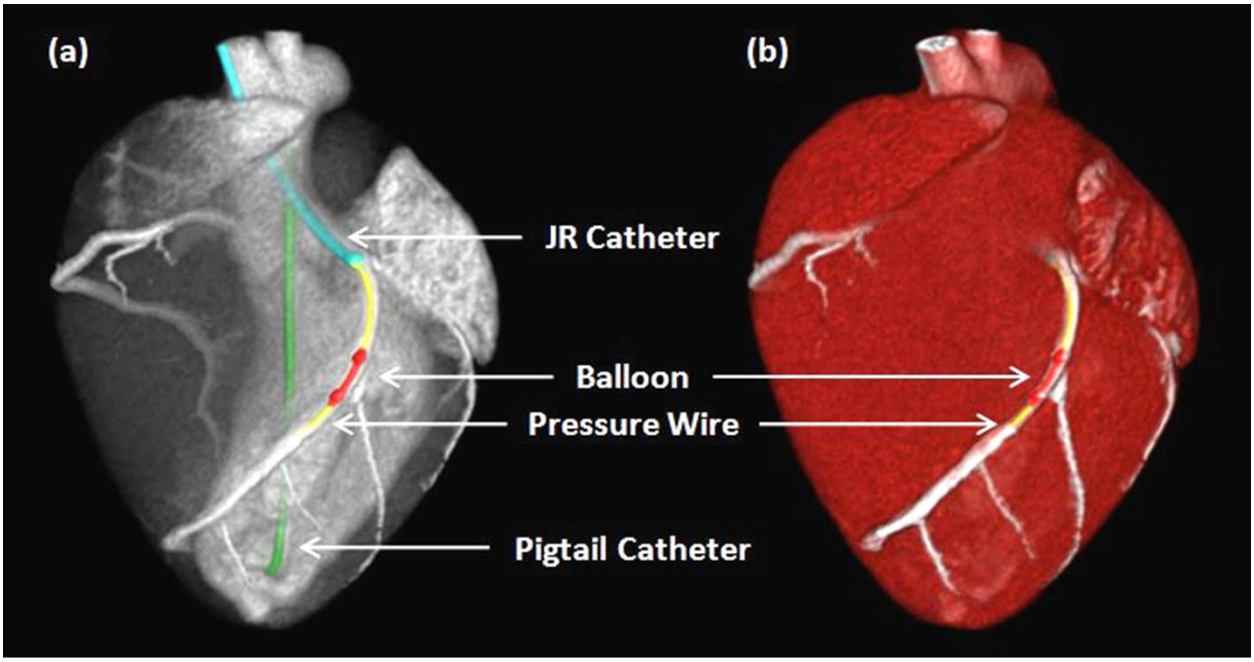

Figure 5.3: Contrast-enhanced (a) CT projection and (b) angiographic images of the interventional setup in the swine model, with the Judkins right (JR) catheter (blue), balloon (red), pressure wire (yellow), and Pigtail catheter (green) displayed.

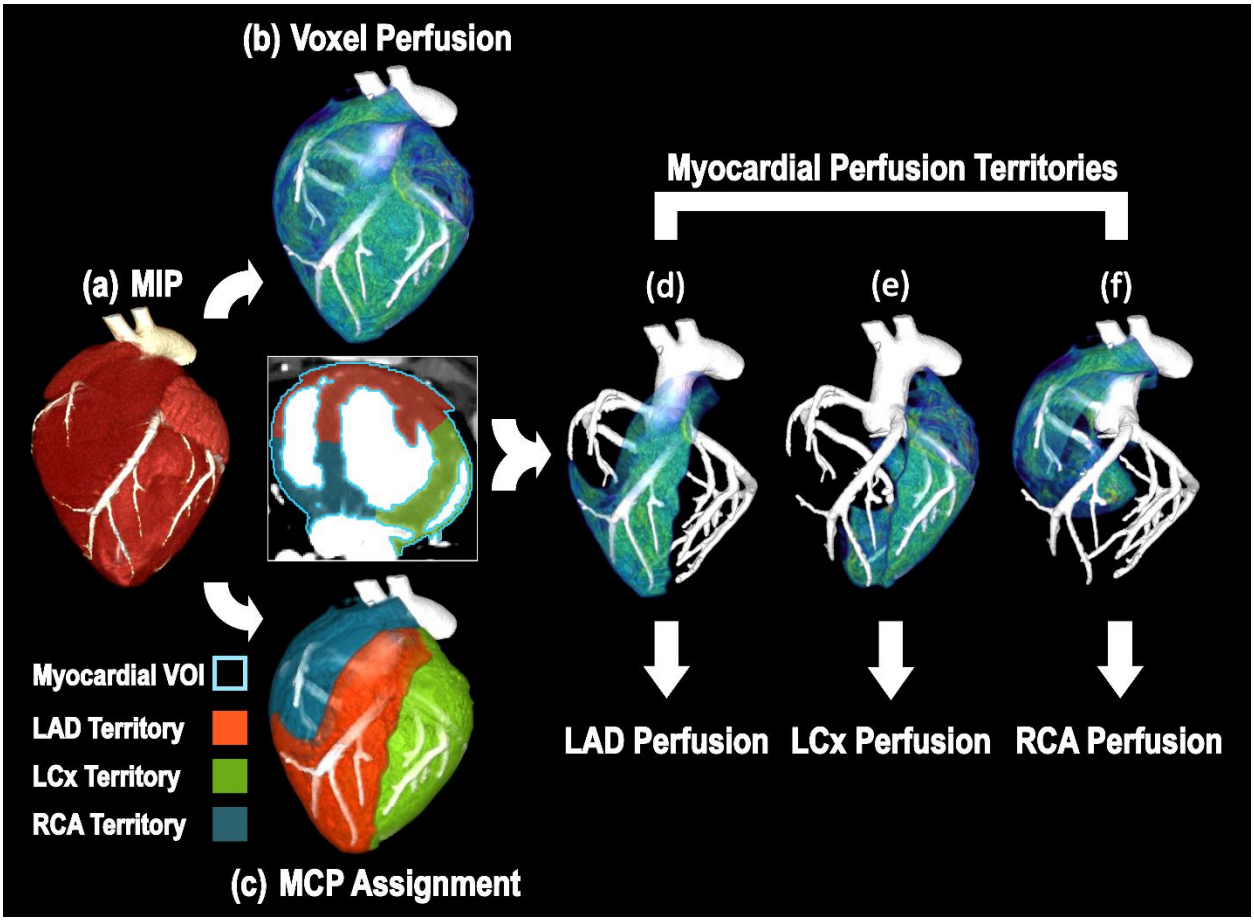

***Figure 5.4:** Image processing scheme for FPA perfusion measurement. (a) The entire heart is segmented from the V1 and V2 maximum-intensity projection image (MIP) resulting in a whole-heart VOI (axial view: light blue outline = whole-heart VOI), (b) voxel-by-voxel perfusion is computed within that whole-heart VOI, (c) minimum-cost-path (MCP) myocardial assignment is performed yielding three vessel-specific sub-VOIs (red = LAD sub-VOI; green = LCx sub-VOI; blue = RCA sub-VOI), and (d-f) vessel-specific perfusion is derived by averaging the voxel-by-voxel perfusion within each sub-VOI.*

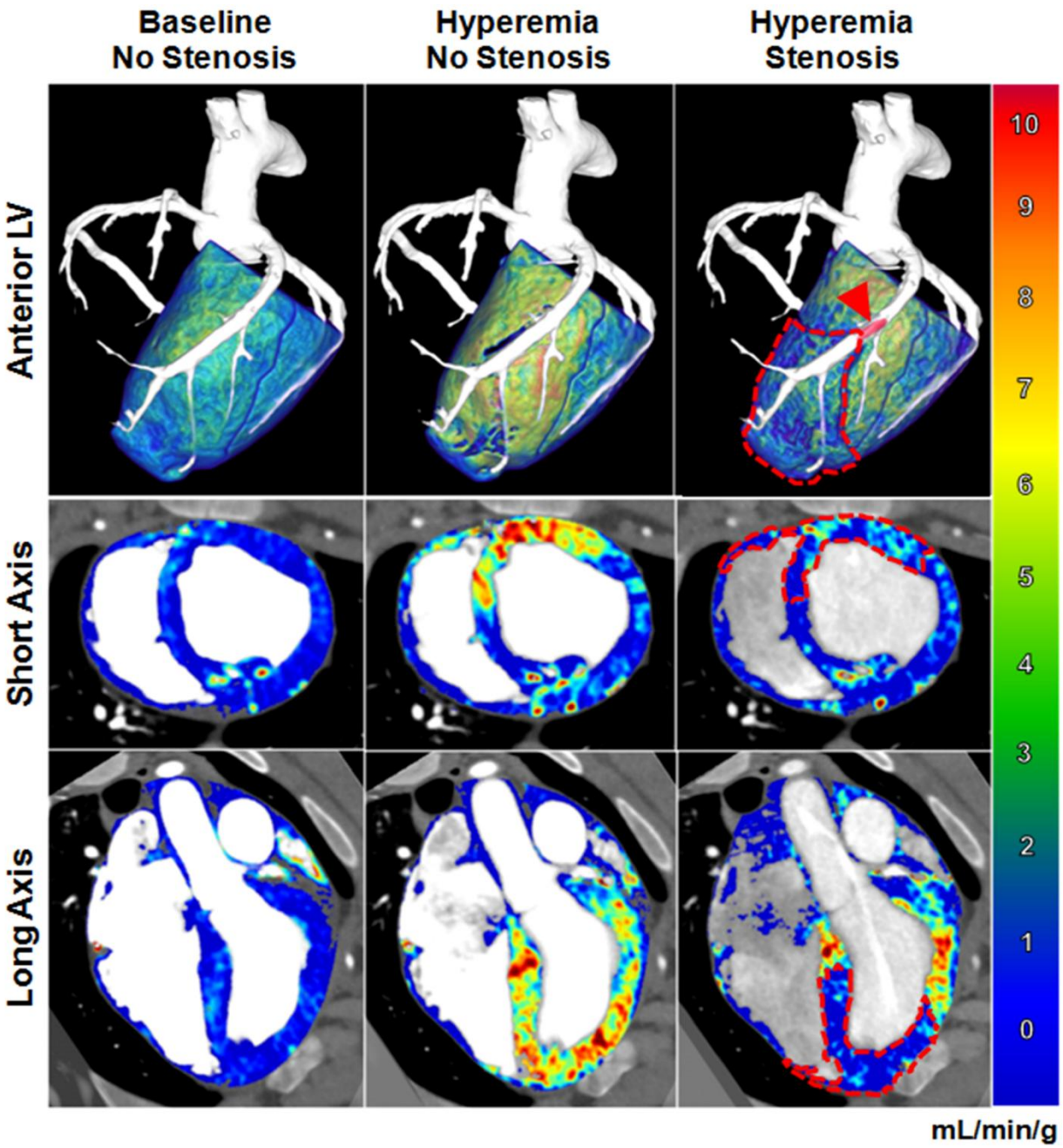

Figure 5.5: Combined angiography and perfusion maps generated by the FPA technique. Several perfusion conditions were induced in the LAD, including (left column) baseline perfusion with no stenosis, (middle column) hyperemic perfusion with no stenosis, and (right column) hyperemic perfusion in the presence of a physiologically significant stenosis. (Top row) Anterior volumetric views of the left ventricle (LV) are shown for 3D visualization of the balloon stenosis position (red arrow) and distal perfusion deficit (red dashed line). (Middle row) Axial and (bottom row) coronal views of both ventricles are also displayed. The color bar indicates quantitative perfusion in mL/min/g.

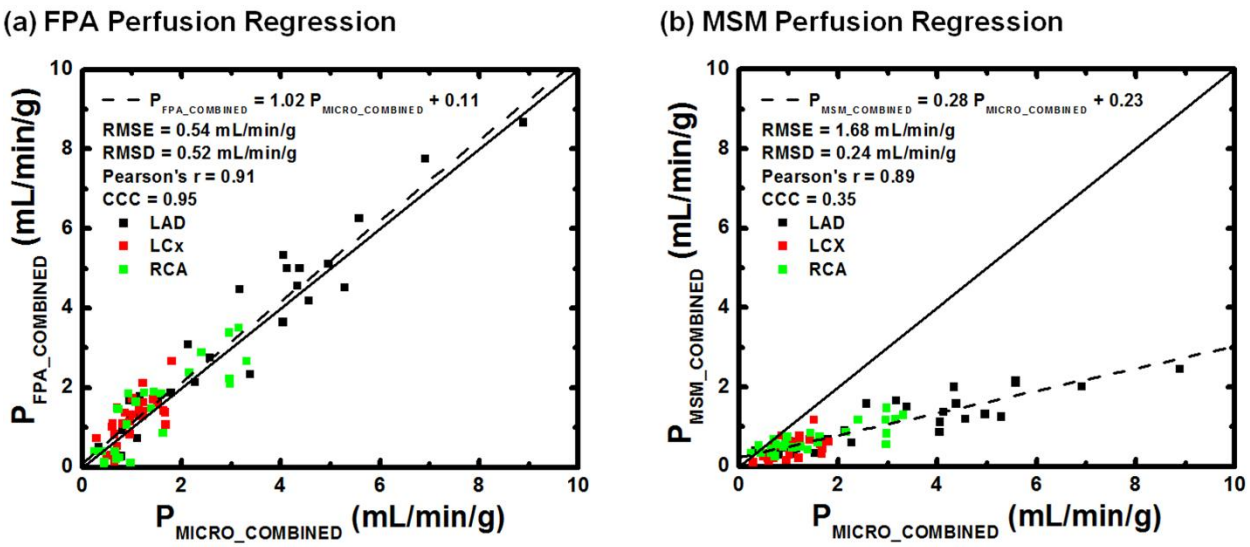

Figure 5.6: (a) Regression of FPA perfusion measurement in all three coronary arteries combined ($P_{FPA\_COMBINED}$) as compared to reference standard microsphere perfusion measurement ($P_{MICRO\_COMBINED}$). (b) Regression of MSM perfusion measurement in all three coronary arteries combined ($P_{MSM\_COMBINED}$) as compared to reference standard microsphere perfusion measurement ($P_{MICRO\_COMBINED}$). CCC indicates Lin's concordance correlation coefficient; RMSD, root-mean-square deviation; RMSE, root-mean-square error.

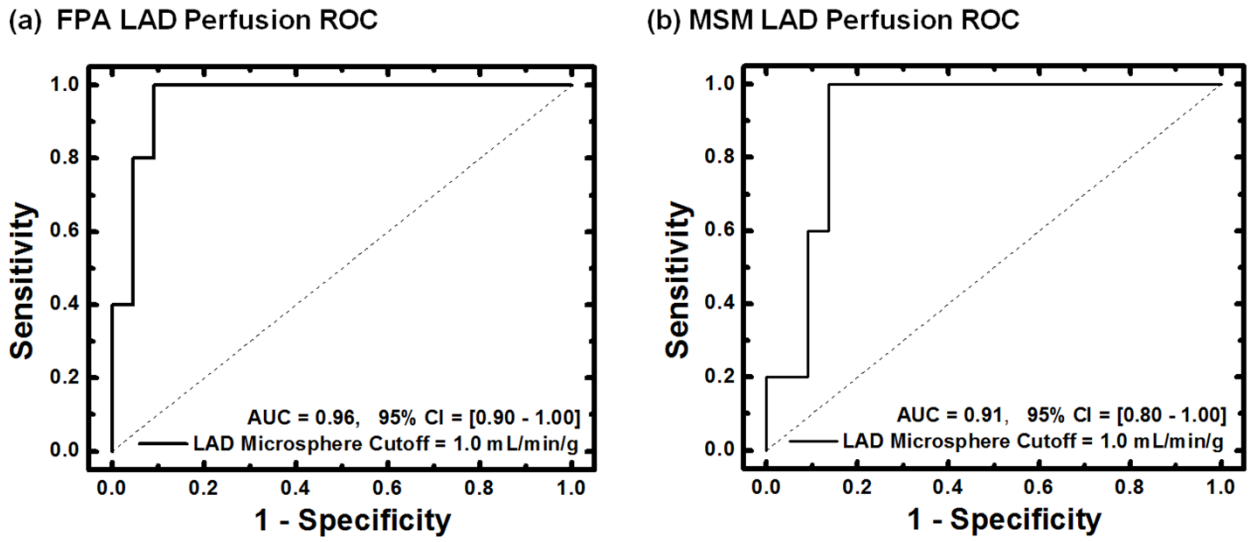

Figure 5.7: (a) FPA-based detection of physiologically significant stenoses in the LAD at maximal hyperemia, (b) MSM-based detection of physiologically significant stenoses in the LAD at maximal hyperemia. Physiologically significant stenoses in the LAD were classified as having reference standard microsphere perfusion values less than 1.0 mL/min/g. ROC indicates receiver operator characteristic; AUC, area under the curve; CI, confidence interval.

CHAPTER 6: LOW-DOSE PROSPECTIVE GLOBAL STRESS PERFUSION MEASUREMENT AS COMPARED TO RETROSPECTIVE PERFUSION MEASUREMENT IN SWINE

Abstract

The purpose of this study was to evaluate a low-dose prospective first-pass analysis (FPA) dynamic CT perfusion technique for accurate submillisievert stress myocardial perfusion measurement. The low-dose FPA technique was evaluated in ten swine (42 ± 12 kg) by direct comparison to a previously validated retrospective FPA technique. For the first two swine, the minimum tube current necessary for accurate FPA perfusion measurement was determined. The remaining eight swine were prospectively assessed at that minimum tube current, with three of those swine having intermediate stenoses with fractional flow reserve severities of 0.70 - 0.90. Specifically, contrast and saline were injected peripherally (370 mgI/mL contrast: 1 mL/kg at 5 mL/s; saline: 0.5 mL/kg at 5 mL/s) followed by dynamic volume scan acquisition with a 320-slice CT scanner. Only two volume scans were acquired for the low-dose prospective FPA technique, while 20 volume scans were acquired for the reference standard retrospective FPA technique. All low-dose prospective stress perfusion measurements were then compared to corresponding reference standard retrospective stress perfusion measurements through regression analysis. The $\mathrm{CTDI}_{\mathrm{vol}}^{32}$ and size-specific dose estimate of the low-dose prospective FPA technique were also determined and were used to estimate effective dose. For the first two swine, accurate perfusion measurement was found to be feasible at a tube current as low as 50 mA. For the remaining eight swine, low-dose prospective

stress perfusion measurements (P_{LOW}) at 50 mA were in good agreement with reference standard retrospective stress perfusion measurements (P_{REF}) at 200 mA (P_{LOW} = 1.07 P_{REF} - 0.09, r = 0.94, RMSE = 0.30 mL/min/g). The $\mathrm{CTDI}_{\mathrm{vol}}^{32}$ and size-specific dose estimate of the low-dose prospective FPA technique were 2.3 and 3.7 mGy, corresponding to an effective dose of 0.52 and 0.83 mSv, respectively. Accurate submillisievert stress myocardial perfusion measurement is feasible using a low-dose prospective FPA dynamic CT perfusion technique.

Introduction

Coronary artery disease (CAD) is a major global health concern. While computed tomography (CT) angiography is a powerful tool for non-invasive assessment of CAD, it is an imperfect guide for percutaneous coronary intervention (PCI) as downstream PCI and optimal medical therapy outcomes are often equivalent[5]. Such discrepancies stem from the fact that CT angiography alone can only assess the morphological severity of segmental stenosis, i.e., it cannot resolve the physiological severity of concurrent multi-vessel, diffuse, and microvascular disease. Hence, guidelines[11-14] recommend additional physiological assessment of CAD to appropriately stratify patient risk and guide downstream intervention. Nevertheless, the primary modalities used for physiological assessment of CAD, i.e., single-photon emission computed tomography (SPECT), stress echocardiography, cardiac magnetic resonance, static positron emission tomography (PET), and static CT only provide metrics of relative perfusion[15, 16, 18-21]. As a result, they cannot resolve the true physiological severity of multiform CAD. Only absolute stress perfusion measurement in mL/min/g can overcome these

limitations, where the spatial distribution of stress perfusion combined with physiologic cutoff thresholds[23, 24] may be used to more reliably stratify patient risk and more properly guide downstream intervention.

Absolute stress perfusion is most commonly measured with dynamic PET[14, 25, 26]. However, limited radiotracer access and high cost preclude its routine clinical use[27]. Fortunately, recent research suggests that absolute stress perfusion measurement is also feasible with dynamic CT[13, 28-30], and can be used in conjunction with CT angiography for improved comprehensive workup of multiform CAD[28, 34]. Nevertheless, the known measurement inaccuracy[38, 116] and high effective dose (~10 mSv)[18, 37, 42] associated with current dynamic CT techniques also preclude its routine clinical use. Hence, there is a need for an improved low-dose dynamic CT perfusion technique.

The purpose of this study was to validate a low-dose prospective first-pass analysis (FPA) dynamic CT perfusion technique against a previously reported retrospective FPA dynamic CT perfusion technique[97, 98, 123]. The central hypothesis was that accurate submillisievert stress myocardial perfusion measurement is feasible using only two whole-heart volume scans that were prospectively acquired at reduced tube current.

Materials and Methods

FPA Dynamic CT Perfusion Theory

As previously described[97, 98, 123], first-pass analysis (FPA) and conservation of mass[117] state that the average perfusion (P_{AVE}) within the entire myocardium is proportional to

the first-pass entry of contrast material mass into the myocardium (dM_C/dt), normalized by the incoming contrast material concentration (C_{in}) and myocardial tissue mass (M_T), prior to contrast material outflow. By extension, the average perfusion (P_{AVE}) is also proportional to the first-pass contrast material concentration change within the myocardium; i.e., the average change in myocardial enhancement (ΔHU_{AVE}) over time. Hence, the integrated change in myocardial enhancement (dM_C/dt), the average change in myocardial enhancement (ΔHU_{AVE}), the average aortic blood pool enhancement (C_{in}), the voxel-by-voxel change in myocardial enhancement (ΔHU), and the total myocardial mass (M_T) may be used in combination to derive voxel-by-voxel perfusion (P_{FPA}), as described by **Equation 1** and **Figure 6.1a** and **6.1b.** Given such a theory, only two whole-heart volume scans, labeled V1 and V2 in **Figure 6.1b**, are mathematically necessary for low-dose FPA dynamic CT perfusion measurement, as previously validated versus invasive fractional flow reserve (FFR) measurement, quantitative microsphere perfusion, and ultrasonic flow probe measurement[97, 98, 123]. Specifically, V1 is defined as the first volume scan after the aortic enhancement exceeds 180 HU, while V2 is defined as the first volume scan at or after the peak of aortic enhancement.

$$\boldsymbol{P_{FPA} = \left(M_T^{-1} C_{in}^{-1} \frac{dM_c}{dt} \right)_{AVE} \cdot \frac{\Delta HU}{\Delta HU_{AVE}}} \qquad \textbf{(1)}$$

General Methods

The study was approved by the Animal Care Committee, was performed on ten male Yorkshire swine (42 ± 12 kg), and had two different experimental aims that were both successfully completed. For the first aim, the accuracy of retrospective FPA perfusion

measurement at several reduced tube currents under rest conditions was assessed in two animals. Specifically, retrospective perfusion measurements were made at 100 kVp and 100, 50, 25, and 10 mA and were compared to corresponding reference standard retrospective FPA perfusion measurements made at 100 kVp and 200 mA[97, 98, 123]. The findings of the first aim were then utilized for the second aim, where the accuracy of low-dose prospective FPA perfusion measurement was assessed in eight animals under stress conditions, with three of the eight animals also having intermediate stenoses with FFR severities of 0.7 - 0.9. Specifically, low-dose prospective perfusion measurements were made at 100 kVp and 50 mA and were compared to corresponding reference standard retrospective FPA perfusion measurements at 100 kVp and 200 mA[97, 98, 123]. All the data was acquired by authors LH, ShM, YZ, PA, and JK between 02/15/2017 and 12/13/2017, and was analyzed by authors LH and ShM between 01/01/2018 and 03/30/2018. LH and YZ were research associates with more than three years of medical imaging research experience and ShM was a research assistant with more than three years of medical imaging research experience. JK was a vascular surgeon with more than ten years of clinical experience and PA was a radiologist with more than fifteen years of clinical experience.

Animal Model Preparation

Anesthesia was induced with Telazol (4.4 mg/kg), Ketamine (2.2 mg/kg), and Xylazine (2.2 mg/kg), and was maintained with 1.5-2.5% Isoflurane (Highland Medical Equipment, Temecula, CA and Baxter, Deerfield, IL). Sheaths were placed (AVANTI®, Cordis Corporation, Miami Lakes, FL) in both femoral veins and were used for IV fluid,

adenosine, and contrast material administration. Additionally, in the last three animals, another sheath was placed in the right carotid artery and was used to pass a Judkins Right (JR) catheter (Cordis Corporation, Miami Lakes, FL) into the left coronary ostium. A pressure wire (PrimeWire PRESTIGE® Pressure Guide Wire, Volcano Corp, Rancho Cordova, CA) was then advanced through the JR catheter into the distal left anterior descending (LAD) coronary artery, and a balloon was passed over the wire into the mid LAD. The balloon was used to generate several sub-occlusive stenoses with fractional flow reserve (FFR) (ComboMap, Volcano Corp., Rancho Cordova, CA) severities of 0.7 – 0.9 at maximal IV stress (240 µg adenosine/kg/min, Model 55-2222, Harvard Apparatus, Holliston, MA).

Aim 1: Tube Current Reduction Methods

Reference Standard Retrospective FPA Dynamic CT Perfusion Protocol: Contrast material (1 mL/kg, Isovue 370, Bracco Diagnostics, Princeton, NJ) was injected (5 mL/s, Empower CTA, Acist Medical Systems, Eden Prairie, MN) followed by a saline chaser (0.5 mL/kg) at the same rate. Whole-heart volume scans were then acquired dynamically at 100 kVp and 200 mA (Aquilion One, Canon Medical Systems, Tustin, CA) over fifteen to twenty seconds to completely capture the aortic enhancement curve, where all volume scans were ECG-gated with a 0.35 second rotation time with 320 x 0.5 mm collimation. After each acquisition, two volume scans (V1 and V2) were selected systematically for reference standard retrospective FPA perfusion measurement, as previously validated versus invasive FFR, quantitative microsphere perfusion, and ultrasonic flow probe measurement[97, 98, 123].

Reduced Tube Current Retrospective FPA Dynamic CT Perfusion Protocol: A ten-minute delay was first employed after each reference standard acquisition to allow for adequate renal clearance of contrast material from the blood pool prior to each reduced tube current acquisition. After each delay, 1 mL/kg of contrast material was again injected (5 mL/s) followed by a saline chaser (0.5 mL/kg) at the same rate. Whole-heart volume scans were then acquired dynamically at 100 kVp and 100, 50, 25, and 10 mA (Aquilion One, Canon Medical Systems, Tustin, CA) over fifteen to twenty seconds to completely capture the aortic enhancement curve, where again, all volume scans were ECG-gated with a 0.35 second rotation time with 320 x 0.5 mm collimation. After each acquisition, two volume scans (V1 and V2) were selected systematically[97, 98, 123] for retrospective perfusion measurement at reduced tube current.

Aim 2: Low-Dose Prospective Acquisition Methods

Reference Standard Retrospective FPA Dynamic CT Perfusion Protocol: For all stress and stenotic conditions, contrast material (1 mL/kg, Isovue 370, Bracco Diagnostics, Princeton, NJ) was injected (5 mL/s, Empower CTA, Acist Medical Systems, Eden Prairie, MN) followed by a saline chaser (0.5 mL/kg) at the same rate. Whole-heart volume scans were then acquired dynamically at 100 kVp and 200 mA (Aquilion One, Canon Medical Systems, Tustin, CA) over fifteen to twenty seconds to completely capture the aortic enhancement curve. All volume scans were ECG-gated with a 0.35 second rotation time with 320 x 0.5 mm collimation. After each acquisition, two volume scans (V1 and V2) were then selected systematically for reference standard retrospective FPA perfusion measurement, as previously validated versus invasive FFR

and quantitative microsphere perfusion measurement[97, 98, 123]. Finally, the time delay (Δt) between V1 and V2 was estimated for each acquisition using automatic time-density-curve analysis (Acquilion One, Canon Medical Systems, Tustin, CA) and was used, in place of a test bolus[124], for proper timing of subsequent low-dose prospective FPA perfusion acquisitions. The entire reference standard retrospective FPA perfusion protocol is shown in **Figure 6.1c.**

Low-Dose Prospective FPA Dynamic CT Perfusion Protocol: A ten-minute delay was first employed after each reference standard acquisition to allow for adequate renal clearance of contrast material from the blood pool prior to each low-dose prospective acquisition. After each delay, 1 mL/kg of contrast material was again injected (5 mL/s) followed by a saline chaser (0.5 mL/kg) at the same rate. Low-dose, 2-mm slab, dynamic bolus tracking at 100 kVp and 50 mA (SureStart, Aquilion One, Canon Medical Systems, Tustin, CA) was then used, with V1 acquired after the aortic enhancement exceeded 180 HU and V2 acquired after V1 using the previously estimated time delay, Δt. For each acquisition, V1 and V2 were prospectively acquired at 100 kVp and 50 mA and were ECG-gated with a 0.35 second rotation time with 320 x 0.5 mm collimation. After each acquisition, V1 and V2 were used for low-dose prospective FPA perfusion measurement. Finally, the $CTDI_{vol}^{32}$ for all low-dose prospective stress perfusion measurements was recorded, with a size-specific dose estimate (SSDE) also determined[118] to account for the effective diameter of each swine used in the study. The $CTDI_{vol}^{32}$ and SSDE were then used, along with a standard chest conversion coefficient of 0.014 mSv/mGy[125] and the 16 cm cranio-caudal coverage, to estimate the effective

dose of low-dose prospective stress perfusion measurement. The entire low-dose prospective FPA perfusion protocol is shown in **Figure 6.1d.**

FPA Dynamic CT Perfusion Image Processing

For both experimental aims, all volume scans were first reconstructed from full projection data at 75% of the R-R interval using AIDR 3D reconstruction[126] and a voxel size of 0.43 x 0.43 x 0.50 mm. The volume scans of interest, i.e. V1 and V2, from each acquisition were then registered and combined into maximum intensity projection (MIP) image volumes. Each MIP was then segmented semi-automatically (Vitrea fX version 6.0, Vital Images, Inc., Minnetonka, MN), yielding the entire myocardium. Voxel-by-voxel perfusion measurements were then computed according to **Equation 1** and were averaged within the entire myocardium to yield global perfusion measurements. All global perfusion measurements for both experimental aims were then quantitatively compared to their corresponding reference standard retrospective perfusion measurements. Additionally, a case-study was performed in a single animal to assess the clinical utility of low-dose prospective stress perfusion measurements in the presence of intermediate severity stenoses with FFR severities of 0.7 - 0.9. Specifically, the stress perfusion maps for the animal were automatically clustered using predefined physiologic cutoff thresholds to yield the amount of myocardial tissue with normal stress perfusion (>2.39 mL/min/g), minimal stress perfusion reduction (1.76 – 2.39 mL/min/g), mild stress perfusion reduction (1.20 – 1.76 mL/min/g), moderate stress perfusion reduction (0.91 – 1.20 mL/min/g), and definite ischemia (0.00 – 0.91 mL/min/g)[24].

Statistical Approach

For the first aim, the retrospective perfusion measurements at reduced tube current were graphically compared to the corresponding reference standard retrospective perfusion measurements at 200 mA. Student's T-tests were also performed to determine if the retrospective perfusion measurements at reduced tube current were significantly different from the corresponding reference standard retrospective perfusion measurements at 200 mA. For the second aim, the low-dose prospective stress perfusion measurements were quantitatively compared to the corresponding reference standard retrospective perfusion measurements through regression, Bland-Altman, root-mean-square-error (RMSE), root-mean-square deviation (RMSD), and Lin's concordance correlation coefficient (CCC)[92]. Student's T-tests were again performed to determine if low-dose prospective stress perfusion measurements were significantly different from corresponding reference standard retrospective stress perfusion measurements. All fit parameter data are reported with 95% confidence intervals displayed in brackets. All other data are reported as mean ± standard deviation. P-values less than 0.05 indicate significant differences. Statistical software was used for all analyses (MatLab 2013a, MathWorks, Natick, MA; PS, Version 3.0, Vanderbilt University, Nashville, TN; SPSS, Version 22, IBM Corporation, Armonk, NY).

Results

General Results:

The heart rate and mean arterial pressure of the ten swine were 94 ± 9 beats per minute and 74 ± 9 mmHg, respectively. For the first experimental aim, rest perfusion at

100, 50, 25, and 10 mA was 0.79 ± 0.37 mL/min/g, 0.69 ± 0.25 mL/min/g, 0.43 ± 0.31 mL/min/g, and 0.27 ± 0.22 mL/min/g, respectively, while reference standard rest perfusion was 0.71 ± 0.33 mL/min/g. The $\mathrm{CTDI}_{\mathrm{vol}}^{32}$ of rest perfusion at 100, 50, 25, and 10 mA was 4.60, 2.30, 1.15, and 0.46 mGy, while the $\mathrm{CTDI}_{\mathrm{vol}}^{32}$ of reference standard rest perfusion measurement was 9.20 mGy. All other mA reduction data are reported in **Table 6.1** and **Figure 6.2**. For the second experimental aim, low-dose prospective stress perfusion was 2.01 ± 0.88 mL/min/g, while reference standard stress perfusion was 1.96 ± 0.77 mL/min/g. The $\mathrm{CTDI}_{\mathrm{vol}}^{32}$ and SSDE for each low-dose prospective stress perfusion acquisition were estimated to be 2.3 and 3.7 ± 0.43 mGy, corresponding to an estimated effective dose of 0.52 and 0.84 ± 0.10 mSv, respectively. All other comparison and dose data are also reported in **Table 6.2.**

Accuracy and Precision Results

For the first experimental aim, rest perfusion measurements at 100 and 50 mA were not significantly different from reference standard rest perfusion measurements ($p = 0.33$ and $p = 0.43$), while rest perfusion measurements at 25 and 10 mA were significantly different from reference standard rest perfusion measurements ($p = 0.04$ and $p = 0.00$). All other tube current reduction mean comparisons data are reported in **Table 6.1**. For the second experimental aim, low-dose prospective stress perfusion (P_{LOW}) and reference standard stress perfusion (P_{REF}) measurements were related by $P_{LOW} = 1.07\ P_{REF} - 0.09$, with a Pearson's correlation of $r = 0.94$, a concordance correlation of $\rho = 0.93$, a root-mean-square-error of 0.30 mL/min/g, and a root-mean-square deviation of

0.29 mL/min/g, as shown in **Figure 6.3** and **Table 6.3**. The 95% confidence intervals for all fit parameter data are shown in **Table 6.3**.

Case-Study Results

For one animal, low-dose prospective stress perfusion maps are displayed for stress perfusion measurement in the absence and presence of a significant LAD stenosis, as shown in **Figure 6.4**. In each case, the amount of myocardial tissue with normal flow (>2.39 mL/min/g), no ischemia but minimal flow reduction (1.76 – 2.39 mL/min/g), no ischemia but mild flow reduction (1.20 – 1.76 mL/min/g), moderate flow reduction (0.91 – 1.20 mL/min/g), and definite ischemia (0.00 – 0.91 mL/min/g)[24] is also reported in **Table 6.4.**

Discussion

Indication of Results

The results of rest perfusion measurement at 100 and 50 mA were in good agreement with reference standard rest perfusion measurement at 200 mA, while rest perfusion measurement at 25 and 10 mA significantly underestimated reference standard rest perfusion measurement. Hence, the results of the first experimental aim suggest that accurate FPA perfusion measurement is feasible at a tube current as low as 50 mA, i.e., at one-quarter of the dose of the previously validated reference standard retrospective FPA technique. Moreover, the results of the second aim go on to demonstrate that accurate low-dose prospective FPA perfusion measurement at 100 kVp and 50 mA is also feasible, as compared to the previously validated reference standard retrospective

FPA technique. First, there were no significant differences between average low-dose prospective stress perfusion measurement and average reference standard retrospective stress perfusion measurement. Second, low-dose prospective stress perfusion measurements agreed with reference standard stress perfusion measurements, demonstrating near unity slope, minimal offset, negligible bias, good concordance correlation, and small RMSE and RMSD. Third, the spatial distribution of low-dose prospective stress perfusion also agreed with the induced flow conditions, where stress perfusion without a stenosis was shown to be normal, while stress perfusion distal to an LAD stenosis with FFR severity of 0.7 was shown to be markedly reduced. The fractional breakdown of stress perfusion throughout the myocardium was also in agreement in each case. In combination, these findings suggest that stress perfusion measurement with the low-dose prospective FPA technique is feasible at a $\mathrm{CTDI}_{\mathrm{vol}}^{32}$ and SSDE of 2.3 and 3.7 ± 0.43 mGy, corresponding to an estimated effective dose of 0.52 and 0.84 ± 0.10 mSv, respectively.

Limitations

This study is not without limitations. For both experimental aims, the perfusion between the reduced tube current or low-dose prospective acquisitions and their corresponding reference standard acquisitions was assumed to be unchanged. However, fluctuations in the animals' vitals between paired acquisitions may have contributed to measurement variance. Hence, considerable effort was made to tightly control ventilation, anesthesia, IV fluid administration, and hemodynamics such that perfusion measurement variance was minimized between acquisitions. Alternatively for the first aim, artificial noise could

have been added to the raw data projections of the reference standard retrospective acquisitions to simulate reduced tube current acquisitions[127], but raw data projection access was not possible; hence, the same validation approach was used for both aims.

Regarding the second experimental aim, the main limitation was the prospective timing of V2. Specifically, given the two-volume acquisition scheme that is central to the FPA technique, V2 must be acquired at or within one cardiac cycle of the peak of the aortic enhancement for perfusion measurements to be accurate[97, 98, 123]. Unfortunately, hemodynamic variability and differences in injection volume negate the use of a fixed time delay between V1 and V2[128-131]. Hence, for the purposes of this study, the time delay (Δt) between V1 and V2 was estimated from each reference standard retrospective FPA perfusion acquisition prior to each subsequent low-dose prospective FPA perfusion acquisition. Clinically, such a time delay prediction can be addressed through the preemptive use of a low-dose diluted test bolus acquisition[124]. Specifically, the geometry of a diluted test bolus emulates that of a true bolus[124]; hence, the correct time-delay can be predicted in advance and used for accurate, prospective acquisition of V2, with negligible increases in contrast and radiation dose per exam.

Another limitation of the study was the small 25 cm effective diameter of the animals used as compared to the average 34 cm effective diameter of patients with CAD[44]. More specifically, when using a fixed tube current, a patient with a large effective diameter will have lower photon flux as compared to a patient with a small effective diameter. Such a relation is problematic at very low tube currents, as photon starvation can lead to

attenuation bias which can lead to perfusion measurement inaccuracy[127]. Fortunately, work by Mirsadraee et al. suggests that a tube current as low as 50 mA can be used over a large range of effective diameters with minimal attenuation bias[127], although measurement noise still increases with effective diameter. Alternatively, exposure control techniques (SureExposure, Acquilion One, Canon Medical Systems, Tustin, CA) may provide a more optimal solution through automatic adjustment of the tube current to maintain the same level of measurement noise at any effective diameter. Given such an approach, a CAD patient with an average effective diameter of 34 cm[44] would receive an effective dose of approximately 1.69 mSv, as estimated by water phantom tests and displayed in **Figure 6.5**. More importantly, the cranial-caudal coverage used in this study was 16 cm, whereas the cranial-caudal coverage necessary for most whole-heart cardiac imaging is only 12 cm[44]. Hence, careful collimation of the cardiac window may also provide 25% more reduction in effective dose, i.e., a CAD patient with an average effective diameter of 34 cm[44] would receive an effective dose of only 1.27 mSv, again as displayed in **Figure 6.5.** Additional dose reduction may also be achievable through larger reductions in tube current combined with better model-based iterative reconstruction algorithms such as FIRST[132]. Thus, the effective dose of the low-dose prospective FPA technique will still be much lower than the 10 mSv average effective dose of existing dynamic CT perfusion techniques[18], even for large effective diameter patients, owing to the fact that only *two* prospective whole-heart volume scans are necessary for accurate FPA perfusion measurement in mL/min/g.

One final limitation of the study was that global perfusion measurements were used for validation of both experimental aims. Specifically, the spatial distribution of stress perfusion combined with physiologic cutoff thresholds[23, 24] is necessary for reliable risk stratification and proper downstream intervention; hence, the value of global perfusion measurement is limited. Fortunately, the FPA technique can spatially resolve perfusion on a voxel-by-voxel basis**.** Nevertheless, voxel-by-voxel perfusion measurement variance depends on image noise which depends on tube current. Hence, at reduced tube currents, spatial perfusion measurement variance is increased. Fortunately, local binning can be used to suppress measurement variance while maintaining sufficient spatial perfusion resolution. More importantly, if low-dose prospective FPA perfusion data is acquired in combination with a CT angiogram[97, 123], minimum-cost-path myocardial assignment[47, 133] can be used to generate coronary vessel-specific territories, i.e., voxel-by-voxel perfusion measurements can be averaged within each territory to yield vessel-specific perfusion measurement, while also suppressing measurement variance[97, 123].

Conclusion

The low-dose prospective FPA technique enables accurate submillisievert measurement of stress myocardial perfusion using only two whole-heart volume scans that are prospectively acquired at reduced tube current. Specifically, the results of the first experimental aim indicate that tube current can be reduced to as low as 50 mA, while maintaining FPA perfusion measurement accuracy – allowing for a 75% reduction in effective dose as compared to the previously validated retrospective FPA technique[97,

[98, 123]. Moreover, the results of the second experimental aim indicate that low-dose prospective FPA perfusion measurement is also feasible, i.e., only two volume scans need to be acquired for accurate low-dose prospective FPA perfusion measurement as compared to the previously validated retrospective FPA technique[97, 98, 123]. Hence, the low-dose prospective FPA technique can dramatically reduce the radiation dose associated with dynamic CT-based assessment of stress perfusion. In summary, the low-dose prospective FPA technique was validated in a swine model and has the potential to be used for accurate submillisievert stress myocardial perfusion measurement.

Tables

Table 6.1. Rest perfusion measurement at reduced tube current and reference standard rest perfusion measurement mean comparison with corresponding dose metrics

Perfusion Metric	200 mA Reference	100 mA	50 mA	25 mA	10 mA
REST (N = 4)					
GLOBAL (mL/min/g)	0.71 ± 0.33	0.79 ± 0.37 (p = 0.33)	0.69 ± 0.25 (p = 0.43)	0.43 ± 0.31 (p = 0.04)	0.27 ± 0.22 (p = 0.00)
$\mathrm{CTDI}_{\mathrm{vol}}^{32}$ (mGy)	9.20	4.60	2.30	1.15	0.46

P-values less than 0.05 indicate significant mean differences in rest perfusion. mA indicates the tube current setting; N, the number of perfusion measurements at each tube current setting; GLOBAL, the entire myocardium; $\mathrm{CTDI}_{\mathrm{vol}}^{32}$, CT dose index per perfusion measurement.

Table 6.2. Low-dose prospective stress perfusion measurement and reference standard retrospective stress perfusion measurement mean comparison with corresponding low-dose prospective stress perfusion dose metrics.

Perfusion Condition	Low-Dose Perfusion (mL/min/g)	Reference Perfusion (mL/min/g)	P-value (α < 0.05)	$CTDI_{vol}^{32}$ (mGy)	SSDE (mGy)	ED (mSv)	SSED (mSv)
STRESS (N = 18)							
GLOBAL	2.01 ± 0.88	1.96 ± 0.77	0.55	2.30	3.74 ± 0.43	0.52	0.84 ± 0.10

P-values less than 0.05 indicate significant mean differences. N indicates the number of perfusion measurements; GLOBAL, the entire myocardium; CTDI, CT dose index; SSDE, size-specific dose estimate; ED, effective dose; SSED, size-specific effective dose.

Table 6.3. Low-dose prospective stress perfusion measurement and reference standard retrospective stress perfusion measurement accuracy and precision analysis

Perfusion Condition	Slope	Intercept	Pearson's r	Lin's CCC	RMSE (mL/min/g)	RMSD (mL/min/g)
STRESS (N = 18)						
GLOBAL	1.07 [0.86, 1.27]	-0.09 [-0.52, 0.35]	0.94 [0.84, 0.98]	0.93 [0.82, 0.97]	0.30	0.29

Brackets indicate 95% confidence intervals. N indicates the number of perfusion measurements; GLOBAL, the entire myocardium; Lin's CCC, Lin's concordance correlation coefficient; RMSE, root-mean-square error; RMSD, root-mean-square deviation.

Table 6.4. Low-dose prospective stress perfusion distribution in the left ventricle of a single animal in the absence and presence of physiologically significant LAD stenosis[24]

Stress Perfusion Cutoff Thresholds (mL/min/g)	FFR = 1.0 LV Mass (%)	FFR = 0.90 LV Mass (%)	FFR = 0.80 LV Mass (%)	FFR = 0.70 LV Mass (%)
0.00 - 0.91 Definite ischemia	5.98	8.98	19.89	25.45
0.91 - 1.20 Moderate reduction	4.60	3.45	3.51	5.69
1.20 - 1.76 Mild reduction	11.67	11.02	9.10	12.47
1.76 - 2.39 Minimal reduction	10.86	19.78	8.87	16.72
2.39 < Normal flow	66.88	56.77	58.64	39.66

All stress perfusion cutoff thresholds are outlined by Johnson and Gould[24]. LAD indicates the left anterior descending coronary artery; FFR, fractional flow reserve; LV, left ventricle.

Figures

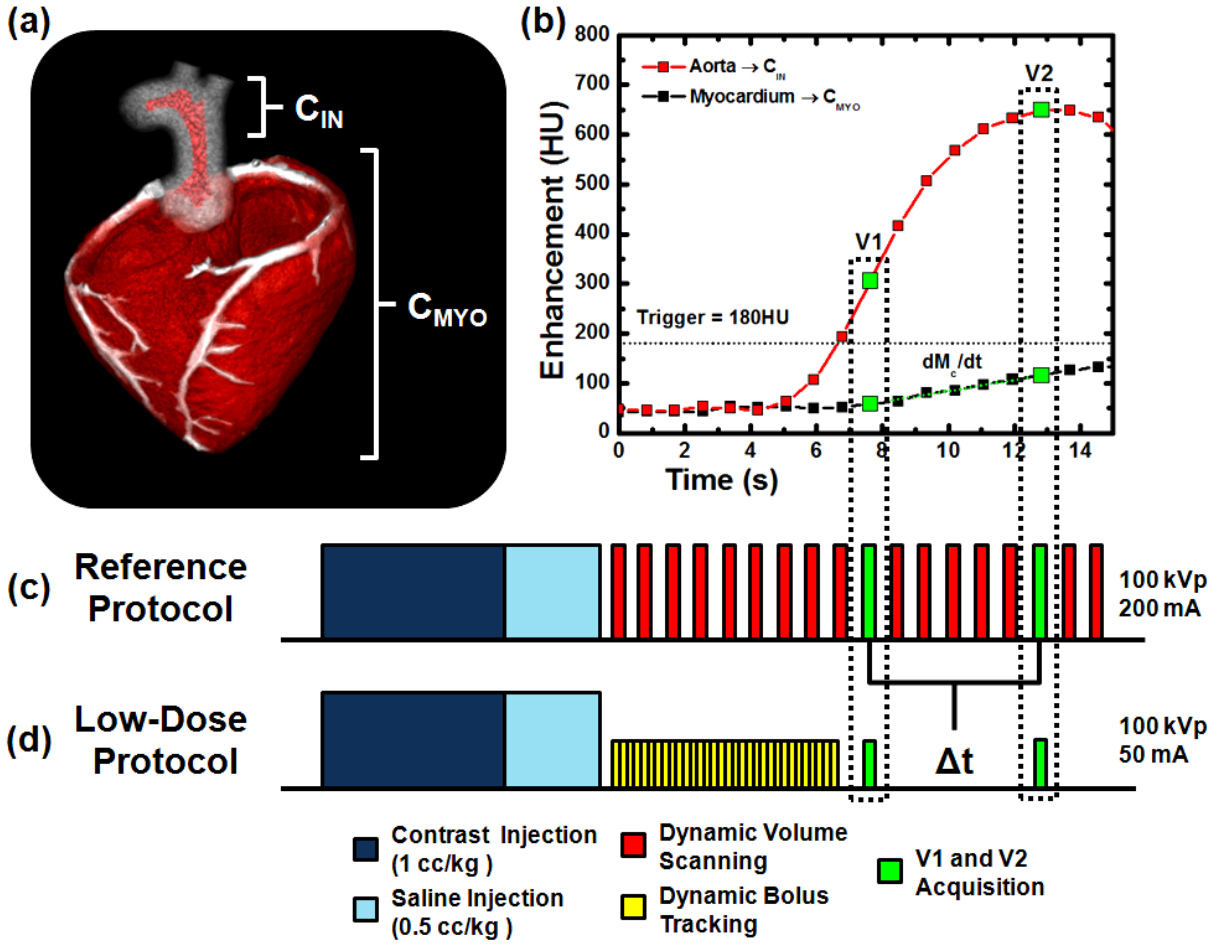

Figure 6.1: First-pass analysis theory and implementation. (a) Whole-heart myocardial perfusion compartment (C_{MYO}) used for first-pass-analysis dynamic CT perfusion measurement. The input concentration (C_{IN}) is derived from the lumen of the aorta. The myocardial mass, M_T in Equation 1, is derived from the whole-heart myocardial perfusion compartment (C_{MYO}). (b) The first-pass enhancement within the aorta and myocardium following contrast and saline injection are shown in red and black, respectively. Two first-pass volume scans, V1 and V2 denoted in green, are used for both reference standard retrospective and low-dose prospective perfusion measurement, respectively. Specifically, the integrated change in myocardial enhancement (dM_C/dt), the average change in myocardial enhancement (ΔHU_{AVE}), the average aortic enhancement (C_{IN}), and the voxel-by-voxel change in myocardial enhancement (ΔHU) between V1 and V2 are used in combination with the total myocardial mass (M_T) to derive voxel-by-voxel perfusion (P_{FPA}). (c) The reference standard retrospective FPA dynamic CT perfusion protocol is comprised of contrast injection followed by dynamic volume scan acquisition at 100 kVp and 200 mA over fifteen to twenty seconds (d) The low-dose prospective FPA dynamic CT perfusion protocol is comprised of contrast injection followed by 2-mm slab dynamic bolus tracking at 100 kVp and 50 mA, threshold-based triggering at 180 HU, then dynamic volume scan acquisition of two volume scans, V1 and V2, at 100 kVp and 50 mA.

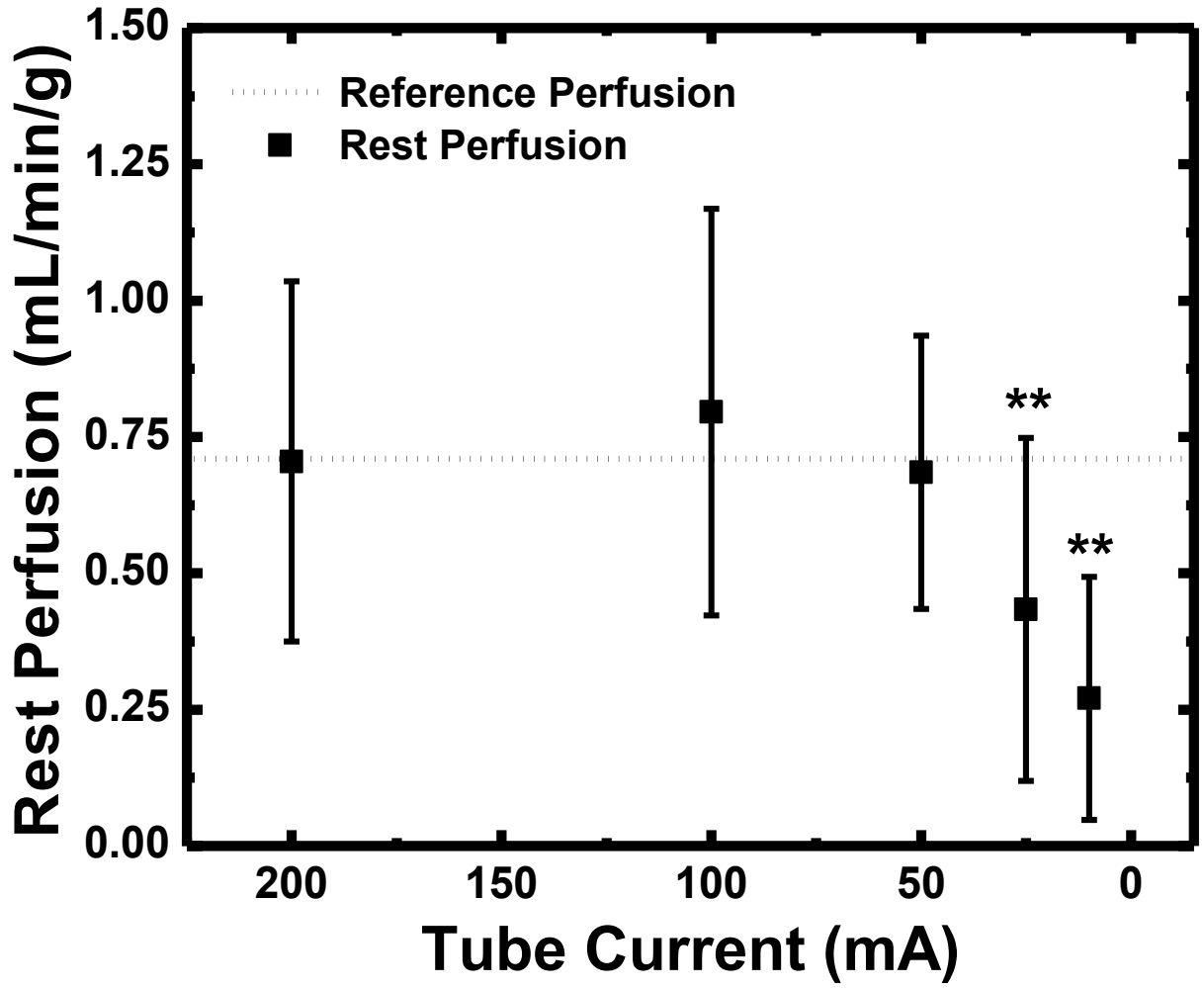

Figure 6.2: Reduced tube current rest perfusion measurement analysis. The graphical analysis compares rest perfusion measurements at several reduced tube current to corresponding reference standard retrospective rest perfusion measurements at 200 mA. mA indicates the tube current in milliamperes. **Indicates a significant difference in rest perfusion measurement.

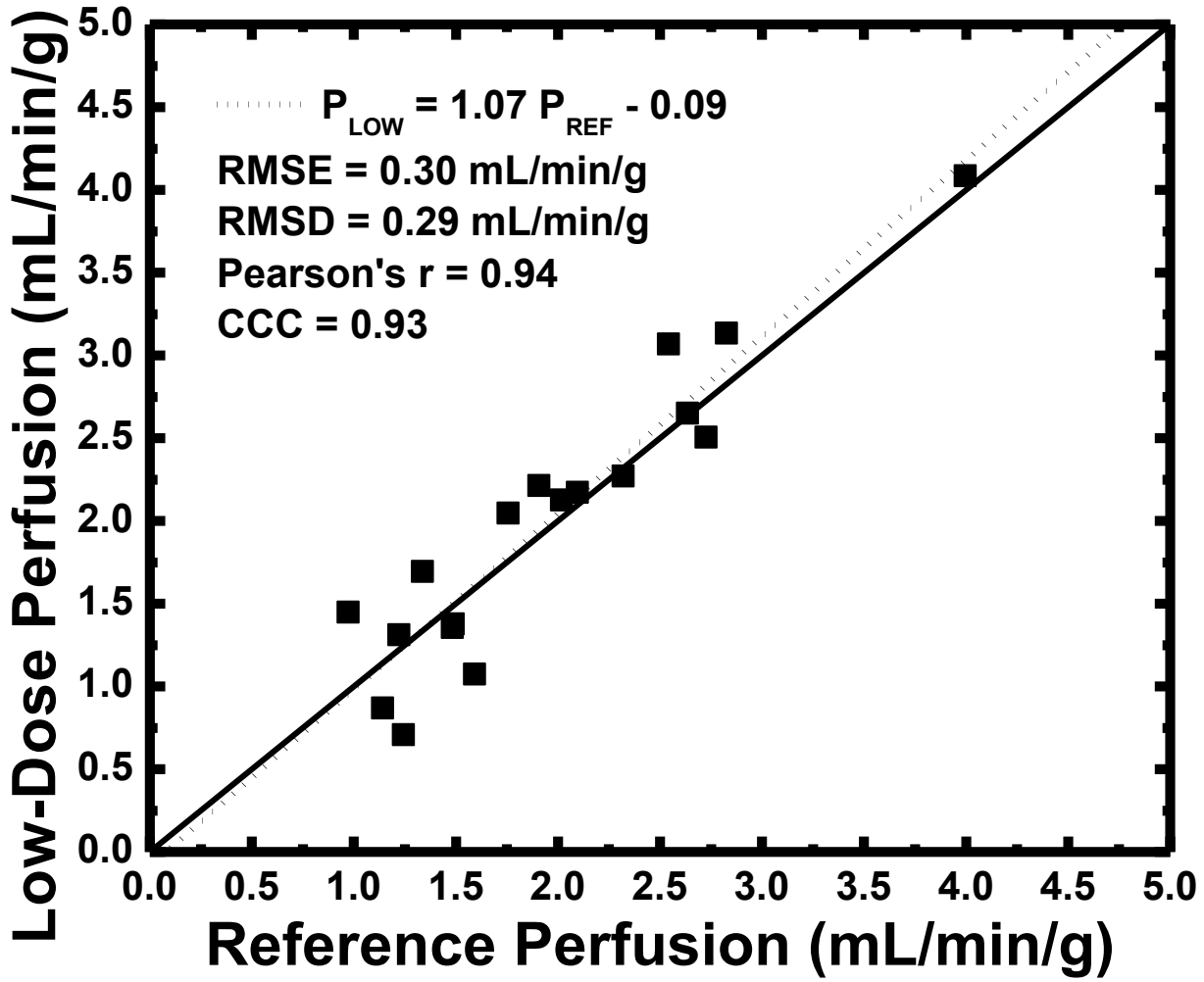

Figure 6.3: Low-dose prospective stress perfusion measurement analysis. The regression analysis compares low-dose prospective stress perfusion measurements at 50 mA (P_{LOW}) to corresponding reference standard retrospective stress perfusion measurements at 200 mA (P_{REF}). RMSE indicates root-mean-square-error; RMSD, root-mean-square-deviation; CCC, Lin's concordance correlation.

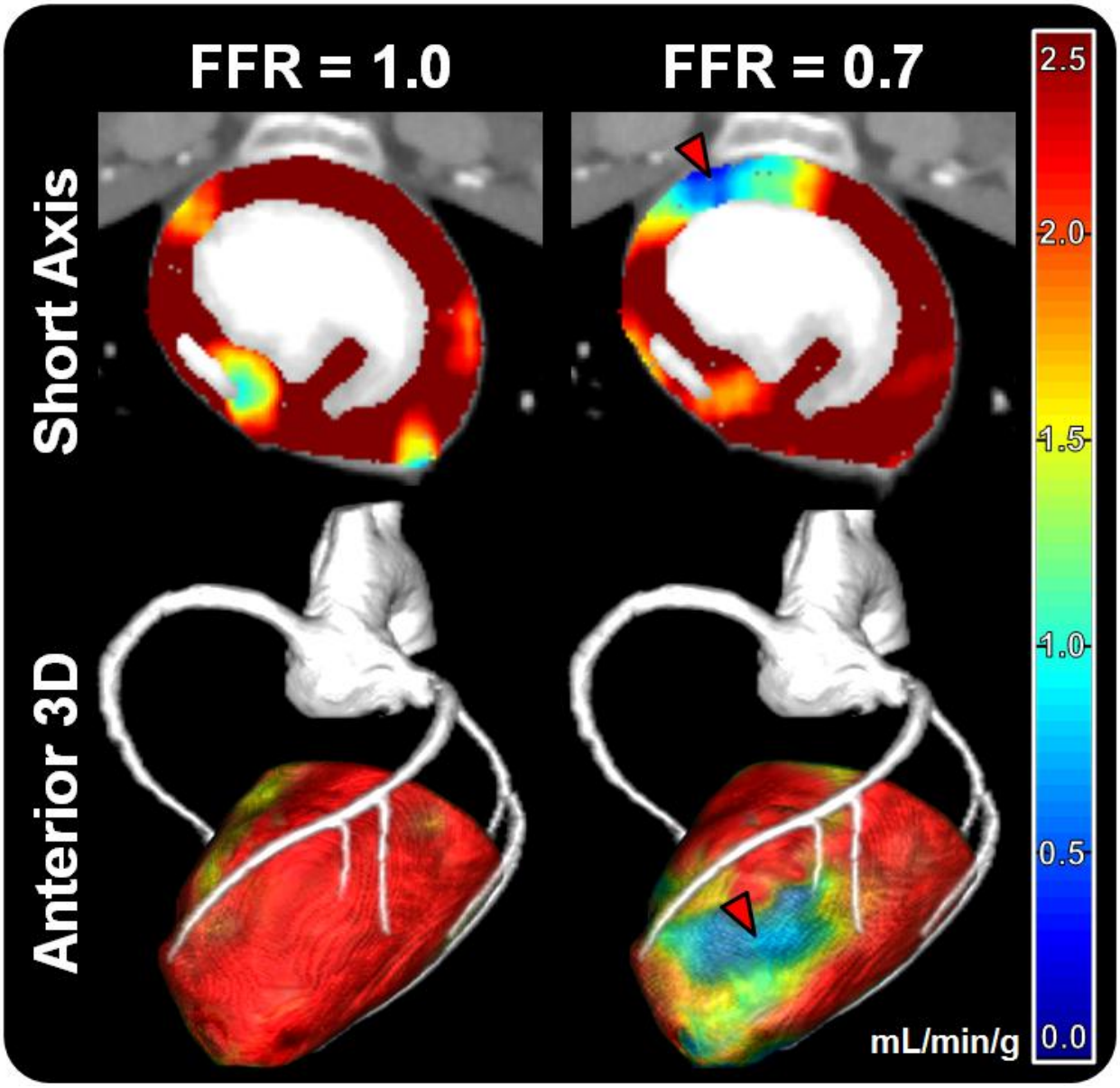

Figure 6.4: Low-dose prospective stress perfusion measurement distribution in the absence and presence of a physiologically significant left anterior descending (LAD) coronary artery stenosis. The perfusion deficit displayed in the short axis view (top row) and anterior 3D view of the left ventricle (bottom row) had an FFR severity of 0.70. The red arrow in the short axis and anterior 3D view of the left ventricle indicates the perfusion defect in the LAD territory. The colorbar indicates low-dose prospective stress perfusion measurement in mL/min/g.

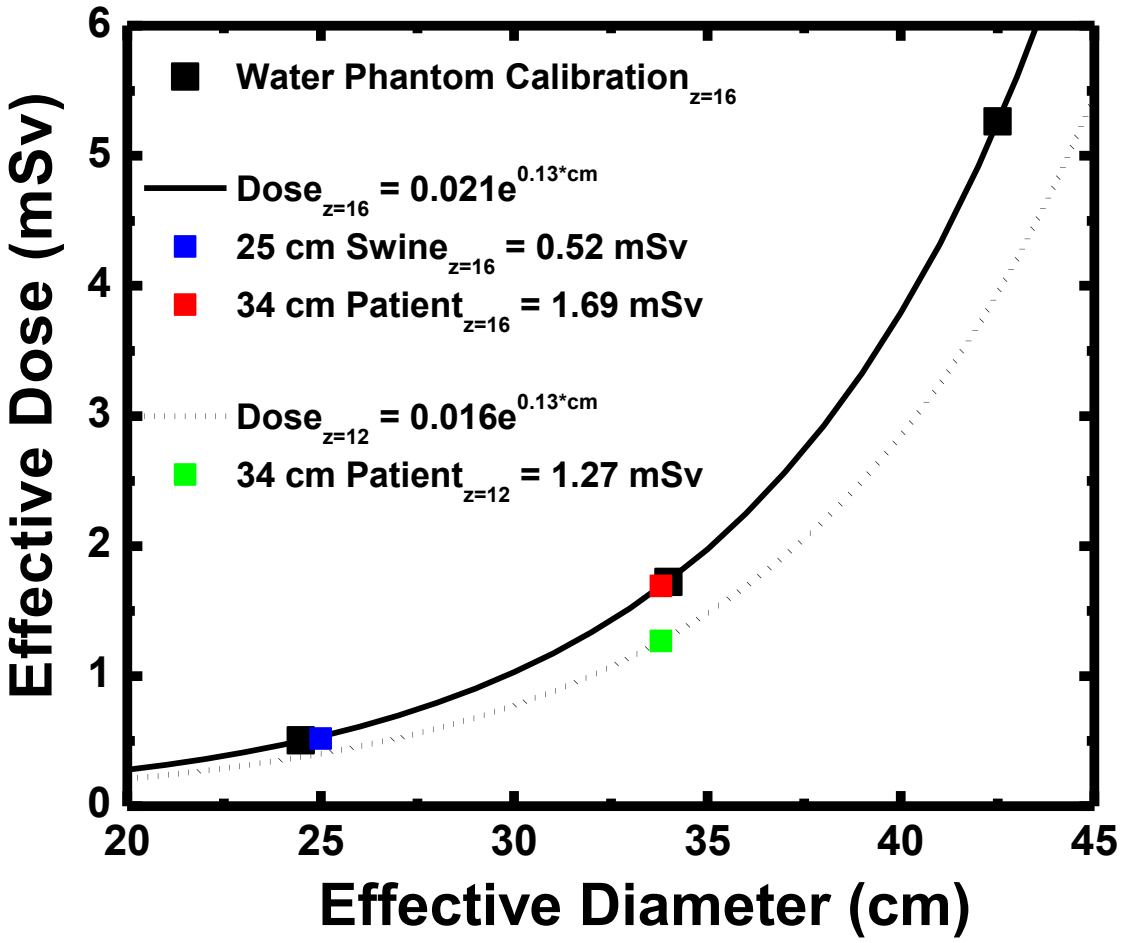

Figure 6.5: Effective dose of the low-dose prospective FPA technique using automatic exposure control. The automatic exposure settings (SureExposure, Acquilion One, Canon Medical Systems, Tustin, CA) were first tuned to match the image noise characteristics that were validated in the 25 cm effective diameter swine. Water phantoms with effective diameters of 24 cm, 34 cm, and 42.5 cm were then used to estimate the effective dose of stress perfusion measurement with the low-dose FPA technique over a range of effective diameters. The effective dose of low-dose stress perfusion measurement in an average 34 cm effective diameter patient is also displayed. All effective dose estimates are shown for a cranio-caudal coverage of 12 cm (z = 12) and 16 cm (z = 16), respectively.

CHAPTER 7: LOW-DOSE PROSPECTIVE VESSEL-SPECIFIC REST PERFUSION, STRESS PERFUSION, CORONARY FLOW RESERVE, AND ANGIOGRAPHY AS COMPARED TO RETROSPECTIVE PERFUSION MEASUREMENT IN SWINE

Abstract

The purpose of this study was to evaluate a low-dose comprehensive cardiac CT technique for combined morphological and physiological assessment of coronary artery disease. The low-dose comprehensive cardiac CT technique, which consists of first-pass analysis (FPA) dynamic CT perfusion, CT angiography, and coronary flow reserve (CFR), was evaluated in twelve swine (43 ± 11 kg) under rest and stress conditions by direct comparison to a previously validated FPA technique. In three of the swine, intermediate stenoses with fractional flow reserve severities of 0.70 - 0.90 were also assessed. Contrast and saline were injected peripherally (370 mgI/mL contrast: 1 mL/kg at 5 mL/s; saline: 0.5 mL/kg at 5 mL/s) followed by dynamic volume scan acquisition with a 320-slice CT scanner. For each perfusion condition, only two volume scans were acquired for the low-dose comprehensive cardiac CT technique, while 20 volume scans were acquired for the reference standard retrospective technique. All of the comprehensive cardiac CT perfusion measurements were then compared to corresponding reference standard perfusion measurements through regression analysis. The $\mathrm{CTDI}_{\mathrm{vol}}^{32}$ and size-specific dose estimate of the comprehensive cardiac CT technique were also computed and used to estimate effective dose.Low-dose comprehensive cardiac CT perfusion measurements (P_{LOW}) were in good agreement

with reference standard perfusion measurements (P_{REF}) (P_{LOW} = 1.04 P_{REF} - 0.08, r = 0.94, RMSE = 0.32 mL/min/g). The $\mathrm{CTDI}_{\mathrm{vol}}^{32}$ of rest perfusion, stress perfusion, CFR, rest perfusion combined with CT angiography, and CFR combined with CT angiography were 2.30, 2.30, 4.60, 5.75, and 8.05 mGy, respectively, with corresponding size-specific dose estimates of 3.66, 3.66, 7.31, 9.14, and 12.80 mGy. In combination, the maximum effective dose and size-specific effective dose of the comprehensive cardiac CT technique were 1.8 and 2.87 mSv, respectively. Accurate morphological and physiological assessment of coronary artery disease is feasible with a low-dose comprehensive cardiac CT technique based on first-pass analysis.

Introduction

Coronary artery disease (CAD) is the leading cause of morbidity and mortality worldwide. As a risk factor, CAD and its resultant ischemic cardiomyopathy are strongly predicative of future cardiac events. While coronary computed tomography (CT) angiography is a powerful tool for assessing CAD risk, it is fundamentally limited in that it can only assess the morphological severity of segmental CAD, but cannot define the physiological severity of concurrent mutli-vessel, diffuse, and microvascular disease. Hence, guidelines recommend additional physiological assessment of CAD, in conjunction with CT angiography[17, 20] for more objective indication of patient risk[11-14]. The primary modalities used for physiological assessment are single-photon emission computed tomography (SPECT), stress echocardiography, cardiac magnetic resonance (CMR), static positron emission tomography (PET), and static CT. However, such modalities only provide metrics of relative perfusion; hence, they still cannot appreciate the true physiological severity of multiform CAD[15, 16, 18-21]. Fortunately, absolute

perfusion measurement with dynamic CT can overcome these limitations[4, 17-19], where the spatial distribution of absolute rest and stress perfusion in mL/min/g combined with physiological cutoff thresholds can be used to reliably stratify patient risk and properly guide intervention[23, 24]. Nevertheless, current dynamic CT perfusion techniques are known to be quantitatively inaccurate[38, 115, 116] and deliver unacceptably high effective radiation doses per imaging exam (~10 mSv)[18, 37, 42], precluding their widespread clinical use. Thus, given the limitations of CT angiography and dynamic CT perfusion, there is a major unmet clinical need for an accurate, low-dose CT technique for combined morphological and physiological assessment of multiform CAD.

The purpose of this study was to address that unmet clinical need through the development and validation of an accurate, low-dose, comprehensive cardiac CT technique based on first-pass analysis (FPA). The central hypothesis was that accurate, low-dose, vessel-specific rest and stress perfusion measurement is feasible while simultaneously providing CT angiography and coronary flow reserve (CFR) using only four volume scans and two contrast injections, respectively.

Materials and Methods

Low-Dose Comprehensive Cardiac CT Theory

First-pass analysis (FPA) and conservation of mass[117] state that the average perfusion (P_{AVE}) within the entire myocardium is proportional to the first-pass accumulation of contrast material mass into the myocardium (dM_C/dt), normalized by the incoming contrast material concentration (C_{in}) and myocardial tissue mass (M_T), prior to contrast

material outflow via the coronary sinus. Moreover, given that the volume of the myocardium is fixed, the average perfusion (P_{AVE}) is also proportional to the first-pass change in contrast material concentration within the myocardium over time (ΔHU_{AVE}). As such, the integrated change in myocardial enhancement (dM_C/dt), the average change in myocardial enhancement (ΔHU_{AVE}), the average aortic blood pool enhancement (C_{in}), the voxel-by-voxel change in myocardial enhancement (ΔHU), and the total myocardial mass (M_T) may be used in combination to derive voxel-by-voxel perfusion (P_{FPA}), as described by **Equation 7.1** and **Figure 7.1a** and **7.1b.** Based on this derivation, only two whole-heart volume scans, labeled V1 and V2 in **Figure 7.1b**, are mathematically necessary for low-dose FPA perfusion measurement, as previously validated versus invasive fractional flow reserve (FFR), quantitative microsphere perfusion, and ultrasonic flow probe measurement[97, 98, 123], where V1 is defined as the first volume scan after the aortic enhancement exceeds 180 HU, while V2 is defined as the first volume scan at or within one cardiac cycle of the peak of aortic enhancement. More importantly, given the temporal location of V2 in relation to the peak of the aortic enhancement, V2 may also be used as a diagnostic quality CT angiogram if the tube current of that volume scan is increased[97, 98]. Thus, low-dose FPA perfusion and CT angiography can be combined into a single exam under rest perfusion conditions using a single contrast injection, as previously described[97, 123]. Additionally, if low-dose FPA stress perfusion measurements are also acquired following the rest exam, co-registered stress perfusion, rest perfusion, coronary flow reserve (CFR), and CT angiography data can all be obtained. Moreover, given the CT angiogram, minimum-cost-path myocardial assignment[47, 97, 123, 133] can also be used to generate coronary vessel-specific territories

such that all stress perfusion, rest perfusion, and CFR data can be assessed in the left anterior descending (LAD), left circumflex (LCx), and right coronary artery (RCA)[97, 123] individually[19, 20].

$$\boldsymbol{P_{FPA} = \left(M_T^{-1} C_{in}^{-1} \frac{dM_c}{dt} \right)_{AVE} \cdot \frac{\Delta HU}{\Delta HU_{AVE}}} \qquad \textbf{(1)}$$

General Methods

The study was approved by the Animal Care Committee and was performed on twelve male Yorkshire swine (43 ± 11 kg). Each animal was imaged with the low-dose comprehensive cardiac CT technique, which consisted of simultaneous FPA perfusion and CT angiography under rest conditions followed by FPA perfusion under stress conditions ten minutes later. Given the CT angiogram, minimum-cost-path myocardial assignment[47, 97, 123, 133] was then performed to generate coronary vessel-specific territories, such that all stress perfusion, rest perfusion data could be assessed in the LAD, LCx, and RCA individually[19, 20]. The ratio of stress to rest perfusion in each vessel was then used to compute CFR. All low-dose, vessel-specific rest and stress perfusion and CFR measurements were then compared to the corresponding reference standard retrospective FPA perfusion and CFR measurements[97, 98, 123]. Of important note, the reference standard retrospective FPA perfusion technique was previously validated versus invasive FFR, quantitative microsphere perfusion, and ultrasonic flow probe measurement[97, 98, 123]. All of the data was acquired by authors LH, ShM, YZ, PA, and JK between 02/15/2017 and 12/13/2017, and was analyzed by authors LH and ShM between 01/01/2018 and 04/20/2018. LH and YZ were research associates with more

than three years of medical imaging research experience and ShM was a research assistant with more than three years of medical imaging research experience. JK was a vascular surgeon with more than ten years of clinical experience and PA was a radiologist with more than fifteen years of clinical experience.

Animal Model Preparation

Anesthesia was induced in twelve animals with Telazol (4.4 mg/kg), Ketamine (2.2 mg/kg), and Xylazine (2.2 mg/kg), and was maintained with 1.5-2.5% Isoflurane (Highland Medical Equipment, Temecula, CA and Baxter, Deerfield, IL). Sheaths were placed (AVANTI®, Cordis Corporation, Miami Lakes, FL) in both femoral veins and were used for IV adenosine and contrast material administration. Additionally, in three of the animals, another sheath was placed in the right carotid artery and was used to pass a Judkins Right (JR) catheter (Cordis Corporation, Miami Lakes, FL) into the left coronary ostium. A pressure wire (PrimeWire PRESTIGE® Pressure Guide Wire, Volcano Corp, Rancho Cordova, CA) was then advanced through the JR catheter into the distal left anterior descending (LAD) coronary artery and a balloon was passed over the wire into the mid LAD. The balloon was then used to generate several sub-occlusive stenoses with fractional flow reserve (FFR, ComboMap, Volcano Corp., Rancho Cordova, CA) severities of 0.7 – 0.9 under maximal IV stress (240 µg adenosine/kg/min, Model 55-2222, Harvard Apparatus, Holliston, MA).

FPA Rest Perfusion and CT Angiography Acquisition Methodology

Reference Standard FPA Rest Perfusion and CT Angiography Protocol: For all rest perfusion conditions, contrast material (1 mL/kg, Isovue 370, Bracco Diagnostics, Princeton, NJ) was injected (5 mL/s, Empower CTA, Acist Medical Systems, Eden Prairie, MN) followed by a saline chaser (0.5 mL/kg) at the same rate. Whole-heart volume scans were then acquired dynamically at 100 kVp and 200 mA (Aquilion One, Canon Medical Systems, Tustin, CA) over fifteen to twenty seconds to completely capture the aortic enhancement curve. Additionally, all volume scans were ECG-gated with a 0.35 second rotation time with 320 x 0.5 mm collimation. After each acquisition, V1 and V2 were selected systematically for reference standard FPA rest perfusion measurement while V2 was also used for CT angiography, as previously validated versus invasive FFR, quantitative microsphere perfusion, and ultrasonic flow probe measurement[97, 98, 123]. Reference standard vessel-specific rest perfusion measurements in the LAD, LCx, and RCA were then derived using the CT angiogram and minimum-cost-path myocardial assignment[47, 97, 123, 133]. Finally, the time delay (ΔT_R) between V1 and V2 was estimated for each acquisition using automatic time-density-curve analysis (Acquilion One, Canon Medical Systems, Tustin, CA) and was used, in place of a test bolus[124], for proper timing of the subsequent low-dose FPA rest perfusion and CT angiography protocol. The entire reference standard FPA rest perfusion and CT angiography protocol is shown in **Figure 7.1c.**

Low-Dose FPA Rest Perfusion and CT Angiography Protocol: A 10-minute delay was first employed after each reference standard rest acquisition to allow for adequate renal clearance of contrast material from the blood pool prior to each low-dose rest acquisition. After each delay, 1 mL/kg of contrast material was again injected (5 mL/s) followed by a saline chaser (0.5 mL/kg) at the same rate. Low-dose, 2-mm slab, dynamic bolus tracking at 100 kVp and 50 mA (SureStart, Aquilion One, Canon Medical Systems, Tustin, CA) was then used, with V1 acquired after the aortic enhancement exceeded 180 HU while V2 was acquired after V1 using the previously estimated time delay, ΔT_R. Of important note, V1 was acquired at 100 kVp and 50 mA while V2 was acquired at 100 kVp and 200 mA. Additionally, both volume scans were ECG-gated with a 0.35 second rotation time with 320 x 0.5 mm collimation. After each acquisition, V1 and V2 were used for low-dose FPA rest perfusion measurement, while V2 was also used for CT angiography. Low-dose vessel-specific rest perfusion measurements in the LAD, LCx, and RCA were then derived using the CT angiogram and minimum-cost-path myocardial assignment[47, 97, 123, 133]. Finally, the $CTDI_{vol}^{32}$ for the low-dose FPA rest perfusion and CT angiography protocol was recorded, with a size-specific dose estimate (SSDE) also determined[118] to account for the effective diameter of each swine used in the study. The $CTDI_{vol}^{32}$ and SSDE were then used, along with a standard chest conversion coefficient of 0.014 mSv/mGy[125] and the 16 cm cranio-caudal coverage, to estimate the effective dose of the low-dose FPA rest perfusion and CT angiography protocol. The entire low-dose FPA rest perfusion and CT angiography protocol is shown in **Figure 1c.**

FPA Stress Perfusion Acquisition Methodology

Reference Standard FPA Stress Perfusion Protocol: For all stress perfusion conditions, contrast material (1 mL/kg, Isovue 370, Bracco Diagnostics, Princeton, NJ) was injected (5 mL/s, Empower CTA, Acist Medical Systems, Eden Prairie, MN) followed by a saline chaser (0.5 mL/kg) at the same rate. Whole-heart volume scans were then acquired dynamically at 100 kVp and 200 mA (Aquilion One, Canon Medical Systems, Tustin, CA) over fifteen to twenty seconds to completely capture the aortic enhancement curve. Additionally, all volume scans were ECG-gated with a 0.35 second rotation time with 320 x 0.5 mm collimation. After each acquisition, V1 and V2 were selected systematically for reference standard FPA stress perfusion measurement, as previously validated versus invasive FFR, quantitative microsphere perfusion, and ultrasonic flow probe measurement[97, 98, 123]. Reference standard vessel-specific stress perfusion measurements in the LAD, LCx, and RCA were then derived using the previously acquired, co-registered, reference standard CT angiogram and minimum-cost-path myocardial assignment[47, 97, 123, 133]. Finally, the time delay (ΔT_S) between V1 and V2 was estimated for each acquisition using automatic time-density-curve analysis (Acquilion One, Canon Medical Systems, Tustin, CA) and was used, in place of a test bolus[124], for proper timing of the subsequent low-dose FPA stress perfusion protocol. The entire reference standard FPA stress perfusion protocol is shown in **Figure 7.1d.**

Low-Dose FPA Stress Perfusion Protocol: A 10-minute delay was first employed after each reference standard stress acquisition to allow for adequate renal clearance of contrast material from the blood pool prior to each low-dose stress acquisition. After

each delay, 1 mL/kg of contrast material was again injected (5 mL/s) followed by a saline chaser (0.5 mL/kg) at the same rate. Low-dose, 2-mm slab, dynamic bolus tracking at 100 kVp and 50 mA (SureStart, Aquilion One, Canon Medical Systems, Tustin, CA) was then used, with V1 acquired after the aortic enhancement exceeded 180 HU while V2 was acquired after V1 using the previously estimated time delay, ΔT_S. Both V1 and V2 were acquired at 100 kVp and 50 mA and were ECG-gated with a 0.35 second rotation time with 320 x 0.5 mm collimation. After each acquisition, V1 and V2 were used for low-dose FPA stress perfusion measurement. Low-dose vessel-specific stress perfusion measurements in the LAD, LCx, and RCA were then derived using the previously acquired, co-registered CT angiogram and minimum-cost-path myocardial assignment[47, 97, 123, 133]. Finally, the $CTDI_{vol}^{32}$ for the low-dose FPA stress perfusion protocol was recorded, with a size-specific dose estimate (SSDE) also determined[118] to account for the effective diameter of each swine used in the study. The $CTDI_{vol}^{32}$ and SSDE were then used, along with a standard chest conversion coefficient of 0.014 mSv/mGy[125] and the 16 cm cranio-caudal coverage, to estimate the effective dose of the low-dose FPA stress perfusion protocol. The entire low-dose FPA stress perfusion protocol is shown in **Figure 7.1d.**

Low-Dose Comprehensive Cardiac CT Image Processing

For both the rest and stress data, all volume scans were first reconstructed from full projection data at 75% of the R-R interval using AIDR 3D reconstruction[126] and a voxel size of 0.43 x 0.43 x 0.5 mm. The four volume scans of interest, i.e., $V1_{REST}$, $V2_{REST}$, $V1_{STRESS}$, and $V2_{STRESS}$, from each acquisition were then registered and combined into

maximum intensity projection (MIP) image volumes. Each MIP was then segmented semi-automatically (Vitrea fX version 6.0, Vital Images, Inc., Minnetonka, MN), yielding the entire myocardium and voxel-by-voxel rest and stress perfusion measurements were computed according to **Equation 1**. The ratio of stress to rest perfusion was then used to derive CFR. Furthermore, in order assess low-dose rest perfusion, stress perfusion, and CFR measurements on a vessel-specific basis, as well as distal to intermediate severity stenoses, the centerlines of the LAD, LCx, and RCA were semi-automatically extracted (Vitrea fX version 6.0, Vital Images, Inc., Minnetonka, MN) from each corresponding CT angiogram, and were used, along with the myocardial segmentations, for minimum-cost-path (MCP) myocardial assignment, yielding three separate coronary perfusion territories, with the LAD territory further partitioned distal to each stenoses, as previously described[47, 97, 123, 133]. All voxel-by-voxel rest perfusion, stress perfusion, and CFR measurements were then averaged within each coronary perfusion territory, yielding vessel-specific measurements. All vessel-specific rest perfusion, stress perfusion, and CFR measurements were then quantitatively compared to their corresponding reference standard retrospective measurements. Additionally, a case-study was performed in a single animal to assess the clinical utility of the low-dose comprehensive cardiac CT technique in the presence of intermediate severity stenoses with FFR severities of 0.7 - 0.9. Specifically, the low-dose stress perfusion data, CFR data, vessel-specific perfusion territory data, and predefined physiological cutoff thresholds[24] were used in combination to yield the mass percent distribution of stress perfusion and CFR in the LAD, LCx, and RCA. The stress perfusion cutoff thresholds were defined as follows: normal (>2.39 mL/min/g), minimal reduction (1.76 – 2.39

mL/min/g), mild reduction (1.20 – 1.76 mL/min/g), moderate reduction (0.91 – 1.20 mL/min/g), and definite ischemia (0.00 – 0.91 mL/min/g)[24]. The CFR cutoff thresholds were defined as follows: normal (>3.37), minimal reduction (2.70 – 3.37), mild reduction (2.03 – 2.70 mL/min/g), moderate reduction (1.74 – 2.03 mL/min/g), definite ischemia (1.00 – 1.74), and myocardial steal (0.00 - 1.00)[24]. The entire low-dose comprehensive cardiac CT image processing scheme is summarized in **Figure 7.2.**

Statistical Approach

Low-dose rest and stress perfusion measurements in the LAD, LCx, and RCA were quantitatively compared to corresponding reference standard perfusion measurements through regression, Bland-Altman, root-mean-square-error (RMSE), root-mean-square deviation (RMSD), and Lin's concordance correlation coefficient (CCC)[92]. Student's T-tests were also performed to determine if low-dose perfusion and CFR measurements in the LAD, LCx, and RCA were significantly different from corresponding reference standard perfusion and CFR measurements. All fit parameter data are reported with 95% confidence intervals displayed in brackets. All other data are reported as mean ± standard deviation. P-values less than 0.5 indicate significant differences. Statistical software was used for all analyses (MatLab 2013a, MathWorks, Natick, MA; PS, Version 3.0, Vanderbilt University, Nashville, TN; SPSS, Version 22, IBM Corporation, Armonk, NY).

Results

General Results

The heart rate and mean arterial pressure of the swine were 93 ± 10 beats per minute and 71 ± 9 mmHg, respectively. On average, low-dose rest perfusion in all three coronary arteries combined was 0.50 ± 0.22 mL/min/g, while corresponding reference standard rest perfusion was 0.58 ± 0.21 mL/min/g. Low-dose stress perfusion in all three coronary arteries combined was 1.93 ± 0.84 mL/min/g, while corresponding reference standard stress perfusion was 1.92 ± 0.73 mL/min/g. Furthermore, for the intermediate severity stenoses, low-dose stress perfusion was 2.07 mL/min/g in the proximal LAD and 1.20 ± 0.32 mL/min/g in the distal LAD, while corresponding reference standard stress perfusion was 2.04 mL/min/g and 1.40 ± 0.40 mL/min/g, respectively. Taken in ratio, low-dose CFR in all three coronary arteries combined was 3.81, while corresponding reference standard CFR was 3.31. Furthermore, for the intermediate severity stenoses, low-dose CFR was 3.56 in the proximal LAD and 2.06 in the distal LAD, while corresponding reference standard CFR was 3.19 and 2.18, respectively. Average low-dose vessel-specific perfusion and CFR measurements in the LAD, LCx, and RCA as compared to average reference standard perfusion and CFR measurements are also shown in **Table 7.1**. Finally, the $\mathrm{CTDI}_{\mathrm{vol}}^{32}$ of rest perfusion, stress perfusion, CFR, rest perfusion combined with CT angiography, and CFR combined with CT angiography were 2.30, 2.30, 4.60, 5.75, and 8.05 mGy, respectively, with corresponding size-specific dose estimates of 3.66, 3.66, 7.31, 9.14, and 12.80 mGy. In combination, the maximum effective dose and size-specific effective dose of the

comprehensive cardiac CT technique were 1.8 and 2.87 mSv, respectively. All other dose data are also reported in **Table 7.2.**

Accuracy and Precision

All low-dose perfusion (P_{LOW}) and reference standard perfusion (P_{REF}) measurements in all three coronary arteries combined under stress and rest perfusion conditions were related by $P_{LOW} = 1.04\ P_{REF} - 0.08$, with a Pearson's correlation of $r = 0.94$, a concordance correlation of $\rho = 0.94$, a root-mean-square-error of 0.32 mL/min/g, and a root-mean-square deviation of of 0.32 mL/min/g, as shown in **Figure 7.3a** and **Table 7.3**, with corresponding Bland-Altman analysis shown in **Figure 7.3b**. All low-dose perfusion (P_{LOW}) and reference standard perfusion (P_{REF}) measurements in all three coronary arteries combined under stress perfusion conditions alone were related by $P_{LOW} = 1.04\ P_{REF} - 0.07$, with a Pearson's correlation of $r = 0.90$, a concordance correlation of of $\rho = 0.89$, a root-mean-square-error of 0.36 mL/min/g, and a root-mean-square deviation of 0.36 mL/min/g, as shown in **Figure 7.3c** and **Table 7.3**, with corresponding Bland-Altman analysis shown in **Figure 7.3d**. All low-dose vessel-specific perfusion measurements in the LAD, LCx, and RCA individually as compared to corresponding reference standard perfusion measurements are also shown in **Table 7.3**.

Application

For one animal with stenoses of FFR severities ranging from 0.9 - 0.7, the low-dose stress perfusion data, CFR data, vessel-specific perfusion territory data, and predefined

physiological cutoff thresholds[24] were used in combination to yield the mass percent distribution of stress perfusion and CFR in the LAD, LCx, and RCA, as displayed in **Figure 7.4**. Low-dose stress perfusion maps and co-registered angiography ($V2_{REST}$) are also displayed for stress perfusion measurement in the absence and presence of a physiologically significant LAD stenosis (FFR = 0.70), are shown in **Figure 7.5**.

Discussion

Indication of Results

The results of low-dose, vessel-specific rest and stress perfusion measurement, as well as CFR measurement, were in agreement with corresponding reference standard measurement. Specifically, there were no significant differences between the average, low-dose, vessel-specific rest and stress perfusion measurements and the corresponding average reference standard perfusion measurements. Moreover, the low-dose rest and stress perfusion measurements also agreed with the corresponding reference standard stress perfusion measurements, demonstrating near unity slope, minimal offset, negligible bias, good concordance correlation, and small RMSE and RMSD. With respect to the case study, the fractional breakdown of stress perfusion and CFR in the LAD, LCX, and RCA also agreed with the physiological severity of the induced stenosis. More specifically, the stress perfusion and CFR in the LAD decreased proportionally as FFR decreased, while the stress perfusion and CFR in the LCx and RCA, i.e., vessels without stenosis, remained normal. Visually, the spatial distribution of low-dose stress perfusion also agreed with the induced flow conditions, where stress perfusion without a stenosis was shown to be normal, while stress perfusion distal to an physiologically significant LAD stenosis with FFR severity of 0.70 was shown to be

markedly reduced. Additionally, the $\mathrm{CTDI}_{\mathrm{vol}}^{32}$ and SSDE of rest perfusion combined with CT angiography, stress perfusion, and CFR were only 8.05 and 12.80 mGy, respectively, corresponding to a maximum effective dose and size-specific effective dose of 1.8 and 2.87 mSv for the comprehensive cardiac CT technique, respectively.

Comparison to Others

Reductions in stress dynamic CT perfusion have been shown to correlate well with reductions in invasive fractional flow reserve[31, 134]. However, there are a wide range of stress perfusion cutoff thresholds that are used to classify the presence or absence of significant multiform CAD[18]. Such variability in stress perfusion can be attributed to natural heterogeneity in microvascular resistance that exists amongst patients[135]. As such, standardized stress perfusion cutoff threshold may be difficult to implement in clinical practice. Fortunately, coronary flow reserve (CFR) used in combination with stress perfusion can account for measurement variability and improve the accuracy of physiological assessment of CAD[24]. Nevertheless, CFR measurement requires baseline perfusion assessment in addition to stress perfusion assessment, increasing the contrast and radiation dose per exam. Moreover, these is a growing body of evidence that supports the need for CT angiography in addition to CT perfusion for improved diagnostic sensitivity and specificity in noninvasive multiform CAD workup[136, 137]. However, the cumulative radiation and contrast dose required to provide rest perfusion, stress perfusion, CFR, and CT angiography together is currently too high to be clinically useful. Several groups have shown that radiation dose can be reduced through tube

voltage and tube current reduction[138, 139], but such reductions remain incremental in that a large number of volume scans are still necessary for perfusion measurement.

Fortunately, the work presented in this study differs from the current state of the field in that the comprehensive cardiac CT technique enables accurate, low-dose, vessel-specific rest and stress perfusion measurement while simultaneously providing CT angiography and coronary flow reserve (CFR) using only four volume scans and two contrast injections, respectively. As a result, the cumulative radiation and contrast dose of CT-based comprehensive morphological and functional assessment of multiform CAD can be dramatically reduced. More importantly, the technique can also provide voxel-by-voxel and vessel specific[47, 133] stress perfusion and CFR measurements in combination, further reducing variability in physiological assessment of CAD. Finally, given the first-pass timing of the V2 volume scan during the low-dose, stress perfusion acquisition, the comprehensive cardiac CT technique can easily be extended by adding cardiac functional analysis (CFA). Specifically, if the stress V2 exposure time is increased, the entire cardiac cycle can be captured, enabling added assessment of cardiac output, ejection fraction, wall motion, and myocardial strain[140, 141].

Limitations

This study is not without limitations. First, the perfusion between the low-dose acquisitions and their corresponding reference standard acquisitions was assumed to be unchanged. However, fluctuations in the animals' vitals between paired acquisitions may have contributed to measurement variance. Hence, considerable effort was made

to tightly control ventilation, anesthesia, IV fluid administration, and hemodynamics such that perfusion measurement variance was minimized between acquisitions. Second, true prospective timing of V2 was not addressed. More specifically, V2 must be acquired at or within one cardiac cycle of the peak of the aortic enhancement for FPA perfusion measurements to be accurate, as well as for CT angiography to be acquired[97, 98, 123]. Unfortunately, hemodynamic variability and differences in injection volume negate the use of a fixed time delay between V1 and V2[128-131]. Hence, the time delay (ΔT_R and ΔT_R) between V1 and V2 for both rest and stress was estimated from the corresponding reference standard perfusion acquisitions, which is not clinically viable. However, such a time delay can also be determined through the preemptive use of a low-dose diluted test bolus acquisition[124]. Hence, proper timing of V2 can be predicted in advance, with negligible increases in contrast and radiation dose per exam.

Third, the swine used in the study had a small effective diameter (23 cm) as compared to the average 34 cm effective diameter of patients with CAD[44]. More specifically, at any given tube current, measurement noise increases with effective diameter. As all of the perfusion and CT angiography volume scans in this study were acquired at tube currents of 50 and 200 mA, respectively, the performance of the comprehensive cardiac CT technique may degrade in larger patients due to increased photon starvation and attenuation bias[127]. Fortunately, exposure control techniques (SureExposure, Acquilion One, Canon Medical Systems, Tustin, CA) enable automatic adjustment of the tube current such that measurement noise is maintained for larger effective diameters, although effective dose will increase proportionally. Using such an approach, a CAD

patient with an average effective diameter of 34 cm[44] will receive a maximum effective dose of approximately 5.20 mSv, for combined rest perfusion, stress perfusion, CFR, and CT angiography, as estimated by water phantom tests. Nevertheless, the cranial-caudal coverage used in this study was 16 cm, whereas the cranial-caudal coverage necessary for most whole-heart cardiac imaging is only 12 cm[44]. Hence, careful collimation of the cardiac window will provide 25% more reduction in effective dose, i.e., a CAD patient with an average effective diameter of 34 cm[44] would receive a maximum effective dose of only 3.90 mSv from comprehensive cardiac CT. Thus, the effective dose of the comprehensive cardiac CT technique will still be substantially lower than the 10 mSv average effective dose of stress perfusion alone with current dynamic CT perfusion techniques[18], even for large effective diameter patients.

One final limitation of the study was that only segmental disease in the LAD was assessed, i.e., multi-vessel, diffuse, and microvascular disease were not considered. Fortunately, the low-dose comprehensive cardiac CT technique can spatially resolve perfusion and CFR on a voxel-by-voxel and vessel-specific basis; hence, detection of focal, gradient, and global perfusion deficits is still feasible. Nevertheless, the accuracy of voxel-by-voxel perfusion and CFR measurement depends on image noise. Fortunately, local binning of voxel-by-voxel measurements can be used to suppress image noise while still maintaining adequate spatial perfusion and CFR resolution. More importantly, minimum-cost-path myocardial assignment[47, 133] can be used to generate coronary vessel-specific territories, i.e., voxel-by-voxel perfusion and CFR

measurements can be averaged within each territory to yield vessel-specific perfusion and CFR measurement, while also suppressing measurement variance[97, 123].

Conclusion

The low-dose comprehensive cardiac CT technique enables accurate, low-dose, vessel-specific rest and stress perfusion measurement while simultaneously providing CT angiography and coronary flow reserve (CFR) using only four volume scans and two contrast injections, respectively. As a result, the total combined radiation and contrast dose of CT-based CAD workup can be dramatically reduced, while also optimizing clinical throughput. Moreover, if the exposure time of the stress V2 volume scan is increased such that the entire cardiac cycle is captured, added assessment of cardiac output, ejection fraction, wall motion, and myocardial strain is also feasible. Hence, the comprehensive cardiac CT technique is unique in that can be tailed to a patient's specific needs, i.e., a patient with a prior history of segmental CAD would benefit from the stress perfusion and CFA arm of the technique, whereas a patient with intermediate risk of CAD would benefit from the full workup, without CFA. Thus, 'one-stop-shop' morphological and physiological assessment of CAD is feasible at a low radiation and contrast dose, making comprehensive CT-based assessment of multiform CAD more accurate, accessible, and impactful to patients in need. In summary, the low-dose comprehensive cardiac CT technique was retrospectively validated in a swine model and has the potential to be used for accurate, low-dose, vessel-specific morphological and physiological assessment of coronary artery disease.

Tables

Table 7.1. Low-dose perfusion and CFR measurement and reference standard perfusion and CFR measurement mean comparison.

Condition	Low-Dose Measurements	Reference Measurements	P-value (α < 0.05)
REST (N)	**(mL/min/g)**	**(mL/min/g)**	
LAD (11)	0.58 ± 0.18	0.64 ± 0.20	0.37
LCx (8)	0.53 ± 0.23	0.62 ± 0.17	0.23
RCA (8)	0.37 ± 0.24	0.46 ± 0.23	0.32
ALL (27)	**0.50 ± 0.22**	**0.58 ± 0.21**	**0.06**
STRESS (N)	**(mL/min/g)**	**(mL/min/g)**	
LAD (27)	1.88 ± 0.83	1.90 ± 0.72	0.76
Normal	2.07 ± 0.83	2.04 ± 0.73	0.64
Stenosis	1.20 ± 0.32	1.40 ± 0.40	0.12
LCx (18)	2.15 ± 0.96	2.14 ± 0.90	0.92
RCA (18)	1.79 ± 0.74	1.76 ± 0.54	0.73
ALL (63)	**1.93 ± 0.84**	**1.92 ± 0.73**	**0.92**
CFR (**)			
LAD	**3.24**	**2.97**	**
Normal	**3.56**	**3.19**	**
Stenosis	**2.06**	**2.18**	**
LCx	**4.05**	**3.45**	**
RCA	**4.83**	**3.83**	**
ALL	**3.83**	**3.31**	**

P-values less than 0.05 indicate significant mean perfusion differences. **Coronary flow reserve (CFR) was computed as the ratio of mean stress to mean rest perfusion; hence, P-values were not computed. N indicates the number of measurements; LAD, left anterior descending perfusion territory; LCx, left circumflex perfusion territory; RCA, right coronary artery perfusion.

Table 7.2. Low-dose comprehensive cardiac CT dose metrics.

Protocol	Total CTDI (mGy)	SSDE (mGy)	ED (mSv)	SSED (mSv)
REST	2.30	3.66 ± 0.43	0.52	0.82 ± 0.10
STRESS	2.30	3.66 ± 0.43	0.52	0.82 ± 0.10
REST, STRESS, CFR	4.60	7.31 ± 0.87	1.03	1.64 ± 0.19
REST + CTA	5.75	9.14 ± 1.08	1.29	2.05 ± 0.24
COMPREHENSIVE CARDIAC CT: REST + CTA, STRESS, CFR	8.05	12.80 ± 3.04	1.80	2.87 ± 0.68

REST indicates rest perfusion measurement; STRESS, stress perfusion measurement; CFR, coronary flow reserve measurement; REST + CTA, rest perfusion measurement combined with CT angiography; CT dose index in mGy; SSDE, size-specific dose estimate in mGy; ED, effective dose in mSv; SSED, size-specific effective dose is mSv.

Table 7.3. Low-dose perfusion measurement and reference standard perfusion measurement accuracy and precision analysis

Condition	Slope	Intercept	Pearson's r	Lin's CCC	RMSE (mL/min/g)	RMSD (mL/min/g)
STRESS+REST (N)						
LAD (38)	1.04 [0.92, 1.15]	-0.09 [-0.29, 0.11]	0.95 [0.91, 0.97]	0.95 [0.90, 0.97]	0.28	0.28
LCx (26)	1.01 [0.87, 1.16]	-0.05 [-0.33, 0.22]	0.96 [0.90, 0.98]	0.95 [0.90, 0.98]	0.32	0.32
RCA (26)	1.09 [0.89, 1.30]	-0.13 [-0.45, 0.18]	0.92 [0.82, 0.96]	0.90 [0.79, 0.96]	0.37	0.36
ALL (90)	**1.04 [0.96, 1.12]**	**-0.08 [-0.22, 0.05]**	**0.94 [0.92, 0.96]**	**0.94 [0.91, 0.96]**	**0.32**	**0.32**
STRESS (N)						
LAD (27)	1.06 [0.88, 1.25]	-0.14 [-0.51, 0.23]	0.92 [0.84, 0.97]	0.91 [0.82, 0.96]	0.31	0.31
LCx (18)	0.98 [0.76, 1.20]	0.04 [-0.47, 0.55]	0.92 [0.80, 0.97]	0.92 [0.79, 0.97]	0.36	0.36
RCA (18)	1.13 [0.73, 1.54]	-0.20 [-0.94, 0.54]	0.83 [0.59, 0.93]	0.79 [0.51, 0.92]	0.41	0.40
ALL (63)	**1.04 [0.91, 1.16]**	**-0.07 [-0.33, 0.19]**	**0.90 [0.85, 0.94]**	**0.89 [0.83, 0.94]**	**0.36**	**0.36**

Brackets indicate 95% confidence intervals. FPA indicates first-pass analysis; kVp, tube voltage; mA, tube current; N, number of perfusion measurements; LAD, left anterior descending perfusion territory; LCx, left circumflex perfusion territory; RCA, right coronary artery perfusion territory; ALL, all coronary perfusion territories combined; Lin's CCC, Lin's concordance correlation coefficient; RMSE, root-mean-square error; RMSD, root-mean-square deviation.

Figures

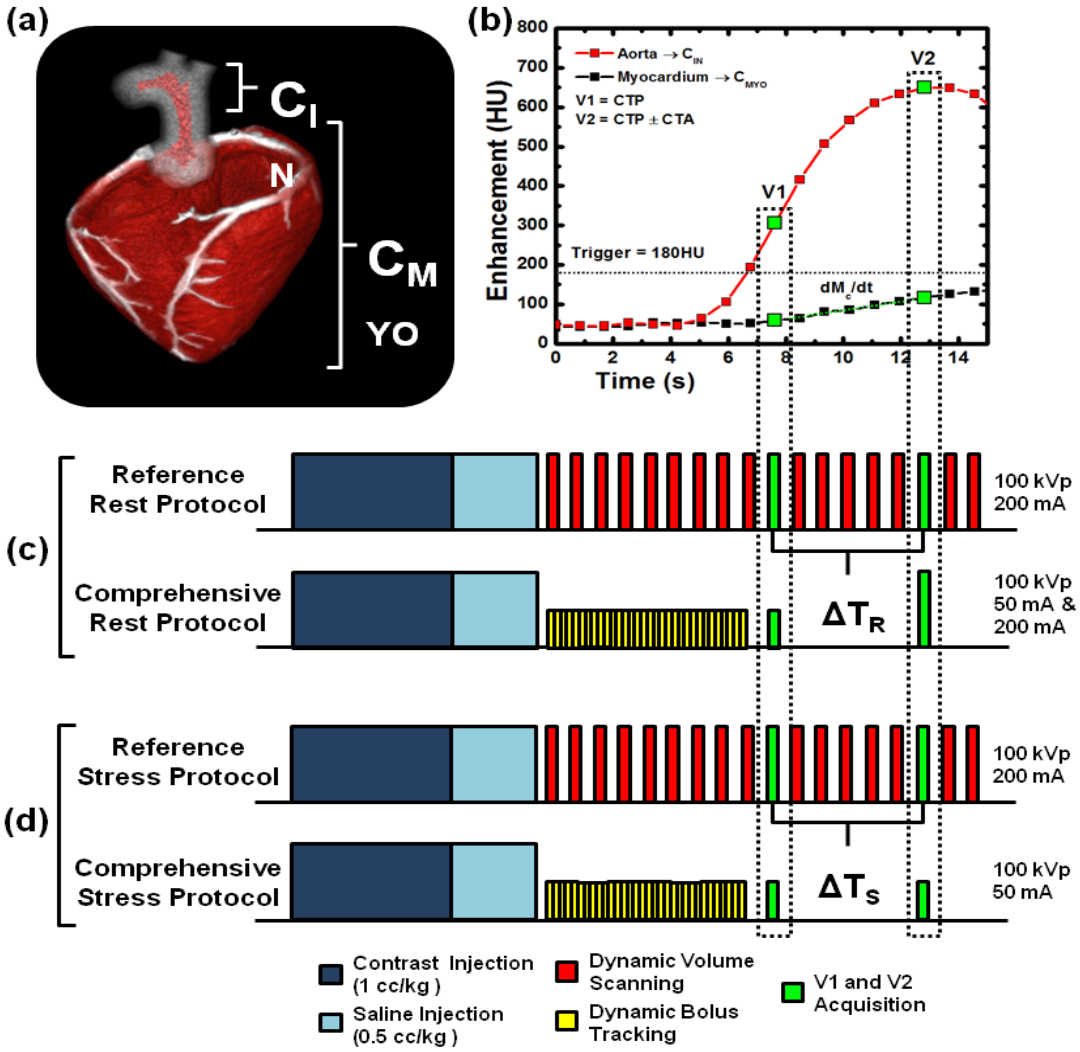

Figure 7.1: Low-dose comprehensive cardiac CT theory and implementation. (a) Whole-heart myocardial compartment (C_{MYO}) used for first-pass-analysis dynamic CT perfusion measurement. The input concentration (C_{IN}) is derived from the lumen of the aorta. The myocardial mass, M_T in Equation 1, is derived from the whole-heart myocardial compartment (C_{MYO}). (b) Following contrast and saline injection, the first-pass enhancement within the aorta and myocardium are shown in red and black, respectively. Two first-pass volume scans, V1 and V2 denoted in green, are then acquired. Both V1 and V2 are used for dynamic CT perfusion (CTP), while V2 may also be used for CT angiography (CTA) acquisition if the tube current of that volume scan is increased. (c) The reference standard FPA rest perfusion and CT angiography protocol is comprised of dynamic volume scan acquisition at 100 kVp and 200 mA over fifteen to twenty seconds. The low dose FPA rest perfusion and CT angiography protocol is comprised of 2-mm slab dynamic bolus tracking at 100 kVp and 50 mA, threshold-based triggering at 180, and acquisition of two volume scans. V1 is acquired at 100 kVp and 50 mA, while V2 is acquired at 100 kVp and 200mA and is used for additional CT angiography. (d) The reference standard FPA stress perfusion protocol is comprised of dynamic volume scan acquisition at 100 kVp and 200 mA over fifteen to twenty seconds. The low dose FPA stress perfusion and protocol is comprised of contrast injection followed by 2-mm slab dynamic bolus tracking at 100 kVp and 50 mA, threshold-based triggering at 180, and acquisition of two volume scans. Both V1 and V2 are acquired at 100 kVp and 50 mA.

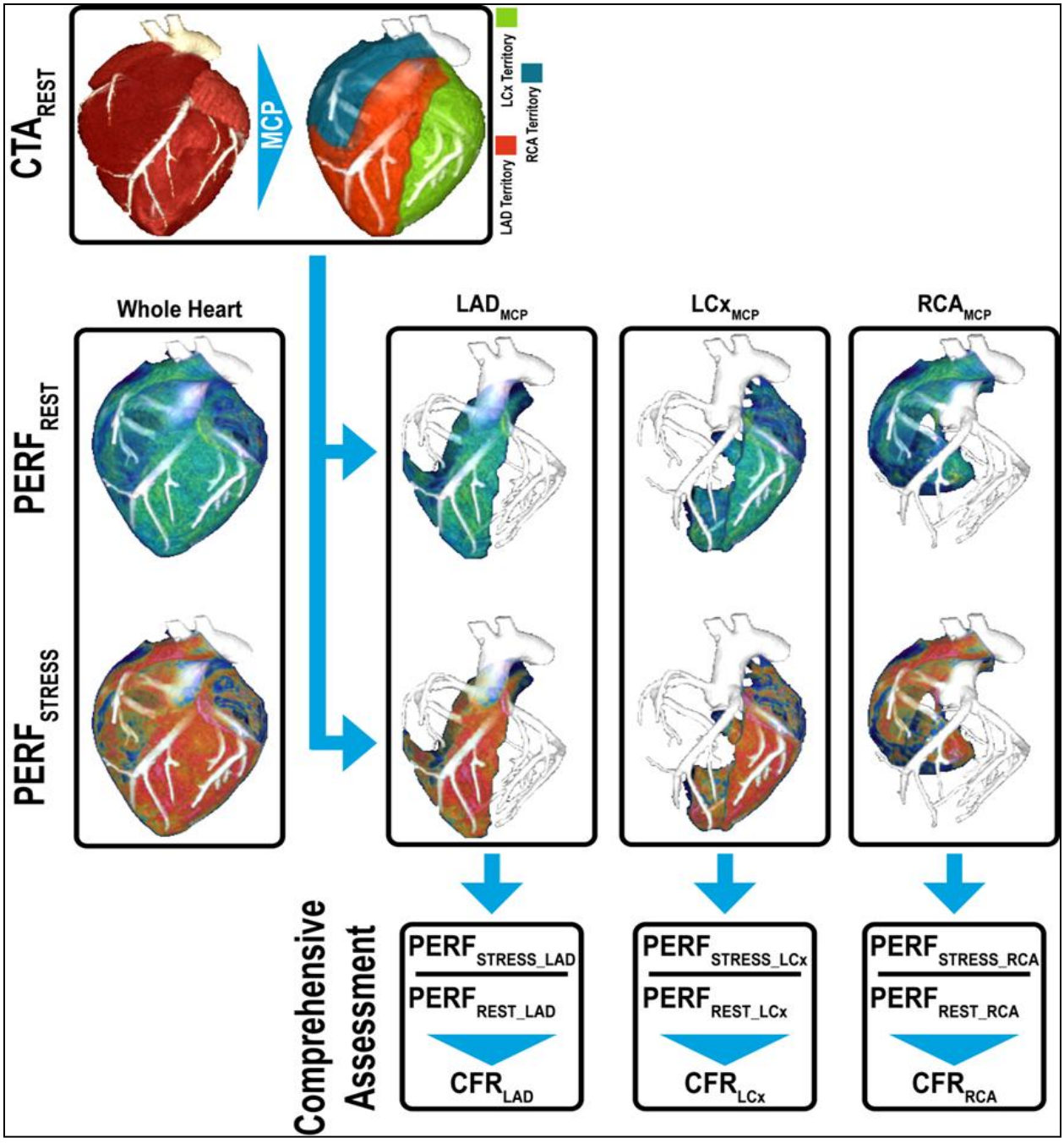

Figure 7.2: Low-dose comprehensive cardiac CT image processing scheme. For each comprehensive cardiac CT assessment, the volume scans of interest ($V1_{REST}$, $V2_{REST}$, $V1_{STRESS}$, and $V2_{STRESS}$) were registered and combined into a maximum intensity projection (MIP) image volume. The MIP was segmented and voxel-by-voxel rest and stress perfusion measurements were computed. The centerlines of the LAD, LCx, and RCA were extracted from the CT angiogram ($V2_{REST}$), and were used for minimum-cost-path (MCP) myocardial assignment, yielding the LAD, LCX, and RCA perfusion territories with the LAD territory further partitioned distal to each stenoses (when present). All voxel-by-voxel rest and stress perfusion measurements were then averaged within each coronary perfusion territory, yielding vessel-specific perfusion measurements. Finally, CFR was computed at the ratio of stress to rest perfusion.

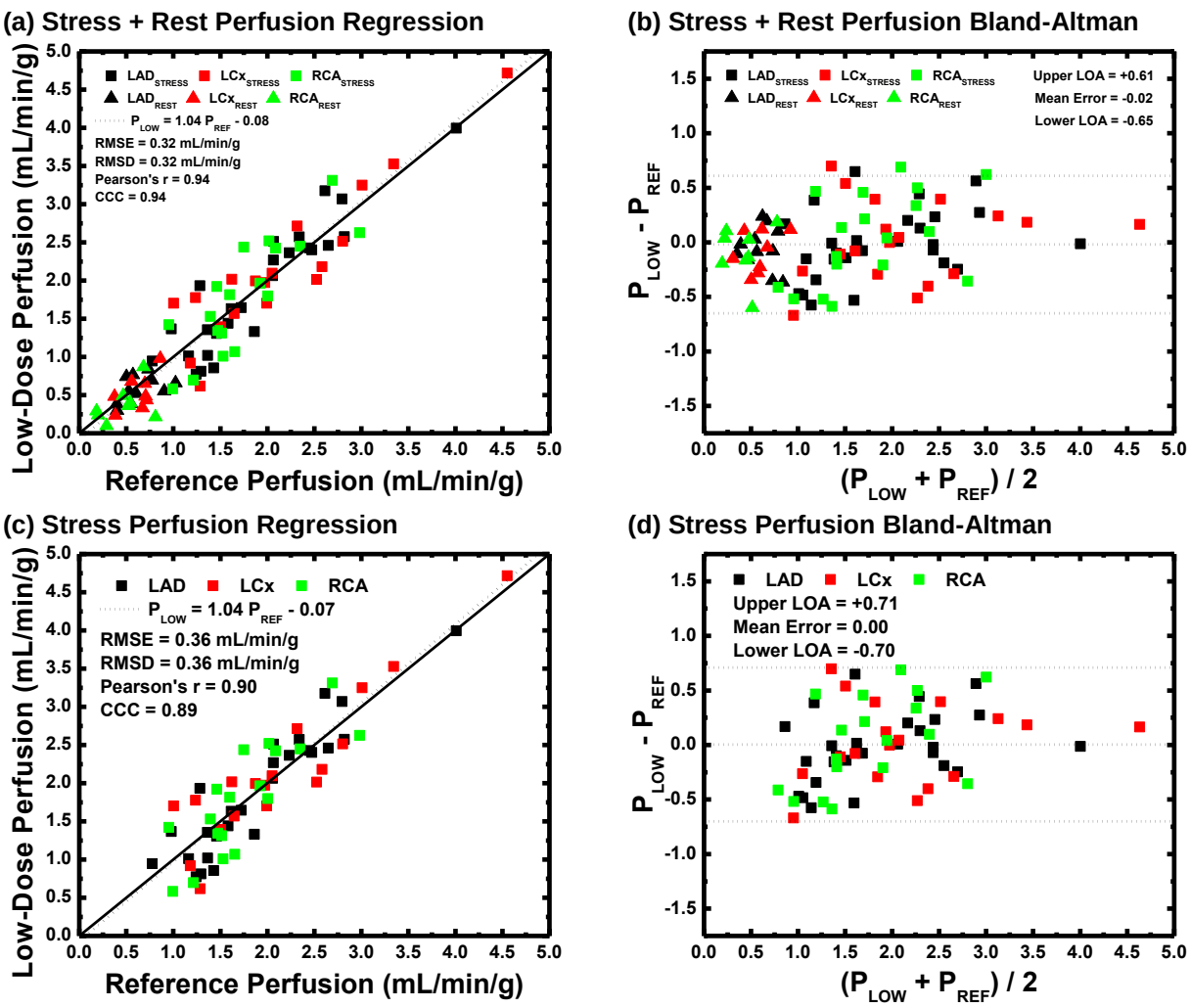

Figure 7.3: Low-dose vessel-specific perfusion measurement analysis. (a) Regression analysis comparing low-dose vessel-specific stress and rest perfusion measurements (P_{LOW}) to corresponding reference standard stress and rest perfusion measurements (P_{REF}). (b) Corresponding low-dose vessel-specific stress and rest perfusion Bland-Altman analysis. (c) Regression analysis comparing low-dose vessel-specific stress only perfusion measurements (P_{LOW}) to corresponding reference standard stress only perfusion measurements (P_{REF}). (d) Corresponding low-dose vessel-specific stress only perfusion Bland-Altman analysis. LAD indicates left anterior descending coronary artery; LCx, left circumflex coronary artery; RCA, right coronary artery; RMSE, root-mean-square-error; RMSD, root-mean-square-deviation; CCC, Lin's concordance correlation; LOA, limits of agreement.

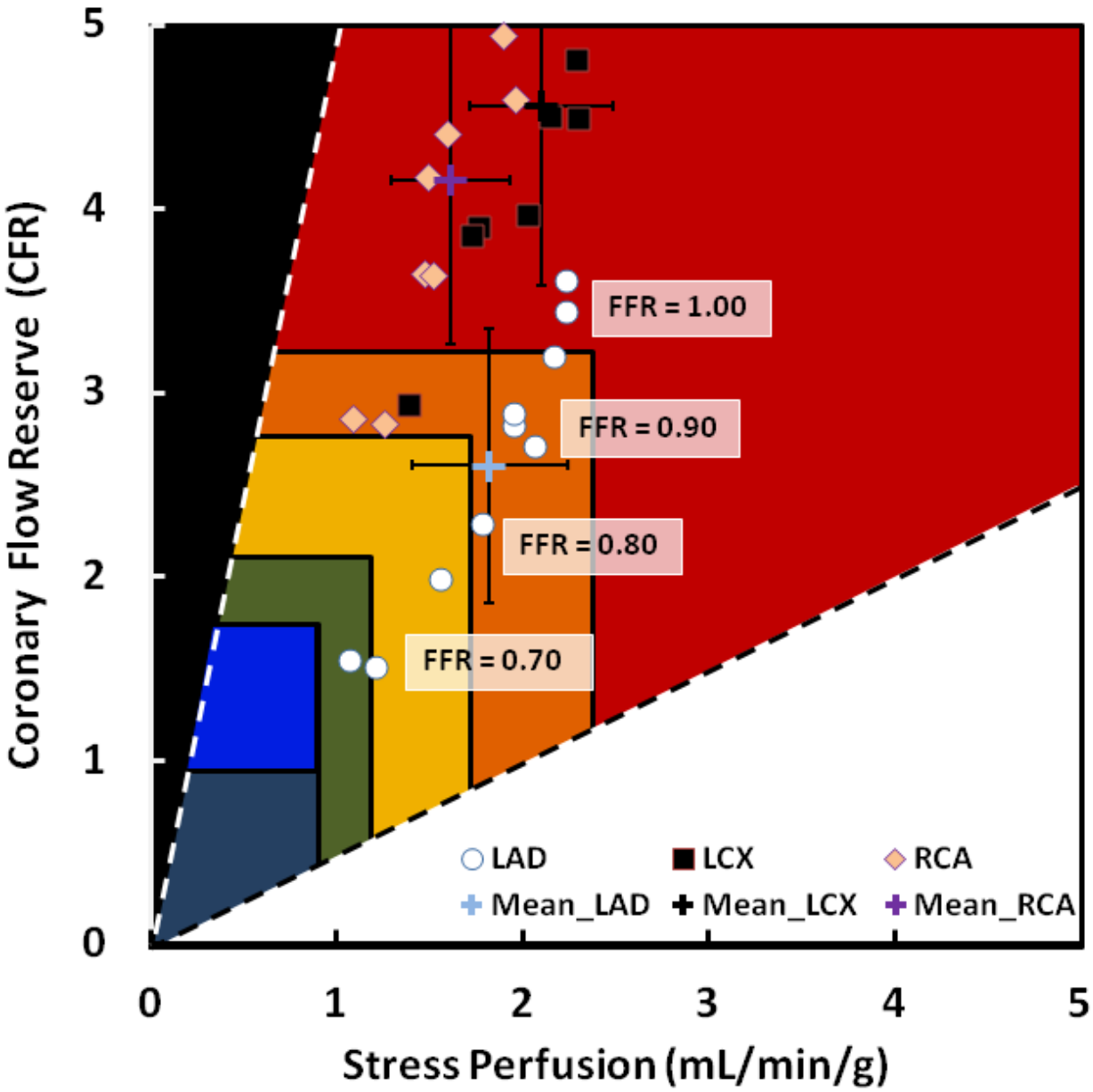

Figure 7.4: Low-dose vessel-specific coronary flow reserve (CFR) versus stress perfusion in the absence and presence of increasing severity LAD stenosis in a single swine. LAD stenoses with fractional flow reserve (FFR) severities of 0.90 - 0.70 are displayed. LAD indicates perfusion and CFR in the left anterior descending territory; LCX, perfusion and CFR in the left circumflex territory; RCA, perfusion and CFR in the right coronary artery territory. Graphical Color Scheme: Red = Normal flow, Orange = No ischemia but minimally reduced; Yellow = No ischemia but mildly reduced; Green = moderately reduced flow capacity; Blue = definite ischemia and/or myocardial steal; Black = predominantly scar.

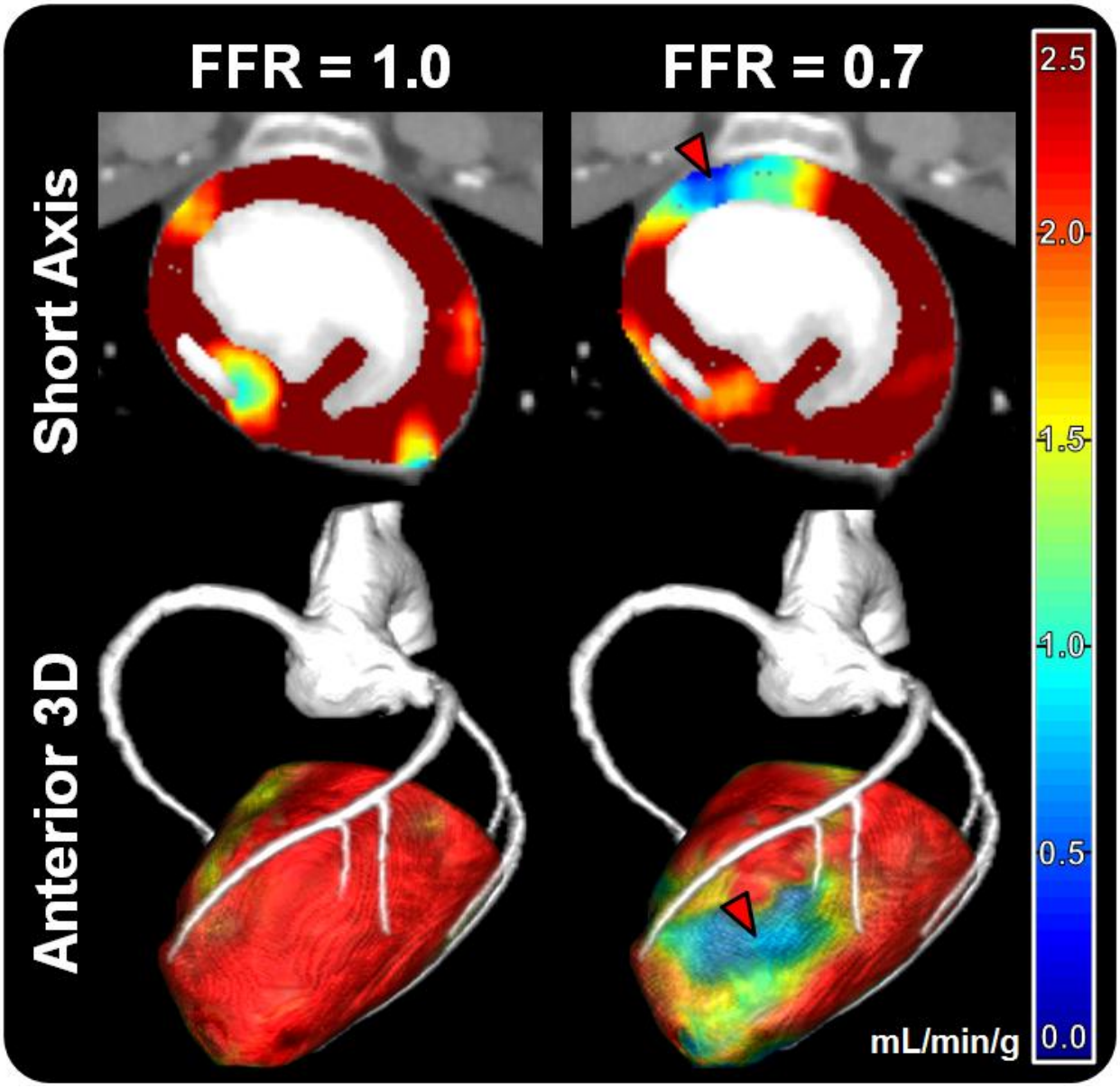

Figure 7.5: Application of the of the low-dose comprehensive cardiac CT technique. Low-dose stress perfusion with co-registered CT angiography is displayed. Stress perfusion measurement is displayed in the absence and presence of a physiologically significant left anterior descending (LAD) coronary artery stenosis. The perfusion deficit displayed in the short axis view (top row) and anterior 3D view of the left ventricle (bottom row) had an FFR severity of 0.70. The red arrow in the short axis and anterior 3D view of the left ventricle indicates the perfusion defect in the LAD territory. The colorbar indicates low-dose stress perfusion measurement in mL/min/g.

CHAPTER 8: PROSPECTIVE ACQUISTION TIMING USING A DILUTED TEST BOLUS AS COMPARED TO AN IDEAL BOLUS IN SWINE

Abstract

The accuracy of coronary computed tomography (CT) angiography depends upon the degree of coronary enhancement as compared to the background noise. Unfortunately, coronary contrast-to-noise ratio (CNR) optimization is difficult on a patient-specific basis. Hence, the objective of this study was to validate a new combined diluted test bolus and CT angiography protocol for improved coronary enhancement and CNR. The combined diluted test bolus and CT angiography protocol was validated in six swine (28.9 ± 2.7 kg). Specifically, the aortic and coronary enhancement and CNR of a standard CT angiography protocol and a new combined diluted test bolus and CT angiography protocol were compared to a reference retrospective CT angiography protocol. Comparisons for all data were made using box-plots, t-tests, regression, Bland-Altman, root-mean-square error and deviation, as well as Lin's concordance correlation. The combined diluted test bolus and CT angiography protocol was found to improve aortic and coronary enhancement by 26% and 13%, respectively, as compared to the standard CT angiography protocol. More importantly, the combined protocol was found to improve aortic and coronary CNR by 29% and 20%, respectively, as compared to the standard protocol. A new combined diluted test bolus and CT angiography protocol was shown to improve coronary enhancement and CNR as compared to an existing standard CT angiography protocol.

Introduction

Coronary computed tomography (CT) angiography is a powerful tool for noninvasive diagnosis of coronary artery disease. However, the accuracy of CT angiography depends upon the degree of coronary enhancement and contrast-to-noise ratio (CNR)[142, 143]. Fortunately, automatic exposure control can be used to optimize image noise[144, 145], while dynamic bolus tracking can be used to trigger CT angiography acquisition[122, 146]. Unfortunately, patient-specific hemodynamic variability renders dynamic bolus tracking unreliable in coronary enhancement optimization[128, 129, 147]. Hence, small volume test bolus injections (10-15 mL) are often used prior to CT angiography acquisition to predict the time-to-peak enhancement[147, 148]. However, the time-to-peak predictions of such test bolus techniques are also known to be highly variable[149-151]; hence, the problem of patient-specific coronary enhancement and CNR optimization remains largely unsolved[128, 147, 149, 152-154].

Fortunately, recent work suggests that the peak enhancement of large volume diluted test bolus injections is highly predictive of CT angiography peak enhancement[124]. Moreover, additional work suggests that bolus injection volume is most predictive of bolus width[130, 131], where the time-to-peak enhancement occurs at one-half the bolus width. Hence, a diluted test bolus of equivalent volume to that of a CT angiography bolus has the potential to accurately predict the time-to-peak enhancement necessary for patient-specific CT angiography optimization. Therefore, the purpose of this study was to validate a new combined diluted test bolus and CT angiography protocol for improved coronary enhancement and CNR. The central hypothesis was that a diluted

test bolus can be used prior to CT angiography acquisition to accurately predict the time-to-peak necessary for optimal coronary enhancement and CNR.

Materials and Methods

General Methods

The study was approved by the Animal Care Committee and was performed in agreement with the “Position of the American Heart Association on Research Animal Use.” Six male Yorkshire swine (28.9 ± 2.7 kg) were used, with two experimental aims of interest. When possible, repeat measurements were made, with both experimental aims successfully completed. All image data was acquired between 05/2017 and 07/2017 and was retrospectively analyzed between 07/2017 and 11/2017

Animal Preparation

Anesthesia was induced with Telazol (4.4 mg/kg), Ketamine (2.2 mg/kg), and Xylazine (2.2 mg/kg), and was maintained with 1.5-2.5% Isoflurane (Highland Medical Equipment, Temecula, CA and Baxter, Deerfield, IL). Sheaths were placed (5Fr, AVANTI®, Cordis Corporation, Miami Lakes, FL) in each femoral vein and were used for drug, fluid, and contrast material administration.

Prediction of Time-To-Peak Enhancement

For each animal, standard un-dilute and diluted test bolus injection protocols were performed followed by dynamic imaging and analysis to determine which test bolus was most predictive of a reference CT angiography bolus time-to-peak enhancement. When

possible, repeat measurements were also made in the six swine, yielding a total of fourteen measurements for the standard test bolus protocol analysis, and a total of twelve measurements for the diluted test bolus protocol analysis.

Standard Test Bolus Protocol: 10 mL of contrast material (Isovue 370, Bracco Diagnostics, Princeton, NJ) was injected (5 mL/s, Empower CTA, Acist Medical Systems, Eden Prairie, MN) followed by saline chaser (0.5 mL/kg) at the same rate. Volume scans were then acquired (Aquilion One, Toshiba America Medical Systems, Tustin, CA) over twenty seconds to capture the time-attenuation-curve, as shown in **Figure 8.1a**.

Diluted Test Bolus Protocol: 10 mL of contrast material was diluted in saline (1 mL/kg) and was injected (5 mL/s) followed by a saline chaser (0.5 mL/kg) at the same rate. Volume scans were then acquired over twenty seconds to capture the time-attenuation-curve, as shown in **Figure 8.1b**.

Reference CT Angiography Bolus Protocol: 1 mL/kg of contrast material was injected (5 mL/s) followed by a saline chaser (0.5 mL/kg) at the same rate. Volume scans were then acquired over twenty seconds to capture the reference CT angiography bolus time-attenuation-curve, as shown in **Figure 8.1c**.

CT Imaging: All dynamic imaging protocols were ECG-gated and were performed at 100 kVp and 200 mA with 320 x 0.5 mm collimation and 16 cm of cranio-caudal coverage.

Additionally, a 10-minute delay was employed after each protocol to allow for adequate clearance of contrast material from the blood pool prior to initiating the next protocol. After imaging was complete, all volume scans were retrospectively reconstructed from full projection data at 75% of the R-R interval using an FC03 kernel and a reconstruction voxel size of 0.43 x 0.43 x 0.50 mm.

Image Processing: For each series of acquisitions, the volume scan with peak aortic enhancement was selected from the reference bolus volumes scans and all test bolus and reference bolus volume scans were deformably registered to that peak enhancement volume scan to minimize motion artifacts[88]. The aorta was then segmented semi-automatically through threshold-based region-growing (Vitrea fX version 6.0, Vital Images, Inc., Minnetonka, MN), producing a vascular volume-of-interest. The vascular volume-of-interest was then radially eroded by two voxels to eliminate partial volume artifact, yielding the central luminal volume of the aorta. Using that central luminal volume, time-attenuation-curves for the test bolus and reference bolus data were produced by computing the average Hounsfield Unit within that luminal volume over time. Time-to-peak enhancement data for each protocol were then extracted with a gamma variate fit function (MatLab 2013a, MathWorks, Natick, MA). The image processing scheme is summarized in **Figure 8.2a.**

Optimization of Enhancement and CNR

For each animal, a standard CT angiography protocol was performed along with a combined diluted test bolus and CT angiography protocol. In each case, the CT dose

index ($CTDI_{VOL}^{32}$) and dose-length-product (DLP) was also recorded. The peak enhancement and CNR for the left anterior descending (LAD), left circumflex (LCx), and right coronary artery (RCA) for the standard and combined protocols were then compared to corresponding data from a reference retrospective CT angiography protocol. When possible, repeat measurements were also made in the six swine, yielding a total of ten measurements for the peak enhancement and CNR analysis.

Standard CT Angiography Protocol: 1 mL/kg of contrast material was injected (5 mL/s) followed by a saline chaser (0.5 mL/kg) at the same rate. Dynamic bolus tracking was used (SureStart, Aquilion One, Toshiba America Medical Systems, Tustin, CA), and a CT angiogram was acquired automatically using a standard clinical protocol with a fixed time delay of four seconds after threshold-based triggering at 180 Hounsfield Units in the aorta, as shown in **Figure 8.3a.**

Combined Diluted Test Bolus and CT Angiography Protocol: 10 mL of contrast material was diluted in saline (1 mL/kg) and was injected (5 mL/s) followed by a saline chaser (0.5 mL/kg) at the same rate. 2-mm slab CINE scanning was then performed in 1.5 second intervals over 20 seconds, and the time-to-peak aortic enhancement was derived. The CT angiography protocol was then manually updated to incorporate the measured time-to-peak. 1 mL/kg of contrast material was then injected (5 mL/s) followed by a saline chaser (0.5 mL/kg) at the same rate. Dynamic bolus tracking was again used, but this time the CT angiogram was acquired using the new time-to-peak

delay after threshold-based triggering at 180 Hounsfield Units in the aorta, as shown in **Figure 8.3b.**

Reference Retrospective CT Angiography Protocol: 1 mL/kg of contrast material was injected (5 mL/s) followed by a saline chaser (0.5 mL/kg) at the same rate. Volume scans were then acquired over twenty seconds to capture the reference retrospective CT angiography time-attenuation-curve, as shown in **Figure 8.3c**.

CT Imaging: All dynamic imaging protocols were ECG-gated and were performed at 100 kVp and 200 mA, where all bolus tracking images had a collimation of 1 x 2.0 mm and all volume scans had a collimation of 320 x 0.50 mm. Additionally, a 10-minute delay was employed after each protocol to allow for adequate clearance of contrast material from the blood pool prior to initiating the next protocol. After imaging was complete, all bolus tracking images and volume scans were retrospectively reconstructed from full projection data at 75% of the R-R interval using an FC03 kernel and a reconstruction voxel size of 0.43 x 0.43 x 2.0 mm and 0.43 x 0.43 x 0.50 mm, respectively.

Image Processing: For each series of acquisitions, the volume scan with peak aortic enhancement was selected from the reference retrospective volumes scans and all CT angiograms and reference retrospective volume scans were deformably registered to that peak enhancement volume scan to minimize motion artifacts[88]. The aorta, LAD, LCx, and RCA were then segmented semi-automatically through threshold-based region-growing (Vitrea fX version 6.0, Vital Images, Inc., Minnetonka, MN), producing

four separate vascular volumes-of-interest. Each vascular volume-of-interest was then radially eroded by two voxels to eliminate partial volume artifact, yielding the central luminal volume of the aorta, LAD, LCx, and RCA. Peak enhancement and CNR data were then computed within each central luminal volume for each protocol, where CNR was defined as the attenuation difference between each central luminal volume and the left ventricular myocardium, divided by the image noise. The image processing scheme is summarized in **Figure 8.2b.**

Statistical Approach

First, the accuracy and precision of both test bolus protocols in prediction of reference bolus time-to-peak aortic enhancement was assessed using regression, Bland-Altman, root-mean-square-error, root-mean-square deviation, and Lin's concordance correlation coefficient[92]. Box-plots were generated, and paired sample t-tests were performed to determine if the time-to-peak enhancement of each protocol was significantly different from the reference protocol ($p < 0.05$). , Next, the accuracy and precision of both CT angiography protocols in prediction of a reference retrospective CT angiography protocol's peak enhancement and CNR was assessed using regression, Bland-Altman, root-mean-square-error, root-mean-square-deviation, and Lin's concordance correlation coefficient[92]. Box-plots were again generated, and paired sample t-tests were again performed to determine if the peak enhancement and CNR of each protocol was significantly different from the reference protocol ($p < 0.05$). Statistical software was used for all analysis (MatLab 2013a, MathWorks, Natick, MA; PS, Version 3.0, Vanderbilt University, Nashville, TN; SPSS, Version 22, IBM Corporation, Armonk, NY).

Results

Prediction of Time-To-Peak Enhancement

The heart rate and mean arterial pressure of the swine were 88 ± 13 beats per minute and 75 ± 19 mmHg, respectively. The test bolus and reference CT angiography bolus enhancement curves are displayed in **Figure 8.4a**, while the test bolus and reference CT angiography bolus time-to-peak data box-plots are shown in **Figure 8.4b**. On average, the time-to-peak data for the standard test bolus and diluted test bolus were 4.9 ± 1.5 ($p = 0.0$) and 6.4 ± 1.6 ($p = 0.9$) seconds, respectively, while the time-to-peak data for the reference CT angiography bolus was 6.2 ± 1.6 seconds. Furthermore, the time-to-peak data for the standard test bolus (TTP_{STB}) and reference CT angiography bolus (TTP_{REF}) were related with a Pearson's correlation of $r = 0.8$ and a concordance correlation of $\rho = 0.6$, as shown in **Figure 8.4c,** with corresponding Bland-Altman analysis displayed in **Figure 8.4d**. Finally, the time-to-peak data for the diluted test bolus (TTP_{DTB}) and reference CT angiography bolus (TTP_{REF}) were related with a Pearson's correlation of $r = 1.0$ and a concordance correlation of $\rho = 1.0$, as shown in **Figure 8.4e,** with corresponding Bland-Altman analysis displayed in **Figure 8.4f**.

Optimization of Enhancement and CNR

The $CTDI_{VOL}^{32}$ and DLP of the standard CT angiography protocol were 4.6 mGy and 73.6 mGy·cm, respectively. The $CTDI_{VOL}^{32}$ and DLP of the diluted test bolus alone were 59.8 mGy and 12.0 mGy·cm, respectively. In combination, the $CTDI_{VOL}^{32}$ and DLP of the combined diluted test bolus and CT angiography protocol were and 64.4 mGy and 85.6 mGy·cm, respectively. Box-plots for the standard, combined, and reference

retrospective CT angiography protocol peak enhancement and CNR data are shown in **Figure 8.5a** and 8.**5b**, respectively, with corresponding paired sample t-test data also shown in **Table 8.1.** Furthermore, for the standard CT angiography protocol, the peak enhancement data ($PEAK_{STAN}$) in both the aorta and coronaries were related to the reference retrospective CT angiography peak enhancement data with a Pearson's correlation of r = 0.8 and a concordance correlation of ρ = 0.8, as shown in **Figure 8.6a** and **Table 8.2,** with corresponding Bland-Altman analysis displayed in **Figure 8.6b**. The CNR data (CNR_{STAN}) in both the aorta and coronaries were also related to the reference retrospective CT angiography CNR data (CNR_{REF}) with a Pearson's correlation of r = 0.9 and a concordance correlation of ρ = 0.8, as shown in **Figure 8.7a** and **Table 8.2,** with corresponding Bland-Altman analysis also displayed in **Figure 8.7b.**

Finally, for the combined diluted test bolus and CT angiography protocol, the peak enhancement data ($PEAK_{COMB}$) in both the aorta and coronaries were related to the reference retrospective CT angiography peak enhancement data ($PEAK_{REF}$) with a Pearson's correlation of r = 1.0 and a concordance correlation of ρ = 1.0, as shown in **Figure 8.6c** and **Table 8.2,** with corresponding Bland-Altman analysis displayed in **Figure 8.6d**. The CNR data (CNR_{COMB}) in both the aorta and coronaries were also related to the reference retrospective CT angiography CNR data (CNR_{REF}) with a Pearson's correlation of r = 1.0 and a concordance correlation of ρ = 1.0, as shown in **Figure 8.7c** and **Table 8.2,** with corresponding Bland-Altman analysis displayed in **Figure 8.7d**. Qualitative multiplanar reformations (MPRs) of the LAD for the standard,

combined, and reference retrospective CT angiography protocols are shown in **Figure 8.5c.**

Discussion

In this study, standard un-dilute and diluted test bolus injection protocols were first performed followed by dynamic imaging and analysis to determine which test bolus was most predictive of reference CT angiography bolus time-to-peak enhancement. A standard CT angiography protocol was then performed along with a combined diluted test bolus and CT angiography protocol, and the peak enhancement and CNR of the LAD, LCx, and RCA for both protocols were then compared to a reference retrospective CT angiography protocol.

The results indicate that a diluted test bolus can be used to accurately predict the time-to-peak enhancement of a CT angiography bolus. However, a standard test bolus was shown to underestimate the time-to-peak enhancement by more than 20%. Furthermore, the diluted test bolus performed better than the standard test bolus in time-to-peak enhancement prediction, demonstrating higher concordance correlation[92] and negligible bias, as compared to the reference CT angiography bolus. Such findings indicate that the enhancement of a diluted test bolus does, in fact, parallel that of a CT angiography bolus, independent of cardiac output.

Moreover, the combined diluted test bolus and CT angiography protocol was found to improve peak aortic and coronary enhancement and CNR by 26%, 13%, 29% and 20%,

respectively, as compared to the standard CT angiography protocol, while only increasing the DLP by 12 mGy·cm. Additionally, the combined diluted test bolus and CT angiography protocol demonstrated better concordance correlation[92] and less bias than the standard CT angiography protocol, as compared to the reference retrospective CT angiography protocol. Such findings indicate that a diluted test bolus can, in fact, be used to significantly improve peak enhancement and CNR through accurate prediction of the time-to-peak necessary for optimal acquisition of the CT angiogram.

Overall, the findings of this study agree with the findings of others regarding optimization of CT angiography. Specifically, the limitations of the standard test bolus in prediction of time-to-peak enhancement agree well with the findings of van Hoe et al. and Kaatee et al., where poor to moderate correlation was found with the actual time-to-peak of the CT angiography bolus[150, 151]. Additionally, with respect to using a test bolus versus dynamic bolus tracking for CT angiography, Nakajima et al. and Rodrigues et al. also found better peak enhancement and CNR when using a test bolus with a patient-specific time delay as compared to dynamic bolus tracking with a fixed time delay[148, 155]. Nevertheless, Nakaura et al. and Platt et al. found no such improvements[147, 152], but this difference is likely attributed to the fact that a standard test bolus has a different time-attenuation-curve as compared to a CT angiography bolus.

To improve test bolus reliability, Masuda et al. evaluated the performance of a diluted and standard test bolus in prediction of peak enhancement of CT angiography in the aorta[124]. Interestingly, they found that peak enhancement for a diluted test bolus was

strongly predictive of peak enhancement for CT angiography, while peak enhancement for a standard test bolus was not ($r = 0.7$ vs. $r = 0.4$). Such findings are further explained by work done by Garcia et al. and Han et al., where injection volume was found to be most predictive of bolus width[130, 131]. That being said, the work of Masuda et al. remained limited to aortic peak enhancement prediction alone. Hence, our study focuses instead on the ability of a diluted test bolus to accurately predict the time-to-peak enhancement of a CT angiography bolus. Moreover, we use those time-to-peak predictions to improve the peak enhancement and CNR of CT angiography in the aorta, LAD, LCx, and RCA.

However, this study is not without limitations. First off, the study was performed on a small number of healthy swine, reducing the power of the study while also limiting assessment of CT angiography quality to coronary enhancement and CNR alone. Hence, validation in a human cohort using CT angiography quality assessment metrics such as CNR, coronary length and number of side branches, stenosis severity, and plaque volume is still necessary[156]. Additionally, while the standard, combined, and reference retrospective CT angiography protocols did employ a mass-adjusted contrast volume (1 mL/kg), the test bolus protocols did not (10 mL). Consequently, the test bolus peak enhancement was higher than the 100-200 Hounsfield Unit enhancement normally seen in human subjects[124, 147], as central blood volume scales proportionally with mass[153, 157]. However, given the analogous relation between the diluted test bolus and standard CT angiography bolus geometries, variations in central blood volume should not impact the diluted test bolus's ability to predict the time-to-peak enhancement for CT

angiography. Hence, 10 mL of contrast was used for the test bolus protocols, as 10-15 mL test bolus injections are used clinically[149].

That being said, the inability of the standard CT angiography protocol to compensate for large variations in cardiac output was likely compounded by the high heart rate and significant heart rate variability of the swine used within this study. However, as cardiac output is the product of both heart rate *and* stroke volume, coronary artery disease patients will still display variations in cardiac output, time-to-peak, and peak enhancement, regardless of beta blockade, due to known variations in stroke work[128, 129]. Hence, it is expected that a combined diluted test bolus and CT angiography protocol will still provide more clinical value than a standard CT angiography protocol alone, although further validation is necessary.

Despite the advantages of the combined diluted test bolus and CT angiography protocol, implementation of such a protocol may be clinically complex. Specifically, the combined protocol requires diluted contrast to be made, injected, and imaged prior to CT angiography; thus, adding time, contrast dose, and effective radiation dose per exam. That being said, exam time can be reduced using injector technology that is capable of co-injection of contrast and saline, i.e., dilution, prior to serial injection of contrast and saline[158]. Moreover, given the time-to-peak, peak enhancement, and CNR gains afforded by using a diluted test bolus, it may be possible to reduce the total volume of contrast necessary for patient-specific CT angiography, while still maintaining adequate image quality. Finally, with respect to effective radiation dose, the advent of

dynamic bolus tracking and iterative reconstruction techniques[159] ensure that the dose of a diluted test bolus is very small (DLP = 12 mGy·cm), as compared to the dose of CT angiography (DLP = 73.6 mGy·cm). Furthermore, there is additional potential to improve dynamic bolus tracking techniques, such that time-to-peak enhancement prediction may be performed without the need for a diluted test bolus, although further validation is necessary.

Conclusion

The combined diluted test bolus and CT angiography protocol uses a low-dose diluted test bolus for time-to-peak enhancement prediction prior to CT angiography. Given the analogous relation between the diluted test bolus and CT angiography bolus, the combined protocol ensures that peak enhancement and CNR are always achieved, independent of central blood volume or cardiac output. In summary, the combined diluted test bolus and CT angiography protocol was retrospectively validated in a swine model and has the potential to improve enhancement and CNR for CT angiography through optimal image acquisition timing.

Tables

Table 8.1: Standard, combined, and reference retrospective CT angiogram peak enhancement and CNR mean comparison

PROTOCOL	CT ANGIOGRAM	REFERENCE	P < 0.05
STANDARD (N)			
AORTA (10)			
Enhancement (HU)	656.4 ± 232.7	824.4 ± 161.4	0.0**
CNR	12.5 ± 5.2	15.9 ± 5.8	0.0**
LAD (10)			
Enhancement (HU)	348.5 ± 77.3	433.8 ± 53.7	0.0**
CNR	5.0 ± 2.7	7.1 ± 3.1	0.0**
LCx (10)			
Enhancement (HU)	347.3 ± 82.4	391.8 ± 73.2	0.2
CNR	4.9 ± 2.8	5.9 ± 2.0	0.2
RCA (10)			
Enhancement (HU)	314.5 ± 77.1	347.6 ± 68.4	0.1
CNR	4.3 ± 3.2	5.3 ± 3.3	0.1
LAD+LCx+RCA (30)			
Enhancement (HU)	336.8 ± 77.8	391.0 ± 72.7	0.0**
CNR	4.8 ± 2.8	6.1 ± 2.9	0.0**
COMBINED (N)			
AORTA (10)			
Enhancement (HU)	828.0 ± 122.5	824.4 ± 161.4	0.9
CNR	16.1 ± 5.4	15.9 ± 5.8	0.6
LAD (10)			
Enhancement (HU)	395.5 ± 94.2	433.8 ± 53.7	0.1
CNR	6.6 ± 3.4	7.1 ± 3.1	0.2
LCx (10)			
Enhancement (HU)	391.1 ± 89.8	391.8 ± 73.1	1.0
CNR	5.5 ± 2.7	5.9 ± 2.0	0.4
RCA (10)			
Enhancement (HU)	354.2 ± 74.4	347.6 ± 68.4	0.9
CNR	5.1 ± 3.3	5.3 ± 3.3	0.7
LAD + LCx + RCA (30)			
Enhancement (HU)	380.3 ± 85.9	391.0 ± 72.7	0.2
CNR	5.7 ± 3.1	6.11 ± 2.9	0.1

CT indicates computed tomography; CNR, contrast-to-noise ratio; N, number of measurements; HU, Hounsfield Units; LAD, left anterior descending; LCx, left circumflex; RCA, right coronary artery; DTB, diluted test bolus. Unless otherwise stated, all peak enhancement and CNR data are MEAN ± STD. **Indicates a p-value less than 0.05, i.e., a significant peak enhancement or CNR difference as compared to the reference.

Table 8.2. Standard, combined, and reference retrospective CT angiogram peak enhancement and CNR regression analysis

PROTOCOL	SLOPE	INTERCEPT	r	CCC	RMSE	RMSD
STANDARD (N)						
AORTA (10)						
Enhancement (HU)	0.9 [0.1, 1.8]	-119.7 [-866.1, 626.6]	0.7 [0.0, 0.9]	0.5 [-0.3, 0.8]	237.2	167.2
CNR	0.7 [0.3, 1.2]	1.2 [-6.2, 8.6]	0.8 [0.3, 1.0]	0.7 [0.1, 0.9]	4.7	3.0
LAD (10)						
Enhancement (HU)	0.5 [-0.6, 1.6]	136.6 [-345.7, 618.8]	0.3 [-0.4, 0.8]	0.2 [-0.5, 0.7]	112.7	69.0
CNR	0.7 [0.3, 1.1]	-0.2 [-3.3, 2.8]	0.8 [0.4, 1.0]	0.7 [0.0, 0.9]	2.7	1.4
LCx (10)						
Enhancement (HU)	0.0 [-0.9, 0.9]	340.5 [-24.6, 705.7]	0.0 [-0.6, 0.6]	0.0 [-0.6, 0.6]	112.9	78.2
CNR	0.9 [0.0, 1.8]	-0.2 [-5.8, 5.4]	0.6 [0.0, 0.9]	0.5 [-0.1, 0.9]	2.3	2.1
RCA (10)						
Enhancement (HU)	0.9 [0.2, 1.5]	19.9 [-194.4, 234.2]	0.8 [0.2, 0.9]	0.7 [-0.1, 0.9]	59.3	48.2
CNR	0.9 [0.5, 1.2]	-0.3 [-2.4, 1.8]	0.9 [0.6,1.0]	0.9 [0.5, 1.0]	1.7	1.3
LAD+LCx+RCA (30)						
Enhancement (HU)	0.4 [0.0, 0.8]	173.8 [22.0, 325.5]	0.4 [0.0, 0.7]	0.3 [-0.1, 0.6]	98.3	70.5
CNR	0.8 [0.6, 1.0]	0.0 [-1.6, 1.6]	0.8 [0.6, 0.9]	0.7 [0.5, 0.9]	2.3	1.7
COMBINED (N)						
AORTA (10)						
Enhancement (HU)	0.7 [0.4, 1.0]	245.7 [7.8, 483.5]	0.9 [0.6, 1.0]	0.9 [0.5, 1.0]	69.8	59.9
CNR	0.9 [0.7, 1.1]	2.0 [-2.0, 5.9]	1.0 [0.8, 1.0]	1.0 [0.8, 1.0]	1.7	1.6
LAD (10)						
Enhancement (HU)	1.4 [0.5, 2.2]	-196.8 [-580.3, 186.6]	0.8 [0.3, 0.9]	0.6 [-0.1, 0.9]	74.4	58.3
CNR	1.0 [0.7, 1.3]	-0.6 [-3.2, 1.9]	0.9 [0.7, 1.0]	0.9 [0.7, 1.0]	1.3	1.2
LCx (10)						
Enhancement (HU)	1.0 [0.5, 1.6]	-15.9 [-242.8, 211.1]	0.8 [0.4, 1.0]	0.8 [0.3, 0.9]	50.5	50.5
CNR	1.2 [0.6, 1.7]	-1.3 [-4.8, 2.3]	0.9 [0.5, 1.0]	0.8 [0.4, 1.0]	1.4	1.3
RCA (10)						
Enhancement (HU)	0.8 [0.2, 1.3]	75.8 [-120.5, 272.1]	0.7 [0.3, 0.9]	0.7 [0.2, 0.9]	50.2	48.0
CNR	0.9 [0.6, 1.2]	0.4 [-1.8, 2.5]	0.9 [0.6, 1.0]	0.9 [0.6, 1.0]	1.4	1.3
LAD+LCx+RCA (30)						
Enhancement (HU)	0.9 [0.6, 1.1]	30.5 [-88.8, 149.7]	0.7 [0.5, 0.9]	0.7 [0.5, 0.9]	59.5	57.1
CNR	1.0 [0.8, 1.2]	-0.2 [-1.4, 1.0]	0.9 [0.8, 1.0]	0.9 [0.8, 1.0]	1.4	1.3

CT indicates computed tomography; CNR, contrast-to-noise ratio; r, Pearson's correlation coefficient; CCC, Lin's concordance correlation coefficient; RMSE, root-mean-square error; RMSD, root-mean-square deviation; N, number of measurements; HU, Hounsfield Units; LAD, left anterior descending; LCx, left circumflex; RCA, right coronary artery; DTB, diluted test bolus. Brackets indicate 95% confidence intervals.

Figures

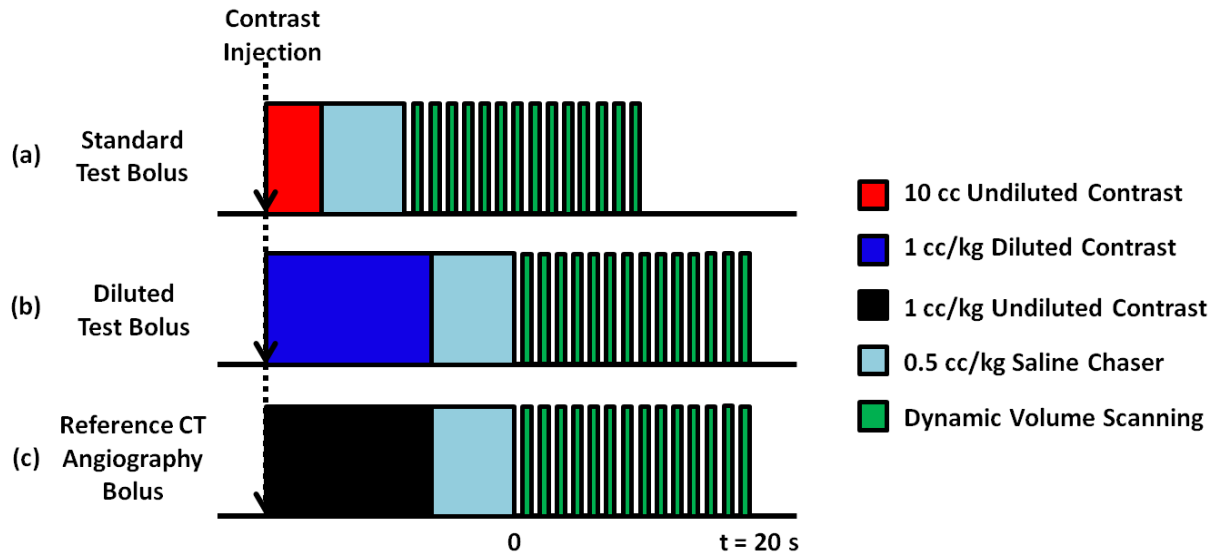

Figure 8.1: Standard, diluted, and reference CT angiography bolus injection protocol comparison. (a) Standard test bolus (STB) injection protocol, (b) diluted test bolus (DTB) injection protocol, (c) reference CT angiography bolus (REF) injection protocol. All bolus injection protocols were followed by the same 20 second dynamic imaging protocol to completely capture each time-attenuation-curve of interest for analysis.

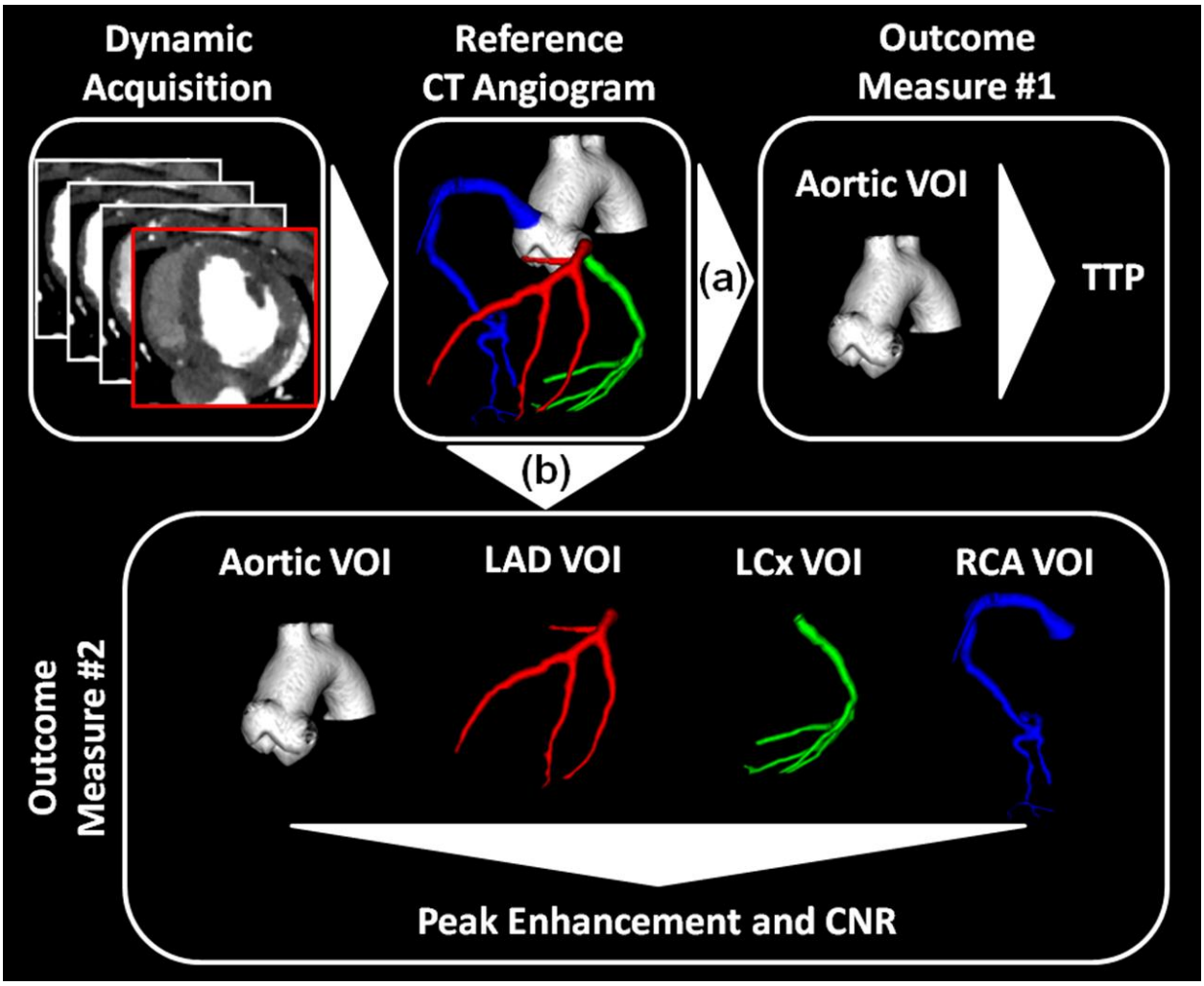

Figure 8.2: Image processing scheme. The peak enhancement volume scan was first selected from the reference computed tomography (CT) angiography bolus protocol data for vascular volume-of-interest (VOI) segmentation and post-processing. (a) The aortic VOI was used to generate time-attenuation-curves for the standard test bolus, diluted test bolus, and reference CT angiography bolus protocol data, and time-to-peak (TTP) enhancement data was then extracted in each case through automatic gamma variate fitting. (b) The aortic VOI, left anterior descending (LAD) VOI, left circumflex (LCx) VOI, and right coronary artery (RCA) VOI were used to compute peak enhancement and contrast-to-noise (CNR) for both standard and combined CT angiography protocols, and all data were then compared to the reference retrospective CT angiography protocol data.

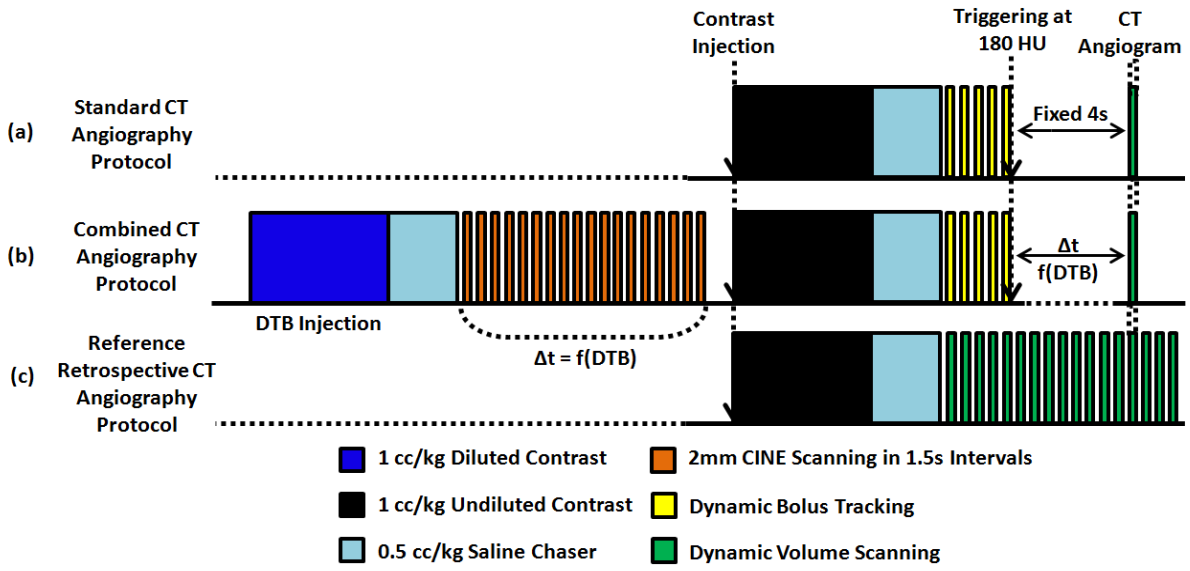

Figure 8.3. Standard, combined, and reference CT angiography acquisition protocol comparison. (a) Standard CT angiography protocol, (b) combined diluted test bolus (DTB) and CT angiography protocol, and (c) reference retrospective CT angiography protocol, where 20 seconds of ECG-gated dynamic imaging was performed to capture peak aortic and coronary enhancement and contrast-to-noise ratio (CNR).

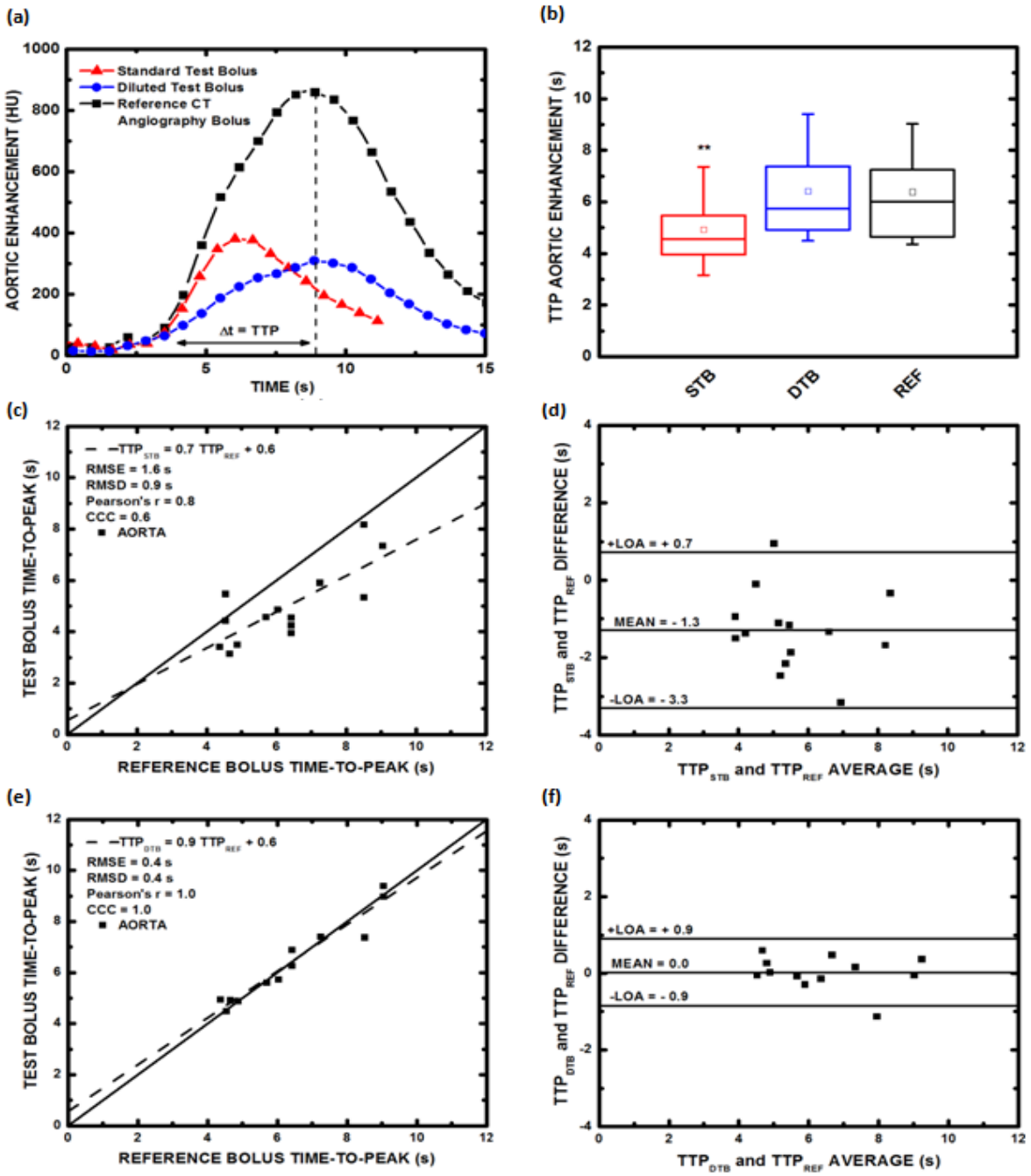

Figure 8.4: Test bolus and reference CT angiography bolus time-to-peak enhancement comparison. (a) Bolus time-attenuation-curve geometry comparison. (b) Bolus time-to-peak (TTP) enhancement box-plot comparison. STB indicates standard test bolus; DTB, diluted test bolus; REF, reference CT angiography bolus. **Indicates a p-value less than 0.05, i.e., a significant time-to-peak difference with the reference CT angiography bolus. (c) Regression analysis comparing the standard test bolus time-to-peak data (TTP_{STB}) to the reference CT angiography bolus time-to-peak data (TTP_{REF}), with (d) corresponding Bland-Altman analysis displayed. (e) Regression analysis comparing the diluted test bolus time-to-peak data (TTP_{DTB}) to the reference CT angiography bolus time-to-peak data (TTP_{REF}), with (f) corresponding Bland-Altman analysis displayed. RMSE indicates root-mean-square error; RMSD, root-mean-square deviation, CCC, Lin's concordance correlation coefficient; LOA, limit of agreement.

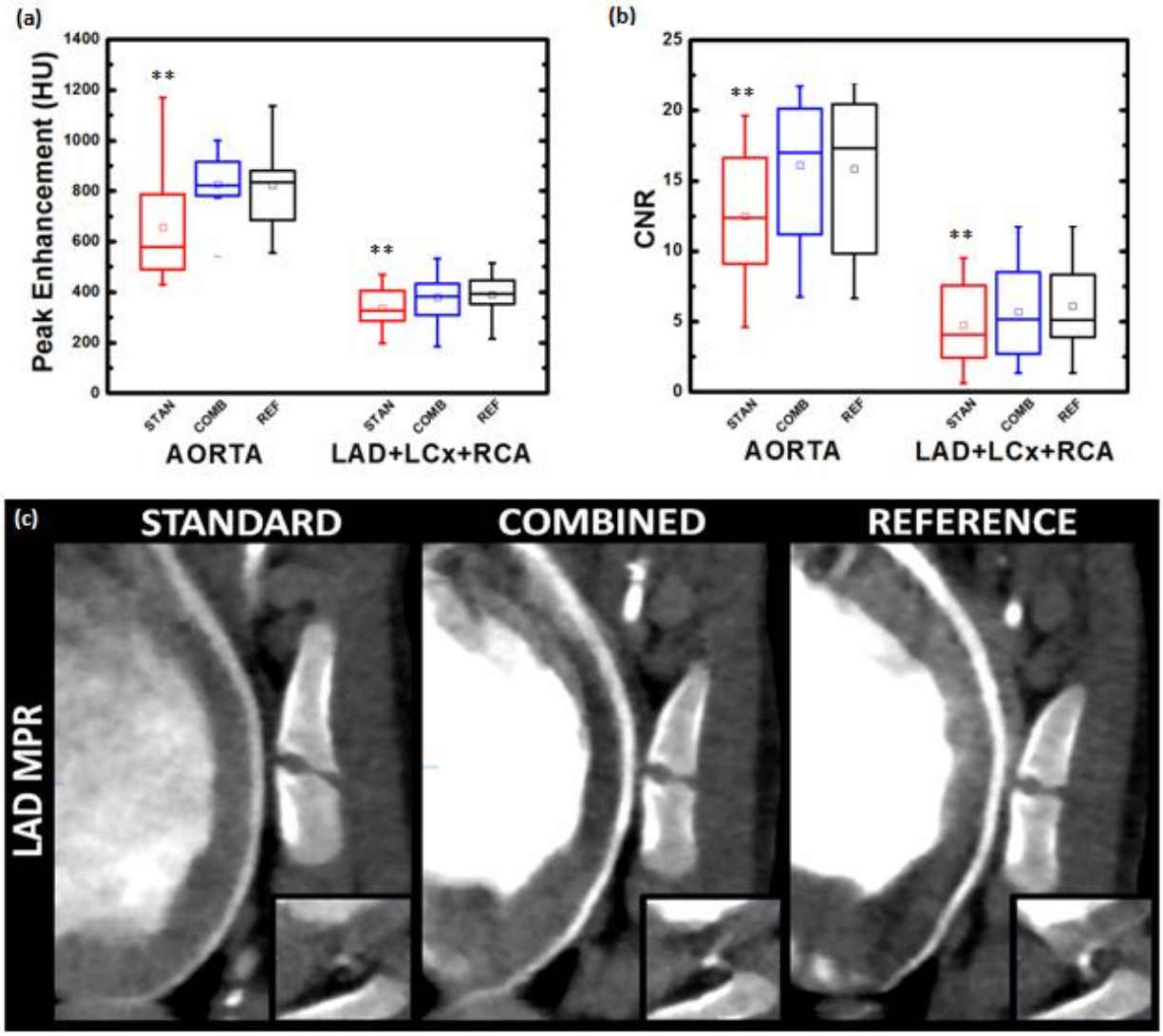

Figure 8.5: Standard, combined, and reference CT angiography peak enhancement and CNR comparison. (a) Aortic and coronary peak enhancement box-plot comparison for the standard and combined CT angiography protocols as compared to a reference retrospective CT angiography protocol. (b) Aortic and coronary CNR box-plot comparison for the standard and combined CT angiography protocols as compared to a reference retrospective CT angiography protocol. (c) Long axis and cross sectional multiplanar reformations (MPRs) of the left anterior descending (LAD) coronary artery for the standard and combined CT angiography protocols as compared to the reference retrospective CT angiography protocol. HU indicates Hounsfield Units; LAD, left anterior descending; LCx, left circumflex; RCA, right coronary artery; **Indicates a p-value less than 0.05, i.e., a significant peak enhancement or CNR difference with the reference retrospective CT angiography data.

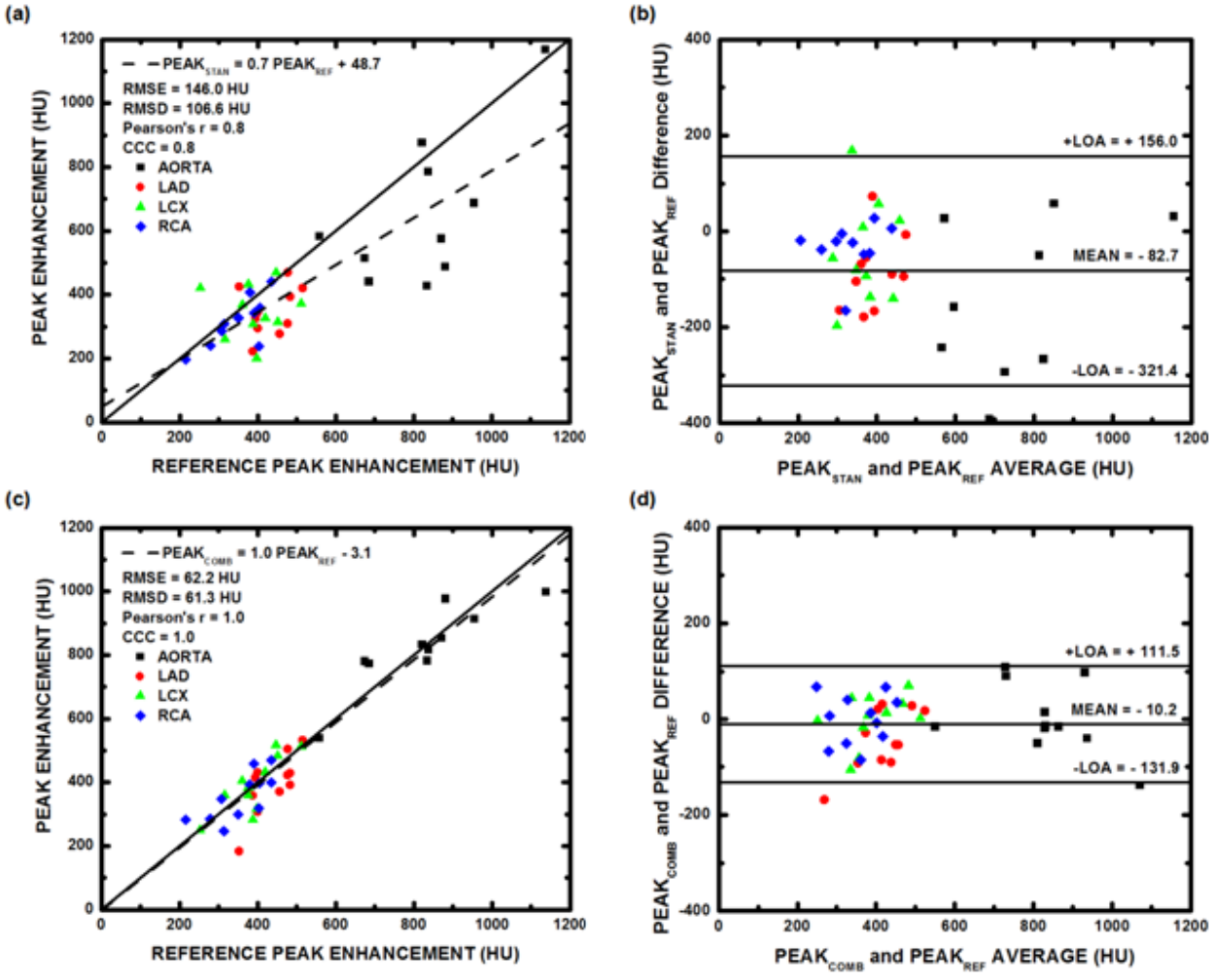

Figure 8.6: Standard, combined, and reference CT angiography peak enhancement regression analysis. (a) Regression analysis comparing the aortic and coronary peak enhancement data from the standard CT angiography protocol ($PEAK_{STAN}$) to corresponding aortic and coronary peak enhancement data from the reference retrospective CT angiography protocol ($PEAK_{REF}$), with (b) Bland-Altman analysis also displayed. (c) Regression analysis comparing the aortic and coronary peak enhancement data from the combined diluted test bolus (DTB) and CT angiography protocol ($PEAK_{COMB}$) to corresponding aortic and coronary peak enhancement data from the reference retrospective CT angiography protocol ($PEAK_{REF}$), with (d) Bland-Altman analysis also displayed. RMSE indicates root-mean-square error; RMSD, root-mean-square deviation; CCC, Lin's concordance correlation coefficient; LAD indicates left anterior descending; LCx, left circumflex; RCA, right coronary artery; LOA, limit of agreement.

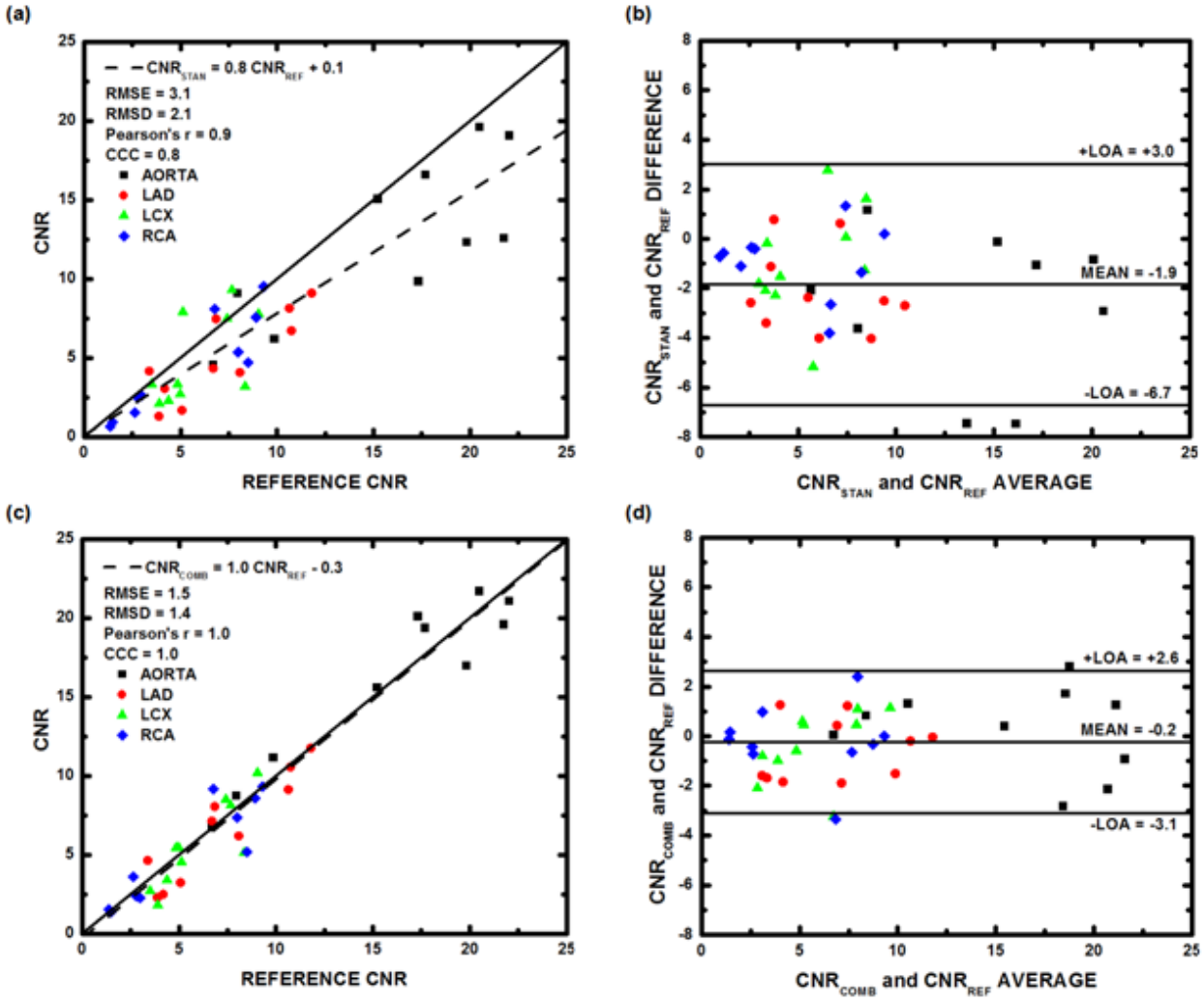

Figure 8.7: Standard, combined, and reference CT angiography CNR regression analysis. (a) Regression analysis comparing the aortic and coronary CNR data from the standard CT angiography protocol (CNR_{STAN}) to corresponding aortic and coronary CNR data from the reference retrospective CT angiography protocol (CNR_{REF}), with (b) Bland-Altman analysis also displayed. (c) Regression analysis comparing the aortic and coronary CNR data from a combined diluted test bolus (DTB) and CT angiography protocol (CNR_{COMB}) to corresponding aortic and coronary CNR data from the reference retrospective CT angiography protocol (CNR_{REF}), with (d) Bland-Altman analysis also displayed. RMSE indicates root-mean-square error; RMSD, root-mean-square deviation; CCC, Lin's concordance correlation coefficient; LAD indicates left anterior descending; LCx, left circumflex; RCA, right coronary artery; LOA, limit of agreement.

CHAPTER 9: PROSPECTIVE ACQUISTION TIMING USING AN OPTIMAL BOLUS TIMING THEORY AS COMPARED TO AN IDEAL BOLUS IN SWINE

Abstract

The feasibility of a low-dose first-pass analysis (FPA) dynamic CT perfusion technique depends upon proper prospective acquisition of two whole-heart volume scans; V1 at the base of the aortic enhancement and V2 at the peak of the aortic enhancement. Hence, the objective of this study was to validate an optimal timing protocol for reliable acquisition of the two volume scans necessary for accurate prospective implementation of low-dose first-pass-analysis (FPA) dynamic CT perfusion technique. Contrast enhanced dynamic CT imaging of twenty-eight male Yorkshire shine (55 ± 24 kg) was performed under rest and stress conditions over twenty to thirty seconds to completely capture the left atrial and aortic enhancement curves. Automatic gamma variate fitting of the left atrial and aortic enhancement curves was then performed. The optimal timing protocol was then retrospectively simulated using the time series data. The protocol consisted of dynamic-bolus-tracking-based triggering in the left atrium, followed by V1 acquisition two seconds after triggering, and V2 acquisition 0.5* Injection Time + d seconds after V1, where “d” was the dispersion delay constant. Using an optimal dispersion delay, a prospective FPA dynamic CT perfusion acquisition scheme was simulated, and all perfusion measurements were quantitatively compared to perfusion measurements with the previously validated reference standard retrospective FPA dynamic CT perfusion technique. Comparisons for all data were made using box-plots,

t-tests, regression, Bland-Altman, root-mean-square error and deviation, as well as Lin's concordance correlation. FPA perfusion measurements with the prospective acquisition simulation ($P_{0.5*InjT+1s}$) were related to the previously validated reference standard retrospective FPA perfusion (P_{REF}) measurements by $P_{0.5*InjT+1s} = 0.95\ P_{REF} + 0.07$ ($r = 0.94$, RMSE = 0.27 mL/min/g, RMSD = 0.04 mL/min/g). The optimal timing protocol was retrospectively validated in twenty-eight swine and has the potential to be used for accurate prospective implementation of a low-dose first-pass-analysis (FPA) dynamic CT perfusion technique.

Introduction

A powerful new first-pass analysis (FPA) dynamic computed tomography perfusion technique is capable of accurate low-dose morphological and physiological assessment of multiform coronary artery disease (CAD)[98, 123, 160]. However, the prospective feasibility of the FPA technique depends upon proper prospective acquisition of two volume scans, V1 and V2, as previously described[98, 123, 160]. By definition, V1 must be acquired as contrast initially arrives in the aorta, while V2 must be acquired at or near the peak of the aortic enhancement. Fortunately, dynamic bolus tracking can be used to reliably trigger and acquire the V1 volume scan[122, 146]. Nevertheless, reliable acquisition of the V2 volume scan at or near the peak of the aortic enhancement proves more difficult. While the time delay between V1 and V2 can be estimated through the preemptive use of a low-dose diluted test bolus acquisition[124], such an acquisition scheme adds time, complexity, contrast dose, and radiation dose; hence, a simpler timing solution is needed.

Unfortunately, patient-specific hemodynamic variability renders arrival time-to-peak difficult to predict[128, 129, 147]. However, an important distinction must be made between arrival time-to-peak and bolus time-to-peak. Arrival time-to-peak is the time delay between initial contrast injection and peak enhancement in the aorta. As such, arrival time-to-peak is dependent on cardiac output and function, i.e., it is patient-specific, and is known to be highly variable[149-151]. However, bolus time-to-peak is the time delay between the base and peak of the aortic enhancement. As such, it is less dependent on cardiac output and function. In fact, work by Garcia et al. and Han et al. suggests that the temporal width of the contrast bolus in the aorta actually depends most on the total contrast bolus volume that is injected[130, 131]. Assuming the injection rate is also fixed, the contrast bolus width in the aorta must also depend on the contrast injection time.

Hence, the purpose of this study was to retrospectively assess and establish a robust relation between the bolus time-to-peak and the contrast injection time. The central hypothesis was that the optimal delay time between the V1 and V2 volume scans is 0.5 * Injection Time + d seconds, where “d” is the dispersion delay. Based on the timing results, an optimal timing protocol was then validated for accurate low-dose prospective implementation of the FPA dynamic CT perfusion technique.

Materials and Methods

Bolus Dispersion and Optimal Peak Timing Theory

Based on work by Garcia et al. and Han et al., it is known that contrast bolus volume is most predictive of the contrast bolus width in the aorta[130, 131]. By extension, assuming

that contrast bolus injection rate is also fixed, the contrast bolus injection time must also be predictive of contrast bolus width in the aorta. Specifically, during contrast injection, the contrast bolus is square in shape, i.e., it has a fixed concentration or enhancement per unit time, as displayed in **Figure 9.1a** and **Figure 9.1b.** However, the vascular resistance and distance to the heart combined with the pustule nature of the circulatory system cause mixing and dispersion, resulting in a broad, approximately gamma variate contrast bolus geometry by the time it reaches the aorta, as displayed in **Figure 9.1b.** Nevertheless, such mixing and dispersion primarily impacts the leading and trailing edges of the bolus uniformly; hence, the temporal center of the bolus should always have the highest contrast concentration. As such, the temporal center of the bolus should also always yield the highest peak enhancement will produce the best performance low-dose prospective first-pass analysis (FPA) dynamic CT perfusion[97, 98, 123]. Moreover, given that the contrast bolus injection time is known, it follows that one-half the injection time plus a fixed dispersion time (*0.5*InjT + d*) should approximately correspond to the temporal center of the contrast bolus in the aorta, as displayed in **Figure 9.1b**.

General Methods

The study was approved by the Animal Care Committee and was performed in agreement with the “Position of the American Heart Association on Research Animal Use.” Contrast enhanced dynamic CT imaging data from twenty-eight male Yorkshire shine (55 ± 24 kg). Five of the swine had significant coronary artery disease generated with a balloon stenosis method as previously described[97, 123] All data was prospectively

acquired and retrospectively analyzed, and there were three experimental aims of interest. For the first aim, the contrast bolus geometry in aorta of each animal was characterized using automatic gamma variate fitting. From the fit curves, the time-to-peak enhancement between the base and peak of the aortic enhancement was extracted and was quantitatively compared to one-half the contrast injection time in order to evaluate the accuracy of the bolus dispersion and optimal peak timing theory. For the second experimental aim, the bolus dispersion and optimal peak timing theory was applied in the context of optimizing prospective FPA dynamic CT perfusion acquisition. Specifically, using the retrospective data, a prospective dynamic bolus tracking, and peak acquisition protocol was simulated, where the peak volume scan was acquired *0.5*InjT + d* seconds after triggering. The dispersion delay, "*d"*, was incrementally increased from 0 - 2 seconds, and the accuracy of peak acquisition was assessed in each case. For the third experimental aim, the impact of the optimal dispersion delay findings of the second aim on the accuracy of FPA dynamic CT perfusion measurement were then assessed in a subset of fourteen animals. Specifically, using the retrospective data, an optimal prospective acquisition scheme was simulated, prospective FPA dynamic CT perfusion was calculated, and all results were quantitatively compared to previously validated retrospective FPA dynamic CT perfusion data from the same fourteen animals[97, 98, 123]. All image data was acquired by authors LH, ShM, YZ, PA, and JK between 03/2016 and 12/2017 and was retrospectively analyzed by author LH, ShM, and YZ between 03/2018 and 04/2018. LH and YZ were research associates with more than three years of medical imaging research experience and ShM was a research assistant with more than two years of

medical imaging research experience. JK was a vascular surgeon with more than ten years of clinical experience and PA was a radiologist with more than fifteen years of clinical experience.

Animal Preparation

Anesthesia was induced with Telazol (4.4 mg/kg), Ketamine (2.2 mg/kg), and Xylazine (2.2 mg/kg), and was maintained with 1.5-2.5% Isoflurane (Highland Medical Equipment, Temecula, CA and Baxter, Deerfield, IL). Sheaths were placed (5Fr, AVANTI®, Cordis Corporation, Miami Lakes, FL) in each femoral vein and were used for drug, fluid, and contrast material administration.

Contrast Enhancement Imaging Protocol

1 mL/kg of contrast material (Isovue 370, Bracco Diagnostics, Princeton, NJ) was injected (5 mL/s, Empower CTA, Acist Medical Systems, Eden Prairie, MN) followed by saline chaser (0.5 mL/kg) at the same rate. Volume scans were then acquired (Aquilion One, Toshiba America Medical Systems, Tustin, CA) dynamically over twenty to thirty seconds to completely capture the base and peak of the time-attenuation-curve, as shown in **Figure 9.1a and Figure 9.1b**. All volume scans were ECG-gated and were acquired at 100 kVp and 200 mA with 320 x 0.5 mm collimation and 16 cm of cranio-caudal coverage. Additionally, a 10-minute delay was employed after each acquisition to allow for adequate clearance of contrast material from the blood pool prior to initiating the next protocol. After imaging was complete, all volume scans were retrospectively reconstructed from full projection data at 75% of the R-R interval using AIDR 3D

reconstruction[126], an FC03 kernal, and a reconstruction voxel size of 0.43 x 0.43 x 0.5 mm.

Aim 1 - Contrast Bolus Parameter Assessment

Automatic Gamma Variate Fitting: For each acquisition, the central lumen of the aorta was first segmented semi-automatically (Vitrea fX version 6.0, Vital Images, Inc., Minnetonka, MN), yielding an aortic vascular volume-of-interest (VOI). Each VOI was then used to automatically generated aortic enhancement curves from each time series dataset. The aortic enhancement curves were then automatically fit via least squares (LSQCurveFit, MatLab 2013a, MathWorks, Natick, MA) using a gamma variate fit function of the form:

$$\boldsymbol{Enhancement(t) = A * \left(\frac{t}{\tau}\right)^{b} * exp^{b*\left(\frac{1-t}{\tau}\right)} + C} \qquad \textbf{Equation. 1}$$

Where *A* is the maximum aortic enhancement, *t* is time, *τ* is both the recay and decay constant, *b* is the recay and decay power, and *C* is the initial pre-contrast enhancement in the aorta. The first and second derivatives of the gamma fit were then computed. Finally, the time-to-peak between the base and peak of the aortic enhancement was calculated as the time difference between the maximum of the second derivative of the gamma variate fit and the ideal peak of the actual gamma variate fit. The gamma fit time-to-peak data was then quantitatively compared to one-half the contrast injection time using regression analysis. Example gamma fits in a 45 kg and 95 kg animal are shown in **Figure 9.2a** and **Figure 9.2b**, respectively.

Differences Under Rest and Stress Conditions: The gamma variate results within a subset of fourteen animals that were imaged dynamically under both rest and rest and stress conditions were also assessed to see if there were pair-wise differences in heart rate, gamma fit time-to-peak, and peak enhancement.

Aim 2 - Optimal Prospective Acquisition of V1 and V2

Optimal Triggering and V1 Acquisition: Based on the results of the first aim, the contrast bolus dispersion and optimal peak timing theory was applied in the context of optimizing prospective FPA dynamic CT perfusion acquisition. Specifically, using the retrospective data, a prospective dynamic bolus tracking, and peak acquisition protocol was simulated. Of important note, when performing dynamic bolus tracking prospectively (SureStart, Aquilion One, Canon Medical Systems, Tustin, CA), the minimum time allowable between bolus-tracking-based triggering and actual volume scan acquisition is two seconds. Such a delay time is problematic for proper prospective FPA dynamic CT perfusion acquisition as two volume scans, V1 and V2 in **Figure 9.1**, must be acquired rapidly. The first volume scan, V1, must be acquired as contrast begins arriving in the aorta, while V2 must be acquired at or near the peak of the aortic enhancement. As such, traditional dynamic-bolus-tracking-based triggering in the aorta followed by acquisition of V1 two seconds later is too slow for proper prospective acquisition of V1.

Fortunately, the left atrium is also in the field-of-view during dynamic bolus tracking; hence, dynamic bolus tracking, and prospective triggering could potentially be performed using the left atrial enhancement instead. Since the left atrium is anatomically more proximal than the aorta, such a triggering solution has the potential to account for the two second scanner delay, such that prospective acquisition of V1 between 100 and 300 HU is accurate and robust. In order to test this hypothesis, the central lumen of the left atrium was segmented semi-automatically (Vitrea fX version 6.0, Vital Images, Inc., Minnetonka, MN), yielding a left atrial vascular volume-of-interest (VOI). Each left atrial VOI was then used to automatically generate left atrial enhancement curves from each time series dataset. The left atrial enhancement curves were then automatically fit via least squares (LSQCurveFit, MatLab 2013a, MathWorks, Natick, MA) using the same gamma variate fit function in **Equation 1**. The left atrial and aortic enhancement curves (from aim 1) were then used in combination to simulate prospective acquisition of V1 using different left atrial trigger thresholds. Specifically, left atrial triggering was simulated at 80, 100, 120, 140, 160, and 180 HU, followed by systematic selection of V1 as the first ECG-gated volume scan 2 seconds after triggering, as shown in **Figure 9.3.** The resulting V1 enhancement was then quantitatively assessed and the left atrial triggering thresholds of 100 and 120HU were used for all remaining analysis.

Optimal Timing and V2 Acquisition: Using the prior left atrial triggering results, the optimal delay time between V1 and V2 for acquisition of V2 at the peak of the aortic enhancement was then assessed. Specifically, based on the bolus dispersion theory as

well as the results of the first aim, the optimal time delay between V1 and V2 was expected to be 0.5*InjT seconds at minimum. As such, prospective left atrial triggering at 100 and 120 HU was simulated, followed by systematic selection of V1 as the first ECG-gated volume scan 2 seconds after triggering. In each case, V2 was then systematically selected as the first ECG-gated volume scan *0.5*InjT + d* seconds after V1, where the dispersion delay "*d*" was iteratively increased as follows: 0.0, 0.5, 1.0, 1.5, 2.0, 2.5, 3.0, 3.5, 4.0 seconds. An example of the prospective simulation is shown in **Figure 9.3**. For each iteration, the cardiac cycle distance of V2 from the ideal peak enhancement was recorded in beats. The result of each left atrial trigger with each 0.5*InjT + d delay were then quantitatively compared through box-plots, paired sample t-tests,

Aim 3 - Accuracy of Prospective Perfusion Measurement

Prospective and Reference Standard Acquisition: The impact of the optimal dispersion delay findings of the second aim on the accuracy of FPA dynamic CT perfusion measurement in mL/min/g were then assessed in a subset of fourteen animals that had previously validated perfusion measurements. More specifically, for each acquisition, V1 and V2 were systematically selected using the optimal prospective acquisition protocol from the second aim. Left atrial triggering thresholds of 100 and 120 HU were both assessed. Prospective FPA dynamic CT perfusion measurements were then computed in each, as previously described[97, 98, 123], and all results were quantitatively compared to the previously validated retrospective FPA dynamic CT perfusion measurements from the same fourteen animals[97, 98, 123].

Imaging Processing and FPA Perfusion Measurement: As previously described[97, 98, 123], the average perfusion (P_{AVE}) in the myocardium is to the first-pass contrast material concentration change within the myocardium; i.e., the average change in myocardial enhancement (ΔHU_{AVE}) over time. Hence, the integrated change in myocardial enhancement (dM_C/dt), the average change in myocardial enhancement (ΔHU_{AVE}), the average aortic blood pool enhancement (C_{in}), the voxel-by-voxel change in myocardial enhancement (ΔHU), and the total myocardial mass (M_T) may be used in combination to derive voxel-by-voxel perfusion (P_{FPA}), as described by **Equation 2.** Given such a theory, only two whole-heart volume scans, labeled V1 and V2 in **Figure 9.1**, are mathematically necessary for low-dose FPA dynamic CT perfusion measurement, as previously validated versus invasive fractional flow reserve (FFR) measurement, quantitative microsphere perfusion, and ultrasonic flow probe measurement[97, 98, 123]. V1 is defined as the first volume scan after the aortic enhancement exceeds 180 HU, while V2 is defined as the first volume scan at or after the peak of aortic enhancement.

$$\boldsymbol{P_{FPA} = \left(M_T^{-1} C_{in}^{-1} \frac{dM_c}{dt} \right)_{AVE} \cdot \frac{\Delta HU}{\Delta HU_{AVE}}} \qquad \textbf{(2)}$$

Hence, for each prospectively simulated acquisition, the V1 and V2 volume scans of interest were first registered and combined into maximum intensity projection (MIP) image volumes. Each MIP was then segmented semi-automatically (Vitrea fX version 6.0, Vital Images, Inc., Minnetonka, MN), yielding the entire myocardium. Voxel-by-voxel perfusion measurements were then computed according to **Equation 2** and were averaged within the entire myocardium to yield global perfusion measurements. All

global perfusion measurements from the prospectively simulated acquisition protocol were then quantitatively compared to their corresponding reference standard retrospective perfusion measurements.

Statistical Approach

For first experimental aim, the gamma variate time-to-peak data was related to the ideal 0.5*InjT data through regression, root-mean-square-error (RMSE), and root-mean-square-deviation (RMSD) analysis. Additionally, the rest and stress subset data were compared graphically through box-plotting as well as quantitatively through paired sample t-tests. For the second experimental aim, optimal V1 triggering and acquisition was assessed graphically through MEAN ± SD comparisons. Moreover, optimal V1 acquisition was assessed graphically through box-plotting as well and quantitatively through paired-sample t-tests. Finally, for the third experimental aim, all perfusions measurements from the prospective simulation protocol were quantitatively compared to the reference standard perfusion measurements using regression, Bland-Altman, root-mean-square-error, root-mean-square deviation, and Lin's concordance correlation coefficient[92]. Statistical software was used for all analysis (MatLab 2013a, MathWorks, Natick, MA; PS, Version 3.0, Vanderbilt University, Nashville, TN; SPSS, Version 22, IBM Corporation, Armonk, NY).

Results

For the first experimental aim, the automatic gamma fit time-to-peak (TTP) data and one-half the injection time data (0.5*InjT) were related by TTP = 1.01 * 0.5 * InjT 2.28,

with a Pearson's correlation of r = 0.98, a root-mean-square-error of 2.28 seconds, and a root-mean-square-deviation of 2.31 seconds, as shown in **Figure 9.4**. The pair-wise box-plot comparisons of the gamma fit data under rest and stress conditions are also shown in **Figure 9.5**, with corresponding mean comparison and paired sample t-test data shown in **Table 9.1.**

For the second experimental aim, the V1 enhancement data resulting from prospective triggering in the left atrium at thresholds ranging from 80 - 180 HU are displayed in **Figure 9.6**. Additionally, with respect to V2 acquisition at the ideal peak, the box-plots for the 100 and 120 HU left atrial trigger data are shown in **Figure 9.7**, with the data from the three most accurate dispersion delays "d" shown for each trigger, respectively. Corresponding paired sample t-test data also shown in **Table 9.2.**

Finally, for the third experimental aim, FPA perfusion measurements in mL/min/g were generated using the most accurate dispersion delay "d = 1s" from the second experiment aim. Specifically, when using a left atrial triggering threshold of 100 HU, FPA perfusion measurements with the prospective acquisition simulation ($P_{0.5*InjT+1s}$) were related to the previously validated reference standard retrospective FPA perfusion (P_{REF}) measurements by $P_{0.5*InjT+1s} = 0.92\ P_{REF} + 0.11$, with a Pearson's correlation of r = 0.94, a concordance correlation of ρ = 0.94, a root-mean-square-error of 0.27 mL/min/g, and a root-mean-square-deviation of 0.07 mL/min/g, as shown in **Figure 9.8a,** with corresponding Bland-Altman analysis displayed in **Figure 9.8b**. Alternatively, when using a left atrial triggering threshold of 120 HU, FPA perfusion measurements

with the prospective acquisition simulation ($P_{0.5*InjT+1s}$) were related to the previously validated reference standard retrospective FPA perfusion (P_{REF}) measurements by $P_{0.5*InjT+1s} = 0.95\ P_{REF} + 0.07$, with a Pearson's correlation of r = 0.94, a concordance correlation of ρ = 0.94, a root-mean-square-error of 0.27 mL/min/g, and a root-mean-square-deviation of 0.04 mL/min/g, as shown in **Figure 9.8c,** with corresponding Bland-Altman analysis displayed in **Figure 9.8d.**

Discussion

Indication of the Results of Aim 1

The results of the first experimental aim indicate that over a large range of injection times (2.5 - 12.5 seconds), one-half the injection time plus a fixed dispersion time of approximately 2.3 seconds (0.5 * InjT + 2.3s) corresponds to the time-to-peak enhancement of the contrast bolus in the aorta. More importantly, based on the pair-wise comparisons, there is was no significant difference in the time-to-peak enhancement between rest an stress conditions, although the stress peak enhancement was significantly lower the rest peak enhancement (p = 0.01). Such findings are important in that they indicate that the contrast bolus volume or time injection time is most predictive of the contrast bolus width in the aorta[130, 131]. As such, the same time delay between V1 and V2 can be used for optimal low-dose FPA perfusion measurement under both rest and stress conditions, independent of changes in cardiac output.

Indication of the Results of Aim 2

The results of the second experimental aim indicate that dynamic-bolus-tracking-based triggering in the left atrium is feasible and should be performed at 100 or 120 HU to ensure that false-triggering is avoided, while also ensuring that V1 is always acquired with an aortic enhancement that is less than 300 HU, i.e., that V1 is acquired right as contrast begins to arrive in the aorta. More importantly, based on the prospective simulation and V2 peak acquisition data as compared to the ideal peak data, a delay time of 0.5* InjT + 1 seconds was found be optimal for acquisition of the ideal peak for both 100 and 120 HU left atrial triggering thresholds. More specifically, there were no significant mean difference in cardiac cycle offset from the ideal peak in both cases ($p = 0.11$, $p = 0.50$), and the RMSE in both cases was less than 2 cardiac cycles, indicating the robustness of the optimal peak timing theory.

Indication of the Results of Aim 3

Finally, with respect to FPA perfusion measurement, when applying the optimal peak timing theory such that an optimal delay of 0.5*InjT + 1 seconds between V1 and V2 was used, FPA perfusion measurements with the prospective acquisition simulation were in good agreement with the previously validated reference standard retrospective FPA perfusion measurements, demonstrating near unity slope, minimal offset, good concordance correlation, and negligible bias. Such findings indicate that the optimal peak timing theory has the potential to be used for accurate, low-dose prospective implementation of the FPA dynamic CT perfusion technique. Moreover, given that the optimal peak timing theory enables accurate acquisition of image data at the peak

enhancement, such findings also have the potential to optimize contrast-to-noise-ratio in both coronary CT angiography and static CT perfusion, although a different triggering protocol and dispersion delay may be necessary.

Limitations

This study is not without limitations. First, while a large range of swine weights and injections times were used, on average the animals were undersized as compared to an average patient with multiform coronary artery disease. Hence, additional work in larger animals may still be necessary to confirm that optimal delay of 0.5*InjT + 1 seconds is robust. Additionally, the majority of the swine used in this study were healthy (only five had significant balloon stenoses); hence, the performance of the optimal delay of 0.5*InjT + 1 seconds was not truly assessed in the presence of poor cardiac function. As a result, additional work in more animals with significant cardiac disease may still be necessary. That being said, the lack of difference between rest and stress data in the pair-wise gamma variate analysis indicates that the optimal delay theory is still robust over a range of cardiac outputs; hence, accurate acquisition of the V2 volume scan at the peak of enhancement may still be feasible in a patient with poor cardiac function. Additionally, as an alternative solution, the V2 time delay can also be predicted through the preemptive use of a low-dose diluted test bolus acquisition[124]. Specifically, the geometry of a diluted test bolus emulates that of a true bolus[124]; hence, the correct time-delay can be predicted in advance and used for accurate, prospective acquisition of V2, although total contrast and radiation dose will be increased. Finally, the optimal delay theory of 0.5*InjT + 1 seconds was developed and assessed retrospectively. While the

simulated prospective acquisition of V1 and V2 for FPA perfusion measurement performed well as compared the previously validated reference standard retrospective FPA perfusion measurement[97, 98, 123], true prospective acquisition of V1 and V2 using the optimal delay theory was not assessed; hence, additional prospective work in more animals may still be necessary.

Conclusion

An optimal timing protocol for accurate low-dose prospective first-pass-analysis (FPA) dynamic CT perfusion was retrospectively developed and validation in twenty-eight swine over a range of injection volumes, injection times, and cardiac outputs. Specifically, dynamic-bolus-tracking-based triggering at 100 or 120 HU in the left atrium resulted in robust acquisition of V1 two seconds later at the start of contrast arrival in the aorta. Additionally, V2 acquisition 0.5*InjT+1 seconds after V1 acquisition resulted in robust acquisition of V2 at the peak of enhancement, yielding accurate low-dose prospective FPA dynamic CT perfusion measurement as compared to a previously validated retrospective FPA dynamic CT perfusion. Moreover, such findings also have the potential to optimize contrast-to-noise-ratio in both coronary CT angiography and static CT perfusion, as the diagnostic accuracy of such techniques depends on acquisition of the peak of enhancement. In summary, the optimal timing protocol was retrospectively validated in twenty-eight swine and has the potential to be used for accurate prospective implementation of a low-dose first-pass-analysis (FPA) dynamic CT perfusion technique.

Tables

Table 9.1: Rest and stress comparison

Parameter (N)	**REST** (MEAN ± SD)	**STRESS** (MEAN ± SD)	**P-Value (α < 0.05)**
Heart Rate (28)	88.50 ± 11.84	94.40 ± 14.58	0.05**
Gamma Fit Time-To-Peak (28)	5.96 ± 1.05	5.76 ± 0.95	0.22
Peak Enhancement (28)	798.75 ± 161.71	702.56 ± 170.85	0.01**

*N indicates the number of measurements; **Indicates a p-value less than 0.05, i.e., a significant difference between rest and stress conditions.*

Table 9.2: Prospective peak acquisition simulation as compared to ideal peak acquisition

Protocol (N)	Cardiac Cycle Difference From Peak (Beats)	P-Value (α < 0.05)	RMSE (Beats)
100 HU LA Trigger (98)			
0.5InjT + 0.5s	-0.98 ± 1.86	0.00**	2.09
0.5InjT + 1.0s	**-0.32 ± 1.92**	**0.11**	**1.95**
0.5InjT + 1.5s	0.43 ± 2.03	0.04**	2.06
120 HU LA Trigger (98)			
0.5InjT + 0.5s	-0.56 ± 1.79	0.00**	1.87
0.5InjT + 1.0s	**0.13 ± 1.85**	**0.50**	**1.84**
0.5InjT + 1.5s	0.86 ± 1.97	0.00**	2.14

*N indicates the number of measurements; HU LA Trigger, dynamic bolus tracking left atrial blood pool trigger threshold; InjT, contrast injection time; RMSE, root-mean-square-error. *Indicates a p-value less than 0.05, i.e., a significant difference as compared to the ideal peak.*

Figures

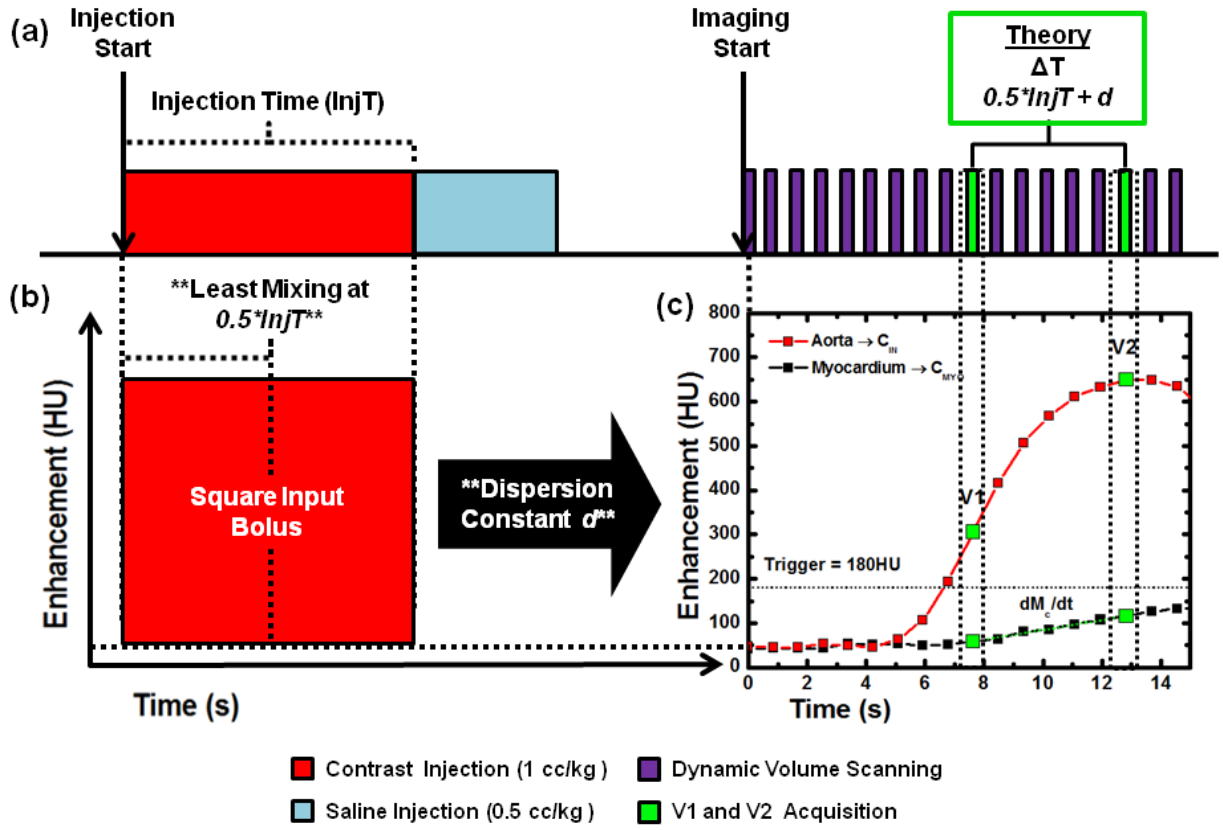

Figure 9.1: Contrast bolus injection protocol and bolus dispersion theory. (a) For all contrast enhanced imaging, contrast was injected at a fixed rate, followed by a saline chaser at the same rate. Dynamic imaging of the heart was then performed. (b) The contrast dispersion bolus theory states that the peak enhancement of the contrast bolus in the aorta occurs at approximately one-half the injection time plus a fixed dispersion time (0.5*InjT + d). Such a theory can be used to optimize acquisition of CT angiography, static CT perfusion, and first-pass analysis (FPA) dynamic CT perfusion as defined by the V2 volume scan.

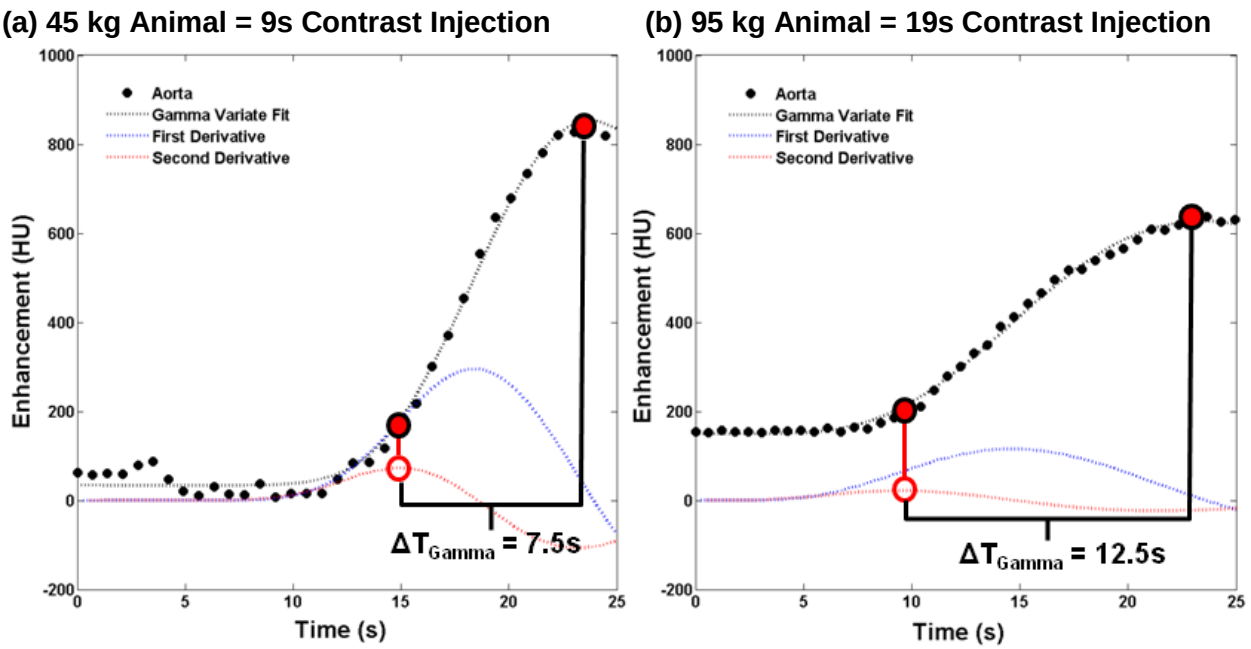

Figure 9.2: Automatic gamma variate fitting of the aortic enhancement in two swine. (a) The gamma fit (black), first derivative (blue), second derivative (red), and time-to-peak (ΔT_{Gamma}) are displayed for a 45 kg animal with a 9 second contrast injection. (b) The gamma fit (black), first derivative (blue), second derivative (red), and time-to-peak (ΔT_{Gamma}) are also displayed for a 95 kg animal with a 19 second contrast injection. As expected, the ΔT_{Gamma} for the 9s injection is proportionally less than the ΔT_{Gamma} for the 19 second contrast injection.

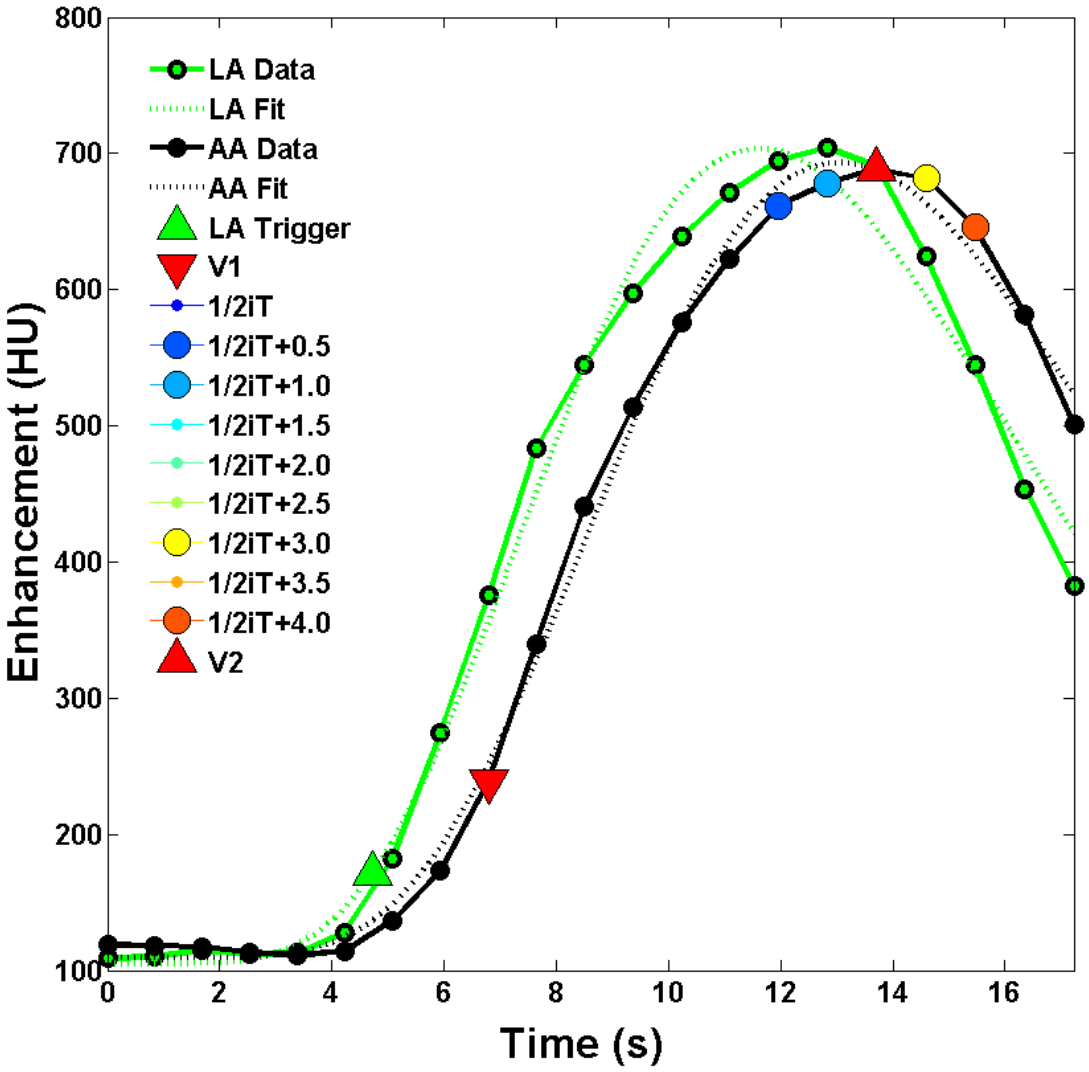

Figure 9.3: Prospective acquisition protocol simulation. For each acquisition, the dynamic data was first used to generate left atrial and aortic enhancement curves. Automatic gamma variate fitting of the left atrial and aortic enhancement curves was then performed. The left atrial gamma variate fit was used to simulate dynamic-bolus-tracking-based triggering (green triangle). V1 was then selected as the first ECG-gated volume scan occurring two seconds after left atrial triggering, while V2 was systematically selected as the first ECG-gated volume scan occurring 0.5*InjT + 0, 0.5, 1.0, 1.5, 2.0, 2.5, 3.0, 3.5, or 4.0 seconds after V1. The cardiac cycle distance of V2 from the ideal peak enhancement (red triangle) was then recorded.

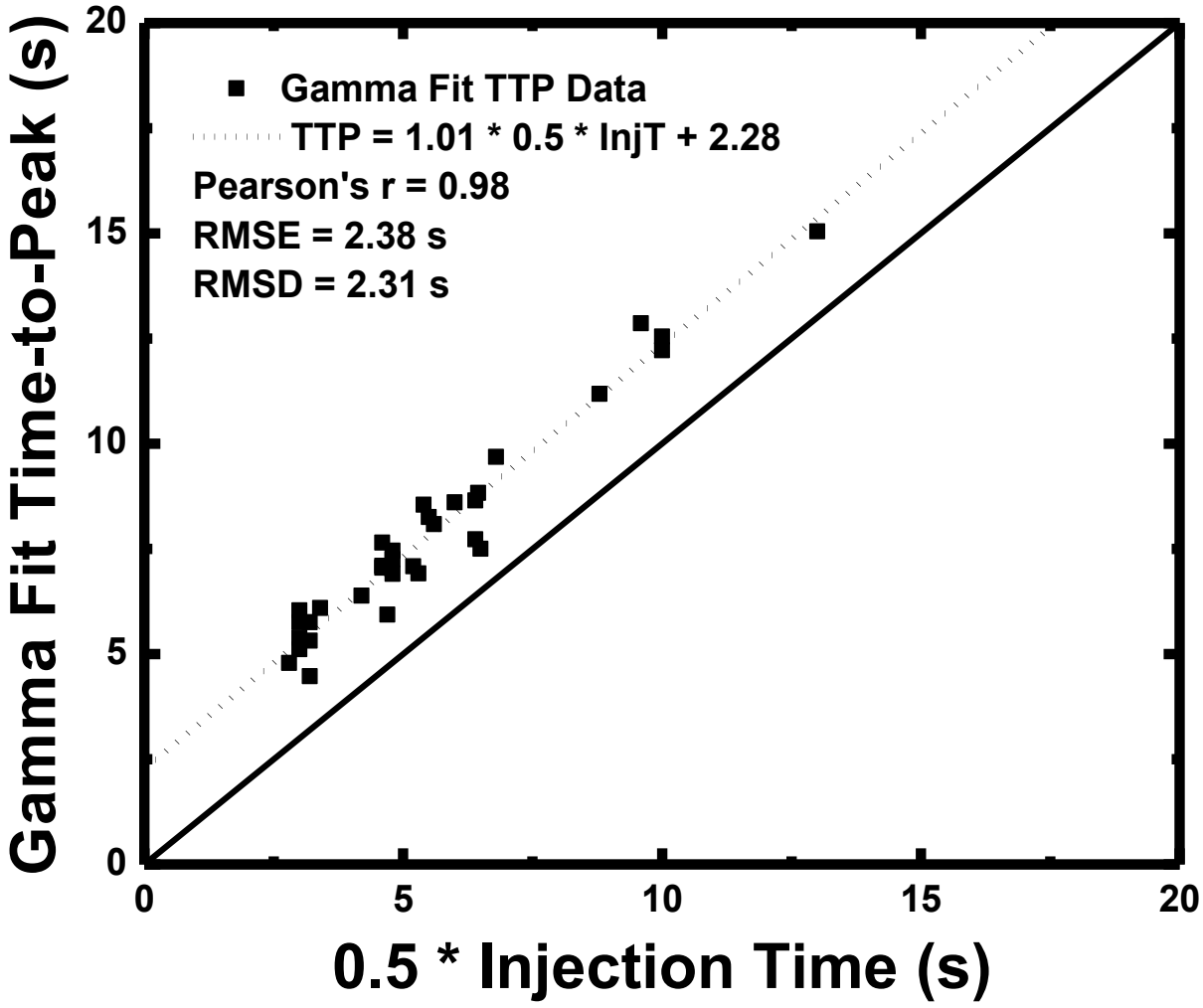

Figure 9.4: Gamma fit time-to-peak data as compared to 0.5* injection time data. The time-to-peak aortic enhancement was retrospectively assessed in 28 animals through automatic gamma variate fitting. The gamma fit time-to-peak data was then quantitatively compared to the ideal bolus timing theory through regression analysis. TTP indicates the time-to-peak of the aortic enhancement, defined as the time between the peak of the second derivative of the gamma fit and the true peak of the gamma fit; InjT, contrast injection time; RMSE, root-mean-square-error. RMSD, root-mean-square-deviation.

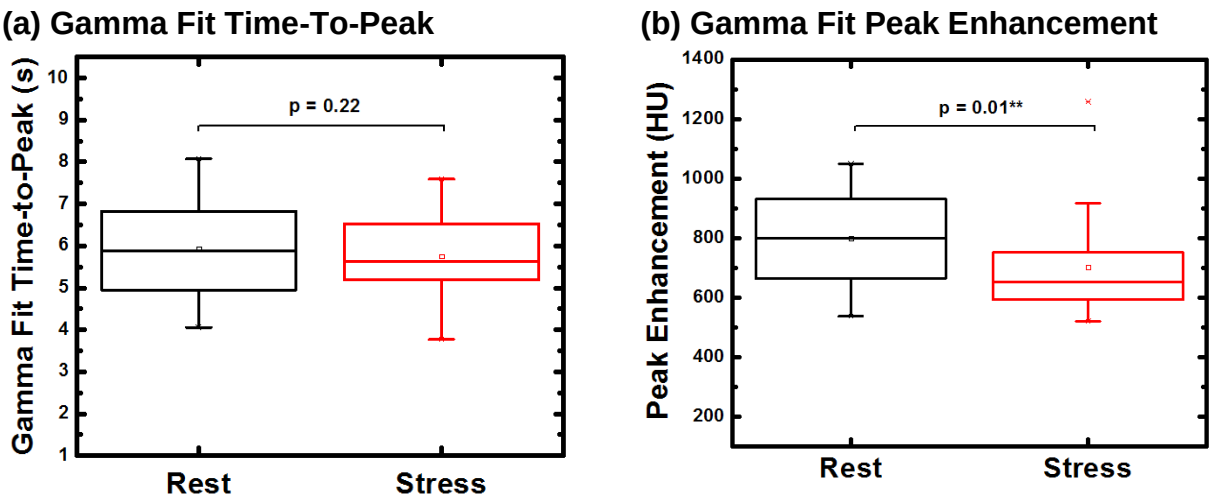

Figure 9.5: Pair-wise gamma fit comparison under rest and stress conditions. Time-to-peak and peak enhancement were retrospectively assessed under rest and stress conditions. (a) Pair-wise gamma-fit time-to-peak box-plots are shown. (b) Pair-wise gamma-fit peak-enhancement box-plots are shown. **Indicates a p-value less than 0.05, i.e., a significant difference between rest and stress conditions.

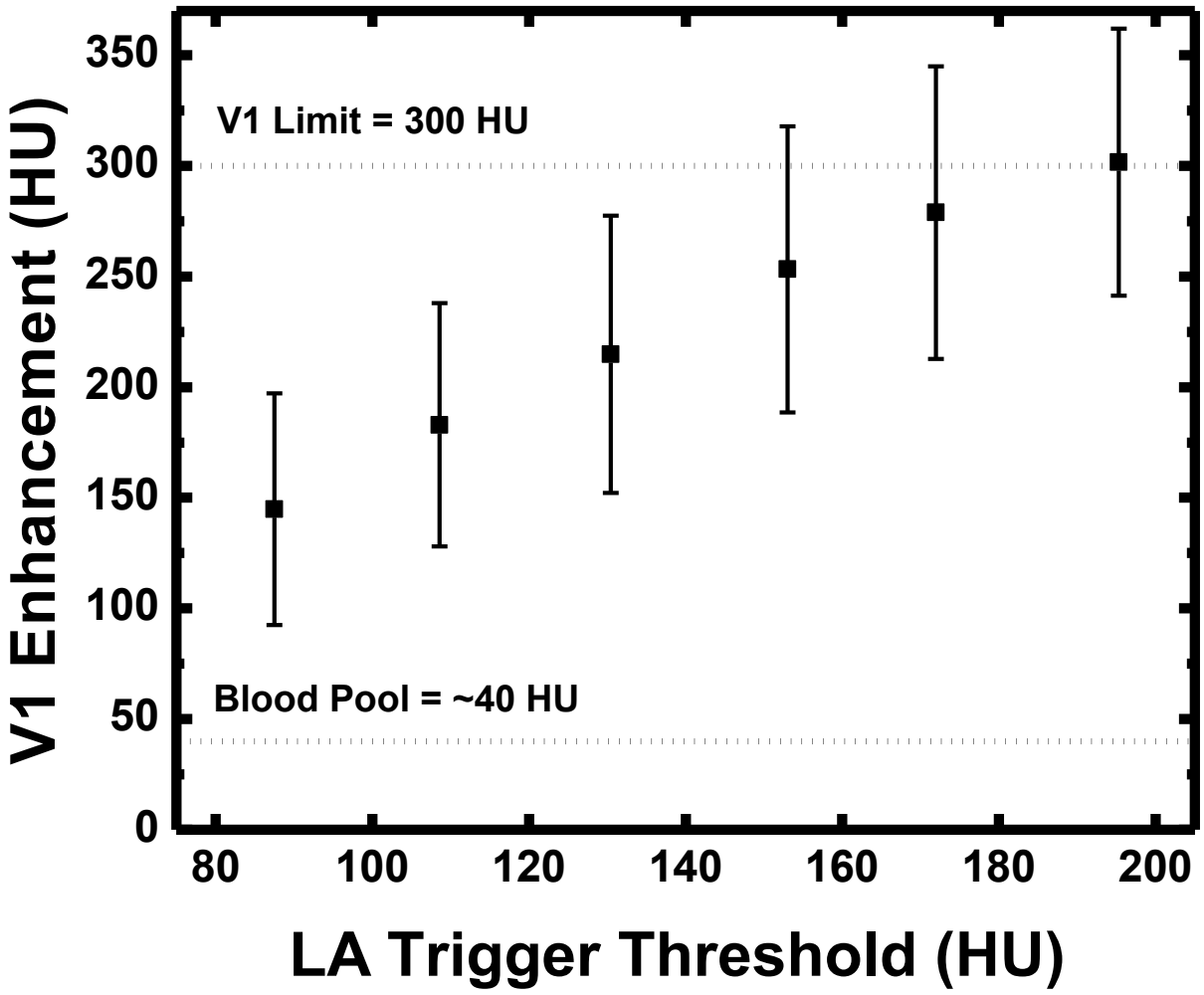

Figure 9.6: Prospective V1 enhancement as a function of left atrial trigger threshold. Left atrial trigger thresholds of 80, 100, 120, 140, 160, and 180 HU were assessed. To avoid false triggering in the left atrium, as well as to avoid V1 enhancement values above 300 HU, left atrial rigger thresholds of 100 and 120 HU were used for all analysis.

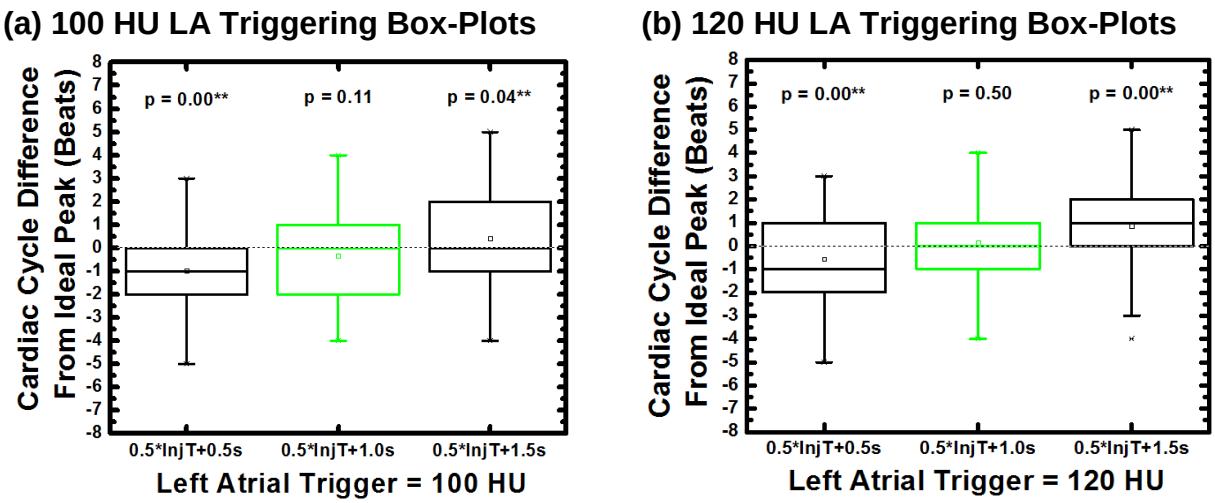

Figure 9.7: Prospective simulation V2 peak acquisition using an optimal delay time as compared to the ideal peak. The box-plots display the cardiac cycle difference (in beats) between the prospectively simulated V2 peak as compared to the ideal peak. (a) V2 cardiac cycle difference from the ideal peak using a 100 HU left atrial trigger as a function of three different dispersion delays. (b) V2 cardiac cycle difference from the ideal peak using a 120 HU left atrial trigger as a function of three different dispersion delays. **Indicates a p-value less than 0.05, i.e., a significant difference between rest and stress conditions. HU indicates Hounsfield Unit; LA, left atrium; InjT, contrast injection time.

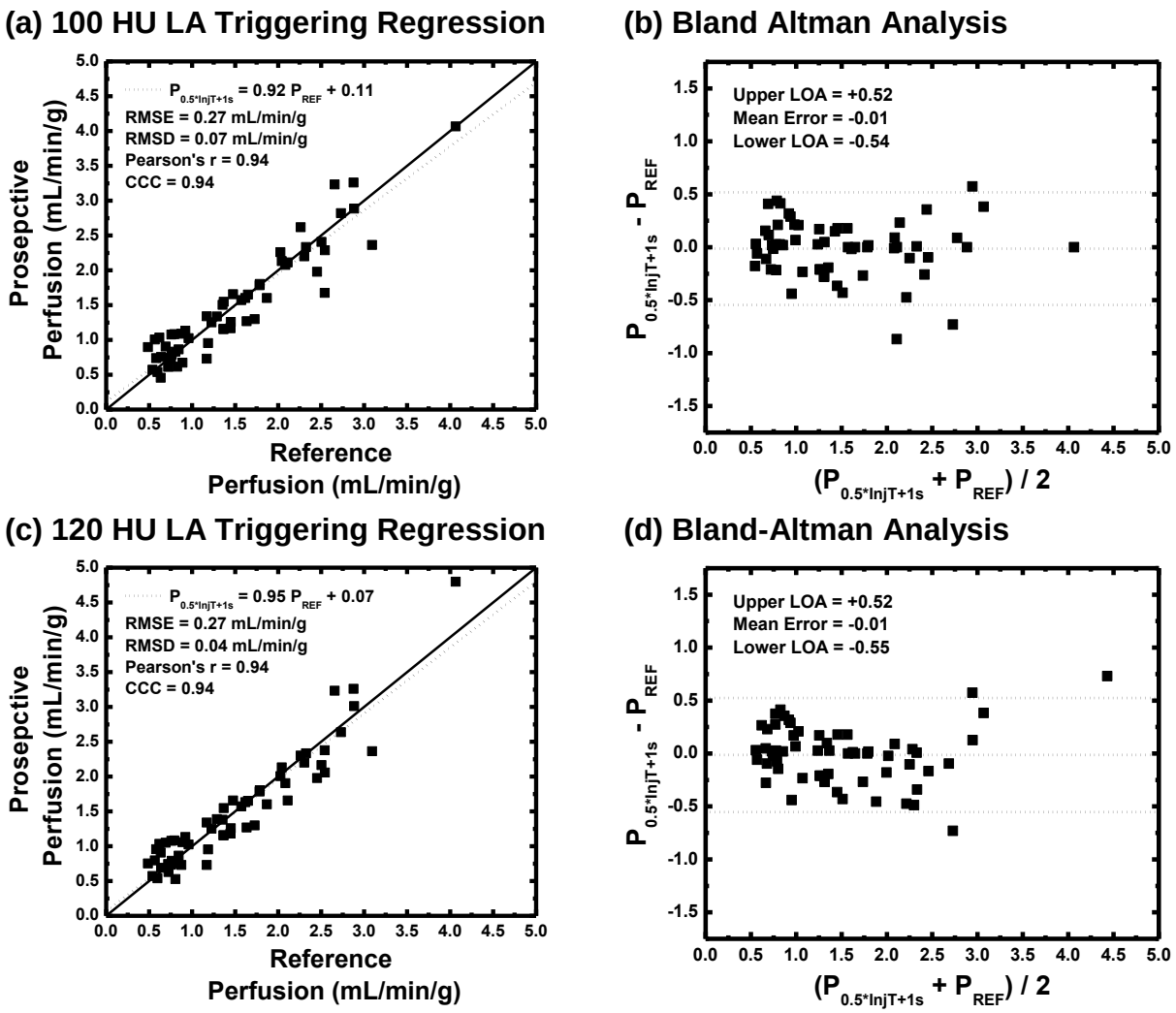

Figure 9.8: FPA perfusion data using the simulated prospective acquisition protocol as compared to the previously validated reference standard retrospective FPA perfusion data. Left atrial triggering thresholds of 100 and 120 HU were used. For the 100 HU left atrial triggering threshold, (a) regression analysis comparing FPA perfusion with the simulated prospective acquisition protocol to reference standard retrospective FPA perfusion is displayed. (b) Corresponding Bland-Altman analysis is also shown. For the 120 HU left atrial triggering threshold, (c) regression analysis comparing FPA perfusion with the simulated prospective acquisition protocol to reference standard retrospective FPA perfusion is displayed. (c) Corresponding Bland-Altman analysis is also shown.

CHAPTER 10: CLINICAL TRANSLATION AND FUTURE DIRECTIONS OF LOW-DOSE COMPREHENSIVE CARDIAC COMPUTED TOMOGRAPHY IN HUMAN SUBJECTS

Abstract

The body of this dissertation research developed and validated a low-dose comprehensive cardiac CT technique based on first-pass analysis for accurate morphological and physiological assessment of multiform coronary artery disease (CAD). First, the accuracy of the technique was retrospectively validated in a phantom model of the heart, as well as in a swine animal model of segmental CAD, through quantitative comparison to ultrasonic flow probe measurement, invasive fractional flow reserve measurement, and quantitative microsphere perfusion measurement. Second, the effective dose reduction capacity of the technique was validated in a swine animal model of segmental CAD through tube current reduction and prospective volume scan acquisition. Third, robust prospective acquisition protocols were validated such that the low-dose comprehensive cardiac CT technique was clinically feasible.

In combination, the next step and future direction of the low-dose comprehensive cardiac CT technique is clinical implementation in human subjects. Specifically, IRB approval was received (HS# 2016-3128) and preliminary investigation of the low-dose comprehensive cardiac CT technique is currently underway. As a case-study, the results of the technique in one patient are also displayed, and future directions also discussed. In summary, the low-dose comprehensive cardiac CT technique has the

potential to be used for accurate, low-dose, vessel-specific morphological and physiological assessment of CAD, making comprehensive CT-based assessment of multiform CAD more accurate, accessible, and impactful to patients in need.

Introduction

Coronary artery disease (CAD) is the leading cause of morbidity and mortality worldwide. As a risk factor, CAD and its resultant ischemic cardiomyopathy are strongly predicative of future cardiac events. While coronary computed tomography (CT) angiography is a powerful tool for assessing CAD risk, it is fundamentally limited in that it can only assess the morphological severity of segmental CAD, but cannot define the physiological severity of concurrent mutli-vessel, diffuse, and microvascular disease. Hence, guidelines recommend additional physiological assessment of CAD, in conjunction with CT angiography, for more objective indication of patient risk. The primary modalities used for physiological assessment are single-photon emission computed tomography (SPECT), stress echocardiography, cardiac magnetic resonance (CMR), static positron emission tomography (PET), and static CT. However, such modalities only provide metrics of relative perfusion; hence, they still cannot appreciate the true physiological severity of multiform CAD. Fortunately, absolute perfusion measurement with dynamic CT can overcome these limitations, where the spatial distribution of absolute rest and stress perfusion in mL/min/g combined with physiological cutoff thresholds can be used to reliably stratify patient risk and properly guide intervention. Nevertheless, current dynamic CT perfusion techniques are known to be quantitatively inaccurate and deliver unacceptably high effective radiation doses

per imaging exam, precluding their widespread clinical use. As such, there is a major unmet clinical need for an accurate, low-dose CT technique for combined morphological and physiological assessment of multiform CAD.

The body of this dissertation research has developed and validated a low-dose comprehensive cardiac CT technique based on first-pass analysis for accurate morphological and physiological assessment of multiform CAD. First, the accuracy of the technique was validated retrospectively in a phantom model of the heart, as compared to reference standard ultrasonic flow probe measurement. From that model, it was determined that only two volume scans were necessary for accurate FPA perfusion measurement[98]. Moreover, the optimal first-pass acquisition scheme of those volume scans at the base and peak of the aortic enhancement was also devised. Next, a minimum-cost-path myocardial assignment algorithm for automatic assignment of coronary perfusion territories using coronary vessel centerlines was validated, as compared to invasive myocardial blush[47, 133]. Using that algorithm, it was determined that the perfusion territories of the left anterior descending (LAD), left circumflex (LCx), and right coronary artery (RCA) can be isolated on a vessel-specific, i.e., a patient-specific basis. Moreover, within a given territory, distal assignment was also devised, such that the perfusion territory distal to a segmental stenosis, i.e., the myocardial-mass-at-risk, can also be isolated.

The accuracy of vessel-specific perfusion measurement in the LAD, LCx, and RCA was then retrospectively validated in a swine animal model of segmental CAD, as compared

to invasive fractional flow reserve and quantitative microsphere perfusion measurement[97, 123]. In combination, the findings indicated that accurate voxel-by-voxel and vessel-specific perfusion measurement in mL/min/g is feasible with the comprehensive cardiac CT technique. Moreover, given that all perfusion measurements were validated using only two volume scans, the findings also indicated that accurate voxel-by-voxel and vessel-specific perfusion measurement in mL/min/g is feasible at a significantly reduced dose, as compared to current dynamic CT perfusion techniques (~10 mSv) [18, 37, 42].

Nevertheless, all accuracy validation was done retrospectively; hence, the effective dose reduction capacity of the comprehensive cardiac CT technique was validated next. Tube current reduction was assessed first, and it was found that accurate perfusion measurement with the comprehensive cardiac CT technique was possible at one-quarter of the previously validated effective dose. Moreover, it was found that low-dose prospective perfusion measurement was possible. Specifically, accurate global and vessel-specific stress and rest perfusion measurements in the LAD, LCx, and RCA could be measured at a dose less than 3 mSv, while simultaneously providing CT angiography and coronary flow reserve (CFR), using only four prospectively acquired volume scans and two contrast injections, respectively.

However, reliable clinical implementation of the comprehensive cardiac CT technique necessitates a robust prospective two-volume acquisition protocol, where the first volume scan is acquired at the base of the aortic enhancement, while the second

volume scan is acquired at or near the peak of the aortic enhancement. As such, two different prospective acquisition protocols were developed and validated. The first protocol employs the preemptive used of diluted test bolus to accurately predict the temporal position of the volumes scans, prior to prospective volume scan acquisition with the low-dose comprehensive cardiac CT technique, as displayed in **Figure 10.1**. The second protocol employs an optimal time delay based on the injection time and bolus dispersion kinetics, such that prospective volume scan acquisition with the low-dose comprehensive cardiac CT technique is simpler and more robust, as displayed in **Figure 10.2**.

In combination, the low-dose comprehensive cardiac CT technique was validated to be accurate, while the total combined radiation and contrast dose of CT-based multiform CAD workup was dramatically reduced. Given these findings, as well the prospective acquisition solutions, the next step and future direction of the low-dose comprehensive cardiac CT technique is clinical implementation in human subjects. Specifically, IRB approval was received (HS# 2016-3128) and preliminary clinical implementation of the low-dose comprehensive cardiac CT technique is currently underway.

Materials and Methods

General Approach

The low-dose comprehensive cardiac CT technique will be used to assess perfusion, CFR, and angiography in patients suspected or known to have CAD, with perfusion values less than 1.0 mL/min/g indicating physiological significance[161]. Such

classification will then be compared to invasive angiography, with >50% cross sectional area reduction indicating morphological significance. Relative perfusion will also be computed and compared to invasive fractional flow reserve (FFR) measurement is FFR data is available, with FFR severities < 0.8 in indicating physiological significance.

Patient Population

Four patients suspected or known to have CAD were initially recruited for the IRB approved low-dose comprehensive CT technique study (HS# 2016-3128). Exclusion criteria included renal failure (estimated glomerular filtration rate < 60 mL/min/1.73m^2), iodine allergy, contraindications to Regadenoson, and pregnancy. Patients with prior heart attacks or revascularization procedures were not excluded.

Low-Dose Comprehensive Cardiac CT Imaging Protocol

For each patient, a scout scanogram was first performed to properly position the heart in the field-of-view. A diluted test bolus was then injected (1mL/kg, 5 mL/s) followed by a saline chaser (0.5 mL/kg, 5 mL/s), and low-dose 2-mm CINE scanning was performed in 1.5 second intervals over 30 seconds. The bolus time-to-peak from the base of the aortic attenuation to the peak of the aortic attenuation was then derived. Next, stress perfusion acquisition was performed. Regadenason was administered (time of action = 2.3 minutes), followed by contrast injection 1 minute later (1 mL/kg, 5mL/s). Dynamic bolus tracking was then performed, where V1 was triggered in the left atrium after the blood pool intensity exceeded 180HU, while V2 was acquired after V1 using the previously determined time-to-peak delay. Fifteen to twenty minutes after the stress

exam, each patient was administered sublingual nitroglycerin and IV metoprolol. the combined rest perfusion and CT angiography exam was then performed. Specifically, contrast was again injected (1 mL/kg, 5mL/s), and dynamic bolus tracking was performed, where V1 was triggered after the left atrial blood pool intensity exceeded 180HU, while V2 (CTA) was acquired at a higher tube current after V1 using the previously determined time-to-peak delay. All dynamic bolus tracking and volume scanning was performed at 100 kVp and with an automatic SureExposure-based tube current using an ultra-low-dose standard deviation setting of 100 HU. All bolus tracking images had a collimation of 1 x 2.0 mm and all volume scans had a collimation of 320 x 0.5 mm. Bolus tracking images and volume scans were then retrospectively reconstructed from full projection data at 75% of the R-R interval using AIDR3D algorithm and an FC03 kernel. The rest and stress protocols of the low-dose comprehensive cardiac CT technique are shown in **Figure 10.1a** and **Figure 10.1b**, respectively.

Image Processing

As previously described[97, 123], all volume scans were first registered[162], combined into a MIP, and segmented semi-automatically to produce a myocardial mask, i.e., a whole-heart perfusion compartment. Given the compartment mass, the average of the AIF, and the integrated and average change in myocardial HU between the volume scans of interest, rest perfusion, stress perfusion, and coronary flow reserve (CFR) measurements were computed. The centerlines of the LAD, LCx, and RCA were then extracted from the CT angiogram ($V2_{REST}$) and used, along with the myocardial mask,

for minimum-cost-path (MCP) myocardial assignment[47], yielding three patient-specific coronary perfusion territories. Given the voxel-by-voxel and vessel-specific perfusion and CFR maps, the fractional breakdown of stress perfusion and CFR in the LAD, LCx, and RCA perfusion territories was also derived, and assessed in conjunction with the CT angiogram.

Statistical Approach

The diagnostic sensitivity, specificity, positive predictive value, negative predictive value, and AUC of the ROC curve for the low-dose comprehensive cardiac CT technique will be determined, with cross-sectional area reductions greater than 50% considered the reference standard for stenosis significance. If FFR is also available, relative perfusion measurements will also be compared to FFR measurements using linear regression and concordance correlation. The R^2, RMSE, and RMSD of measurement will also be determined, with Bland-Altman analysis used to graphically assess systematic bias. The diagnostic sensitivity, specificity, positive predictive value, negative predictive value, and AUC of the ROC curve for relative perfusion will also be determined, with FFRs less than or equal to 0.80 considered to the reference standard for functional significance.

Results

Single Patient Case Study: The CT angiographic data identified a morphologically significant calcified stenosis in the proximal LAD, as displayed in **Figure 10.3.** Regadenson induced myocardial stress also resulted in marked reduction in stress

perfusion and CFR in distal LAD territory, indicating physiologically significant segmental disease caused by the morphologically significant stenosis, as displayed in **Figure 10.3.** Further analysis of the average stress perfusion and CFR in the LAD, LCx, and RCA perfusion territories is also displayed in **Figure 10.4b,** where **Table 10.1** and **Table 10.2** go on to describe the fractional breakdown of stress perfusion and CFR in the LAD, LCx, and RCA perfusion territories, respectively.

Discussion

Indication of Results: A cohort of at least fifty patients must first be recruited and assessed with the low-dose comprehensive cardiac CT technique before any major conclusions can be drawn. However, in the preliminary case-study of a 100 kg patient with suspected CAD, the low-dose comprehensive cardiac CT technique was able to detect a morphologically and physiologically significant stenosis in the proximal LAD. Moreover, the total effective dose of the entire exam was only 6.9 mSv for voxel-by-voxel and vessel-specific stress perfusion, rest perfusion, and CFR, while simultaneously providing CT angiography. The effective dose of stress perfusion alone was 2.4 mSv; substantially lower than the 10 mSv average effective dose of stress perfusion alone with current dynamic CT perfusion techniques[18],

Future Directions

Optimization of the Protocol: After the first round of preliminary studies the low-dose comprehensive cardiac CT protocol was modified. Specifically, it was difficult to reduce the patients' heart rates after the stress protocol prior to the rest protocol; hence, the

temporal order of rest and stress were switched, as displayed in **Figure 10.1** and **Figure 10.2**. Additionally, in order to minimize the risk of renal damage, the total contrast dose was reduced by 30% from 1 mL/kg to 0.7 mL/kg. Moreover, in order to reduced the effective dose of the low-dose comprehensive cardiac CT technique by 25%, the cranio-caudal coverage was reduced from 16 cm to 12 cm.

Improvement of the Technique: Given the first-pass timing of the V2 volume scan during the low-dose, stress perfusion acquisition, the comprehensive cardiac CT technique has the potential to be extended by adding cardiac functional analysis (CFA). Specifically, if the stress V2 exposure time is increased, the entire cardiac cycle can be captured, enabling added assessment of cardiac output, ejection fraction, wall motion, and myocardial strain[140, 141]. Moreover, the low-dose comprehensive cardiac CT technique dramatically reduced the dose of CT-based multiform CAD workup, but additional effective dose reduction may still be feasible. Specifically, tube voltage optimization, better tube current modulation, and improved iterative reconstruction techniques (FIRST)[43, 66, 132] may be used to further reduce the effective dose of the comprehensive cardiac CT technique, although additional validation is still necessary. Moreover, beam hardening reduces the diagnostic accuracy of the comprehensive cardiac CT technique. While standard beam hardening corrections are already used (FC03 reconstruction kernal), better image-based or projection-based beam hardening correction algorithms[68, 69]. More importantly, widespread utilization of the low-dose comprehensive cardiac CT technique depends upon the availability of whole-heart imaging systems. Fortunately, such systems are becoming more prevalent. Additionally,

128- and 256-slice CT scanners with eight centimeters of cranio-caudal coverage are also becoming more prevalent, with a recent report[110] indicating that it is possible to image the entire heart within eight centimeters of cranio-caudal coverage if systolic-phase data is acquired during an end-expiratory breath hold. Hence, the reach of the low-dose comprehensive cardiac CT technique may also be extended to clinical centers with 128- and 256-slice CT scanner technology, although further validation is still necessary.

Conclusion

In summary, coronary artery disease (CAD) is the leading cause of morbidity and mortality worldwide. Given the inherent limitations of CT angiography and current dynamic CT perfusion techniques, there is a major unmet clinical need for an accurate, low-dose CT technique for combined morphological and physiological assessment of multiform CAD. This dissertation research addresses that unmet clinical need through the development, validation, and preliminary clinical translation of an accurate, low-dose, comprehensive cardiac CT technique based on first-pass analysis (FPA). The comprehensive technique can accurately assess vessel-specific stress and rest perfusion, while simultaneously providing cardiac functional analysis (CFA), CT angiography, and coronary flow reserve (CFR), respectively. Thus, morphological and physiological assessment of CAD is feasible using a single low-dose exam, making comprehensive CT-based assessment of multiform CAD more accurate, accessible, and impactful to patients in need.

Tables

Table 10.1: Low-dose comprehensive cardiac CT stress perfusion distribution in the left ventricle of a 100 kg patient[24]

Stress Perfusion Thresholds (mL/min/g)	LV Mass (g)	LAD Mass (g)	LCx Mass (g)	RCA Mass (g)
0.00 - 0.91 (Definite ischemia)	18.33 (18.89%)	15.13 (28.05%)	0.00 (0.00%)	1.38 (4.51%)
0.91 - 1.20 (Moderate reduction)	8.05 (8.30%)	5.88 (10.91%)	0.00 (0.00%)	1.85 (6.04%)
1.20 - 1.76 (No ischemia, mild reduction)	21.18 (21.83%)	12.95 (24.01%)	0.05 (2.40%)	7.35 (24.07%)
1.76 - 2.39 (No ischemia, minimal reduction)	22.94 (23.64%)	11.75 (21.78%)	0.91 (43.51%)	8.87 (29.05%)
> 2.39 (Normal flow)	26.52 (27.34%)	8.23 (15.25%)	1.13 (54.09%)	11.10 (36.33%)

***Table 10.2: Low-dose comprehensive cardiac CT* CFR distribution in the left ventricle of a 100 kg patient[24]**

CFR Thresholds	LV Mass (g)	LAD Mass (g)	LCx Mass (g)	RCA Mass (g)
0.0 - 1.00 (Myocardial steal)	14.91 (15.37%)	12.28 (22.77%)	0.00 (0.00%)	0.94 (3.08%)
1.0 - 1.74 (Definite ischemia)	16.81 (17.32%)	12.23 (22.67%)	0.00 (0.00%)	3.92 (12.82%)
1.74 - 2.03 (Moderate reduction)	8.10 (8.35%)	4.95 (9.18%)	0.00 (0.15%)	2.83 (9.27%)
2.03 - 2.70 (No ischemia, mild reduction)	20.34 (20.97%)	11.44 (21.20%)	0.45 (21.50%)	7.57 (24.77%)
2.70 - 3.37 (No ischemia, minimal reduction)	17.34 (17.87%)	7.34 (13.61%)	0.95 (45.53%)	7.31 (23.92%)
> 3.37 (Normal flow)	19.52 (20.11%)	5.70 (10.57%)	0.69 (32.82%)	7.98 (26.13%)

Figures

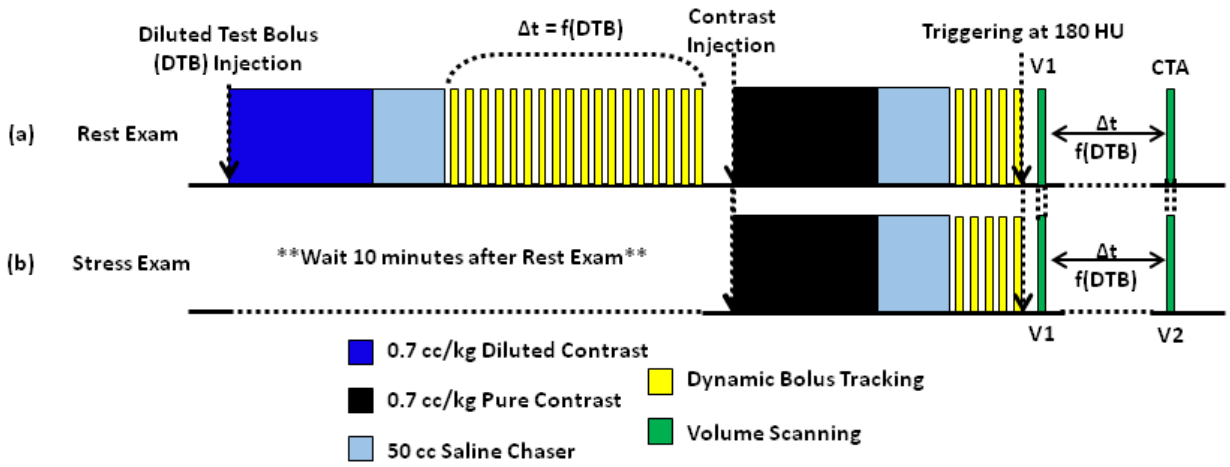

Figure 10.1: Preemptive diluted test bolus and low-dose comprehensive cardiac CT technique protocol (a) The Rest Exam consists of a preemptive diluted test bolus and time-to-peak calculation, followed by prospective volume scan acquisition of rest perfusion and CT angiography data (b) The Stress Exam consist of prospective volume scan acquisition of stress perfusion data using the same diluted test-bolus-based time delay as was used for the rest perfusion and CT angiography protocol.

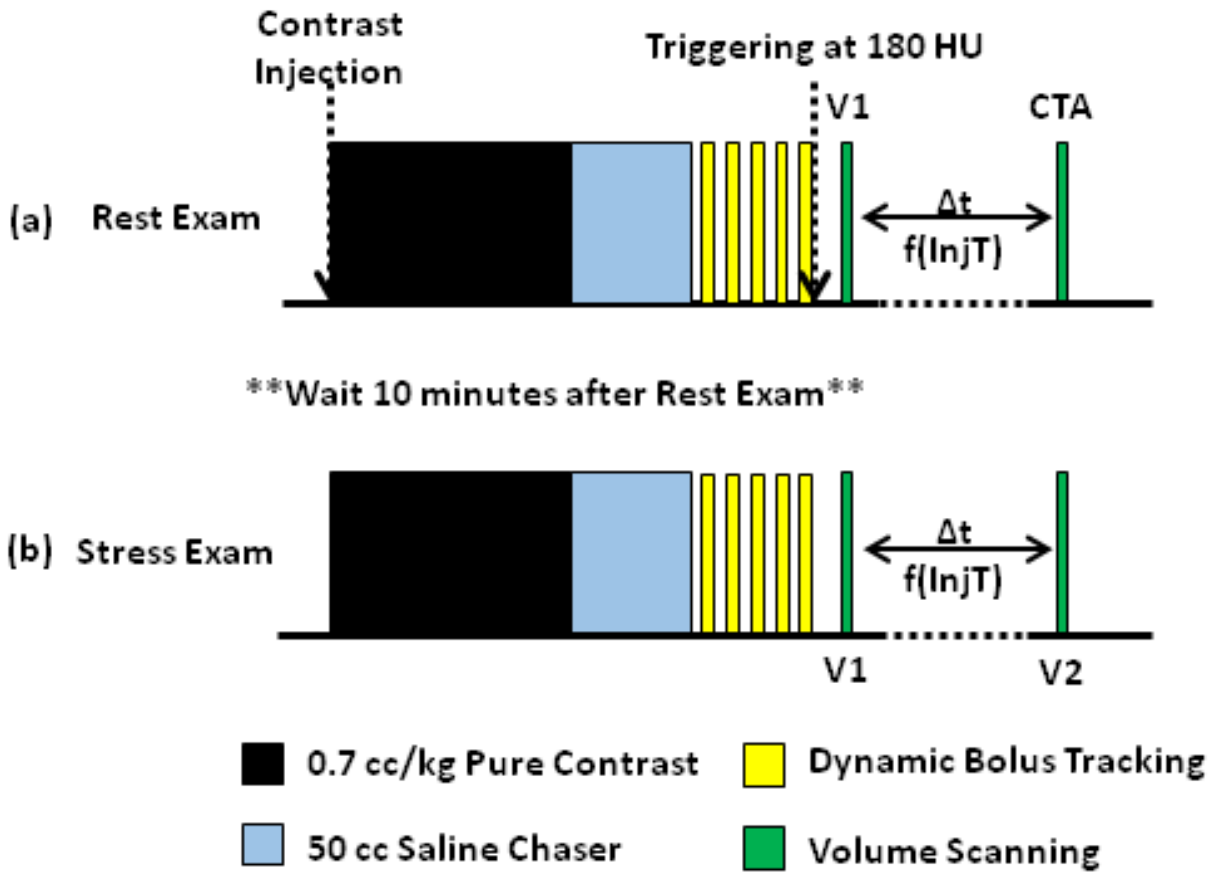

Figure 10.2: Low-dose comprehensive cardiac CT technique protocol that employs an optimal injection-time-based acquisition (a) The Rest Exam uses an optimal injection-time-based acquisition protocol and consists of prospective volume scan acquisition of rest perfusion and CT angiography data (b) The Stress exam also uses the same optimal injection-time-based acquisition protocol and consists of prospective volume scan acquisition of stress perfusion data.

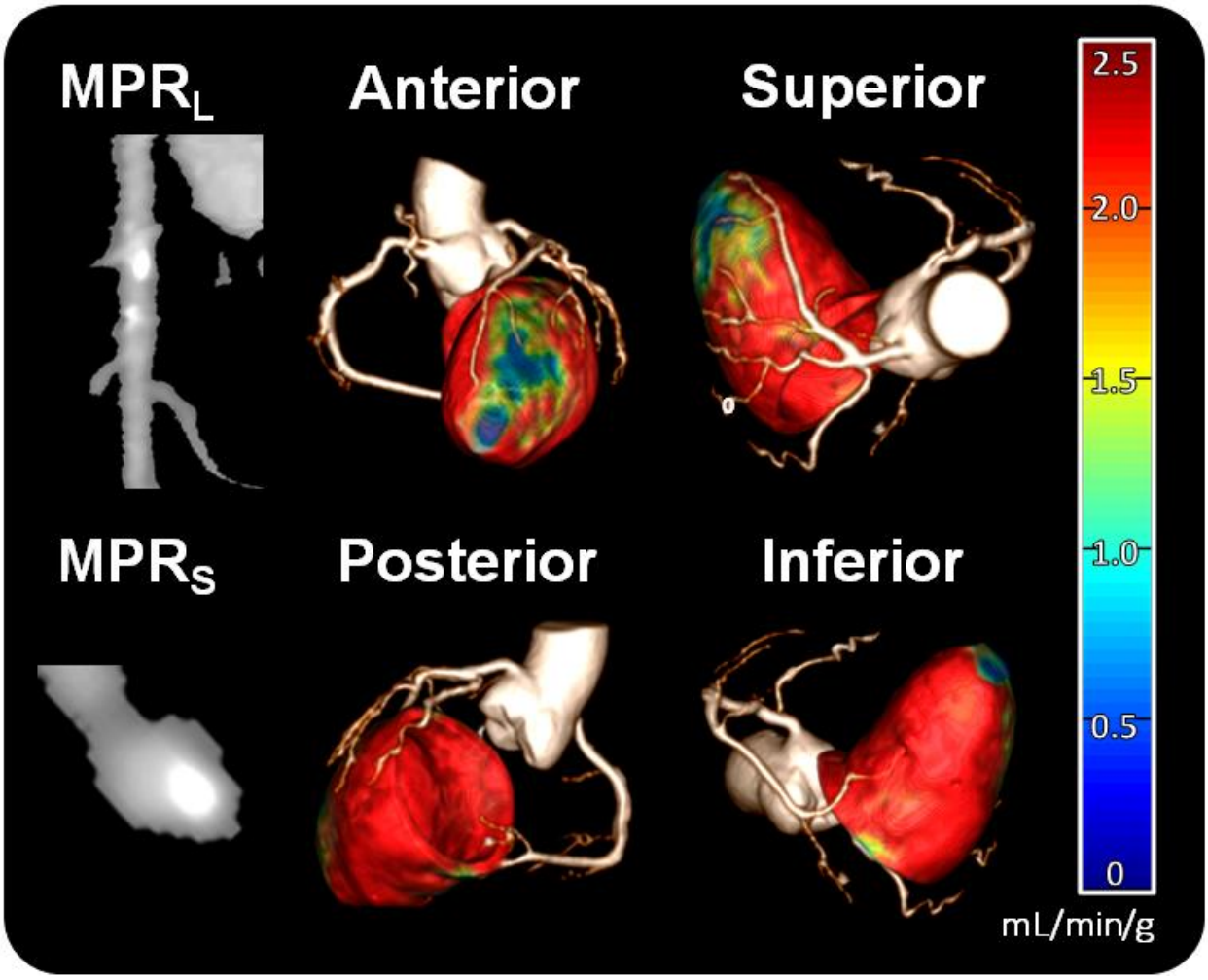

Figure 10.3: : Co-registered stress perfusion and CT angiography with the low-dose comprehensive cardiac CT technique in a 100 kg a patient. Multiple views are displayed in 3D. A morphologically significant calcified stenosis is seen in the long and short axis multiplanar reformations of the LAD (MPR_L and MPR_S). Moreover, a physiologically significant stress perfusion defect is seen in the distal perfusion territory of the LAD (anterior and superior views). The color bar indicates stress perfusion in mL/min/g. Color Scheme: Red = Normal flow, Orange = No ischemia but minimally reduced; Yellow = No ischemia but mildly reduced; Green = moderately reduced flow capacity; Blue = definite ischemia and/or myocardial steal; Black = predominantly scar.

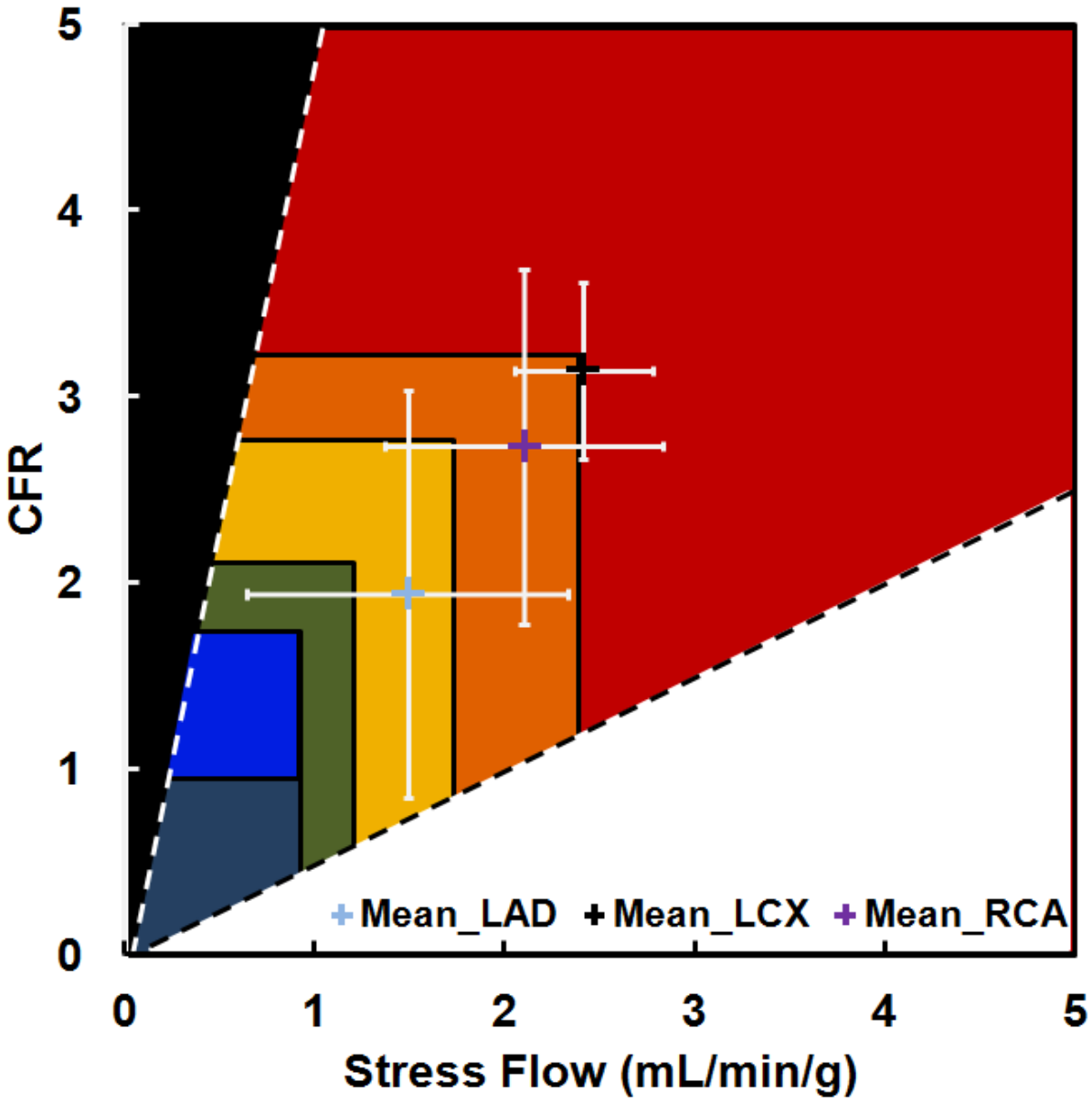

Figure 10.4: Vessel-specific CFR versus stress perfusion measurement with the low-dose comprehensive cardiac CT technique in a 100 kg patient with coronary artery disease. LAD indicates perfusion and CFR in the left anterior descending territory; LCX, perfusion and CFR in the left circumflex territory; RCA, perfusion and CFR in the right coronary artery territory. Color Scheme: Red = Normal flow, Orange = No ischemia but minimally reduced; Yellow = No ischemia but mildly reduced; Green = moderately reduced flow capacity; Blue = definite ischemia and/or myocardial steal; Black = predominantly scar.

REFERENCES

1. Fisher L. Coronary-artery surgery study (cass) - a randomized trial of coronary-artery bypass-surgery - survival-data. *Circulation*. 1983;68:939-950
2. Topol EJ, Nissen SE. Our preoccupation with coronary luminology. The dissociation between clinical and angiographic findings in ischemic heart disease. *Circulation*. 1995;92:2333-2342
3. Miller JM, Rochitte CE, Dewey M, Arbab-Zadeh A, Niinuma H, Gottlieb I, Paul N, Clouse ME, Shapiro EP, Hoe J, Lardo AC, Bush DE, de Roos A, Cox C, Brinker J, Lima JA. Diagnostic performance of coronary angiography by 64-row ct. *N Engl J Med*. 2008;359:2324-2336
4. Meijboom WB, Meijs MF, Schuijf JD, Cramer MJ, Mollet NR, van Mieghem CA, Nieman K, van Werkhoven JM, Pundziute G, Weustink AC, de Vos AM, Pugliese F, Rensing B, Jukema JW, Bax JJ, Prokop M, Doevendans PA, Hunink MG, Krestin GP, de Feyter PJ. Diagnostic accuracy of 64-slice computed tomography coronary angiography: A prospective, multicenter, multivendor study. *J Am Coll Cardiol*. 2008;52:2135-2144
5. Boden WE, O'Rourke RA, Teo KK, Hartigan PM, Maron DJ, Kostuk WJ, Knudtson M, Dada M, Casperson P, Harris CL, Chaitman BR, Shaw L, Gosselin G, Nawaz S, Title LM, Gau G, Blaustein AS, Booth DC, Bates ER, Spertus JA, Berman DS, Mancini GB, Weintraub WS. Optimal medical therapy with or without pci for stable coronary disease. *N Engl J Med*. 2007;356:1503-1516

6. Zir LM, Miller SW, Dinsmore RE, Gilbert JP, Hawthorne JW. Interobserver variability in coronary angiography. *Circulation*. 1976;53:627-632

7. DeRouen TA, Murray JA, Owen W. Variability in the analysis of coronary arteriogram. *Circulation*. 1977;55:324-328

8. Topol EJ, Nissen SE. Our preoccupation with coronary luminology. The dissociation between clinical and angiographic findings in ischemic heart disease [see comments]. *Circulation*. 1995;92:2333-2342

9. Di Carli M, Czernin J, Hoh CK, Gerbaudo VH, Brunken RC, Huang SC, Phelps ME, Schelbert HR. Relation among stenosis severity, myocardial blood flow, and flow reserve in patients with coronary artery disease. *Circulation*. 1995;91:1944-1951

10. Bartunek J, Sys SU, Heyndrickx GR, Pijls NH, De Bruyne B. Quantitative coronary angiography in predicting functional significance of stenoses in an unselected patient cohort. *J Am Coll Cardiol*. 1995;26:328-334

11. Pijls NH, Fearon WF, Tonino PA, Siebert U, Ikeno F, Bornschein B, van't Veer M, Klauss V, Manoharan G, Engstrom T, Oldroyd KG, Ver Lee PN, MacCarthy PA, De Bruyne B. Fractional flow reserve versus angiography for guiding percutaneous coronary intervention in patients with multivessel coronary artery disease: 2-year follow-up of the fame (fractional flow reserve versus angiography for multivessel evaluation) study. *J Am Coll Cardiol*. 2010;56:177-184

12. De Bruyne B, Pijls NHJ, Kalesan B, Barbato E, Tonino PAL, Piroth Z, Jagic N, Möbius-Winkler S, Rioufol G, Witt N, Kala P, MacCarthy P, Engström T, Oldroyd KG, Mavromatis K, Manoharan G, Verlee P, Frobert O, Curzen N,

Johnson JB, Jüni P, Fearon WF. Fractional flow reserve–guided pci versus medical therapy in stable coronary disease. *New England Journal of Medicine*. 2012;367:991-1001

13. Chen MY, Rochitte CE, Arbab-Zadeh A, Dewey M, George RT, Miller JM, Niinuma H, Yoshioka K, Kitagawa K, Sakuma H, Laham R, Vavere AL, Cerci RJ, Mehra VC, Nomura C, Kofoed KF, Jinzaki M, Kuribayashi S, Scholte AJ, Laule M, Tan SY, Hoe J, Paul N, Rybicki FJ, Brinker JA, Arai AE, Matheson MB, Cox C, Clouse ME, Di Carli MF, Lima JAC. Prognostic value of combined ct angiography and myocardial perfusion imaging versus invasive coronary angiography and nuclear stress perfusion imaging in the prediction of major adverse cardiovascular events: The core320 multicenter study. *Radiology*. 2017;284:55-65
14. Murthy VL, Naya M, Foster CR, Hainer J, Gaber M, Di Carli G, Blankstein R, Dorbala S, Sitek A, Pencina MJ, Di Carli MF. Improved cardiac risk assessment with noninvasive measures of coronary flow reserve. *Circulation*. 2011;124:2215-2224
15. Doukky R, Hayes K, Frogge N, Balakrishnan G, Dontaraju VS, Rangel MO, Golzar Y, Garcia-Sayan E, Hendel RC. Impact of appropriate use on the prognostic value of single-photon emission computed tomography myocardial perfusion imaging. *Circulation*. 2013;128:1634-1643
16. Rieber J, Huber A, Erhard I, Mueller S, Schweyer M, Koenig A, Schiele TM, Theisen K, Siebert U, Schoenberg SO, Reiser M, Klauss V. Cardiac magnetic resonance perfusion imaging for the functional assessment of coronary artery

disease: A comparison with coronary angiography and fractional flow reserve. *Eur Heart J*. 2006;27:1465-1471

17. Tonino PA, De Bruyne B, Pijls NH, Siebert U, Ikeno F, van' t Veer M, Klauss V, Manoharan G, Engstrom T, Oldroyd KG, Ver Lee PN, MacCarthy PA, Fearon WF. Fractional flow reserve versus angiography for guiding percutaneous coronary intervention. *N Engl J Med*. 2009;360:213-224
18. Danad I, Szymonifka J, Schulman-Marcus J, Min JK. Static and dynamic assessment of myocardial perfusion by computed tomography. *European Heart Journal - Cardiovascular Imaging*. 2016;17:836-844
19. Ziadi MC, Dekemp RA, Williams KA, Guo A, Chow BJ, Renaud JM, Ruddy TD, Sarveswaran N, Tee RE, Beanlands RS. Impaired myocardial flow reserve on rubidium-82 positron emission tomography imaging predicts adverse outcomes in patients assessed for myocardial ischemia. *J Am Coll Cardiol*. 2011;58:740-748
20. Hagemann CE, Ghotbi AA, Kjær A, Hasbak P. Quantitative myocardial blood flow with rubidium-82 pet: A clinical perspective. *Am J Nucl Med Mol Imaging*. 2015;5:457-468
21. Hajjiri MM, Leavitt MB, Zheng H, Spooner AE, Fischman AJ, Gewirtz H. Comparison of positron emission tomography measurement of adenosine-stimulated absolute myocardial blood flow versus relative myocardial tracer content for physiological assessment of coronary artery stenosis severity and location. *JACC Cardiovasc Imaging*. 2009;2:751-758
22. Johnson NP, Johnson DT, Kirkeeide RL, Berry C, De Bruyne B, Fearon WF, Oldroyd KG, Pijls NH, Gould KL. Repeatability of fractional flow reserve despite

variations in systemic and coronary hemodynamics. *JACC Cardiovasc Interv*. 2015;8:1018-1027

23. Johnson NP, Gould KL, Di Carli MF, Taqueti VR. Invasive ffr and noninvasive cfr in the evaluation of ischemia: What is the future? *Journal of the American College of Cardiology*. 2016;67:2772-2788
24. Johnson NP, Gould KL. Integrating noninvasive absolute flow, coronary flow reserve, and ischemic thresholds into a comprehensive map of physiological severity. *JACC Cardiovasc Imaging*. 2012;5:430-440
25. Herzog BA, Husmann L, Valenta I, Gaemperli O, Siegrist PT, Tay FM, Burkhard N, Wyss CA, Kaufmann PA. Long-term prognostic value of 13n-ammonia myocardial perfusion positron emission tomography added value of coronary flow reserve. *J Am Coll Cardiol*. 2009;54:150-156
26. Schwaiger M. Myocardial perfusion imaging with pet. *J Nucl Med*. 1994;35:693-698
27. Bateman TM. Advantages and disadvantages of pet and spect in a busy clinical practice. *J Nucl Cardiol*. 2012;19 Suppl 1:S3-11
28. Lubbers M, Coenen A, Kofflard M, Bruning T, Kietselaer B, Galema T, Kock M, Niezen A, Das M, van Gent M, van den Bos E-J, van Woerkens L, Musters P, Kooij S, Nous F, Budde R, Hunink M, Nieman K. Comprehensive cardiac ct with myocardial perfusion imaging versus functional testing in suspected coronary artery disease. *The Multicenter, Randomized CRESCENT-II Trial*. 2017
29. Bamberg F, Hinkel R, Schwarz F, Sandner TA, Baloch E, Marcus R, Becker A, Kupatt C, Wintersperger BJ, Johnson TR, Theisen D, Klotz E, Reiser MF,

Nikolaou K. Accuracy of dynamic computed tomography adenosine stress myocardial perfusion imaging in estimating myocardial blood flow at various degrees of coronary artery stenosis using a porcine animal model. *Invest Radiol*. 2012;47:71-77

30. Schwarz F, Hinkel R, Baloch E, Marcus RP, Hildebrandt K, Sandner TA, Kupatt C, Hoffmann V, Wintersperger BJ, Reiser MF, Theisen D, Nikolaou K, Bamberg F. Myocardial ct perfusion imaging in a large animal model: Comparison of dynamic versus single-phase acquisitions. *JACC Cardiovasc Imaging*. 2013;6:1229-1238
31. Bamberg F, Becker A, Schwarz F, Marcus RP, Greif M, von Ziegler F, Blankstein R, Hoffmann U, Sommer WH, Hoffmann VS, Johnson TR, Becker HC, Wintersperger BJ, Reiser MF, Nikolaou K. Detection of hemodynamically significant coronary artery stenosis: Incremental diagnostic value of dynamic ct-based myocardial perfusion imaging. *Radiology*. 2011;260:689-698
32. Wang Y, Qin L, Shi X, Zeng Y, Jing H, Schoepf UJ, Jin Z. Adenosine-stress dynamic myocardial perfusion imaging with second-generation dual-source ct: Comparison with conventional catheter coronary angiography and spect nuclear myocardial perfusion imaging. *AJR Am J Roentgenol*. 2012;198:521-529
33. Bateman TM. Advantages and disadvantages of pet and spect in a busy clinical practice. *J Nucl Cardiol*. 2012;19:3-11
34. Ko BS, Cameron JD, Leung M, Meredith IT, Leong DP, Antonis PR, Crossett M, Troupis J, Harper R, Malaiapan Y, Seneviratne SK. Combined ct coronary angiography and stress myocardial perfusion imaging for hemodynamically

significant stenoses in patients with suspected coronary artery disease: A comparison with fractional flow reserve. *JACC Cardiovasc Imaging*. 2012;5:1097-1111

35. Mahnken AH, Klotz E, Pietsch H, Schmidt B, Allmendinger T, Haberland U, Kalender WA, Flohr T. Quantitative whole heart stress perfusion ct imaging as noninvasive assessment of hemodynamics in coronary artery stenosis: Preliminary animal experience. *Investigative Radiology*. 2010;45:298-305
36. Christian TF, Frankish ML, Sisemoore JH, Christian MR, Gentchos G, Bell SP, Jerosch-Herold M. Myocardial perfusion imaging with first-pass computed tomographic imaging: Measurement of coronary flow reserve in an animal model of regional hyperemia. *Journal of nuclear cardiology*. 2010;17:625-630
37. Rossi A, Merkus D, Klotz E, Mollet N, de Feyter PJ, Krestin GP. Stress myocardial perfusion: Imaging with multidetector ct. *Radiology*. 2014;270:25-46
38. Bindschadler M, Modgil D, Branch KR, La Riviere PJ, Alessio AM. Comparison of blood flow models and acquisitions for quantitative myocardial perfusion estimation from dynamic ct. *Phys Med Biol*. 2014;59:1533-1556
39. Pijls NH, Uijen GJ, Hoevelaken A, Arts T, Aengevaeren WR, Ros HS, Fast JH, Van Leeuwen KL, Van der Werf T. Mean transit time for the assessment of myocardial perfusion by videodensitometry. *Circulation*. 1990;81:1331-1340
40. Weininger M, Schoepf UJ, Ramachandra A, Fink C, Rowe GW, Costello P, Henzler T. Adenosine-stress dynamic real-time myocardial perfusion ct and adenosine-stress first-pass dual-energy myocardial perfusion ct for the

assessment of acute chest pain: Initial results. *European Journal of Radiology*. 2012;81:3703-3710

41. Huber AM, Leber V, Gramer BM, Muenzel D, Leber A, Rieber J, Schmidt M, Vembar M, Hoffmann E, Rummeny E. Myocardium: Dynamic versus single-shot ct perfusion imaging. *Radiology*. 2013;269:378-386
42. Ho KT, Chua KC, Klotz E, Panknin C. Stress and rest dynamic myocardial perfusion imaging by evaluation of complete time-attenuation curves with dual-source ct. *JACC Cardiovasc Imaging*. 2010;3:811-820
43. Einstein AJ. Multiple opportunities to reduce radiation dose from myocardial perfusion imaging. *Eur J Nucl Med Mol Imaging*. 2013;40:649-651
44. Chen MY, Shanbhag SM, Arai AE. Submillisievert median radiation dose for coronary angiography with a second-generation 320-detector row ct scanner in 107 consecutive patients. *Radiology*. 2013;267:76-85
45. Ziemer BP, Hubbard L, Lipinski J, Molloi S. Dynamic ct perfusion measurement in a cardiac phantom. *Int J Cardiovas Imag*. 2015;31:1451-1459
46. Seiler C, Kirkeeide RL, Gould KL. Measurement from arteriograms of regional myocardial bed size distal to any point in the coronary vascular tree for assessing anatomic area at risk. *Journal of the American College of Cardiology*. 1993;21:783-797
47. Le H, Wong JT, Molloi S. Estimation of regional myocardial mass at risk based on distal arterial lumen volume and length using 3d micro-ct images. *Computerized medical imaging and graphics : the official journal of the Computerized Medical Imaging Society*. 2008;32:488-501

48. Pijls NH, De Bruyne B, Peels K, Van Der Voort PH, Bonnier HJ, Bartunek JKJJ, Koolen JJ. Measurement of fractional flow reserve to assess the functional severity of coronary-artery stenoses. *New England Journal of Medicine*. 1996;334:1703-1708

49. Klocke FJ, Simonetti OP, Judd RM, Kim RJ, Harris KR, Hedjbeli S, Fieno DS, Miller S, Chen V, Parker MA. Limits of detection of regional differences in vasodilated flow in viable myocardium by first-pass magnetic resonance perfusion imaging. *Circulation*. 2001;104:2412-2416

50. Bamberg F, Becker A, Schwarz F, Marcus RP, Greif M, von Ziegler F, Blankstein R, Hoffmann U, Sommer WH, Hoffmann VS. Detection of hemodynamically significant coronary artery stenosis: Incremental diagnostic value of dynamic ct-based myocardial perfusion imaging. *Radiology*. 2011;260:689-698

51. Rossi A, Uitterdijk A, Dijkshoorn M, Klotz E, Dharampal A, Van Straten M, Van Der Giessen WJ, Mollet N, Van Geuns R-J, Krestin GP. Quantification of myocardial blood flow by adenosine-stress ct perfusion imaging in pigs during various degrees of stenosis correlates well with coronary artery blood flow and fractional flow reserve. *European Heart Journal–Cardiovascular Imaging*. 2013;14:331-338

52. Mullani NA, Gould KL. First-pass measurements of regional blood flow with external detectors. *J Nucl Med*. 1983;24:577

53. Le HQ, Wong JT, Molloi S. Allometric scaling in the coronary arterial system. *The international journal of cardiovascular imaging*. 2008;24:771-781

54. Lipton M, Higgins C, Farmer D, Boyd D. Cardiac imaging with a high-speed cine-ct scanner: Preliminary results. *Radiology*. 1984;152:579-582

55. Wolfkiel CJ, Ferguson J, Chomka E, Law W, Labin I, Tenzer M, Booker M, Brundage B. Measurement of myocardial blood flow by ultrafast computed tomography. *Circulation*. 1987;76:1262-1273

56. Molloi S, Zhou Y, Kassab GS. Regional volumetric coronary blood flow measurement by digital angiography: In vivo validation. *Academic Radiology*. 2004;11:757-766

57. Molloi S, Qian YJ, Ersahin A. Absolute volumetric blood flow measurements using dual-energy digital subtraction angiography. *Med. Phys.* 1993;20:85-91

58. Molloi S, Ersahin A, Tang J, Hicks J, Leung CY. Quantification of volumetric coronary blood flow with dual-energy digital subtraction angiography. *Circulation*. 1996;93:1919-1927

59. Molloi S, Bednarz G, Tang J, Zhou Y, Mathur T. Absolute volumetric coronary blood flow measurement with digital subtraction angiography. *Int J Cardiac Imag*. 1998;14:137-145

60. Chiribiri A, Schuster A, Ishida M, Hautvast G, Zarinabad N, Morton G, Otton J, Plein S, Breeuwer M, Batchelor P, Schaeffter T, Nagel E. Perfusion phantom: An efficient and reproducible method to simulate myocardial first-pass perfusion measurements with cardiovascular magnetic resonance. *Magn Reson Med*. 2013;69:698-707

61. Ulzheimer S, Kalender WA. Assessment of calcium scoring performance in cardiac computed tomography. *Eur Radiol*. 2003;13:484-497

62. Bamberg F, Marcus RP, Becker A, Hildebrandt K, Bauner K, Schwarz F, Greif M, von Ziegler F, Bischoff B, Becker HC, Johnson TR, Reiser MF, Nikolaou K, Theisen D. Dynamic myocardial ct perfusion imaging for evaluation of myocardial ischemia as determined by mr imaging. *JACC Cardiovasc Imaging*. 2014;7:267-277

63. AAPM. The measurement, reporting, and management of radiation dose in ct. *AAPM*. 2008

64. George RT, Silva C, Cordeiro MA, DiPaula A, Thompson DR, McCarthy WF, Ichihara T, Lima JA, Lardo AC. Multidetector computed tomography myocardial perfusion imaging during adenosine stress. *J Am Coll Cardiol*. 2006;48:153-160

65. Bastarrika G, Ramos-Duran L, Rosenblum MA, Kang DK, Rowe GW, Schoepf UJ. Adenosine-stress dynamic myocardial ct perfusion imaging: Initial clinical experience. *Invest Radiol*. 2010;45:306-313

66. Greif M, von Ziegler F, Bamberg F, Tittus J, Schwarz F, D'Anastasi M, Marcus RP, Schenzle J, Becker C, Nikolaou K, Becker A. Ct stress perfusion imaging for detection of haemodynamically relevant coronary stenosis as defined by ffr. *Heart*. 2013;99:1004-1011

67. Rossi A, Dharampal A, Wragg A, Davies LC, van Geuns RJ, Anagnostopoulos C, Klotz E, Kitslaar P, Broersen A, Mathur A, Nieman K, Hunink MG, de Feyter PJ, Petersen SE, Pugliese F. Diagnostic performance of hyperaemic myocardial blood flow index obtained by dynamic computed tomography: Does it predict functionally significant coronary lesions? *Eur Heart J Cardiovasc Imaging*. 2014;15:85-94

68. Kitagawa K, George RT, Arbab-Zadeh A, Lima JA, Lardo AC. Characterization and correction of beam-hardening artifacts during dynamic volume ct assessment of myocardial perfusion. *Radiology*. 2010;256:111-118

69. Stenner P, Schmidt B, Allmendinger T, Flohr T, Kachelrie M. Dynamic iterative beam hardening correction (dibhc) in myocardial perfusion imaging using contrast-enhanced computed tomography. *Invest Radiol*. 2010;45:314-323

70. Haridasan V, Nandan D, Raju D, Rajesh GN, Sajeev CG, Vinayakumar D, Muneer K, Babu K, Krishnan MN. Coronary sinus filling time: A novel method to assess microcirculatory function in patients with angina and normal coronaries. *Indian Heart J*. 2013;65:142-146

71. Varnauskas E. Long-term results of prospective randomized study of coronary-artery bypass-surgery in stable angina-pectoris. *Lancet*. 1982;2:1173-1180

72. Davies RF, Goldberg AD, Forman S, Pepine CJ, Knatterud GL, Geller N, Sopko G, Pratt C, Deanfield J, Conti CR. Asymptomatic cardiac ischemia pilot (acip) study two-year follow-up: Outcomes of patients randomized to initial strategies of medical therapy versus revascularization. *Circulation*. 1997;95:2037-2043

73. Madsen JK, Grande P, Saunamaki K, Thayssen P, Kassis E, Eriksen U, Rasmussen K, Haunso S, Nielsen TT, Haghfelt T, Fritz-Hansen P, Hjelms E, Paulsen PK, Alstrup P, Arendrup H, Niebuhr-Jorgensen U, Andersen LI. Danish multicenter randomized study of invasive versus conservative treatment in patients with inducible ischemia after thrombolysis in acute myocardial infarction (danami). Danish trial in acute myocardial infarction. *Circulation*. 1997;96:748-755

74. Hachamovitch R, Hayes SW, Friedman JD, Cohen I, Berman DS. Comparison of the short-term survival benefit associated with revascularization compared with medical therapy in patients with no prior coronary artery disease undergoing stress myocardial perfusion single photon emission computed tomography. *Circulation*. 2003;107:2900-2907

75. Shaw LJ, Berman DS, Maron DJ, Mancini GB, Hayes SW, Hartigan PM, Weintraub WS, O'Rourke RA, Dada M, Spertus JA, Chaitman BR, Friedman J, Slomka P, Heller GV, Germano G, Gosselin G, Berger P, Kostuk WJ, Schwartz RG, Knudtson M, Veledar E, Bates ER, McCallister B, Teo KK, Boden WE. Optimal medical therapy with or without percutaneous coronary intervention to reduce ischemic burden: Results from the clinical outcomes utilizing revascularization and aggressive drug evaluation (courage) trial nuclear substudy. *Circulation*. 2008;117:1283-1291

76. Cerqueira MD, Weissman NJ, Dilsizian V, Jacobs AK, Kaul S, Laskey WK, Pennell DJ, Rumberger JA, Ryan T, Verani MS. Standardized myocardial segmentation and nomenclature for tomographic imaging of the heart. A statement for healthcare professionals from the cardiac imaging committee of the council on clinical cardiology of the american heart association. *Circulation*. 2002;105:539-542

77. Ortiz-Perez JT, Rodriguez J, Meyers SN, Lee DC, Davidson C, Wu E. Correspondence between the 17-segment model and coronary arterial anatomy using contrast-enhanced cardiac magnetic resonance imaging. *JACC Cardiovasc Imaging*. 2008;1:282-293

78. Pereztol-Valdes O, Candell-Riera J, Santana-Boado C, Angel J, Aguade-Bruix S, Castell-Conesa J, Garcia EV, Soler-Soler J. Correspondence between left ventricular 17 myocardial segments and coronary arteries. *Eur Heart J*. 2005;26:2637-2643

79. Thomassen A, Petersen H, Johansen A, Braad PE, Diederichsen AC, Mickley H, Jensen LO, Gerke O, Simonsen JA, Thayssen P, Hoilund-Carlsen PF. Quantitative myocardial perfusion by o-15-water pet: Individualized vs. Standardized vascular territories. *Eur Heart J Cardiovasc Imaging*. 2015:970-976

80. Javadi MS, Lautamaki R, Merrill J, Voicu C, Epley W, McBride G, Bengel FM. Definition of vascular territories on myocardial perfusion images by integration with true coronary anatomy: A hybrid pet/ct analysis. *J Nucl Med*. 2010;51:198-203

81. Donato P, Coelho P, Santos C, Bernardes A, Caseiro-Alves F. Correspondence between left ventricular 17 myocardial segments and coronary anatomy obtained by multi-detector computed tomography: An ex vivo contribution. *Surg Radiol Anat*. 2012;34:805-810

82. Rafflenbeul W, Urthaler F, Lichtlen P, James TN. Quantitative difference in "critical" stenosis between right and left coronary artery in man. *Circulation*. 1980;62:1188-1196

83. Carlsson M, Saeed M. Intracoronary injection of contrast media maps the territory of the coronary artery: An mri technique for assessing the effects of locally delivered angiogenic therapies. *Acad Radiol*. 2008;15:1354-1359

84. Kurata A, Kono A, Sakamoto T, Kido T, Mochizuki T, Higashino H, Abe M, Coenen A, Saru-Chelu RG, de Feyter PJ, Krestin GP, Nieman K. Quantification of the myocardial area at risk using coronary ct angiography and voronoi algorithm-based myocardial segmentation. *Eur Radiol*. 2015;25:49-57

85. Ide S, Sumitsuji S, Yamaguchi O, Sakata Y. Cardiac computed tomography-derived myocardial mass at risk using the voronoi-based segmentation algorithm: A histological validation study. *J Cardiovasc Comput Tomogr*. 2017;11:179-182

86. Cerci RJ, Arbab-Zadeh A, George RT, Miller JM, Vavere AL, Mehra V, Yoneyama K, Texter J, Foster C, Guo W, Cox C, Brinker J, Di Carli M, Lima JA. Aligning coronary anatomy and myocardial perfusion territories: An algorithm for the core320 multicenter study. *Circ Cardiovasc Imaging*. 2012;5:587-595

87. Faber TL, Santana CA, Garcia EV, Candell-Riera J, Folks RD, Peifer JW, Hopper A, Aguade S, Angel J, Klein JL. Three-dimensional fusion of coronary arteries with myocardial perfusion distributions: Clinical validation. *J Nucl Med*. 2004;45:745-753

88. Modat M, Ridgway GR, Taylor ZA, Lehmann M, Barnes J, Hawkes DJ, Fox NC, Ourselin S. Fast free-form deformation using graphics processing units. *Comput Methods Programs Biomed*. 2010;98:278-284

89. McCormick M, Liu X, Jomier J, Marion C, Ibanez L. Itk: Enabling reproducible research and open science. *Front Neuroinform*. 2014;8:13

90. Sethian JA. A fast marching level set method for monotonically advancing fronts. *Proceedings of the National Academy of Sciences*. 1996;93:1591-1595

91. O HLGMLLYYBNO. Effect of variable gain on computerized texture analysis on digitized mammograms. *SPIE Proceedings*. 2010

92. Lin LI. A concordance correlation coefficient to evaluate reproducibility. *Biometrics*. 1989;45:255-268

93. Dice LR. Measures of the amount of ecologic association between species. *Ecology*. 1945;26:297-302

94. Li H, Giger ML, Huo Z, Olopade OI, Lan L, Weber BL, Bonta I. Computerized analysis of mammographic parenchymal patterns for assessing breast cancer risk: Effect of roi size and location. *Med Phys*. 2004;31:549-555

95. Li H, Giger ML, Lan L, Janardanan J, Sennett CA. Comparative analysis of image-based phenotypes of mammographic density and parenchymal patterns in distinguishing between brca1/2 cases, unilateral cancer cases, and controls. *Journal of medical imaging (Bellingham, Wash.)*. 2014;1:031009

96. Kerl JM, Ravenel JG, Nguyen SA, Suranyi P, Thilo C, Costello P, Bautz W, Schoepf UJ. Right heart: Split-bolus injection of diluted contrast medium for visualization at coronary ct angiography. *Radiology*. 2008;247:356-364

97. Hubbard L, Ziemer B, Lipinski J, Sadeghi B, Javan H, Groves EM, Malkasian S, Molloi S. Functional assessment of coronary artery disease using whole-heart dynamic computed tomographic perfusion. *Circ Cardiovasc Imaging*. 2016;9:1-8

98. Ziemer BP, Hubbard L, Lipinski J, Molloi S. Dynamic ct perfusion measurement in a cardiac phantom. *Int J Cardiovasc Imaging*. 2015;31:1451-1459

99. Li H, Giger ML, Lan L, Bancroft Brown J, MacMahon A, Mussman M, Olopade OI, Sennett C. Computerized analysis of mammographic parenchymal patterns

on a large clinical dataset of full-field digital mammograms: Robustness study with two high-risk datasets. *J Digit Imaging*. 2012;25:591-598

100. Detre KM, Wright E, Murphy ML, Takaro T. Observer agreement in evaluating coronary angiograms. *Circulation*. 1975;52:979-986

101. Tobis JM, Mallery J, Mahon D, Lehmann K, Zalesky P, Griffith J, Gessert J, Moriuchi M, McRae M, Dwyer ML, et al. Intravascular ultrasound imaging of human coronary arteries in vivo. Analysis of tissue characterizations with comparison to in vitro histological specimens. *Circulation*. 1991;83:913-926

102. Robbins SL, Rodrequez FL, Wragg AL, Fish SJ. Problems in quantitation of coronary atheroscelerosis. *Am J Cardiol*. 1966;18:153-159

103. Vlodaver Z, Frech R, Van Tassel RA, Edwards JE. Correlation of the antemortem coronary angiogram and the postmortem specimen. *Circulation*. 1973;47:162-169

104. White CW, Wright CB, Doty DB, Hiratza LF, Eastham CL, Harrison DG, Marcus ML. Does visual interpretation of the coronary arteriogram predict the physiologic importance of a coronary stenosis? *New England Journal of Medicine*. 1984;310:819-824

105. Kono AK, Coenen A, Lubbers M, Kurata A, Rossi A, Dharampal A, Dijkshoorn M, van Geuns RJ, Krestin GP, Nieman K. Relative myocardial blood flow by dynamic computed tomographic perfusion imaging predicts hemodynamic significance of coronary stenosis better than absolute blood flow. *Invest Radiol*. 2014;49:801-807

106. Kern MJ, Lerman A, Bech JW, De Bruyne B, Eeckhout E, Fearon WF, Higano ST, Lim MJ, Meuwissen M, Piek JJ, Pijls NH, Siebes M, Spaan JA. Physiological assessment of coronary artery disease in the cardiac catheterization laboratory: A scientific statement from the american heart association committee on diagnostic and interventional cardiac catheterization, council on clinical cardiology. *Circulation*. 2006;114:1321-1341

107. Kern MJ, Samady H. Current concepts of integrated coronary physiology in the catheterization laboratory. *J Am Coll Cardiol*. 2010;55:173-185

108. Danad I, Uusitalo V, Kero T, Saraste A, Raijmakers PG, Lammertsma AA, Heymans MW, Kajander SA, Pietilä M, James S, Sörensen J, Knaapen P, Knuuti J. Quantitative assessment of myocardial perfusion in the detection of significant coronary artery disease: Cutoff values and diagnostic accuracy of quantitative [(15)o]h2o pet imaging. *J Am Coll Cardiol*. 2014;64:1464-1475

109. Baile EM, Paré PD, D'yachkova Y, Carere RG. Effect of contrast media on coronary vascular resistance: Contrast-induced coronary vasodilation. *Chest*. 1999;116:1039-1045

110. Kurata A, Kawaguchi N, Kido T, Inoue K, Suzuki J, Ogimoto A, Funada J, Higaki J, Miyagawa M, Vembar M, Mochizuki T. Qualitative and quantitative assessment of adenosine triphosphate stress whole-heart dynamic myocardial perfusion imaging using 256-slice computed tomography. *Plos One*. 2013;8:e83950

111. Hadamitzky M, Freissmuth B, Meyer T, Hein F, Kastrati A, Martinoff S, Schomig A, Hausleiter J. Prognostic value of coronary computed tomographic angiography

for prediction of cardiac events in patients with suspected coronary artery disease. *JACC Cardiovasc Imaging*. 2009;2:404-411

112. Meijboom WB, Van Mieghem CA, van Pelt N, Weustink A, Pugliese F, Mollet NR, Boersma E, Regar E, van Geuns RJ, de Jaegere PJ, Serruys PW, Krestin GP, de Feyter PJ. Comprehensive assessment of coronary artery stenoses: Computed tomography coronary angiography versus conventional coronary angiography and correlation with fractional flow reserve in patients with stable angina. *Journal of the American College of Cardiology*. 2008;52:636-643

113. Johnson NP, Gould KL, Di Carli MF, Taqueti VR. Invasive ffr and noninvasive cfr in the evaluation of ischemia: What is the future? *J Am Coll Cardiol*. 2016;67:2772-2788

114. Bartoli CR, Okabe K, Akiyama I, Coull B, Godleski JJ. Repeat microsphere delivery for serial measurement of regional blood perfusion in the chronically instrumented conscious canine. *J Surg Res*. 2008;145:135-141

115. Schwarz F, Hinkel R, Baloch E, Marcus RP, Hildebrandt K, Sandner TA, Kupatt C, Hoffmann V, Wintersperger BJ, Reiser MF, Theisen D, Nikolaou K, Bamberg F. Myocardial ct perfusion imaging in a large animal model: Comparison of dynamic versus single-phase acquisitions. *JACC: Cardiovasc Imaging*. 2013;6:1229-1238

116. Ishida M, Kitagawa K, Ichihara T, Natsume T, Nakayama R, Nagasawa N, Kubooka M, Ito T, Uno M, Goto Y, Nagata M, Sakuma H. Underestimation of myocardial blood flow by dynamic perfusion ct: Explanations by two-

compartment model analysis and limited temporal sampling of dynamic ct. *J Cardiovasc Comput Tomogr*. 2016;10:207-214

117. Molloi S, Zhou Y, Kassab GS. Regional volumetric coronary blood flow measurement by digital angiography: In vivo validation. *Acad Radiol*. 2004;11:757-766

118. Boone J, Strauss K, Cody D, McCollough C, McNitt-Gray M, Toth T, Goske M, Frush D. Size-specific dose estimates (ssde) in pediatric and adult body ct examinations: Report of aapm task group 204. *College Park, MD: American Association of Physicists in Medicine*. 2011

119. Dupont WD, Plummer WD. Power and sample size calculations for studies involving linear regression. *Controlled clinical trials*. 1998;19:589-601

120. Eldridge SM, Ukoumunne OC, Carlin JB. The intra-cluster correlation coefficient in cluster randomized trials: A review of definitions. *Int Stat Rev*. 2009;77:378-394

121. Schwinn DA, McIntyre RW, Reves JG. Isoflurane-induced vasodilation: Role of the alpha-adrenergic nervous system. *Anesth Analg*. 1990;71:451-459

122. Schweiger GD, Chang PJ, Brown BP. Optimizing contrast enhancement during helical ct of the liver: A comparison of two bolus tracking techniques. *AJR Am J Roentgenol*. 1998;171:1551-1558

123. Hubbard L, Lipinski J, Ziemer B, Malkasian S, Sadeghi B, Javan H, Groves EM, Dertli B, Molloi S. Comprehensive assessment of coronary artery disease by using first-pass analysis dynamic ct perfusion: Validation in a swine model. *Radiology*. 2018;286:93-102

124. Masuda T, Funama Y, Imada N, Sato T, Yamagami T, Tatsugami F, Awai K. Prediction of aortic enhancement on coronary cta images using a test bolus of diluted contrast material. *Acad Radiol*. 2014;21:1542-1546

125. Halliburton SS, Abbara S, Chen MY, Gentry R, Mahesh M, Raff GL, Shaw LJ, Hausleiter J. Scct guidelines on radiation dose and dose-optimization strategies in cardiovascular ct. *J Cardiovasc Comput Tomogr*. 2011;5:198-224

126. Di Cesare E, Gennarelli A, Di Sibio A, Felli V, Splendiani A, Gravina GL, Barile A, Masciocchi C. Assessment of dose exposure and image quality in coronary angiography performed by 640-slice ct: A comparison between adaptive iterative and filtered back-projection algorithm by propensity analysis. *La Radiologia medica*. 2014;119:642-649

127. Mirsadraee S, Weir NW, Connolly S, Murchison JT, Reid JH, Hirani N, Connell M, van Beek EJ. Feasibility of radiation dose reduction using aidr-3d in dynamic pulmonary ct perfusion. *Clin Radiol*. 2015;70:844-851

128. Sakai S, Yabuuchi H, Chishaki A, Okafuji T, Matsuo Y, Kamitani T, Setoguchi T, Honda H. Effect of cardiac function on aortic peak time and peak enhancement during coronary ct angiography. *European Journal of Radiology*. 2010;75:173-177

129. Bae KT, Heiken JP, Brink JA. Aortic and hepatic contrast medium enhancement at ct. Part ii. Effect of reduced cardiac output in a porcine model. *Radiology*. 1998;207:657-662

130. Garcia P, Genin G, Bret PM, Bonaldi VM, Reinhold C, Atri M. Hepatic ct enhancement: Effect of the rate and volume of contrast medium injection in an animal model. *Abdom Imaging*. 1999;24:597-603

131. Han JK, Kim AY, Lee KY, Seo JB, Kim TK, Choi BI, Lhee CS, Han MC. Factors influencing vascular and hepatic enhancement at ct: Experimental study on injection protocol using a canine model. *J Comput Assist Tomogr*. 2000;24:400-406

132. Ohno Y, Yaguchi A, Okazaki T, Aoyagi K, Yamagata H, Sugihara N, Koyama H, Yoshikawa T, Sugimura K. Comparative evaluation of newly developed model-based and commercially available hybrid-type iterative reconstruction methods and filter back projection method in terms of accuracy of computer-aided volumetry (cadv) for low-dose ct protocols in phantom study. *Eur J Radiol*. 2016;85:1375-1382

133. Malkasian S, Hubbard L, Dertli B, Kwon J, Molloi S. Quantification of vessel-specific coronary perfusion territories using minimum-cost path assignment and computed tomography angiography: Validation in a swine model. *In Review*. 2018

134. Rossi A, Papadopoulou SL, Pugliese F, Russo B, Dharampal AS, Dedic A, Kitslaar PH, Broersen A, Meijboom WB, van Geuns RJ, Wragg A, Ligthart J, Schultz C, Petersen SE, Nieman K, Krestin GP, de Feyter PJ. Quantitative computed tomographic coronary angiography: Does it predict functionally significant coronary stenoses? *Circ Cardiovasc Imaging*. 2014;7:43-51

135. Kim EY, Chung WJ, Sung YM, Byun SS, Park JH, Kim JH, Moon J. Normal range and regional heterogeneity of myocardial perfusion in healthy human myocardium: Assessment on dynamic perfusion ct using 128-slice dual-source ct. *Int J Cardiovasc Imaging*. 2014;30 Suppl 1:33-40

136. Cury RC, Kitt TM, Feaheny K, Blankstein R, Ghoshhajra BB, Budoff MJ, Leipsic J, Min JK, Akin J, George RT. A randomized, multicenter, multivendor study of myocardial perfusion imaging with regadenoson ct perfusion vs single photon emission ct. *J Cardiovasc Comput Tomogr*. 2015;9:103-112 e101-102

137. George RT, Mehra VC, Chen MY, Kitagawa K, Arbab-Zadeh A, Miller JM, Matheson MB, Vavere AL, Kofoed KF, Rochitte CE, Dewey M, Yaw TS, Niinuma H, Brenner W, Cox C, Clouse ME, Lima JA, Di Carli M. Myocardial ct perfusion imaging and spect for the diagnosis of coronary artery disease: A head-to-head comparison from the core320 multicenter diagnostic performance study. *Radiology*. 2014;272:407-416

138. Fujita M, Kitagawa K, Ito T, Shiraishi Y, Kurobe Y, Nagata M, Ishida M, Sakuma H. Dose reduction in dynamic ct stress myocardial perfusion imaging: Comparison of 80-kv/370-mas and 100-kv/300-mas protocols. *Eur Radiol*. 2014;24:748-755

139. Kim SM, Cho YK, Choe YH. Adenosine-stress dynamic myocardial perfusion imaging using 128-slice dual-source ct in patients with normal body mass indices: Effect of tube voltage, tube current, and iodine concentration on image quality and radiation dose. *Int J Cardiovasc Imaging*. 2014;30 Suppl 2:95-103

140. Pourmorteza A, Schuleri KH, Herzka DA, Lardo AC, McVeigh ER. A new method for cardiac computed tomography regional function assessment: Stretch quantifier for endocardial engraved zones (squeez). *Circ Cardiovasc Imaging*. 2012;5:243-250

141. Pourmorteza A, Schuleri KH, Herzka DA, Lardo AC, McVeigh ER. Regional cardiac function assessment in 4d ct: Comparison between squeez and ejection fraction. *2012 Annual International Conference of the IEEE Engineering in Medicine and Biology Society*. 2012:4966-4969

142. Cademartiri F, Mollet NR, Lemos PA, Saia F, Midiri M, de Feyter PJ, Krestin GP. Higher intracoronary attenuation improves diagnostic accuracy in mdct coronary angiography. *AJR Am J Roentgenol*. 2006;187:430-433

143. Cademartiri F, Mollet NR, van der Lugt A, McFadden EP, Stijnen T, de Feyter PJ, Krestin GP. Intravenous contrast material administration at helical 16-detector row ct coronary angiography: Effect of iodine concentration on vascular attenuation. *Radiology*. 2005;236:661-665

144. Papadakis AE, Perisinakis K, Damilakis J. Automatic exposure control in ct: The effect of patient size, anatomical region and prescribed modulation strength on tube current and image quality. *European Radiology*. 2014;24:2520-2531

145. Ghoshhajra BB, Engel L-C, Károlyi M, Sidhu MS, Wai B, Barreto M, Shanmugam U, Hoffmann U, Brady TJ, Kalra M, Abbara S. Cardiac computed tomography angiography with automatic tube potential selection: Effects on radiation dose and image quality. *J Thorac Imaging*. 2013;28:40-48

146. Eisa F, Brauweiler R, Peetz A, Hupfer M, Nowak T, Kalender WA. Optical tracking of contrast medium bolus to optimize bolus shape and timing in dynamic computed tomography. *Phys Med Biol*. 2012;57:173-182

147. Nakaura T, Awai K, Yanaga Y, Namimoto T, Utsunomiya D, Hirai T, Sugiyama S, Ogawa H, Aoyama M, Yamashita Y. Low-dose contrast protocol using the test bolus technique for 64-detector computed tomography coronary angiography. *Jpn J Radiol*. 2011;29:457-465

148. Rodrigues JC, Mathias H, Negus IS, Manghat NE, Hamilton MC. Intravenous contrast medium administration at 128 multidetector row ct pulmonary angiography: Bolus tracking versus test bolus and the implications for diagnostic quality and effective dose. *Clin Radiol*. 2012;67:1053-1060

149. Cademartiri F, van der Lugt A, Luccichenti G, Pavone P, Krestin GP. Parameters affecting bolus geometry in cta: A review. *J Comput Assist Tomogr*. 2002;26:598-607

150. van Hoe L, Marchal G, Baert AL, Gryspeerdt S, Mertens L. Determination of scan delay time in spiral ct-angiography: Utility of a test bolus injection. *J Comput Assist Tomogr*. 1995;19:216-220

151. Kaatee R, Van Leeuwen MS, De Lange EE, Wilting JE, Beek FJ, Beutler JJ, Mali WP. Spiral ct angiography of the renal arteries: Should a scan delay based on a test bolus injection or a fixed scan delay be used to obtain maximum enhancement of the vessels? *J Comput Assist Tomogr*. 1998;22:541-547

152. Platt JF, Reige KA, Ellis JH. Aortic enhancement during abdominal ct angiography: Correlation with test injections, flow rates, and patient demographics. *AJR Am J Roentgenol*. 1999;172:53-56

153. Bae KT, Seeck BA, Hildebolt CF, Tao C, Zhu F, Kanematsu M, Woodard PK. Contrast enhancement in cardiovascular mdct: Effect of body weight, height, body surface area, body mass index, and obesity. *AJR Am J Roentgenol*. 2008;190:777-784

154. Nakaura T, Awai K, Yauaga Y, Nakayama Y, Oda S, Hatemura M, Nagayoshi Y, Ogawa H, Yamashita Y. Contrast injection protocols for coronary computed tomography angiography using a 64-detector scanner: Comparison between patient weight-adjusted- and fixed iodine-dose protocols. *Investigative Radiology*. 2008;43:512-519

155. Yoshikazu Nakajima, Toshiki Yoshimine, Hiroyoshi Yoshida, Keiji Sakashita, Mitsutoyo Okamoto, Masanobu Kishikawa, Keiichi Yagi, Junichiro Yokota, Toru Hayakawa. Computerized tomography angiography of ruptured cerebral aneurysms: Factors affecting time to maximum contrast concentration. *J Neurosurg*. 1998;88:663-669

156. Ferencik M, Nomura CH, Maurovich-Horvat P, Hoffmann U, Pena AJ, Cury RC, Abbara S, Nieman K, Fatima U, Achenbach S, Brady TJ. Quantitative parameters of image quality in 64-slice computed tomography angiography of the coronary arteries. *Eur J Radiol*. 2006;57:373-379

157. Bae KT. Intravenous contrast medium administration and scan timing at ct: Considerations and approaches. *Radiology*. 2010;256:32-61

158. Indrajit IK, Sivasankar R, D'Souza J, Pant R, Negi RS, Sahu S, Hashim PI. Pressure injectors for radiologists: A review and what is new. *Indian J Radiol Imaging*. 2015;25:2-10

159. Halliburton SS, Tanabe Y, Partovi S, Rajiah P. The role of advanced reconstruction algorithms in cardiac ct. *Cardiovasc Diagn Ther*. 2017;7:527-538

160. Hubbard L, Ziemer B, Lipinski J, Sadeghi B, Javan H, Groves EM, Malkasian S, Molloi S. Functional assessment of coronary artery disease using whole-heart dynamic computed tomographic perfusion. *Circ Cardiovasc Imaging*. 2016;9

161. Johnson NP, Gould KL, Di Carli MF, Taqueti VR. Invasive ffr and noninvasive cfr in the evaluation of ischemiawhat is the future? *Journal of the American College of Cardiology*. 2016;67:2772-2788

162. Modat M, Ridgway GR, Taylor ZA, Lehmann M, Barnes J, Hawkes DJ, Fox NC, Ourselin S. Fast free-form deformation using graphics processing units. *Comput Methods Programs Biomed*. 2010;98:278-284